University of Sheffield

Structure-Property Relationships of Elastomers Containing Thermally Reversible Diels-Alder Bonds

Jennifer Catherine Hughes

A thesis submitted in partial fulfilment of the requirements for the degree of

Doctor of Philosophy

The University of Sheffield

School of Mathematical and Physical Sciences

Chemistry

October 2024

Declaration

I, **Jennifer Hughes**, confirm that the thesis is my own work. I am aware of the University's Guidance on the Use of Unfair Means (www.sheffield.ac.uk/ssid/unfair-means). This work has not previously been presented for an award at this, or any other, university. All the work is the original work of the author, except where acknowledged.

Jennifer Hughes October 2024

- All DMA data was obtained by Nicholas Hawkins (Department of Engineering, University of Oxford).
- All SAXS and WAXS data was obtained by Yi Zhang (ISIS Neutron and Muon Source).
- The solid-state frequency sweep data in Chapter 2 was obtained by Nictharkarn Soontornnon (University of Sheffield).

Acknowledgments

I would like to take this opportunity to thank every member of the Slark research group, in particular my PhD supervisor Professor Andrew Slark and postdoc Dr. James Wilson for their continuous support, guidance and feedback throughout this project. Their knowledge and expertise have allowed me to thrive within the research environment. I am extremely grateful for such a wonderful opportunity to learn and grow as in induvial as well as part of a team. I would like to thank Yi-Zhang who I met at the Young Researchers meeting (YRM) conference back in 2022. Since then, he has selflessly carried out many valuable SAXS and WAXS experiments for me and widened my morphology knowledge, even if it hurt my head at times! Another big thanks goes to Nicholas Hawkins, who has provided me with top quality DMA data and taught me a lot about thermal analysis, including the opportunity to visit Oxford university to see their facilities. I would also like to thank EPSRC for the funding.

I would especially like to thank Simon for being such a supportive friend and fantastic PhD mentor when I first started out in the Slark group during my master's degree (feels like an incredibly long time ago now), I honestly don't know what I would have done without you! James, you have also gone above and beyond as a friend and a colleague to make sure my PhD experience was good one and I am forever grateful for that. I am also grateful for all of my office, lunch and lab friends that have kept me sane along this crazy journey (you all know who you are), our mutual support and motivation has kept each other going and cheered me up tremendously when needed. Not to mention the after-work pints, socials and Christmas dinners certainly helped too.

An enormous thank you to my mum, dad, and sister. Your unwavering support, encouragement, and visits to Sheffield (mostly to our favourite food spots) have really meant a lot to me.

Abstract

The fast reversibility of the furan-maleimide Diels-Alder (DA) reaction, and high equilibrium conversion at room temperature make it an attractive candidate to design elastomers with thermal healing and reprocessing abilities. Applications and reprocessing techniques impose specific requirements, which can be met by the vast tuneability of design parameters within DA-polymers. This thesis greatly expands the fundamental understanding of structure-property relationships within DA polymer systems.

Chapter 2 explores self-healing thermoplastic polyurethanes comprising DA-cycloadducts (DA-TPUs) with various soft segment (SS) backbones. The thermoreversibility of molecular weight is demonstrated *via* SEC and sol-gel transitions. The thermomechanical and morphological properties were dependent on SS backbone, with phase-separated and semi-crystalline DA-TPUs displaying optimised properties.

In **Chapter 3** the synthesis of DA-TPUs comprising different molecular weight poly(ε-caprolactone) (PCL) SS is described. PCL crystallinity was found to dominate material properties over DA-cycloadduct concentration. The synthesis of DA-TPUs comprising different concentrations of poly(ε-caprolactone urethane) (PEU) and poly(1,4-butadiene urethane) (PBU) backbones is explored, showing that the morphology and thermomechanical properties varied systematically with PBU : PEU composition, with DA-(50PBU-*co*-50PEU) displaying a synergistic effect.

Chapter 4 describes the synthesis of trifuran cross-linkers comprising ester, urethane, or urea functional groups and their subsequent copolymerisation with different telechelic PU bismaleimides (from **Chapter 2**) to give 12 reversibly cross-linked DA-networks. Enhanced network strength and thermal stability was demonstrated *via* increased cross-linker hydrogen bonding, demonstrating synergistic reinforcement.

Chapter 5 investigates the effect of equivalent concentration of maleimide and furan functional groups (f_g) or furan backbone on the thermomechanical properties of polyester DA-

networks. Increasing f_g, through the use of low molecular weight bismaleimides, increased network strength, stiffness, and thermal stability whilst flexibility decreased. DA-networks incorporating highly crystalline 1,3,5-trifuryl benzoate exhibited higher tensile strength, toughness, and thermal stability than those containing amorphous FGE-FAM (synthesised from the ring-opening addition of furfuryl glycidyl ether with furfuryl amine).

Table of contents

List of Figures

List of Tables

List of Schemes

List of Abbreviations

ΔH_m	Enthalpy change of melting
$\Delta H_{m(HS)}$	Enthalpy change of melting of the hard segment
ΔH_{mPCL}	Enthalpy change of melting of PCL
ΔH_{rDA}	Enthalpy change of retro-Diels-Alder
ε_b	Strain at break
σ_b	Tensile stress at break
ATR-FTIR	Attenuated Total Reflectance Fourier-transform infrared
BDA	1,4-Butanediamine
BD	1,4-Butanediol
BMI	*N,N'*-(4,4'-methylene diphenyl) bismaleimide
CAN	Covalent adaptable network
CE	Chain extender
DA	Diels-Alder
DAP	1,3-Diaminopropane
DBDTL	Dibutyltin dilaurate
DCM	Dichloromethane
1,12-DD	1,12-Dodecanediol
$Đ_M$	Dispersity
DMA	Dynamic mechanical analysis
DMF	Dimethylformamide
DMSO	Dimethyl sulfoxide
DOSY	Diffusion-ordered ^{1}H NMR spectroscopy
d-spacing	Average interdomain spacing
DSC	Differential scanning calorimetry

EDA	Ethylene diamine
ESI-MS	Electrospray ionisation mass spectroscopy
$E'_{rubbery}$	Rubbery plateau modulus
E_y	Young's modulus
E'	Storage modulus
E''	Loss modulus
FA	Furfuryl alcohol
FAM	Furfuryl amine
f_g	Equivalent concentration of furan and maleimide groups
FGE	Furfuryl glycidyl ether
FMA	Furfuryl methacrylate
FTIR	Fourier-transform infrared
HDI	Hexamethylene diisocyanate
HEMI	2-Hydroxyethyl maleimide
HOMO	Highest unoccupied molecular orbital
HPBD	Hydrogenated polybutadiene
HS	Hard segment
$HS_{wt\%}$	Hard segment weight percent
HTPB	Hydroxyl-terminated polybutadiene
IPDI	Isophorone diisocyanate
LUMO	Lowest unoccupied molecular orbital
6-MCA	6-Maleimidocaproic acid
MDI	4,4'-methylene diphenyl diisocyanate
M_n	Number average molecular weight
M_w	Weight average molecular weight
m/z	Mass-to-charge-ratio

N	Number of monomers present at given time
N_0	Number of monomers at the start of reaction
NCO	Isocyanate
NEt_3	Triethylamine
NMR	Nuclear magnetic resonance
NPG	Neopentyl glycol
p	Extent of reaction
PBD	Poly(1,4-butadiene)
PBU	Poly(1,4-butadiene urethane)
PCL	Poly(ε-caprolactone)
PCL.LA	Poly(ε-caprolactone).Lactic acid
PDMS	Poly(dimethylsiloxane)
PEG	Poly(ethylene glycol)
PET	Poly(ethylene terephthalate)
PEU	Poly(ester urethane)
PMMA	Poly(methyl methacrylate)
PPG	Poly(propylene glycol)
ppm	Parts per million
PTFE	Poly(tetrafluoroethylene)
PTMG	Poly(tetrahydrofuran)
PTSA	p-Toluenesulphonic acid
PU	Polyurethane
P1075	Priamine™ 1075
q	Modulus of the scattering vector
q_{max}	Maximum peak intensity of q
r	Stoichiometric ratio of monomers

rDA	retro-Diels-Alder
ROP	Ring-opening polymerisation
SAXS	Small-angle X-ray scattering
SEC	Size-exclusion chromatography
SS	Soft segment
$T_{deg5\%}$	5% mass degradation temperature
T_f	Temperature of viscous flow
T_g	Glass transition temperature
T_{gel}	Degelation temperature
$T_{g(HS)}$	Glass transition temperature of the hard segment
$T_{g(SS)}$	Glass transition temperature of the soft segment
T_m	Melting temperature
T_{mHS}	Melting temperature of the hard segment
T_{mPCL}	Melting temperature of PCL
TDI	Toluene diisocyanate
TF	Trifunctional
TFBZ	1,3,5-trifuryl benzoate
TGA	Thermogravimetric analysis
THF	Tetrahydrofuran
TOF	Time of flight
TPE	Thermoplastic elastomer
TPU	Thermoplastic polyurethane
T_{rDA}	Temperature of retro-Diels-Alder
U_T	Modulus of toughness
WAXS	Wide-angle X-ray scattering

$wt\%_{HS}$	Weight percent hard segment
$wt\%_{MDI}$	Weight percent MDI
$wt\%_{SS}$	Weight percent soft segment
$\overline{X}_n$	Number average degree of polymerisation

1. Introduction

1.1 Step-growth polymerisation

Step-growth polymerisation refers to a types of polymerisation mechanism whereby bi-functional or multifunctional monomers react initially to form dimers (***Figure 1.1 (A)***). Dimers then react with monomers to form trimers. Eventually dimers and trimers react with one another to produce oligomers which continue to react, forming high molecular weight polymers.[1] This is why the average molecular weight increases slowly at low conversions and high extents of reaction are required to obtain high molecular weights (***Figure 1.1 (B)***).

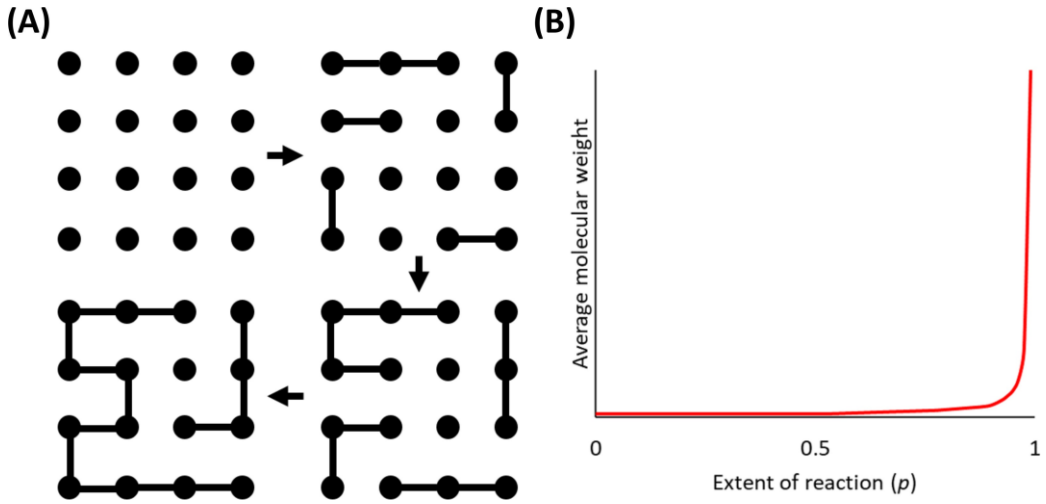

Figure 1.1 (A) *Generic representation of a step growth polymerisation (black dots represent monomers and black chains represent oligomers and polymers).* ***(B)*** *variation of molecular weight with extent of reaction (p) for step-growth polymerisation.*

The extent of reaction, p, can be calculated using the following equation*:*

$$p = \frac{N_0 - N}{N_0}$$

where N_0 is the number of monomers at the start of the reaction and N is the number of monomers present after time t.[2] The Carothers equation can then be applied to calculate the number average degree of polymerisation, $\bar{X}_n$, for the reaction of two monomers in equimolar quantities:

$$\bar{X}_n = \frac{1}{(1-p)}$$

This equation highlights how a high monomer conversion is necessary to achieve a high degree of polymerisation, for example a p of 0.98 is required for $\bar{X}_n$= 50, whilst a small increase of p to 0.99

doubles this to $\bar{X}_n$ = 100. Using the molecular weight of the repeating monomer unit, M_0, the number average molecular weight, M_n, and weight average molecular weight, M_w, can be calculated:

$$M_n = M_0 \frac{1}{1-p}$$

$$M_w = M_0 \frac{1+p}{1-p}$$

The dispersity, $Đ_M$, can then be calculated using the following equation, which simplifies to 1 + p.

$$Đ_M = \frac{M_w}{M_n} = 1 + p$$

This demonstrates that for linear polymers the maximum value of $Đ_M$ = 2, when monomer conversion is 100% or $p = 1$, but for branched polymers where multifunctional monomers are used $Đ_M$ can be much higher. For step-growth polymerisations where there is one monomer present in stoichiometric excess the Carothers equation becomes:

$$\bar{X}_n = \frac{(1+r)}{(1+r-2rp)}$$

where r is the stoichiometric ratio and is always less than 1. At the end of the reaction when $p = 1$ this equation simplifies to:

$$\bar{X}_n = \frac{(1+r)}{(1-r)}$$

showing that stoichiometric equivalence ($r = 1$) of bi-functional monomers is required to yield high molecular weight linear polymers. This equation demonstrates how stoichiometric control can be employed to target specific molecular weights for desired properties. High monomer purity and the absence of side reactions are also required to obtain high molecular weights.

1.2 Polyaddition versus polycondensation

There are two categories of step-growth polymerisation: polyaddition and polycondensation. Polyaddition occurs when the propagation steps are addition reactions, but small molecules are not evolved during these steps. An important example of polyaddition is the reaction of diols with diisocyanates to form urethane linkages in the synthesis of polyurethanes (PUs), which was discovered by Otto Bayer and co-workers in 1937 (***Scheme 1.1***).[3] Since their invention PUs have developed extensively, and now occupy a substantial share of the polymer market, with an estimated value of $73 billion in 2021.[4] This is a consequence of their excellent mechanical properties, durability, and diverse properties, as the only polymer class to encompass thermosetting, thermoplastic, and elastomeric materials.[5] PU versatility can be attributed to the extensive range of raw materials available, which gives rise to tunable properties such as flexibility, hardness, strength, insulation, and hydrolytic resistance. This makes PUs useful for diverse commercial applications such as footwear, construction, and automotive industries in the form of foams, coatings, adhesives, sealants, and elastomers.[6]

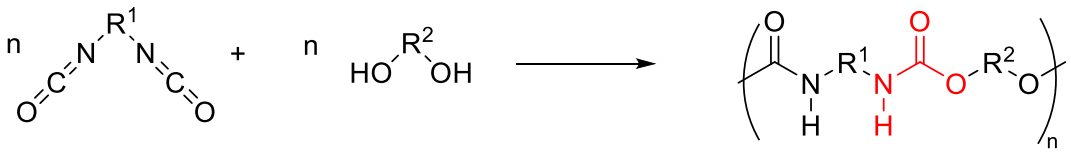

Scheme 1.1 *Polyaddition reaction between a diisocyanate and diol to yield a polyurethane. Urethane linkage highlighted in red.*

Polycondensation involves propagation steps which are condensation reactions where low molecular weight molecules are evolved. A significant example of polycondensation is the reaction between dicarboxylic acids and diols to form polyesters, which liberates water (***Scheme 1.2***). Polycondensations often require high temperatures, increased pressure, and catalysts to obtain high molecular weights.[7] Efficient removal of water is also typically required to drive the equilibrium forwards.

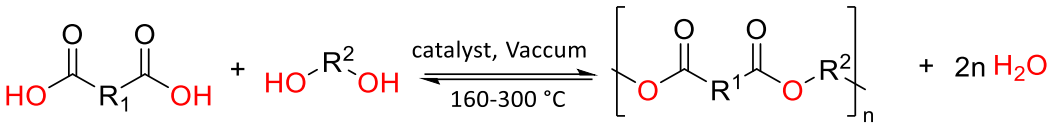

Scheme 1.2 *Generic synthesis of a polyester from the reaction between a dicarboxylic acid and a diol.*

Polyesters are another popular subclass of polymers, which started with the early research of Carothers in 1926. Discouraged by their low melting points and susceptibility to hydrolysis, Carothers' work on polyesters was left incomplete, instead he shifted his focus towards polyamides, specifically the production of Nylon, one of the first synthetic fibres. Carothers' work was recovered by British scientists Whinfield and Dickson, who patented poly(ethylene terephthalate) (PET) in 1941.[8] PET has since become one of the most common and economically viable polyesters, with fundamental applications in plastic water bottles and commercial synthetic fibres such as Terylene® due to its high strength and chemical resistance. In 2019 around 30.5 million metric tonnes of PET were produced worldwide.[9]

1.3 Thermoplastics and Thermosets

Polymers can be classified as thermoplastics or thermosets based on their behaviour when subjected to heat. Thermoplastics contain high molecular weight, entangled polymer chains which associate *via* non-covalent, intermolecular interactions such as Van der Waals forces, hydrogen (H-) bonding and π-π stacking. These weak interactions are susceptible to solvation and heating, transforming the thermoplastic from a solid to a viscous fluid. In this state, thermoplastics can be repeatedly reshaped and remoulded using traditional polymer processing techniques such as extrusion, injection, or compression moulding.[10] The melting/solidifying process in thermoplastics is fully reversible due to the absence of chemical bonding.[11] Despite this, thermoplastics often display weaker mechanical properties, solvent, and temperature resistance compared to thermosetting polymers, making them less suitable for intensive applications that require durability. Most thermoplastics are semi-crystalline, comprising amorphous and crystalline characteristics, where the degree of crystallinity lies in the range of 10-80% and affects the polymer properties.[12] Semi-crystalline polymers display highly

ordered molecular structures with broad melting ranges often up to 30 °C wide. Amorphous thermoplastics contain polymer chains with irregular molecular orientation, which are anisotropic of thermal properties. Examples of industrially relevant thermoplastics include polyethylene, polypropylene, poly(vinyl chloride), polystyrene and polycarbonate.[13,14]

Thermosetting polymers avoid such limitations by containing strong, irreversible, covalent cross-links between polymer chains to form a three-dimensional network. Such cross-links provide superior mechanical properties, temperature, solvent, and chemical resistance to thermosetting polymers, meaning they are more suitable for high-performance applications, such as structural adhesives construction materials and coatings.[15-17] Thermosetting polymers are obtained by irreversibly curing a soft solid or viscous liquid prepolymer (resin).[18] This means that upon cooling thermosets form a permanent, solid network that cannot be remolded or recycled upon heating, hence thermosets must be cured in the desired shape. The mechanism of cross-linking depends on the application and the chemistry involved, for example thermoset elastomers such as poly(isoprene) (natural rubber) and styrene-butadiene rubber are typically cured with sulphur in a process called vulcanisation. Vulcanisation occurs when some allylic C-H bonds are replaced by chains of sulphur that link with a cure site on another polymer chain.[19] Polymer chains of acrylic resins, vinyl esters, and polyesters, comprising unsaturated sites along the backbone, are commonly linked *via* free radical initiated copolymerisation with unsaturated monomer diluents.[20] Epoxy resins can homopolymerise upon the addition of heat and anionic or cationic catalysts, or copolymerise with multifunctional cross-linking agents.[21] Thermoset PUs are formed from the nucleophilic addition of polyisocyanates and polyols, where the degree of cross-linking is established by the functionality and ratio of reactants.[22]

1.4 Elastomers

Elastomers are polymers that display rubber like elasticity, which can stretch in response to macroscopic stresses and return quickly to their original shape after removal of a deforming force.[23] Polymer chains in elastomers are typically held together *via* weak intermolecular forces or a low degree of cross-links, leading to relatively low Young's modulus and high fracture strains compared to other materials. The term elastomer is commonly used interchangeably with rubber, though the latter typically refers to vulcanised material. Elastomers tend to be amorphous polymers with sub-ambient glass transition temperature (T_g) values, so that at room temperature they can undergo substantial molecular reconformation without the breaking of covalent bonds.[24] Elastomers are usually thermosets, although thermoplastic elastomers are also common.[25] The molecular structure of elastomers can be envisaged as a ''spaghetti and meatball'' structure, where the meatballs signify cross-links (***Figure 1.2***). In an unstressed polymer, the individual chains are random coils which are tangled in an irregular way. The coils ''straighten out'' under stretching so that the long chains can reconfigure themselves to distribute the applied stress. When the stress is removed, the covalent or physical cross-links ensure that the elastomer returns to its original coiled state as the intermolecular forces are greatest in this arrangement. Elastomers can be referred to as 'entropy springs', meaning that the major driving force for their elasticity is the increase in entropy ($+\Delta S$) *i.e* disorder and number of accessible chain conformations upon polymer chain contraction. This entropic contribution significantly decreases Gibb's free energy, meaning ΔG becomes more negative, where $\Delta G = \Delta H - T\Delta S$.[26]

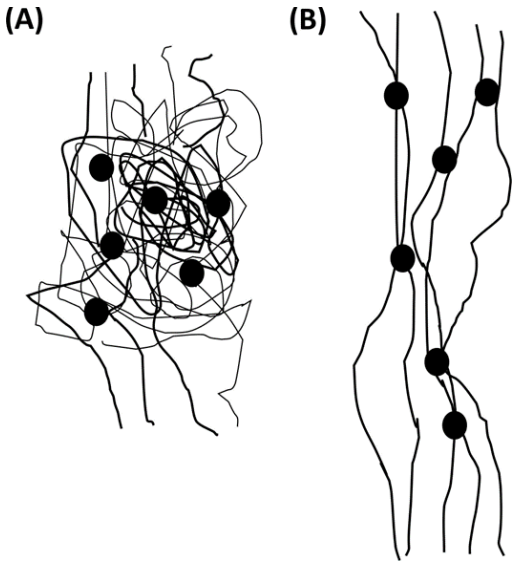

Figure 1.2 *''Spaghetti and meatball'' representation of molecular structure of elastomers* ***(A)*** *unstressed polymer and* ***(B)*** *same polymer under stress. Dots represent cross-links.*

Elastomers can be natural rubber (*cis*-polyisoprene) or synthetic including unsaturated rubbers that can be cured *via* sulphur vulcanisation such as butadiene rubber (*cis*-polybutadiene), chloroprene rubber (CR), styrene-butadiene rubber (SBR), and nitrile rubber or saturated rubbers that can be cured by sulphur vulcanisation *i.e* epichlorohydrin rubber (ECO), acrylic rubber (ACM), and silicone rubber (SI). Other important types of elastomers are polyurethane (PU) and polysulphide rubber.[27] Elastomers are used in diverse industries such as automobile, construction, renewable energy, oil and gas and biomedical applications due to their high impact resistance, thermal stability and chemical resistance.[28]

1.5 Polyurethanes

1.5.1 PU composition

PUs are segmented, multiblock copolymers comprising alternating flexible soft segments (SS) and rigid hard segments (HS), which are covalently bonded *via* urethane linkages (***Figure 1.3***).[29] The HS contains short chain diisocyanates and chain extenders (CEs), whilst the SS comprises long chain diols known as polyols.[30] A wide variety of PUs can be prepared by varying the HS : SS molar ratio, reaction conditions, and monomer structures resulting in a large variation in physio-mechanical properties.[31]

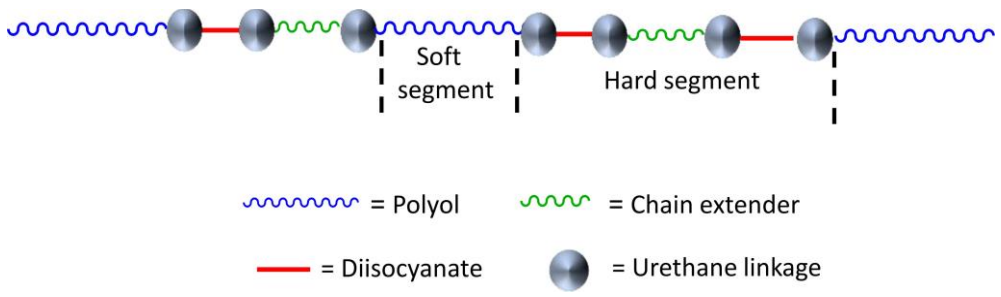

Figure 1.3 *Representation of PU composition comprising alternating hard and soft domains.*

1.5.2. PU soft segment

The SS of a PU typically contains flexible, polyol chains with molecular weights between 1000 – 5000 $g.mol^{-1}$ providing optimum material properties.[32] Below this value, PUs are unable to adequately phase separate. Lower molecular weights also reduce the ability of the SS to strain-crystallise, an important mechanical strengthening mechanism.[33] On the other hand, higher SS molecular weights can cause practical problems, such as extremely high viscosities during industrial bulk polymerisations, leading to mixing and pumping difficulties, as well as problems achieving high conversions.[33] The promotion of phase separation, resulting from using higher molecular weight SS chains, also reduces fractional conversion, which needs to be high in step-growth polymerisation to achieve high TPU molecular weights. Some of these problems can be resolved by using solution polymerisation methods, but such methods do not lend themselves to commercial scale synthesis due to associated negative environmental and health impacts. The molecular weight, crystallinity, flexibility, and structure of SS chains directly influence the mechanical and low temperature properties of the final PU, such as the T_g.[34] A low SS T_g is required for good low temperature properties and to maximise the service temperature of the PU. Substantial research has been conducted on the effect of SS molecular weight on PU properties, in the absence of any other structural changes. For example, Ma *et al.* synthesised a library of biodegradable poly(urethane urea)s with the same HS chemistry and content whilst altering SS molecular weight.[35] They discovered that increasing SS molecular weight correlated to a decrease in initial modulus. Ma *et al.* further reported that a larger SS chain length led to a decrease in permanent deformation due to a reduction in HS organisation.[35] Additionally, Gisselfalt

and Helgee reported that increasing SS length increased the degree of PU phase separation, causing a decrease in SS mobility, evidenced by lower T_g values and a resulting reduction in modulus.[36] Semi-crystalline polyols have been found to display an opposite effect, whereby increased molecular weight leads to an increased degree of crystallinity, which in turn increases modulus and ultimate tensile strength of the final PU.[35]

The most widely used PU SSs are polyester, polyether, and poly(1,4-butadiene) (PBD) polyols. Polyester polyols are typically synthesised *via* step-growth polycondensations of diacids such as adipic acid, with short chain diols, like ethylene glycol and propylene glycol (***Figure 1.4 (a)***). Polyester polyols are usually more viscous and expensive than polyether polyols.[37] Despite this, polyesters allow for a polar matrix with a high degree of H-bonding which helps to create strong bonds. This means that PUs incorporating polyester SS exhibit high tensile strength and hardness, with the potential for strain-induced crystallisation.[38] Polyester polyols are more susceptible to hydrolysis than polyether or PBD polyols, as they contain repeat ester linkages with significant dipole charges. Polyester polyols can have low or high T_g values and be amorphous or semi-crystalline, depending on their backbone structure. Polyether polyols, such as poly(propylene glycol) (PPG) and poly(ethylene glycol) (PEG), are usually syntheised *via* the acid or base catalysed ring-opening polymerisation (ROP) of propylene oxide and ethylene oxide with an active hydrogen-containing compound (***Figure 1.4 (b)***).[39] Polyether polyols originate from relatively cheap raw materials, meaning that they are more cost effective than other polyols. Polyether polyols also display excellent hydrolysis resistance and low temperature flexibility. However, PUs containing polyether SS often suffer from poor mechanical properties, due to the lack of H-bonding.

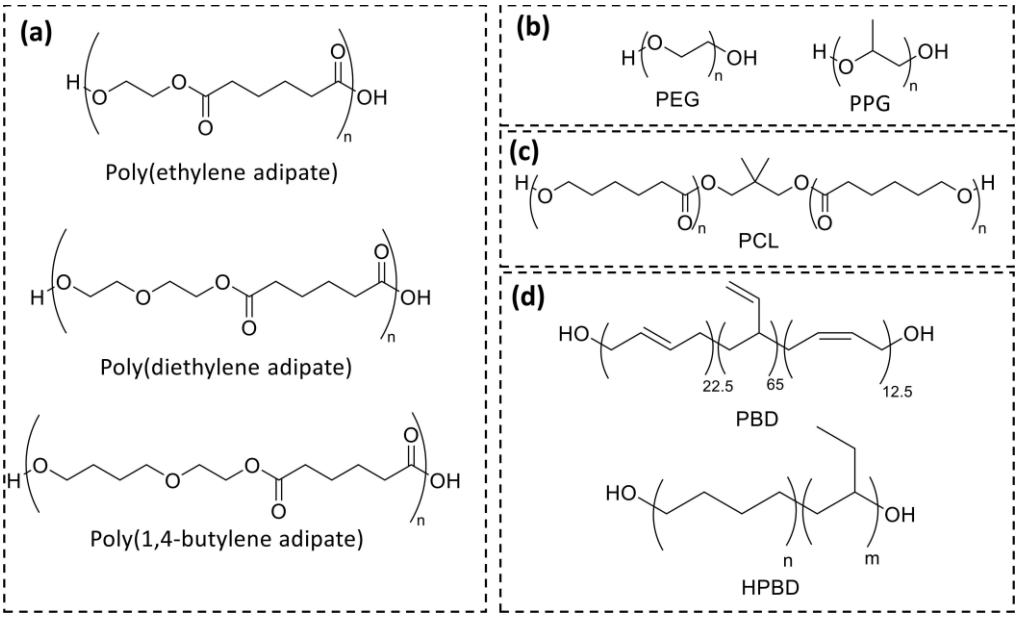

Figure 1.4 *Structures of commonly used polyols in the synthesis of PUs.* ***(a)*** *polyesters,* ***(b)*** *polyethers,* ***(c)*** *poly(ε-caprolactone) and* ***(d)*** *poly(1,4-butadiene)s.*

High performance polyester polyols, such as poly(ε-caprolactone) (PCL), are produced *via* the ROP of lactones, in this case of ε-caprolactone, with nucleophilic 'initiator' multifunctional alcohols (R-[-OH]$_f$]), using various catalysts like stannous octoate (***Figure 1.4 (c)*** and ***Scheme 1.3***).[40]

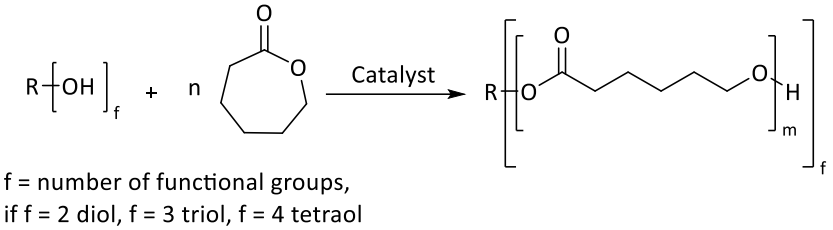

Scheme 1.3 *General reaction scheme for the ROP of ε-caprolactone with an initiator diol to produce poly(ε-caprolactone).*

ROP offers several advantages over traditional polyester synthesis, as it is capable of producing higher molecular weight polymers with more targeted control over monomer conversion and narrower dipsersities. However, ROP is considered less industrially viable as it is a slower process, involving air sensitive techniques which can be difficult to produce on a commercial scale.[41]

PCL is a semi-crystalline, biodegradable polyester with a melting point of approximately 60 °C and a low T_g of -60 °C, resulting in enhanced low temperature properties.[42,43] PCL is often reserved for speciality PUs, where it imparts outstanding impact, hydrolysis, oil, and solvent resistance. PCL is a SS known to strain-crystallise, producing tough materials with high tensile strengths and tear resistance.[44] PCL polyols are also less susceptible to hydrolytic degradation than traditional polyester polyols, as they contain less polar, longer hydrocarbon chains with a lower concentration of ester groups. A broad range of 'initiator' multifunctional alcohols can be used to ring-open ε-caprolactone, enabling the design of PCL polyols with customised properties. The initiator functionality, *f*, defines the functionality of the resulting polyol (diol, triol, tetraol) whilst the structure affects the final PU properties. For example, neopentyl glycol (NPG) is a bulky/hindered diol which is used due to its reduced tendency to crystallise and enhanced hydrolytic stability, whilst hexane-1,2-diol yields PUs with superior tensile and thermal properties in addition to high cut-chip resistance.

Low dispersity ($Đ_M$ < 1.1) PBD is synthesised *via* anionic polymerisation of 1,4-butadiene in a hydrocarbon solvent, such as hexane, using a butyllithium (BuLi) initiator.[45] The propagation occurs *via* a 1,4- or a 1,2-Michael-addition, followed by termination when methanol is added. Hydroxyl-terminated PBD (HTPB) is synthesised *via* epoxidation of PBD, followed by chain cleavage to form aldehyde end-groups, which are then reduced to form hydroxyl end groups. Hydrogenation of HTPB produces hydroxyl-terminated hydrogenated PBD (HTHPB). PUs synthesised from HTPB can be functionalised to obtain specific physical properties, producing PUs which can be highly elastic or tough and rigid. HTPB-based PUs can be used in various applications, such as rigid foam insulation panels, durable elastomeric wheels, tyres, and rocket propellant, demonstrating their versatility. Additionally, PUs containing HTPB often display superior hydrolytic stability and low temperature flexibility due to their hydrocarbon nature.[46] Despite this, the mechanical properties of HTPB-based PUs are usually inferior to polyester PUs, on account of the lower miscibility between non-polar HTPB SSs and polar HSs, causing unfavourable, early phase separations.[47] In this case phase separation is

bad because it negatively influences the formation of segmented block copolymers. However, when phase separation occurs at a later stage in PU polymerisation it can be applied to enhance mechanical strength, facilitate order on a wide range of length scales, or to add localised functionalities to a material.[48,49]

1.5.3 PU hard segment

PU HS is more compact than SS, comprising shorter components which associate *via* non-covalent interactions, such as H-bonds and π–π stacking to form rigid, physically crosslinked clusters dispersed in a flexible SS polymer matrix. The strength of these interactions dictates the mechanical properties of PUs, whilst the thermal stability acquired by these interactions determines the high temperature behaviour of PUs.[50] Longer HS blocks generally lead to better phase separation and resulting PU properties, but at the same relative HS fraction, longer blocks can contribute to difficulties in synthesis.[33] The morphology and degree of crystallinity within the HS are determined by diisocyanate and CE structure, for example less branching and higher symmetry leads to improved packing with more regular HS-HS interactions.[51] Different percentages of HS content, traditionally 15, 30, 45 or 60% are used in PU compositions to tune the resulting properties. Increasing HS content above 30% often changes long-range connectivity of HS, resulting in an increase in mechanical strength in the PU.[52] Increasing HS content typically increases elastic properties such as Young's modulus and rubbery-plateau modulus, whilst various elastomeric properties like elongation and stress at break decrease.[53] Many researchers have studied the complex PU structure-property relationships associated with varying HS content.[54-56]

1.5.3.1 Isocyanate reactivity

Di- or poly- functional isocyanates are highly reactive unsaturated compounds containing two or more NCO groups. Primary reactions of NCO involve polyadditions with alcohols and amines to yield urethane and urea bonds, respectively (***Scheme 1.4 (A)*** and ***(D)***). At elevated temperatures, the high reactivity of NCO allows for secondary reactions with urethanes and ureas to form allophanates and

biurets, respectively (***Scheme 1.4 (B)*** and ***(E)***). Depending on the aim, these reactions can lead to premature cross-linking and unwanted side products or be desired to provide a cross-linking mechanism which enhances network mechanical properties. Isocyanates can also react with water to form a primary amine and carbon dioxide *via* an unstable carbamic acid intermediate (***Scheme 1.4 (C)***).[57] The produced carbon dioxide gas can be useful as a 'blowing agent' for application in PU foams. However, in PU elastomer applications water can compete with the desired CE compound for preferential reaction with NCO leading to unwanted side reactions. The primary amine formed from the initial reaction of water with NCO can react with more NCO to produce urea compounds which can subsequently react with NCO groups to form biurets. Atmospheric moisture should therefore be excluded in PU synthesis by conducting polymerisations under vacuum or inert atmosphere.

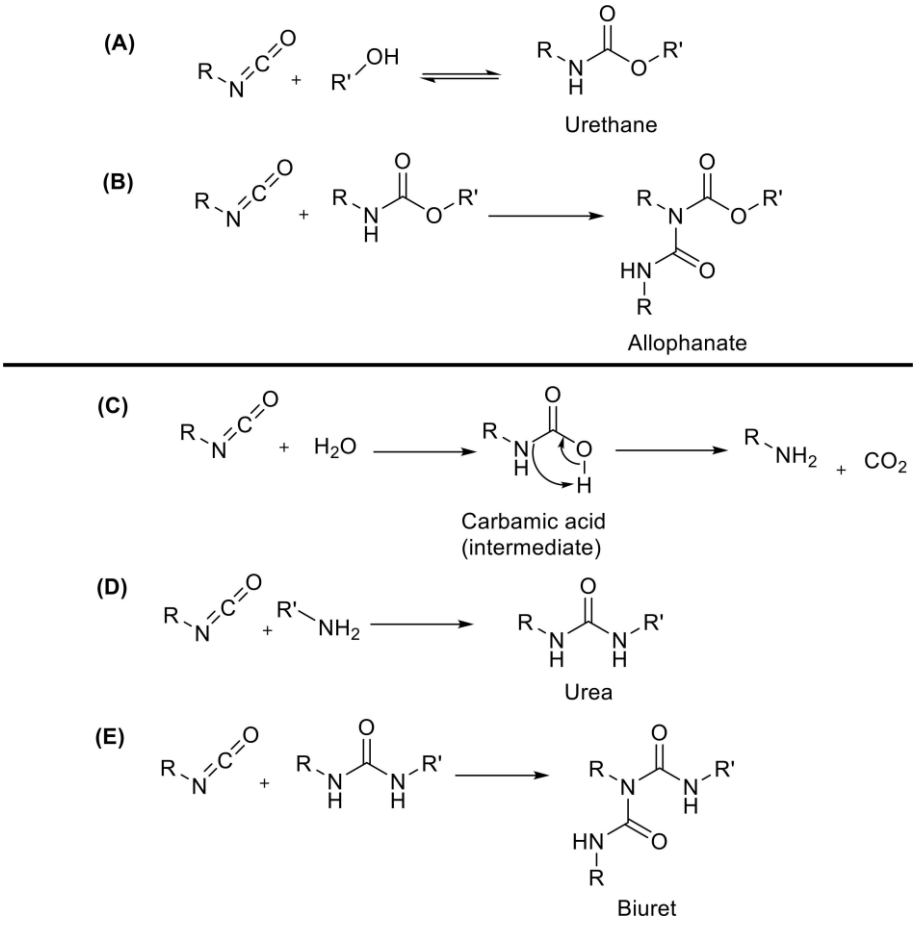

Scheme 1.4 *Summary reactions of isocyanate with* ***(A)*** *alcohol,* ***(B)*** *urethane,* ***(C)*** *water,* ***(D)*** *amine and* ***(E)*** *urea.*

1.5.3.2 Isocyanate structure

Diisocyanates can be classified as aromatic or aliphatic, depending on their structure. Aromatic diisocyanates are generally more popular as the aryl rings provide structural rigidity and conjugation to PU chains increasing their overall polarity and restricting free rotation.[58] The NCO functional groups in aromatic diisocyanates are also more susceptible to nucleophilic attack due to the greater electron-withdrawing effect of the aryl rings, which increase electrophilicity of the NCO carbon atoms.[59] This means that PU polymerisations using aromatic diisocyanates display faster rates of reaction. The two most common aromatic diisocyanates in the PU industry are methylene diphenyl diisocyanate (MDI) and toluene diisocyanate (TDI), which make up 90% of the total diisocyanate market.[60] Both can exist in several isomers (***Figure 1.5***). The symmetric isomers (4,4'-MDI and 2,6-TDI) contain NCO groups of equal reactivity, whilst the asymmetric isomers (2,4-MDI, and 2,4-TDI) introduce preferential reactivity.[61] PUs incorporating symmetric diisocyanates exhibit stronger mechanical properties, on account of better chain packing, promoting H-bonding and crystallisation.[62] The higher volatility and toxicity of TDI make it less attractive, hence MDI is often preferred as it is a solid at room temperature.[60] However, TDI is favoured in applications, such as flexible foams, as it contains one less aromatic ring than MDI meaning it can provide more flexibility to the PU.[60] Aromatic PUs have a tendency to yellow with prolonged exposure to UV light, due to a photo-Fries rearrangement of the urethane group around the aromatic ring, forming a quinone-imide structure.[63] This means that aliphatic isocyanates, in particular hexamethylene diisocyanate (HDI) and isophorone diisocyanate (IPDI), are preferred in applications like paints and coatings where enhanced light, thermal and hydrolytic stability are necessary.[64] Urethanes formed over a longer time by aliphatic diisocyanates are also typically more stable than those formed from aromatic diisocyanates.[65]

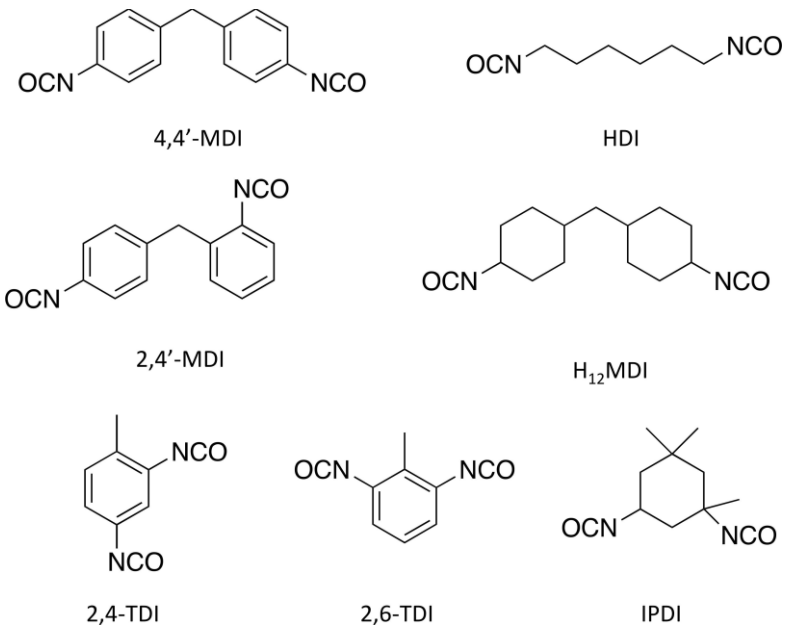

Figure 1.5 *Structures of common aromatic and aliphatic diisocyanates used in PU synthesis.*

1.5.3.3 Chain extenders

CEs are low molecular weight diols or diamines that typically react NCO-terminated prepolymers to form urethane and urea linkages, building PU molecular weight and increasing the HS block length.[66] By doing this, CEs can enhance the number of chain entanglements and favourable interactions within PUs thereby improving mechanical properties.[67] Diamine CEs usually provide PUs with increased modulus and tensile strength but decreased elongation compared to diol CEs, due to bidentate H-bonding between the formed urea groups.[66] The tendency of diamine CEs to produce biuret cross-links in addition to their highly rapid and exothermic reactions with NCO limit their usage, especially in the formulation of TPUs.[68] Like diisocyanates, CEs can be aromatic or aliphatic.

The first example of a CE was water which reacts with NCO to produce PU and carbon dioxide which 'blows' the block copolymer into a solid supramolecular foam.[69] However, outside of PU foam applications, water has little advantage. Examples of more commonly used diol CEs in TPUs are 1,4-butanediol (BD), 1,2-propanediol (PD), neopentyl glycol (NPG) and 2-methyl-1,3-propanediol (MPD) (***Figure 1.6***). The shape, structure and functionality of CEs determine the rigidity and density of H-bonds in the HS blocks.[68] Symmetrical BD is the most popular CE for PUs in structural applications as

it produces highly regular and well-packed HSs, forming dense physical networks which provide superior mechanical performance.[70] Ethylene diamine (EDA), butane-1,4-diamine (BDA), and 1,3-diaminopropane (DAP) are common amine CEs which have been used extensively to make PUs for biomedical applications.

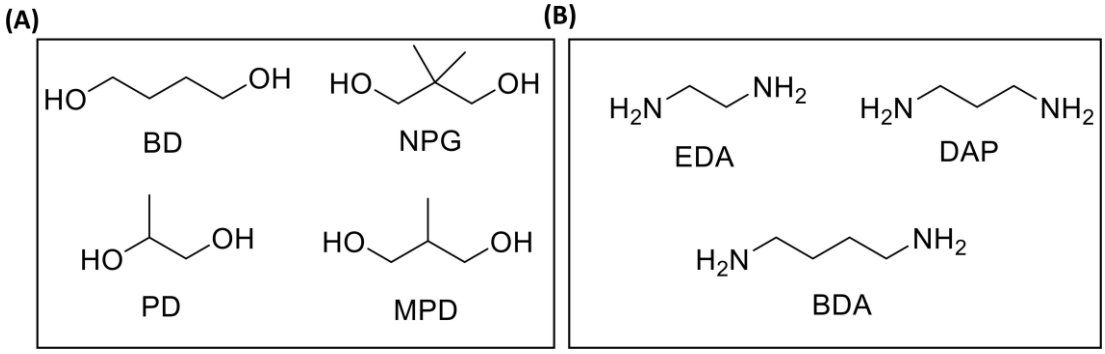

Figure 1.6 *Structures of* ***(A)*** *common diol CEs and* ***(B)*** *common diamine CEs used for PU synthesis.*

1.5.4 PU morphology

PUs exhibit microphase separated morphologies, driven by the thermodynamic incompatibility between polar HSs and non-polar SSs (***Figure 1.7***).[71] Despite the significantly increased entropy upon mixing ($\Delta_{mix}S$) the hard and soft segments, the absence of favourable enthalpic interactions ($\Delta_{mix}H$) between the contrasting segments usually results in mutual immiscibility.[72] At high temperatures the segments will become miscible if the free energy of mixing is negative ($\Delta_{mix}G < 0$), where $\Delta_{mix}G = \Delta_{mix}H - T\Delta_{mix}S$ but as the PU cools the HSs associate *via* H-bonding to form physically cross-linked clusters which are immiscible with the SS, triggering spinodal decomposition and subsequent phase separation. Macrophase separation is prevented *via* the formation of covalent urethane bonds between the hard and soft blocks, instead leading to microphase separation.

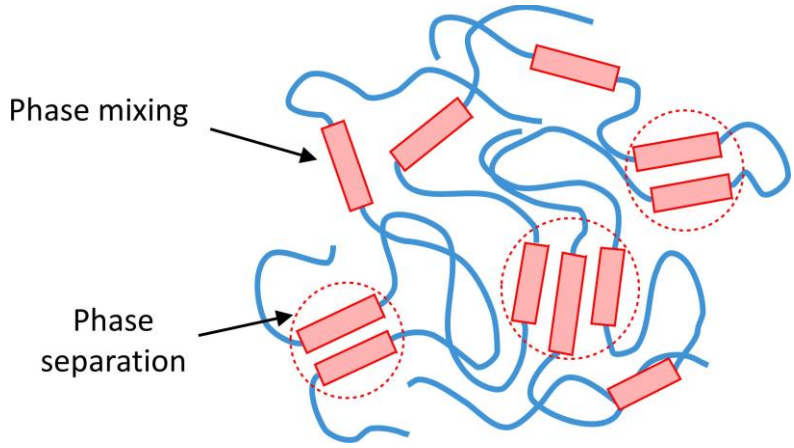

Figure 1.7 *Representation of PU morphology. Blue lines represent SS polyol, red blocks represent HS, and the red dashed circles symbolise a phase change.*

The degree of microphase separation can be controlled by changing the compatibility between the hard and soft segments, which will affect the final PU properties. T_g reflects the degree of miscibility between the segments. For example, a highly phase separated PU will typically display two T_g values which can be assigned to the separate hard and soft segments, whilst a predominantly phase mixed PU will exhibit a single T_g which lies between the T_g values of the hard and soft domains.

At low HS contents, the HSs form discrete 'pseudo-crystalline' domains which act as rigid physical cross-linking sites, reinforcing the amorphous SS matrix and enhancing the strength and elasticity of the network.[73] Increasing HS content results in increased hard domain interconnectivity and a transition from discrete to continuous hard domains.[33] When stress is applied to a PU, the SS chains can reorientate from a mostly entangled state by extending in the direction of force, whilst the HSs remain unaffected, preventing permanent deformation of the SS. When the stress is removed, the SS chains can relax and resume their original conformation.[74] When a TPU heated, the hard domains melt, transforming the material into a viscous melt. Upon cooling, the H-bonds within the HS can reform, meaning the TPU regains its strength.[75]

TPU elastomers display three distinct regions on a plot of modulus against temperature, namely the glassy plateau, the rubbery plateau, and the viscous fluid region (***Figure 1.8***). The glassy plateau,

defined as the region below the T_g of the SS, is where the TPU is brittle and adopts a frozen glassy state due to negligible chain motion. As the TPU approaches the T_g the modulus drops due to the onset of segmental chain motion. The region above the T_g and below the melting temperature (T_m) of the TPU is defined as the rubbery plateau, also known as the service temperature range, where a relatively stable modulus is retained. This region defines the temperature limits in which the TPU is required to operate and is where optimum material properties are achieved. Above the T_m the polymer is molten and acts as a viscous fluid.

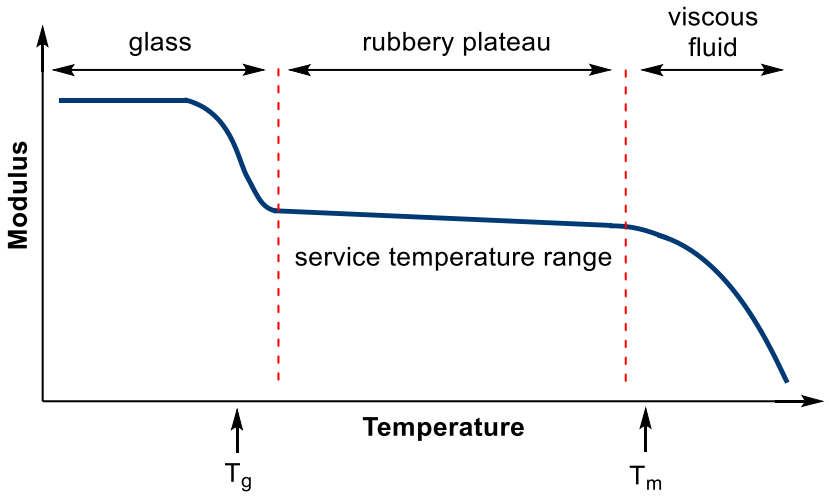

Figure 1.8 *Graph showing typical changes in TPU modulus as a function of temperature.*

1.5.5 PU polymerisation method

PU polymerisation can be performed *via* two different methods, known as the one-shot and two-shot method. The one-shot method is a commonly used industrial technique to prepare PUs as it is simple, quick, and economically viable. It involves combing the polyol, CE, and other desired reactants such as catalysts and fillers in 'one-shot', followed by the addition of diisocyanate to produce the final PU.[76] The simultaneous reaction of NCO with polyol and CE usually leads to a random distribution of soft and hard segments in the macromolecular backbone of the obtained PU.[77] This reaction is also highly exothermic, meaning it can cause the final product to thermally 'self-destruct', so no orderly polymeric structure is formed.[78] In the two-shot method, commonly referred to as the prepolymer method, polyol first reacts with a stoichiometric excess of diisocyanate to give an NCO-terminated

prepolymer.[79] This intermediate species is then reacted with an excess of diol or diamine CE in a second step to yield an OH or NH-terminated PU. The properties of the prepolymer which is obtained in the first step depend on the molar ratio of NCO : OH, viscosity, the presence or absence of water, and the properties of diisocyanates and polyols.[80] The prepolymer method offers more control over the molecular structure and provides a more even distribution of hard and soft segments, leading to enhanced PU mechanical properties over PUs prepared by the one-shot method.[81] The prepolymer method is also considered a safer process as some of the chemical energy is already used up forming the prepolymer and there are still NCO groups that are available to react.

1.6 Covalent adaptable networks

Covalent adaptable networks (CANs) are polymer networks which closely resemble thermosetting polymers; however they incorporate dynamic covalent bonds, which can exchange upon the application of an external stimulus such as light, heat or pH, enabling the network to rearrange its topology on a molecular level.[82] These dynamic cross-links allow CANs to display reprocessing, recycling, self-healing, and reshaping properties, thereby bridging the gap between thermoplastics and thermosets.[83-85] CANs can be classified as associative or dissociative, depending on the underlying bond exchange mechanism and their resulting temperature dependence (***Figure 1.9***).[86]

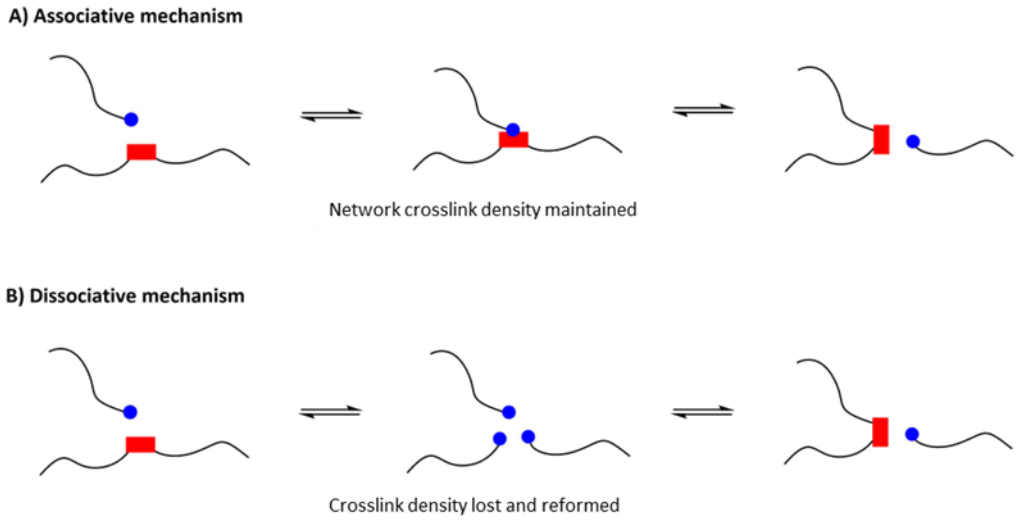

Figure 1.9 *CANs divided into two groups:* ***A)*** *associative and* ***B)*** *dissociative based on exchange mechanisms which proceed respectively, with or without a temporary net loss of cross-link density.*

During an associative exchange mechanism, a cross-link is only broken when a new covalent bond has formed with a different reaction partner *via* an addition-elimination pathway. This mechanism therefore proceeds without a temporary net loss of cross-link density (***Figure 1.9 A)***).[87] Associative CANs maintain network integrity upon heating, preventing depolymerisation. This means that they typically display a gradual decrease in viscosity and retention of insolubility in inert solvents in addition to high creep-resistance at elevated temperatures. The first reported associative CANs in 2005 involved photo-mediated, free-radical addition-fragmentation chain transfer reactions by incorporating ally sulphide moieties.[88] In 2011, a new class of associative CANs, coined ''vitrimers'' was introduced by Lieber *et al.*, based on catalytic transesterification within epoxy/acid or epoxy/anhydride polyester-based networks.[89] They demonstrated that the permanent polyester/polyol networks exhibited a gradual decrease in viscosity upon heating, a distinctive feature of vitreous silica.[86] Since then, the chemistry platform of associative CANs has developed well, with noteworthy examples including transamidation of vinylogous urethanes,[90,91] transesterification using boronic esters,[92] and dynamic exchange of thioesters with thiols.[93] Above the topology freezing temperature, all of the mentioned exchange mechanisms are fast, enabling viscous flow.[94] Consequently, associative CANs can be thermally reshaped and recycled. Despite this, due to their relatively high viscosity at elevated temperatures high-pressure reprocessing techniques, such as injection and compression moulding must be used.[95]

In a dissociative exchange mechanism, the opposite occurs: bond dissociation precedes bond reformation *via* an elimination/addition pathway. When a stimulus is applied, the equilibrium will shift to the dissociated state, leading to a temporary decrease in network cross-link density (***Figure 1.9 B)***). In the case of a thermoreversible system, when a sufficient amount of heat is applied net covalent bond dissociation occurs and the dissociative CAN experiences a loss of network integrity, leading to a sudden drop in viscosity. This leads to viscous flow, stress-relaxation, and solubility in good solvents at high temperatures due to very fast topology rearrangements.[96] Upon cooling, the dynamic cross-links will reform, usually to the same extent as in the starting material, preserving desirable

thermosetting properties. These dynamic cross-links enable facile thermal (re-)processing of polymeric networks, requiring lower pressures and temperatures than those required for associative CANs. The most explored chemical platform for the design and synthesis of dissociative CANs is the thermoreversible Diels-Alder (DA) reaction between furans and maleimides.[97,98] Other notable examples of dissociative CAN chemistry are triazolinedione Alder-ene reactions,[99,100] hindered-urea exchange,[101,102] and alkoxyamine dynamic bonds.[103-105]

1.7 Diels-Alder chemistry

1.7.1 Diels-Alder reaction

The DA cycloaddition reaction, discovered by Otto Diels and Kurt Alder in 1928, is a pericyclic reaction which occurs between a conjugated diene and dienophile to give a cyclohexene derivative (***Scheme 1.5***).[106] The reaction takes place *via* a concerted mechanism, in which three π-bonds are broken whilst two σ-bonds and a π-bond are simultaneously formed.[107] The reaction proceeds *via* a cyclic transition state with six delocalised π-electrons, benefitting from aromatic stabilisation. The DA reaction can be classified as a [4+2] cycloaddition, as it involves the four π-electrons of the diene and the two π-electrons of the dienophile. According to the Woodward-Hoffmann rules, these [4+2] cycloadditions are activated by heat, opposed to [4+4] and [2+2] cycloadditions, which are activated *via* light-irradiation.[108]

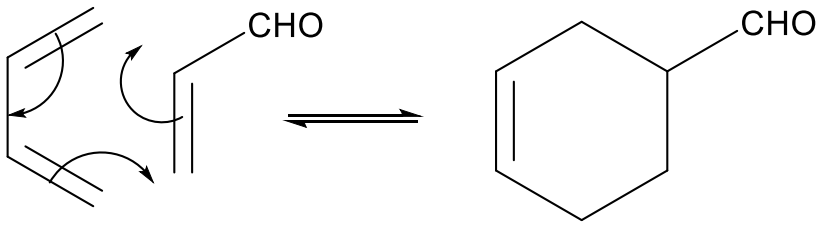

Scheme 1.5 *The Diels-Alder reaction between a conjugated diene and a substituted dienophile to give a substituted cyclohexene derivative.*

DA-cycloaddition is driven by the rapid formation of energetically stable σ-bonds, due to perfect alignment of the involved p-orbitals. It can be considered as a ''click'' reaction due to its modularity, high yields, regiospecificity, and insensitivity towards solvent parameters, oxygen, and water.[109] For a

successful DA reaction to occur, the diene must adopt a pseudo s-*cis* conformation due to geometrical constraints associated with the s-*trans* conformation, involving an extremely strained σ-bond. This means that cyclic dienes, such as furan and cyclopentadiene, which have a fixed s-*cis* conformation, are ideal for DA reactions. The dienophile is an alkene or alkyne, which is typically attached to an electron-withdrawing substituent such as carbonyl compounds, nitro compounds, nitriles, or sulphones to provide extra conjugation, known as 'activating' the dienophile. To understand why, it is necessary to consider the frontier molecular orbitals of the reactants.[110]

σ-bond formation occurs *via* the interaction between the highest occupied molecular orbital (HOMO) of the diene (ψ_2) with the lowest unoccupied molecular orbital (LUMO) of the dienophile (π*) (***Figure 1.10***). This interaction is thermally allowed since the orbitals involved have matching symmetry and are of similar energy.[111] The newly formed σ-bonds are also lower in energy, meaning they are more stable and preferred. The energy of the dienophile LUMO can be lowered by incorporating adjacent electron-withdrawing substituents, making it electron poor, whilst the energy of the diene HOMO can be increased by attaching electron-donating groups, making it electron-rich. This decreases the ψ_2 HOMO/ π* LUMO energy gap, allowing for better orbital overlap and an increased rate of reaction.

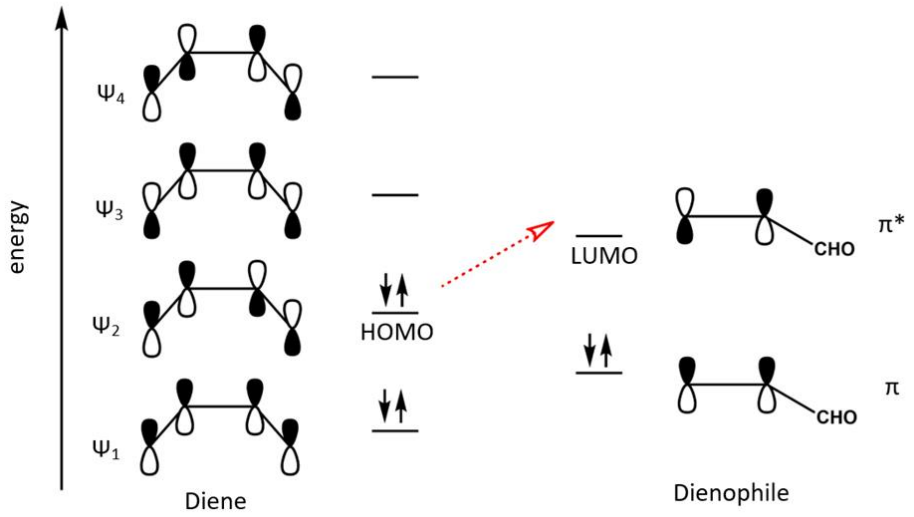

Figure 1.10 *Molecular orbital diagram displaying the thermally allowed transition from the diene HOMO to the dienophile LUMO.*

Inverse electron demand DA reactions can also occur which involve overlap between the HOMO of the dienophile and the LUMO of the diene.[110] This alternative transition is less likely due to presence of a larger energy gap. Despite this, attaching electron-withdrawing groups to the diene and electron-donating groups to the dienophile can alter the HOMO/LUMO energy gap enough to make this reaction preferred. A typical DA reaction has negative values of both enthalpy, Δ*H* and entropy, Δ*S* due to the formation of energetically stable σ-bonds and the combination of two reactants to give one product, giving more order. This means that at every temperature a dynamic equilibrium exists, such that at low temperatures cycloadducts form preferentially, but at high temperatures the equilibrium favours dissociation in the microscopic reverse of the DA reaction, known as the retro Diels-Alder (rDA) reaction.

Depending on the suprafacial approach of the diene and dienophile, the forward DA reaction can produce two diastereoisomers, known as the *endo* and the *exo* cycloadducts (***Figure 1.11 (a)***).[112] The *endo* isomer, where the bulkier sides of the diene and dienophile overlap, is the kinetically favoured product. This is because the overlap allows stabilisation of the transition state by secondary interactions between the extended π orbitals of the diene and dienophile, reducing its activation energetic barrier. (***Figure 1.11 (b)*** and ***(c)***). However, the *endo* isomer is less thermodynamically stable than the *exo* isomer on account of greater steric hindrance. The *exo* isomer is formed when the bulkier, heteroatom sides of the diene and dienophile lie away from each other, resulting in fewer secondary orbital interactions to lower the energic barrier of the transition state, causing it to form at a slower rate. The *exo* DA-adducts are thermodynamically favoured as they experience less steric hindrance than the *endo* DA-adducts, leading to a more negative Gibbs free energy of reaction, $\Delta_r G°$.[113]

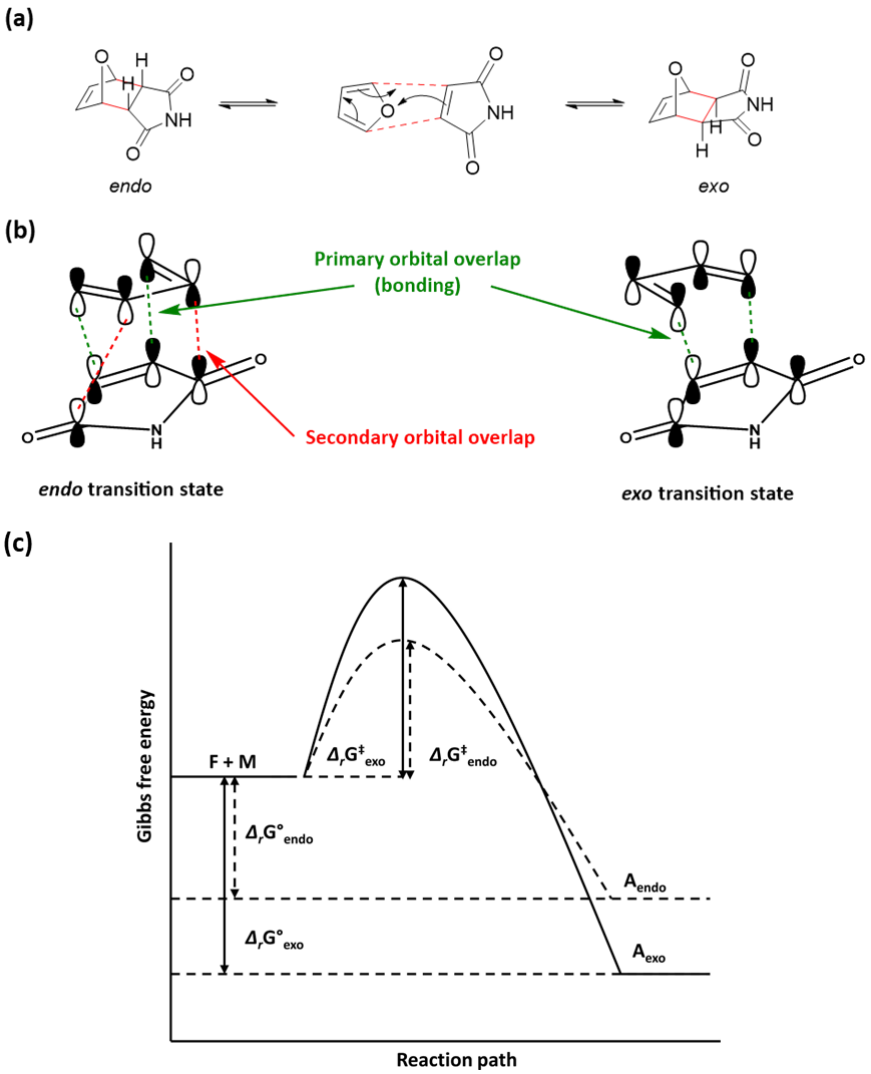

Figure 1.11 (a) *Reaction of furan and maleimide to form endo and exo diastereoisomers,* ***(b)*** *transition states leading to endo and exo isomers using molecular orbitals and* ***(c)*** *Gibbs free energy profiles showing the activation energy barriers, $\Delta G^{\ddagger}$, and the standard Gibbs free energies of reaction, $\Delta_r G°$, for furan and maleimide.*

A wide variety of conjugated dienes and dienophiles have been used in the literature to participate in this thermoreversible DA reaction, such as anthracene-maleimide,[114,115] anthracene-fullerene,[116] fulvene-cyanofurmarate,[117] cyclopentadiene-cyanodithioester,[118] cyclopentadiene-(di) cyclopentadiene,[119,120] and furan-maleimide (***Table 1.1***).

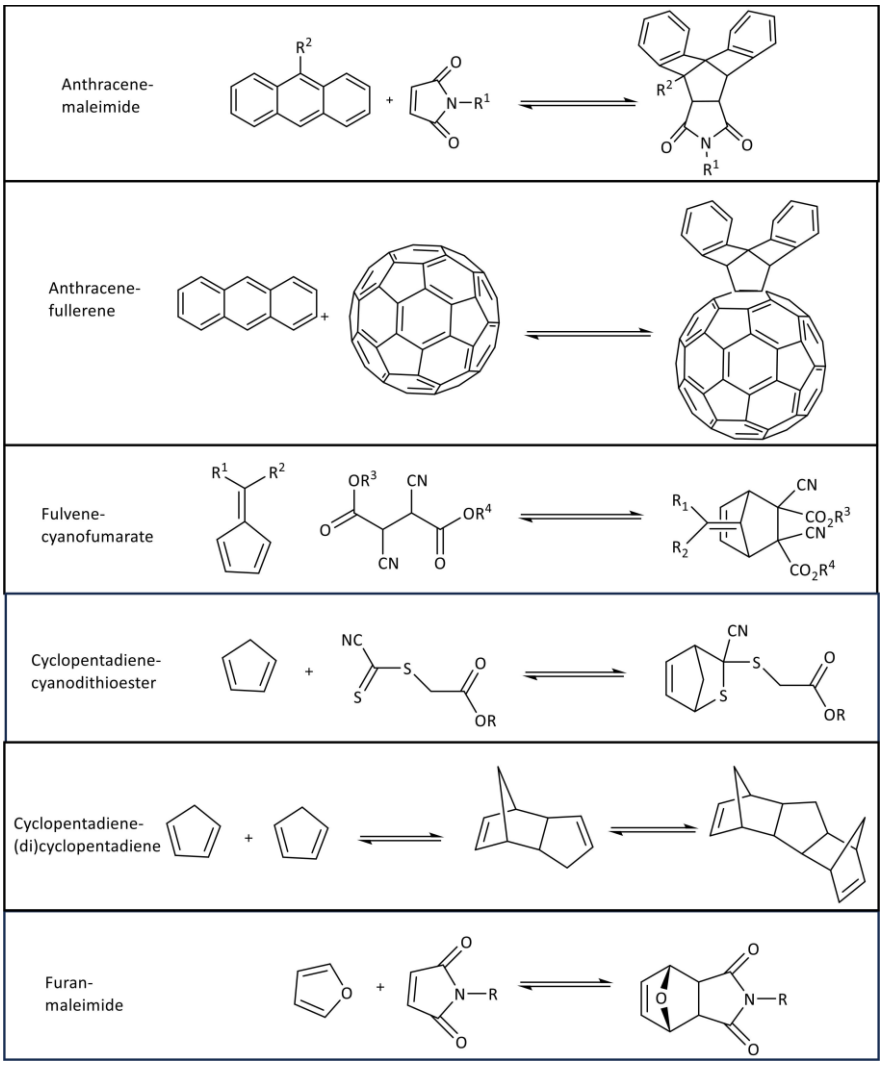

Table 1.1 *Summary of diene-dienophile pairings used in recent literature.*

Furan and maleimide derivatives have become the most popular diene-dienophile pairing throughout literature, since these reactants lead to a dynamic equilibrium with fast reaction kinetics and high equilibrium conversion at ambient temperature, with minimal side reactions.[121,122] The furan-maleimide rDA reaction also occurs at relatively low temperatures (≥ 110 °C), which are viable and non-degradative to practically all macromolecular structures, opening the door to recyclable networks and self-healing materials.[123,124]

The first reversible DA network based on furan-maleimide chemistry was patented by Craven in 1969.[125] However, it took until 2002 when Wudl *et al*. applied this chemistry to synthesise self-healing networks with properties similar to cross-linked epoxy resins for DA-chemistry to regain a lot of

interest.[126] They reported that DA polymer networks constructed with dynamic covalent bonds possess an estimated bond energy of 93 kJ.mol^{-1}, only slightly lower than typical covalent bonds (150-550 kJ.mol^{-1}). This means that DA-networks exhibit similar mechanical properties, such as Young's modulus and toughness values to traditional thermoset networks at ambient temperature. Moreover, since the DA cross-links in the polymer networks are thermoreversible, upon heating through the degelation temperature (T_{gel}) the DA-bonds will break, meaning the previously viscoelastic material will start displaying viscous flow behaviour. This enables DA-CANs to be thermally reprocessed, reshaped, and recycled, unlike conventional thermosets.[127] Consequently, furan-maleimide DA chemistry has been applied to several polymer networks, including polyurethane,[128-132] epoxy,[133-135] polyacrylate,[136-138] and polysiloxane,[139-141] to create self-healing and thermally reprocessable materials for diverse applications such as elastomers, adhesives, coatings, and composites.

Various thermoplastic polymers incorporating furan-maleimide DA bonds have also been reported with different spacer chemistries.[142-144] In all cases, the DA bonds allowed for a reversible change in molecular weight with temperature, achieving lower melt viscosities and enhanced processability than traditional thermoplastics. However, most of these polymeric systems used *N,N*'-(4,4'-methylene diphenyl) bismaleimide (BMI), a low molecular weight monomer which is toxic and inappropriate for consumer or industrial applications.

1.7.2 Maleimide side reactions

Increasing the temperature, which is required for the thermal processing and healing of DA-networks, accelerates the rDA reaction and shifts the equilibrium to regenerate the furan and maleimide functional precursors. However, at high temperatures, these reactive moieties can undergo unwanted, irreversible side reactions. One of the most well-documented side reactions is the radical homopolymerisation of maleimide moieties, which takes place at temperatures above 150 °C (***Scheme 1.6***).[145] One way to minimise maleimide homopolymerisation is to add a radical scavenger such as

benzene-1,4-diol (hydroquinone), during the synthesis procedure.[146] The radical scavenger will neutralise any radicals formed, preventing the initiation of the homopolymerisation.

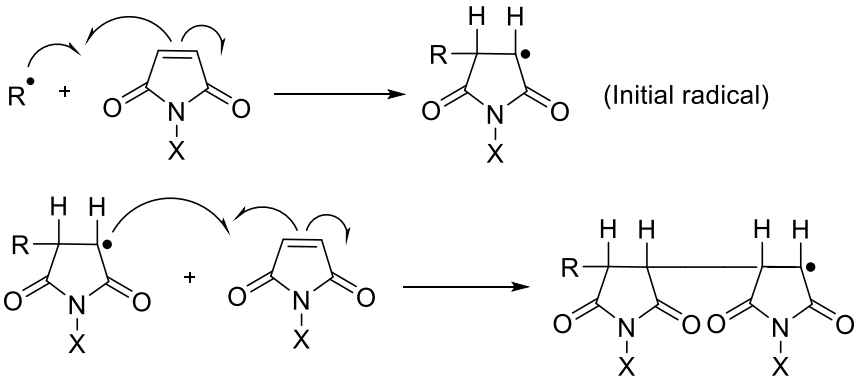

Scheme 1.6 *Free radical homopolymerisation of maleimide.*

Another prominent side reaction is the Michael-addition reaction, which can occur between primary or secondary amines with maleimides between 100 and 180 °C (***Scheme 1.7***).[147] This means that in DA networks it is imperative to avoid of formation of any unreacted amines as they will consume maleimides to form irreversible cross-links, reducing the thermal reversibility of the system.

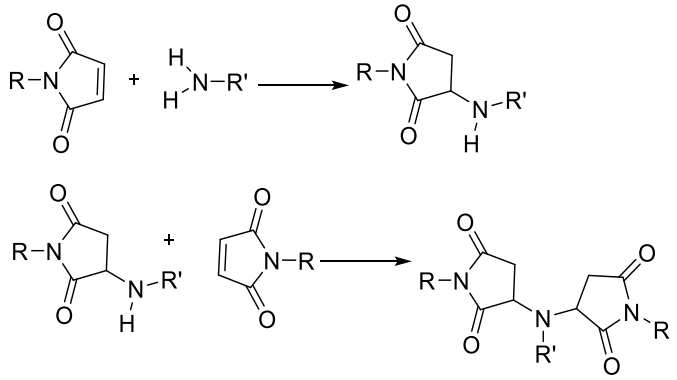

Scheme 1.7 *Michael-addition reaction of primary or secondary amine with maleimide.*

1.7.3 Design parameters in DA

The three major design parameters which have been summarised in the literature to influence DA polymer network properties are: the monomer functionality, the stoichiometric ratio of the maleimide and furan reactive groups, and the equivalent concentration of maleimide and furan functional groups (f_g in kg.mol^{-1}) which correlates to the concentration of DA-cycloadducts at room temperature (***Figure 1.12***).[148] By carefully controlling these design parameters researchers can tailor the mechanical,

manufacturing, and self-healing properties of DA-polymers to meet the requirements for specific applications. These design parameters are often interconnected, meaning that optimising one parameter may require altering the others to achieve the final desired property.

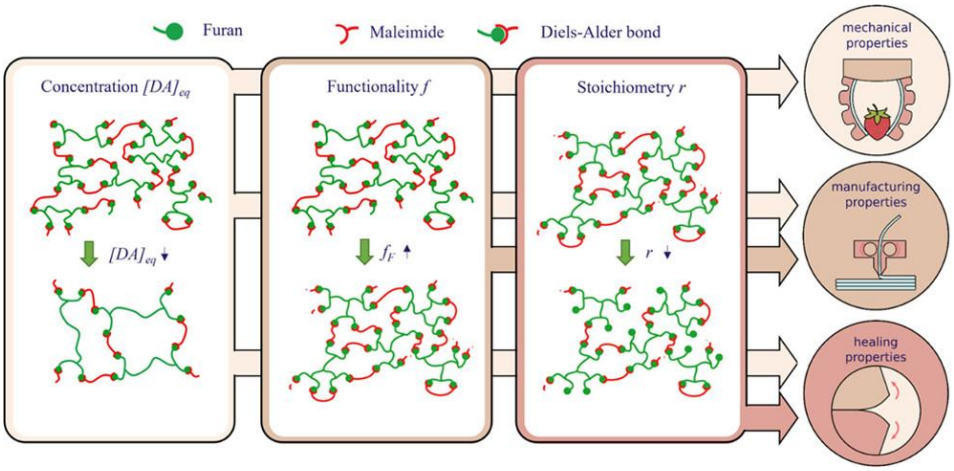

Figure 1.12 *Summary of three main networks design parameters in DA-polymer networks. Reprinted with permission from Macromolecules,* ***2022****, 13, 5947-5513. Copyright 2024 American Chemical Society.*[148]

The thermomechanical properties of DA networks, including the viscoelastic behaviour at different temperatures, can be varied *via* the cross-link density, which correlates to the concentration of DA-cycloadducts at room temperature.[149] The cross-link density can be influenced by the molar mass per DA functional group of the monomer units, as well as the molar ratio between them.[150] Higher DA-concentrations have been found to push the T_g and T_{gel} to higher temperatures yet decrease self-healing rates due to the reduction of mobility caused by additional DA cross-links.[151] Brancart and coworkers demonstrated that by changing the DA cross-link density whilst keeping other network parameters constant the mechanical properties could be varied over several orders of magnitude, with Young's modulus ranging from the MPa to GPa scale.[148] They also discovered that higher DA-cycloadduct concentrations caused a decrease in mobility, which increased the temperature of self-healing. Li *et al*. demonstrated that the T_{gel} and the resulting rheological behaviour of DA networks could also be highly influenced by monomer functionality, with minimal change in mechanical properties at room temperature.[152] Moreover, research has been conducted by Vanderborght *et al.*

on increasing the T_{gel} by using furan compounds with a higher degree of functionality for fused filament fabrication.[153] They determined that higher furan functionalities speeded up reaction kinetics during printing, leading to faster solidification and improving both print speed and resolution. Researchers have also revealed that lowering the maleimide- to-furan stoichiometric ratio, by using excess furan, led to faster DA-bond formation and faster self-healing, whilst the mechanical properties and T_{gel} values remained hardly unchanged.[148]

1.8 Aims

Whilst the chemistry platforms for dissociative dynamic polymers are developing well, a recent perspective has highlighted the need for better understanding of materials behaviour.[87] The main goal of the work outlined in this thesis is therefore to ''*investigate novel structure property relationships of Diels-Alder based polymers with thermal healing and reprocessing properties*''. This thesis aims to answer the fundamental research question ''*can we use the current knowledge of Diels-Alder design parameters from the literature to design new ones?*'' To successfully achieve the primary objective of this research, the succeeding chapters of this dissertation will delve into addressing the follow research questions (RQ):

RQ1: What range of properties can be achieved by altering the soft segment of TPUs containing Diels-Alder cycloadducts?

Incorporating DA chemistry into thermoplastic polyurethanes (TPUs) enables a thermoreversible change in molecular weight, lowering melt viscosity and improving thermal processing efficiency, in addition to providing thermal healing properties. Whilst research has be carried out into TPUs containing Diels-Alder cycloadducts (DA-TPUs), previous work has focussed on fixing the DA-TPU soft segment (SS) whilst changing other DA-design parameters. The work outlined in **Chapter 2** aims to thoroughly compare DA-TPUs synthesised using four different polyols of M_n of 2,000 g.mol^{-1} in order to alter SS structure independent of DA-cycloadduct concentration. This work illustrated that a wide range of thermal, mechanical and morphological properties can be achieved *via* altering SS structure,

with the unsaturated polybutadiene DA-TPU (DA-PBD) displaying enhanced thermal stability due to phase separation and the semi-crystalline poly(ε-caprolactone) DA-TPU (DA-PCL) exhibiting optimised mechanical properties. Moreover, this work confirmed excellent thermal healing and reprocessing properties of the DA-TPU materials using mild conditions.

RQ2: What range of properties can be achieved by altering the soft segment molecular weight in DA-TPUs?

In the first part of **Chapter 3**, the effect of changing PCL SS molecular weight and consequently the equivalent concentration of furan and maleimide functional groups (f_g) in the DA-TPUs on the resulting material properties was studied comprehensively. To achieve this, PCL polyols of M_n = 1000, 2000, and 4000 g.mol^{-1} were copolymerised with excess 4,4'-methylene diphenyl diisocyanate (MDI) followed by furfuryl alcohol (FA) or 2-hydroxyethyl maleimide (HEMI) to provide furan or maleimide terminated PU prepolymers. The corresponding prepolymers were then copolymerised at ambient temperature to yield DA-TPUs comprising PCL SS molecular weight (DA-1KPCL, DA-2KPCL, and DA-4KPCL). It was demonstrated that DA-TPUs comprising higher molecular weight PCL provided stronger mechanical properties due to enhanced PCL crystallinity. Despite this, the thermal stability of the DA-TPUs decreased with increasing PCL molecular weight/ decreasing f_g as less thermal energy was required to dissociate a lower concentration of DA-cycloadducts.

RQ3: Is it possible to synthesise DA-TPUs comprising mixed soft segments, and can we alter properties by altering the composition of such segments?

Rubber waste is a major issue as a consequence of its slow degradation and poor recyclability. While annually hundreds of papers are published on the synthesis of novel DA-based polymers, no literature study to date has explored DA-TPUs comprising two SS's. In order to take advantage of the merits and overcome the drawbacks of DA-PBD and DA-PCL from **Chapter 2**, the second part of **Chapter 3** aims to explore the use of DA chemistry to synthesise DA-TPUs **combining both** PBD and PCL SSs *via* the copolymerisation furan and maleimide terminated

poly(butadiene urethane) and poly(ε-caprolactone urethane) prepolymers. This approach will be adopted to yield three DA-(PBU-*co*-PEU) copolymers containing varying amounts of PBU : PEU segments (25, 50 and 75 wt.%). This work demonstrated proof of concept for the use DA chemistry to make recyclable elastomers with superior properties from incompatible precursors. Moreover, it was illustrated that material properties could be systematically varied with PBU : PEU composition, with DA-(50PBU-*co*-50PEU) displaying a pronounced synergistic effect.

RQ4: Can dual-dynamic networks provide a synergistic approach?

By researching covalent adaptable networks (CANs) this work aims to design recyclable elastomers which can potentially bridge the gap between current thermoplastic and thermoset elastomers. To achieve this, **Chapter 4** describes the synthesis of 12 PU based dual-dynamic networks made *via* the copolymerisation of the telechelic bismaleimides from **Chapter 2** with trifunctional furans comprising isocyanurate cores and either ester, urethane or urea functionality. This work demonstrated that increased cross-linker hydrogen bonding systematically increased the DA network delegation temperature (T_{gel}), crucial for processing, by upto 40 °C, confirming synergistic reinforcement of the DA covalent cross-links from non-covalent interactions. Network tensile strength also improved with degree of cross-linker hydrogen bonding whilst flexibility decreased. All networks showed high gel fractions in THF confirming high degrees of cross-linking whilst displaying excellent recovery of mechanical properties after 3 thermal reprocessing cycles, demonstrating recyclability. Moreover, the effect of cross-linking was determined by comparing the thermomechanical properties of the DA PU-CANs to the corresponding linear DA-TPUs from **Chapter 2** with the same SS backbone, showing that tensile strength and thermal stability increased whilst flexibility decreased upon cross-linking.

RQ4: Is it possible to synthesise polyester-based CANs derived from biobased monomers?

Due to the increased demand for biobased monomers and the shift away from the use of toxic isocyanates **Chapter 5** aims to focus on the synthesis and structure-property relationships of

polyester-based CANs. Two furan cross-linkers were synthesised *via* the ring-opening addition of furfuryl glycidyl ether (FGE) with either vegetable oil dimer diamine (Priamine 1075) or furfuryl amine (FAM) to produce tetrafunctional FGE-P1075 or trifunctional FGE-FAM, respectively, where all monomers can be derived from biomass. 1,3,5-trifuryl benzoate (TFBZ) was also synthesised *via* the reaction of 1,3,5-benzenetricarbonyl chloride with furfuryl alcohol to provide a highly crystalline, rigid alternative to the highly flexible FGE-FAM cross-linker. Different molar mass bismaleimides were syntheised *via* the Fischer-esterification of various hydrocarbon polyols with 6-maleimodic caproic acid (6-MCA). Copolymerisation of these bismaleimides with the various furan cross-linkers enabled independent variation of either network f_g/concentration of DA cross-links or trifuran backbone structure. This work demonstrated that increasing f_g increased network strength, stiffness, and thermal stability whilst flexibility decreased. Furthermore, DA-networks incorporating TFBZ provided higher tensile strength, toughness, and thermal stability than those containing FGE-FAM.

1.9 References

[1] G. Odian, *Principles of Polymerization*, Wiley-Interscience, New York, 1991 edn., 1991.

[2] W. H. Carothers, T. *Faraday Soc.*, 1936, **32**, 39-49.

[3] J. Brandrup, E. H. Immergut, E. A. Grulke, A. Abe and D. R. Bloch, *Polymer handbook*, Wiley New York, 1999.

[4] G. V. Research, *Polyurethane Market Size, Share & Trends Analysis Report by Product* (Rigid Foam, Flexible Foam), By Application (Construction, Furniture & Interiors), By Region, And Segment Forecasts, 2022 - 2030, Report 978-1-68038-262-4, San Francisco, 2022.

[5] H. W. Engels. H. G. Pirkl, R. Albers, R. W. Albach, J. Krause, A. Hoffman, H. Casselman, *Angew.Chem. Int. Ed.*, 2013, **52**, 9422-9441.

[6] G. Woods, *The ICI Polyurethanes Book*, ICI Polyurethanes and John Wiley and Sons, New York, 1990, 2nd ed, pp 7-14, 32-35.

[7] H. Wang, H. Li, C. K. Lee, N. S. Mat Nanyan and G. S. Tay, *Polymers*, 2022, **14**, 5059.

[8] Whinfield, J.R. and Dickson, J.T., 1941. Improvements relating to the manufacture of highly polymeric substances. *British Patent*, *578*, p.79.

[9] M. E. Rogers, T. E. Long and S. Richard Turner, in *Synthetic Methods in Step-Growth Polymers*, 2003, pp. 1–16.

[10] P.K. Mallick, in *Materials design and manufacturing of lightweight vehicles*, Woodhead publishing, Cambridge, 2021, 2nd edn, pp 187-228.

[11] E. R. Larson, in *Thermoplastic Material Selection*, ed. E. R. Larson, William Andrew Publishing, 2015, pp.19-56.

[12] N. Kumar, P. D. Ukey, V. Francis, R. P. Singh, and S. Sahu, in *Polymers for 3D Printing*, ed. J. Izdebska-Podsiadły, William Andrew Publishing, 2022, pp. 307-323.

[13] S. Hassan, M. Heinrich, B. Cecen, J. Prakash and Y. S. Zhang, in *Biomaterials for Organ and Tissue Regeneration*, eds. N. E. Vrana, H. Knopf-Marques and J. Barthes, Woodhead Publishing, 2020, pp. 669-707.

[14] M. Mandal, G. Gogoi, N. Dutta, and T. K. Maji, in *Handbook of Polymer Nanocomposites for Industrial Applications*, ed. C. M. Hussain, Elsevier, 2021, pp. 587-615.

[15] T. Engels, in *Thermosets*, ed. Q. Guo, Woodhead Publishing, 2012, pp. 228-253.

[16] S. Agarwal and R. K. Gupta, in *Thermosets (2nd Edition)*, ed. Q. Guo, Elsevier, pp. 279-302.

[17] S. Agarwal and R. K. Gupta, in *Thermosets (2nd Edition)*, ed. Q. Guo, Elsevier, pp. 369-400.

[18] J. P. Pascault and R. J. J. Williams, in *Thermosets*, ed. Q. Guo, Woodhead Publishing, 2012, pp. 3-27.

[19] A. Y. Coran, in *The Science and Technology of Rubber (4th Edition)*, eds. J. E. Mark, B. Erman and C. M. Roland, Academic Press, Boston, 2013, pp. 337-381.

[20] T. J. Mao, *J. Polym. Sci., Polym. Lett. Ed.*, 1978, **16**, 201–201.

[21] B. Ellis, in *Chemistry and Technology of Epoxy Resins*, Springer Netherlands, 1993, pp. 1–36.

[22] T. Li, X. Zhang, W. Yang, Y. Zhang, W. Wu and Y. Luo, *Polymer*, 2024, **290**, 126586.

[23] R. Tarodiya and A. Levy, *Powder Technology*, 2021, **387**, 527-559.

[24] K. M. Salleh, M. Mostapha, K. S. Lau and S. Zakaria, in *Elastomer Blends and Composites*, eds. S. M. Rangappa, J. Parameswaranpillai, S. Siengchin and T. Ozbakkaloglu, Elsevier, 2022, pp. 331-351.

[25] A. L. Skov and P. Sommer-Larsen, in *Dielectric Elastomers as Electromechanical Transducers*, eds. F. Carpi, D. De Rossi, R. Kornbluh, R. Pelrine and P. Sommer-Larsen, Elsevier, Amsterdam, 2008, pp. 25-32.

[26] M. Rinnbauer, in *Encyclopedia of Lubricants and Lubrication*, ed. T. Mang, Springer Berlin Heidelberg, Berlin, Heidelberg, 2014, pp. 475-477.

[27] I. M. Alarifi, *Adv .Ind. Eng .Polym. Res.*, 2023, **6**, 451-464.

[28] T. Pervez and F. S. Al-Jahwari, in *Encyclopedia of Renewable and Sustainable Materials*, eds. S. Hashmi and I. A. Choudhury, Elsevier, Oxford, pp. 131-147.

[29] Y. He, D. Xie, X. Zhang, *J. Mater. Sci.*, 2014, **49**, 7339-7352.

[30] Lee, C.-F.et al, *Appl. Sci*. 2021, **11**, 698.

[31] R. Al Nakib, A. Toncheva, V. Fontaine, J. Vanheuverzwijn, J.-M. Raquez and F. Meyer, *J. Appl. Polym. Sci.*, 2022, **139**, 51666.

[32] C. Hepburn, in *Polyurethane Elastomers*, ed. C. Hepburn, Springer Netherlands, Dordrecht, 1992, pp. 51-106.

[33] T. J. Touchet and E. M. Cosgriff-Hernandez, in *Advances in Polyurethane Biomaterials*, eds. S. L. Cooper and J. Guan, Woodhead Publishing, 2016, pp 3-22.

[34] D. Randall and S. Lee, *The Polyurethanes Book*, Wiley, New York, 3rd edn., 2003.

[35] Z. Ma, Y. Hong, D. M. Nelson, J. E. Pichamuthu, C. E. Leeson and W. R. Wagner, *Biomacromolecules*, 2011, **12**, 3265-3274.

[36] K. Gisselfält and B. Helgee, *Macromol. Mater. Eng.*, 2003, **288**, 265-271.

[37] A. Domanska and A. Boczkowska, *Polym. Degrad. Stab.*, 2014, **108**, 175-181.

[38] A. Das and P. Mahanwar, *Adv. Ind. Eng. Polym. Res.*, 2020, **3**, 93-101.

[39] A.-L. Broca, C. Mantzaridis, D. Tunca and S. Carlotti, *Prog. Polym. Sci*, 2013, **38**, 845-873.

[40] M. Labet, W. Thielemans, *Chem. Soc. Rev*., 2009, **38** (12), 3484-504.

[41] H. Phan, K. Kortsen, G. Englezou, B. Couturaud, A. J. Nedoma, A. K. Pearce and V. Taresco, *J. Polym. Sci.*, 2020, **58**, 1911-1923.

[42] P. D. O. Coulembiera, J. L. Hedrick, P. Dubois, *Prog. Polym. Sci.*, 2006, **31**, 723- 747.

[43] K. Žukiene, V. Jankauskaitė, V. Betingytė, A. Baltušnikas, *J. Appl. Polym. Sci.,* 2013. **1286**, 2186-2196.

[44] L. D. Morbitzer and H. Hespe, *J. App. Polym. Sci.*, 1972, **16**, 2697-2708.

[45] A. Ryan, O. Mykhaylyk, C. Fernyhough, M. Okura, P. Fairclough and R. Graham, *Eur. Polym. J.*, 2011, **47**, 447-464.

[46] J. O. Akindoyo, M. D. H. Beg, S. Ghazali, M. R. Islam, N. Jeyaratnam and A. R. Yuvaraj, *RSC Adv.*, 2016, **6**, 114453-114482.

[47] M. Spirkova, *J. Appl. Polym. Sci*., 2002, **85**, 84.

[48] Y. Liu, *J. Appl. Polym. Sci.*, 2013, **127**, 3279-3292.

[49] Y. S. Lipatov, *J. Macromol. Sci., Part B: Phys*., 2006, **45**, 871–888.

[50] K. Kojio, S. Nozaki, A. Takahara and S. Yamasaki, *J. Polym. Res.*, 2020, **27**, 140.

[51] S. McCreath, P. Boinard, E. Boinard, P. Gritter and J. J. Liggat, *Int. J. Adhes. Adhes*, 2018, **86**, 84-97.

[52] M. Strankowski, *Inter. J. Polym. Sci.*, **2018**, 1090753.

[53] K. Rohm and I. Manas-Zloczower, *Mech. Mater*, 2023, **180**, 104627.

[54] A. Aneja and G. L. Wilkes, *Polymer*, 2003, **44**, 7221-7228.

[55] A. Stribeck, B. Eling, E. Pöselt, M. Malfois and E. Schander, *Macromol. Chem. Phys*, 2019, **22.**

[56] S. Abouzahr, G. L. Wilkes and Z. Ophir, *Polymer*, 1982, **23**, 1077-1086.

[57] M. Modesti, N. Baldoin and F. Simioni, *Eur. Polym. J*., 1998, **34**, 1233-1241.

[58] D. J. Liaw, *J. Appl. Polym. Sci*., 1997, **66**, 1251-1265.

[59] G. Odion, in *Principles of Polymerisation*, Wiley-Interscience, New York, 1991, 3rd edn, pp 234-240.

[60] M. F. Sonnenschein, in *Polyurethanes: Science, Technology, Markets and Trends*, John Wiley and Sons, New Jersey, 2015, pp 12-19, 26, 28-34, 55, 61-95, 116-117.

[61] L. Nagy, T. Nagy, Á. Kuki, M. Purgel, M. Zsuga and S. Kéki, *Int. J. Chem. Kinet*., 2017, **49**, 643-655.

[62] K. Kojio, S. Nozaki, A. Takahara and S. Yamasaki, *J. Polym. Res*, 2020, **27**, 140.

[63] L. Irusta and M. J. Fernandez-Berridi, *Polym. Degrad. Stab.*, 1999, **63**, 113-119.

[64] E. Yilgör, E. Yurtsever, I. Yilgör, *Polymer*, 2002, **43**, 6561-6568.

[65] D. K. C. a. D. C. Webster, *Prog. Polym. Sci*., 2009, **34**, 1068-1133.

[66] T. J. Touchet and E. M. Cos Griff-Hernandez, in *Advances in Polyurethane Biomaterials*, eds. S. L. Cooper and J. Guan, Woodhead Publishing, 2016, pp. 3-22.

[67] C.-H. Tsou, H.-T. Lee, H.-A. Tsai, H.-J. Cheng, and M.-C. Suen, *Polym. Degrad. Stabil*., 2013, **98**, 643-650.

[68] A. D. Padsalgikar, in *Plastics in Medical Devices for Cardiovascular Applications*, ed. A. D. Padsalgikar, William Andrew Publishing, 2017, pp. 53-82.

[69] G. Holden, H. R. Kricheldorf and R. P. Quirk, in *Thermoplastic Elastomers*, Hanser, Germany, 3rd edn., 2004.

[70] N. Akram, S. Saleem, K. M. Zia, M. Saeed, M. Usman, S. Maqsood, N. Mumtaz and W. G. Khan, J. *Polym. Res*., 2021, **28**, 1-15.

[71] B.-X. Cheng, W.-C. Gao, X.-M. Ren, X.-Y. Ouyang, Y. Zhao, H. Zhao, W. Wu, C.-X. Huang, Y. Liu, X.-Y. Liu, H.-N. Li, and R. K. Y. Li, *Polym. Test.*, 2022, **107**, 107489.

[72] A.-V. Ruzette and A. Mayes, *Macromolecules*, 2001, **34**, 1894–1907.

[73] C. Li, S. L. Goodman, R. M. Albrecht and S. L. Cooper, *Macromolecules*, 1988, **21**, 2367-2375.

[74] S. C. F. Wanga, Q. Wua, R. Zhang and P. Sun, *Polymer*, 2019, **163**, 154-161.

[75] G. Holden, in *Understanding thermoplastic elastomers*, Hanser Verlag, 2000.

[76] S. L. Axelrood, C. W. Hamilton, and K. C. Frisch., *Ind. Eng. Chem*., 1961, **53** (11), 889.

[77] I. Yilgör, E. Yilgör and G. L. Wilkes, *Polymer*, 2015, **58**, A1-A36.

[78] C. Prisacariu, in *Polyurethane Elastomers: From Morphology to Mechanical Aspects*, Springer, New York, 2011, pp 3-6, 23-37, 61-66, 108-111.

[79] C. P. Buckley, C. Prisacariu and C. Martin, *Polymer*, 2010, **51**, 3213-3224.

[80] P. Kasprzyk, E. Głowińska and J. Datta, *Eur. Polym. J.*, 2021, **157**, 110673.

[81] A. Reghunadhan and S. Thomas, in *Polyurethane Polymers*, eds. S. Thomas, J. Datta, J. T. Haponiuk and A. Reghunadhan, Elsevier, Amsterdam, 2017, pp 1-16.

[82] S. J. Rowan, S. J. Cantrill, G. R. Cousins, J. K. Sanders, and J. F. Stoddart, *Angew. Chem. Int. Ed. Engl*, 2002, **41**, 898-952.

[83] S. Huang, et al, *Eur. Polym. J.*, 2020, **141**, 110094.

[84] C. J. Kloxin, T. F. Scott, B. J. Adzima and C. N. Bowman, *Macromolecules*, 2010, **43**, 2643–2653.

[85] C. J. Kloxin and C. N. Bowman, *Chem. Soc. Rev.*, 2013, **42**, 7161–7173.

[86] W. Denissen, J. M. Winne and F. E. Du Prez, *Chem. Sci.*, 2016, **7**, 30-38.

[87] J. M. Winne, L. Leibler and F. E. Du Prez, *Polym. Chem.,* 2019, **10**, 6091-6108.

[88] T. F. Scott, C. N. Bowman, C. D. Wayne and A. D. Schneider, *Science*, 2005, **308**, 1615–1617

[89] D. Montarnal, M. Capelot, F. Tournilhac and L. Leibler, *Science (1979)*, 2011, **334**, 965–968.

[90] W. Denissen, G. Rivero, R. Nicolaÿ, L. Leibler, J. M. Winne and F. E. Du Prez, *Adv. Funct. Mater*., 2015, **25**, 2451–2457.

[91] W. Denissen, M. Droesbeke, R. Nicolaÿ, L. Leibler, J. M. Winne and F. E. Du Prez, *Nat. Commun*., 2017, **8**, 14857.

[92] M. Röttger, T. Domenech, R. Van Der Weegen, A. Breuillac, R. Nicolaÿ and L. Leibler, *Science*, 2017, **356**, 62–65.

[93] B. T. Worrell, S. Mavila, C. Wang, T. M. Kontour, C. H. Lim, M. K. McBride, C. B. Musgrave, R. Shoemaker and C. N. Bowman, *Polym. Chem*., 2018, **9**, 4523–4534.

[94] M. Capelot, M. M. Unterlass, F. Tournilhac and L. Leibler, *ACS. Macro. Lett.*, 2012, **1**, 789-792.

[95] L. Imbernon, E. K. Oikonomou, S. Norvez and L. Leibler, *Polym. Chem.*, 2015, **6**, 4271-4278.

[96] C. J. Kloxin and C. N. Bowman, *Chem. Soc. Rev.*, 2013, **42**, 7161-7173.

[97] B. J. Adzima, H. A. Aguirre, C. J. Kloxin, T. F. Scott and C. N. Bowman, *Macromolecules*, 2008, 41, 9112–9117.

[98] A. J. Inglis, L. Nebhani, O. Altintas, F. G. Schmidt and C. Barner-Kowollik, *Macromolecules*, 2010, 43, 5515–5520.

[99] S. Billiet, K. De Bruycker, F. Driessen, H. Goossens, V. Van Speybroeck, J. M. Winne and F. E. Du Prez, *Nat. Chem*., 2014, **6**, 815–821.

[100] H. A. Houck, K. De Bruycker, S. Billiet, B. Dhanis, H. Goossens, S. Catak, V. Van Speybroeck, J. M. Winne and F. E. Du Prez, *Chem. Sci*., 2017, **8**, 3098–3108.
[101] H. Ying, Y. Zhang and J. Cheng, *Nat. Commun*., 2014, **5**, 3218.

[102] L. Zhang and S. J. Rowan, *Macromolecules*, 2017, **50**, 5051– 5060.

[103] C. e. Yuan, M. Z. Rong and M. Q. Zhang, *Polymer*, 2014, **55**, 1782-1791.

[104] H. Otsuka, K. Aotani, Y. Higaki, A. Takahara, *J. Am. Chem. Soc*. 2003,**125**, 4064

[105] H. Otsuka, *Polym. J.*, 2013, **45**, 879-891.

[106] O. Diels and K. Alder, *Justus Liebigs Ann Chem*, 1928, **460**, 98–122.

[107] R. B. Woodward and T. J. Katz, *Tetrahedron*, 1959, **5**, 70–89.

[108] R. Hoffmann and R. B. Woodward, *J. Am. Chem. Soc.*, 1965, **87**, 2046-2048.

[109] X. Wang, F. Schmidt, D. Hanaor, P. H. Kamm, S. Li and A. Gurlo, *Addit. Manuf*, 2019, **27**, 80-90.

[110] H. P. Figeys and A. Mathy, *Tetrahedron Lett.*, 1981, **22**, 1393–1396.

[111] Piet W.N.M. van Leeuwen, in *Encyclopedia of Physical Science and Technology,* Academic press, 2003, 3rd edition, pp 457-490.

[112] J. A. Berson, R. D. Reynolds and W. M. Jones, *J. Am. Chem. Soc.*, 1956, **78**, 6049-6053.

[113] A. Cuvellier, R. Verhelle, J. Brancart, B. Vanderborght, G. Van Assche and H. Rahier, *Polym. Chem.*, 2019, **10**, 473-485.

[114] J. A. Syrett, G. Mantovani, W. R. S. Barton, D. Price, and D. M. Haddleton, *Polym. Chem.*, 2010, **1**, 102-106.

[115] N. Yoshie, S. Saito and N. Oya, *Polymer*, 2011, **52**, 6074-6079.

[116] J. Kötteritzsch, R. Geltner, J. F. Ahner, M. Abend, S. Zechel, J. Vitz, S. Hoeppener, B. Dietzek, M. Schmitt, J. Popp, U. S. Schubert and M. D. Hager, *J. App. Polym. Sci.,* 2018, **135**, 45916.

[117] P. Reutenauer, E. Buhler, P. J. Boul, S. J. Candau and J.-M. Lehn, *Chem. Eur. J.*, 2009, **15**, 1893-1900.

[118] K. K. Oehlenschlaeger, J. O. Mueller, J. Brandt, S. Hilf, A. Lederer, M. Wilhelm, R. Graf, M. L. Coote, F. G. Schmidt and C. Barner-Kowollik, *Adv. Mat.*, 2014, **26**, 3561-3566.

[119] E. B. Murphy, E. Bolanos, C. Schaffner-Hamann, F. Wudl, S. R. Nutt and M. L. Auad, *Macromolecules*, 2008, **41**, 5203-5209.

[120] J. S. Park, K. Takahashi, Z. Guo, Y. Wang, E. Bolanos, C. Hamann-Schaffner, E. Murphy, F. Wudl and H. T. Hahn, *J. Compos. Mater.*, 2008, **42**, 2869-2881.

[121] X. Liu, P. Du, L. Liu, Z. Zheng, X. Wang, T. Joncheray and Y. Zhang, *Polym. Bull.*, 2013, **70**, 2319–2335.

[122] P. van den Tempel, E. O. van der Boon, J. G. M. Winkelman, A. V. Krasnikova, D. Parisi, P. J. Deuss, F. Picchioni and R. K. Bose, *Polymer*, 2023, **274**, 125884.
[123] A. Gandini, *Macromolecules*, 2008, **41**, 9491–9504.

[124] A. Gandini, *Prog. Polym. Sci*., 2013, **38**, 1-29.

[125] J. M. Craven, Cardiff; Wilmington. *Cross-Linked Thermally Reversible Polymers Produced from Condensation Polymers with Pendant Furan Groups Cross-Linked with Maleimides*. U.S. Pat. WO 3435003, March 25, 1969, **28 (2)**, 131–134.

[126] X. Chen, M. A. Dam, K. Ono, A. Mal, H. Shen, S. R. Nutt, K. Sheran, and F. Wudl, *Science (1979)*, 2002, **295**, 1698–1702.

[127] S. D. Bergman and F. Wudl, *J. Mater. Chem.*, 2008, **18**, 41-62.

[128] L. M. Sridhar, M. O. Oster, D. E. Herr, J. B. D. Gregg, J. A. Wilson, and A. T. Slark, *Green. Chem.*, 2020, **22**, 8669-8679.

[129] G. Rivero, L.-T. T. Nguyen, X. K. D. Hillewaere and F. E. D. Prez, *Macromolecules*, 2014, **47**, 2010-2018.

[130] Y. Heo and H. A. Sodano, *Adv. Funct. Mater.*, 2014, **24**, 5261-5268.

[131] G. Fu, L. Yuan, G. Liang and A. Gu, *J. Mater. Chem. A.*, 2016, **4**, 4232-4241.

[132] B. Willocq, F. Khelifa, J. Brancart, G. Van Assche, P. Dubois and J. M. Raquez, *RSC. Adv.*, 2017, **7**, 48047-48053.

[133] X. Kuang, G. Liu, X. Dong, X. Liu, J. Xu and D. Wang, *J. Polym. Sci. A. Polym. Chem.*, 2015, **53**, 2094-2103.

[134] T. S. Coope, D. H. Turkenburg, H. R. Fischer, R. Luterbacher, H. van Bracht and I. Bond, *Smart. Mater. Struct.*, 2016, **25**.

[135] J. Chi, G. Zhang, Q. Xie, C. Ma and G. Zhang, *Prog. Org. Coat.*, 2020, **139**, 105473.

[136] A. A. Kavitha and N. K. Singha, *Macromolecules*, 2010, **43**, 3193-3205.

[137] D. Li, Y. Zhang, L. Yuan, G. Liang, and A. Gu, *Polym. Int.*, 2020, **69**, 110-120.

[138] G. Fortunato, E. Tatsi, B. Rigatelli, S. Turri and G. Griffini, *Macromol. Mater. Eng*, 2020, **305**, 1900652.

[139] Q. Yan, L. Zhao, Q. Cheng, T. Zhang, B. Jiang, Y. Song and Y. Huang, *Ind. Eng. Chem. Res*., 2019, **58**, 21504-21512.

[140] Z. Gou, Y. Zuo and S. Feng, *RSC. Adv.*, 2016, **6**, 73140-73147.

[141] J. Zhao, R. Xu, G. Luo, J. Wu and H. Xia, *J. Mater. Chem. B.*, 2016, **4**, 982-989.

[142] A. Gandini, D, Coelho and A. J. D Silvestre, *Eur. Polym. J.*, 2008, **44**, 4029.

[143] J. D. Mayo and A. Adronov, *J. Polym. Sci. A. Polym. Chem.*, 2013, **51**, 5056-5066.

[144] L. Feng, Z. Yu, Y. Bian, J. Lu, X. Shi and C. Chai, *Polymer*, 2017, **124**, 48-59.

[145] A. V. Tungare and G. C. Martin, *J. App. Polym. Sci.*, 1992, **46**, 1125-1135.

[146] B. T. McReynolds, K. D. Mojtabai, N. H. G. Penners, G. Kim, S. J. Lindholm, Y. Lee, J. D. McCoy and S. Chowdhury, *Polymers*, 2023, **15**.

[147] J. L. Hopewell, G. A. George and D. J. T. Hill, *Polymer*, 2000, **41**, 8221-8229.

[148] S. Terryn, J. Brancart, E. Roels, R. Verhelle, A. Safaei, A. Cuvellier, B. Vanderborght and G. Van Assche, *Macromolecules*, 2022, **55**, 5497-5513.

[149] S. Terryn, G. Mathijssen, J. Brancart, D. Lefeber, G. V. Assche and B. Vanderborght, *Bioinspir. Biomim.*, 2015, **10**.

[150] F. Orozco, J. Li, U. Ezekiel, Z. Niyazov, L. Floyd, G. M. R. Lima, J. G. M. Winkelman, I. Moreno-Villoslada, F. Picchioni and R. K. Bose, *Eur. Polym. J.*, 2020, **135**, 109882.

[151] H. H. Winter, *Polym. Eng. Sci*, 1987, **27**, 1698-1702.

[152] X. Li, F. Becquart, M. Taha, J.-C. Majesté, J. Chen, S. Zhang, and N. Mignard, *Soft Mat.*, 2020, **16**, 2815-2828.

[153] E. Roels, S. Terryn, J. Brancart, R. Verhelle, G. Van Assche and B. Vanderborght, *Soft Robotics*, 2020, **7**, 711-723.

2. TPUs Containing Thermally Reversible Diels-Alder Cycloadducts

2.1 Introduction

Thermoplastic elastomers (TPEs) are widely used materials, which combine the elasticity of rubber with the thermal processability of thermoplastics.[1] Applications of TPEs range from sealants and adhesives to bio-implants and flexible electronics.[2,3] Six main types of TPEs exist, including thermoplastic polyurethanes (TPUs), styrenic block copolymers (TPS), thermoplastic vulcanizates (TPV), thermoplastic polyolefins blends (TPO), thermoplastic copolyesters (TPE) and thermoplastic polyamides (TPA).[4]

TPUs remain a popular choice due to their versatility, chemical resistance, and durability.[5] The beneficial properties of TPUs result from their dual phase morphology, comprising alternating crystallisable, high T_g hard segments (HS) and elastomeric, low T_g soft segments (SS).[6] Thermodynamic incompatibility between these segments leads to microphase separated structures, whereby the degree of separation can be altered by changing the HS : SS ratio and the structure or polarity of the segments.[7]

Despite TPUs having robust mechanical properties, they often display high melt viscosities due to HS association *via* strong inter urethane H-bonding interactions, which persist in the melt. The high molecular weight PU chains also persist in the melt, contributing further to a high melt viscosity. Consequently, current TPUs can only be reprocessed *via* industrial methods, such as injection moulding or hot melt extrusion, which require demanding conditions involving high pressure and temperature, limiting potential applications.[8]

One way to resolve these issues is to design TPUs which contain Diels-Alder (DA) dynamic covalent bonds, enabling a reversible change in molecular weight with temperature. The forward DA reaction would dominate at ambient temperature, providing a mechanically robust solid, whilst the retro DA (rDA) reaction would preferentially occur at higher temperatures (above 100 °C), providing a low melt viscosity liquid. This could therefore enable less demanding and more effective reprocessing, recycling, and self-healing. A well-documented diene-dienophile pairing is electron-rich furan with electron-

deficient maleimide due to their high reactivity under mild conditions, without the need for a catalyst, whilst avoiding by-product formation.[9]

Several reports in the literature have investigated linear TPUs containing DA-cycloadducts (DA-TPUs), across a variety of polymer backbones. Work by Feng *et al.* in 2017 studied DA-TPUs by copolymerising poly(propylene glycol) (PPG) based furan-terminated PU prepolymers with *N,N'*-(4,4'-methylene diphenyl) bismaleimide (BMI).[10] The DA-TPU exhibited a tensile strength of upto 6.5 MPa whilst the conventional TPU comprising 1,4-butanediol as chain extender (BDO-TPU) only achieved a tensile strength of 0.63 MPa. Moreover, polarised optical microscopy images and tensile testing also revealed that the DA-TPU achieved a self-healing efficiency of 71% after heat treatment of 120 °C for 15 minutes or 60 °C for 24 hours, whilst the cracks in BDO-TPU could only be partially repaired, with a low self-healing efficiency of 19%. Polyester based DA-TPUs containing varying DA-cycloadduct concentrations have also been studied, demonstrating that high adhesive strengths can be achieved whilst enhancing melt processability.[11] A further study by Lakatos *et al.* reported DA-TPUs containing poly(ε-caprolactone) (PCL) SS, displaying shape memory effects.[12] Elastomeric materials were produced with a range of mechanical properties determined by the PCL molecular weight and diisocyanate type, but recyclability was not considered. Research has also been conducted in poly(1,4-butadiene) (PBD), isophorone diisocyanate (IPDI)-based DA-TPUs for use in binder films in energetic composites, where high self-healing efficiency was controlled by DA-cycloadduct concentration.[13] Moreover in 2023, Wu *et al*. synthesised a series of DA-TPUs from PPG, polydimethylsiloxane (PDMS), IPDI, furfuryl alcohol (FA) and BMI. They discovered that the mechanical and self-healing properties of the DA-TPUs could be tuned by varying the relative concentrations of the PPG and PDMS-OH SS.[14]

Whilst DA chemistry has been applied to various TPU backbones, it is important to highlight that the majority of these studies use the low molecular weight BMI monomer, which is highly toxic when liberated upon the rDA reaction and unsuitable for practical consumer or industrial

applications. Additionally, none of the existing literature has independently explored the effect of SS polymer backbone on DA-TPUs properties. This work therefore aims to fill in this gap by synthesising and comparing four DA-TPUs which incorporate different SS backbones, whilst keeping other design parameters, such as DA-cycloadduct concentration barely unchanged. The effect of SS structure on the thermomechanical and morphological properties of resulting DA-TPUs will be evaluated, for potential use in self-healing, recyclable elastomers.

2.2 Results and discussion

2.2.1 Synthesis and characterisation of maleimide- and furan-terminated PU prepolymers

To achieve this, four commercially available polyols with a M_n of approximately 2000 g.mol^{-1} were chosen, so that the equivalent concentration of furan and maleimide functional groups (f_g) and thus concentration of DA-cycloadducts in the final DA-TPUs remained similar. Two PCL-based diols, initiated with neopentyl glycol (NPG): **Capa® 2200J**, a semi-crystalline PCL and **Capa® 8025D**, an amorphous 75:25 random copolymer of ε-caprolactone and lactic acid (PCL.LA), were compared with two amorphous PBD based polyols: **Krasol® LBH P 2000**, hydroxyl-terminated unsaturated PBD and **Krasol® HLBH P 2000**, hydroxyl-terminated hydrogenated PBD (HPBD) (***Figure* 2.1**). These specific polyols were chosen to independently investigate the effect of SS crystallinity (PCL versus PCL.LA), double bonds (PBD versus HPBD) and polarity (PCL.LA versus PBD or HPBD) on the thermomechanical and morphological properties of the final DA-TPU copolymers.

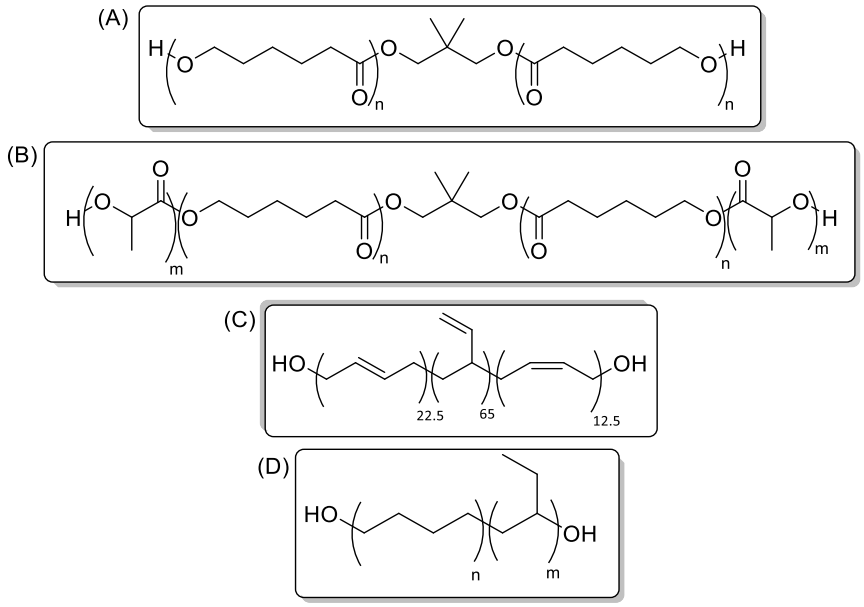

Figure 2.1 *Structures of commercial polyols, (A)* ***Capa® 2200J*** *(PCL), (B)* ***Capa® 8025D*** *(PCL.LA), (C)* ***Krasol® LBH P2000*** *(PBD) and (D)* ***Krasol® HLBH P 2000*** *(HPBD).*

Linear DA-TPUs (**DA-X**) were synthesised from corresponding polyols *via* consecutive addition reactions then copolymerisation, whereby **X** represents PCL, PCL.LA, PBD or HPBD backbone (***Scheme 2.1***). Initially, polyol was copolymerised with excess 4,4'-methylene diphenyl diisocyanate (MDI) at a stoichiometry of 2.0 : 1.0 NCO : OH, to form an isocyanate (NCO) terminated prepolymer (***Step 1***). This was followed by the reaction of terminal NCO groups with either furfuryl alcohol (FA), (***step 2a***) or 2-hydroxyethyl maleimide (HEMI), (***step 2b***) at a stoichiometry of 1.1 : 1.0 OH : NCO to yield the corresponding furan- (**PPF-X**) or maleimide-terminated (**PPM-X**) PU prepolymers.

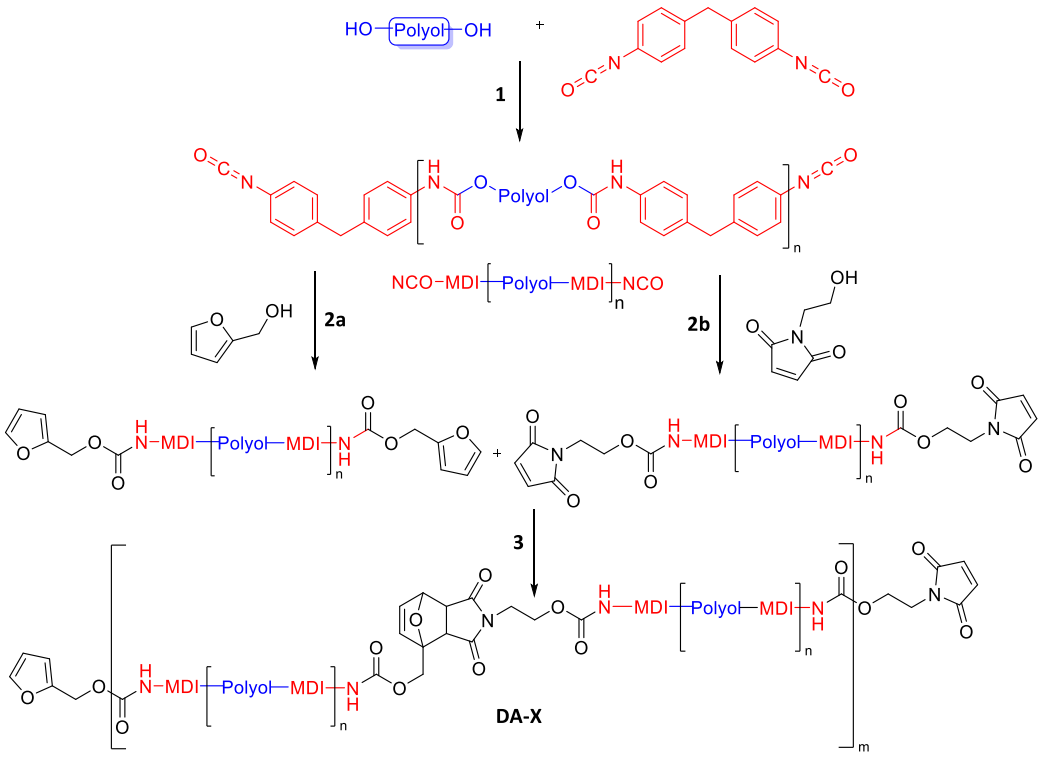

Scheme 2.1 *1) Bulk, 110 °C for 1 hour. 2a) or 2b) Bulk, 120 °C for 1.5-2 hours. 3) Solvent casting in* CH_2Cl_2 *at ambient temperature.*

Eight PU prepolymers were synthesised in total (the **PPF-X** and **PPM-X** prepolymers for each polyol backbone). Size exclusion chromatography (SEC) analysis of the PU prepolymers confirmed a modest increase in apparent molecular weight compared to the starting polyols, as a result of the reagent stoichiometry (***Table 2.1***).

Table 2.1 *Molecular weight characterisation of polyols and corresponding* ***PPF-X*** *and* ***PPM-X*** *prepolymers.*

Material	M_n [a] (g.mol^{-1})	M_w [a] (g.mol^{-1})	$Đ_M$ [a]
PCL	1,900	3,600	1.9
PPM-PCL	8,000	16,200	2.0
PPF-PCL	7,200	14,400	2.0
PCL.LA	2,200	4,400	1.9
PPM-PCL.LA	6,400	12,700	2.0
PPF-PCL.LA	6,400	13,600	2.1
PBD	3,000	3,300	1.1
PPM-PBD	7,400	12,400	1.7
PPF-PBD	7,600	13,400	1.8
HPBD	2,700	3,300	1.2
PPM-HPBD	7,900	15,000	1.9
PPF-HPBD	7,300	14,400	2.0

[a] *Determined by SEC analysis, against poly(methyl methacrylate) (PMMA) standards in* $CHCl_3$.

^{1}H NMR spectroscopy of the PU prepolymers revealed resonances associated with the aromatic urethane (G-J) and maleimide (M) or furan (L-N) end-groups, using the ^{1}H NMR spectra of **PPM-PCL** and **PPF-PCL** for demonstration (**Figure 2.2**). The ^{1}H NMR spectrum of **PPM-PCL** displayed resonances at δ = 4.32 (K) and 4.16 (F') ppm, corresponding to the methylene units of the HEMI and PCL backbones directly adjacent to a urethane group, demonstrating covalent linkage between HEMI and PCL with MDI (***Figure* 2.2 *(B)***). The ^{1}H NMR spectrum of **PPF-PCL** also displayed resonances at δ = 5.16 (K) and 4.17 (F') ppm, representing the methylene units of FA and PCL backbones adjacent to a urethane group, showing covalent linkage between FA and PCL with MDI (***Figure* 2.2 *(C)***).

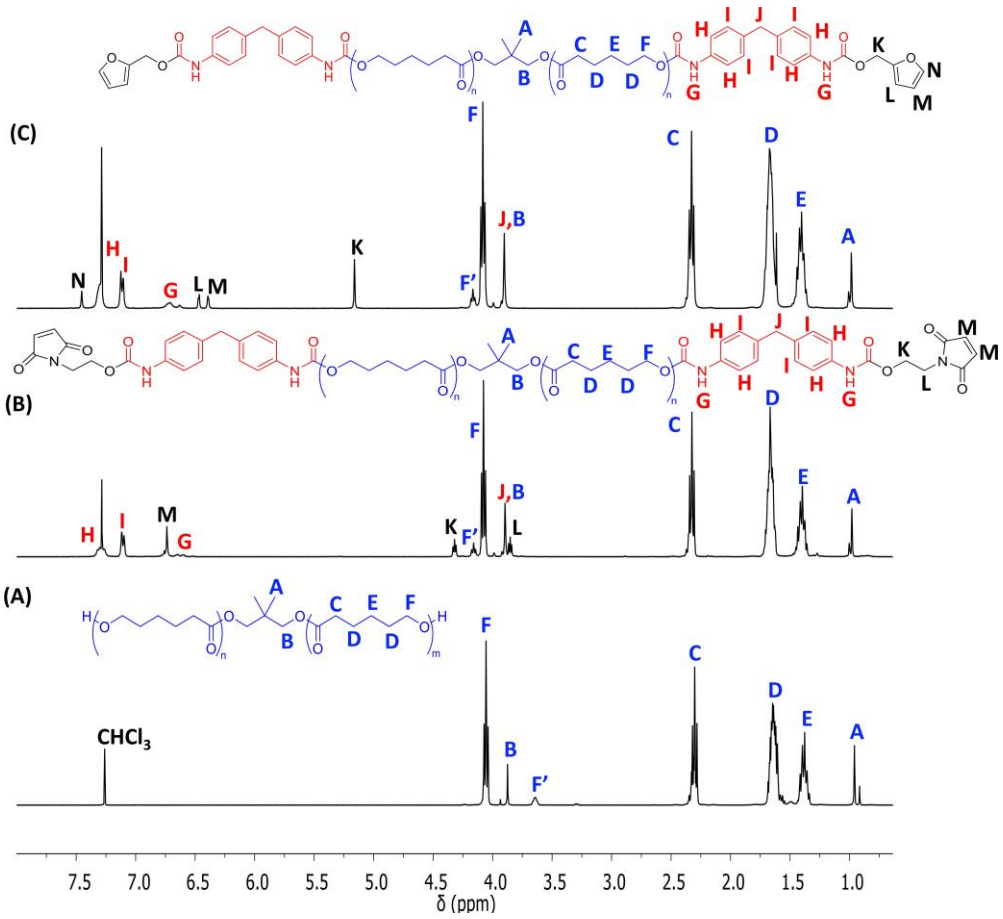

Figure 2.2 *^{1}H NMR spectra of* ***(A) PCL*** *polyol,* ***(B) PPM-PCL*** *and* ***(C) PPF-PCL*** *(400 MHz, $CDCl_3$, 298 K).*

ATR-FTIR spectroscopy confirmed successful consecutive addition reactions, using the synthesis of **PPM-PCL** and **PPF-PCL** for demonstration (***Figure* 2.3** and ***Table 2.2***). After end-capping with MDI, the O-H stretching vibration of PCL at ν_{max} = 3442 cm^{-1}, disappeared, whilst resonances at ν_{max} = 3330 and 1528 cm^{-1} emerged, representing N-H and C-N stretching in the newly formed urethane bonds, respectively. An FTIR band at ν_{max} = 1598 cm^{-1} also appeared in the NCO-terminated PCL prepolymer (**PCL-NCO**), representing aromatic C=C stretching in the phenyl rings of MDI. The FTIR spectra of **PPM-PCL** and **PPF-PCL** showed complete disappearance of the -NCO stretching vibration at ν_{max} = 2260 cm^{-1}, indicating that all the free NCO from **PCL-NCO** had successfully reacted with HEMI or FA groups.[15] After the addition of HEMI or FA, bands at ν_{max} = 696 or 730 cm^{-1} also appeared, which can be assigned to the maleimide B1 antisymmetric ring deformation mode and C-H out of plane bending from the furan arene ring, respectively.[16,17]

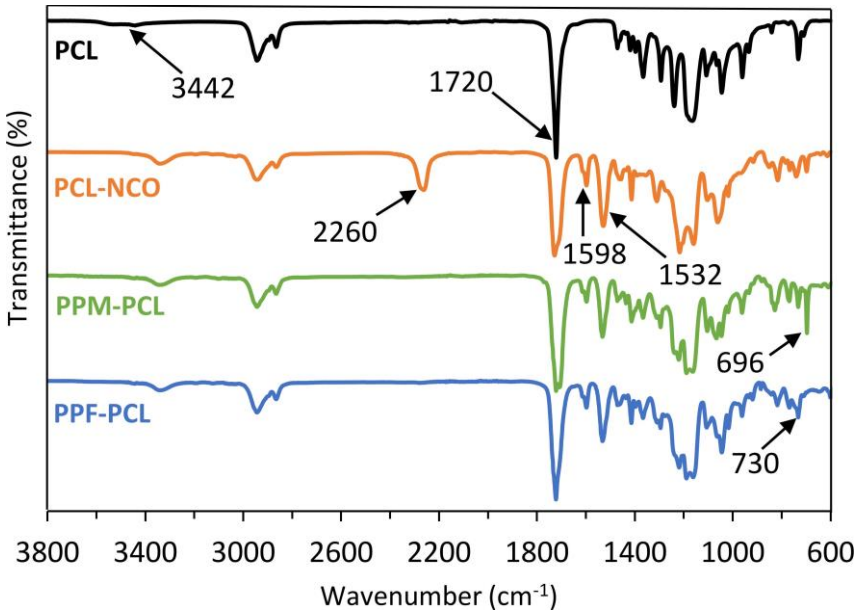

Figure 2.3 *Overlayed ATR-FTIR spectra of* ***PCL*** *polyol,* ***PCL-NCO****,* ***PPM-PCL****, and* ***PPF-PCL****.*

Table 2.2 *Wavenumbers of significant functional groups during the synthesis of* ***PPM-PCL*** *and* ***PPF-PCL****.*

Sample	Wavenumber (cm^{-1}) [a]					
	O-H	N-H	NCO	C=O	Ar C=C	C-N
PCL	3342	-	-	1723	-	-
PCL-NCO	-	3330	2260	1730/1702	1598	1524
PPM-PCL	-	3336	-	1722/1704	1594	1528
PPF-PCL	-	3336	-	1720/1705	1594	1527

[a] *obtained from ATR-FTIR analysis.*

ATR-FTIR analysis of the carbonyl region revealed that copolymerisation of PCL with MDI broadened the PCL ester carbonyl absorption at ν_{max} = 1720 cm^{-1}, due to the emergence of shoulders at ν_{max} = 1730 and 1710 cm^{-1}, representing free and H-bonded urethane carbonyls, respectively (***Figure* 2.4**).[18] **PPM-PCL** and **PPF-PCL** displayed broad absorptions between ν_{max} =1730-1710 cm^{-1}, resulting from the overlap of PCL ester carbonyl and urethane carbonyl stretching. **PPM-PCL** presented an additional FTIR absorbance at ν_{max} = 1700 cm^{-1}, corresponding to the stretching of imide carbonyls from maleimide functional groups.[19]

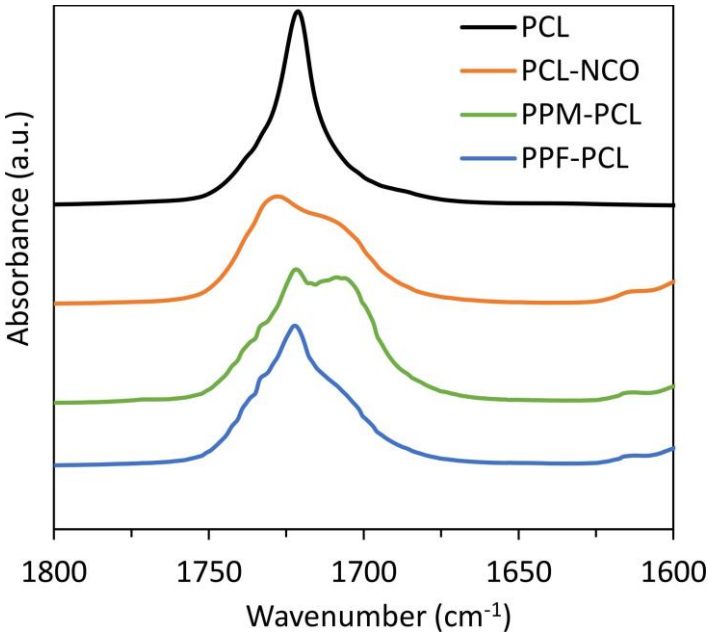

Figure 2.4 *ATR-FTIR spectra of the carbonyl region in* ***PCL, PCL-NCO, PPM-PCL,*** *and* ***PPF-PCL****.*

Since hydrogen (H-) bonding is the driving force of the energetically favourable phase separation in PUs, the morphological composition of the PU prepolymers with different SS backbones can be compared *via* FTIR analysis of the carbonyl stretching regions (***Figure* 2.5**).[20] H-bonding within the HS occurs between the secondary amine and carbonyl groups of urethane, whilst in phase mixed HS-SS, H-bonding occurs between the secondary amine group of the urethane and the ester carbonyl groups in PCL. Carbonyl peaks within PU FTIR spectra can be split into free, non-H bonded, urethane carbonyl between ν_{max} = 1733-1730cm^{-1}, strongly H-bonded urethane carbonyl in phase-separated confirmations at ν_{max} = 1700-1683 cm^{-1} and loosely H-bonded urethane carbonyl in disordered, phase-mixed confirmations appearing between ν_{max} = 1723-1705 cm^{-1}.[21-23]

PPF-PCL and **PPF-PCL.LA** displayed broad carbonyl stretching bands with strong absorptions between ν_{max} = 1720-1730 cm^{-1}, resulting the overlap of PCL ester and free urethane carbonyl stretching, with only small shoulders appearing at ν_{max} = 1710 cm^{-1} for loosely H-bonded, phase-mixed, urethane carbonyl stretching (***Figure* 2.5 *(A)***). Conversely, **PPF-PBD** and **PPF-HPBD** displayed strong carbonyl stretching absorptions at ν_{max} = 1700 cm^{-1}, indicating the presence of strongly H-bonded urethane carbonyls in ordered, phase-separated confirmations, with only small shoulders appearing at ν_{max} =

1733 cm^{-1} representing free, non-H bonded urethane carbonyl. This is likely due to microphase separation driven by the large polarity difference between non-polar PBD SS and polar HS (reaction products of MDI and FA or HEMI). The same trend existed in the **PPM-X** prepolymers, but an additional absorption appeared at ν_{max} = 1700 cm^{-1}, which can be assigned to the imide carbonyl groups of maleimide (***Figure* 2.5 *(B)***). The PBD and HPBD-PU prepolymers exhibited lower normalised absorbance values, as they do not contain ester carbonyl which significantly contributes to the strong absorptions at ν_{max} = 1720 cm^{-1} in the polyester-based PU prepolymers.

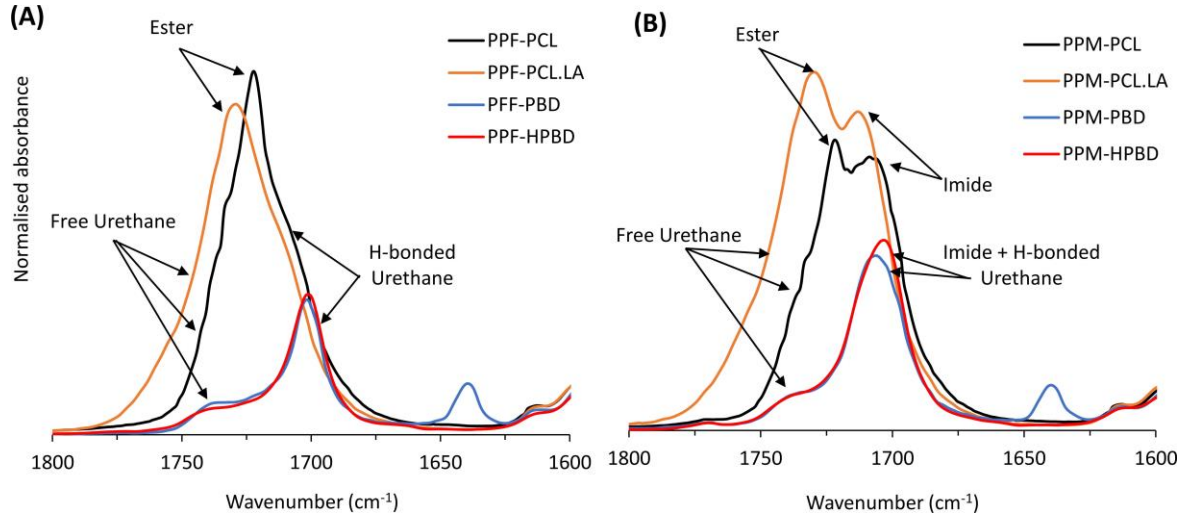

***Figure 2.5** ATR-FTIR spectra of **(A) PPF-X** and **(B) PPM-X** prepolymers in the carbonyl region. Peaks normalised against $V_{C\text{-}N}$ band of –C(=O)-NH- at 1528 cm^{-1}.*

Differential scanning calorimetry (DSC) was performed on the polyols and the corresponding **PPM-X** and **PPF-X** prepolymers to compare their thermal properties (***Figure* 2.6** and ***Table 2.3***). Only the 1st heating cycle is discussed as the structures do not reform within the timescale of the DSC experiment. The T_g of all polyol backbones increased after copolymerisation with MDI and HEMI or FA, due to the introduction of interurethane and polar end-group H-bonding in addition to π-π stacking between MDI phenyl rings, which restrict polymer chain motion.[24] **PPM-PCL** and **PPF-PCL** displayed sub-ambient T_g values and endotherms between 32 and 45 °C (T_{mPCL}), corresponding to the melting of semi-crystalline PCL segments (***Figure* 2.6 *(A)***).[25] The enthalpy of the melting endotherm in the PCL polyol (ΔH_{mPCL}) decreased significantly after copolymerisation, indicating that incorporating MDI and polar end-groups

disrupts the order of PCL chains and reduces crystallinity. Like PCL.LA polyol, **PPM-PCL.LA** and **PPF-PCL.LA** were both amorphous liquids with sub-ambient T_g values. (***Figure* 2.6 *(B)***) Despite PBD and HPBD polyols being amorphous liquids, the corresponding furan- and maleimide-terminated PU prepolymers were solids, presenting multiple melting endotherms between 36 and 118 °C (T_{mHS} and ΔH_{mHS}), suggesting a degree of HS order (***Figure* 2.6 *(C)*** and ***(D)***). **PPF-PBD** also exhibited an upper T_g at 44 °C. This order is likely to originate from microscale phase separation of non-polar PBD or HPBD SSs from polar HSs, in agreement with FTIR data. **PPM-PBD** and **PPM-HPBD** displayed further melt endotherms between 146 and 148 °C, suggesting polar end-group association, driven by favourable intermolecular H-bonding between maleimide imide carbonyls and urethane NH groups, which can be enhanced in such a hydrophobic matrix.[26] It should be noted that the DSC thermogram of **PPM-PBD** exhibited a steep exothermic incline above 160 °C. This is likely due to the Alder-ene reaction, known to occur between maleimides and alkenes with an allylic hydrogen at high temperatures.[27]

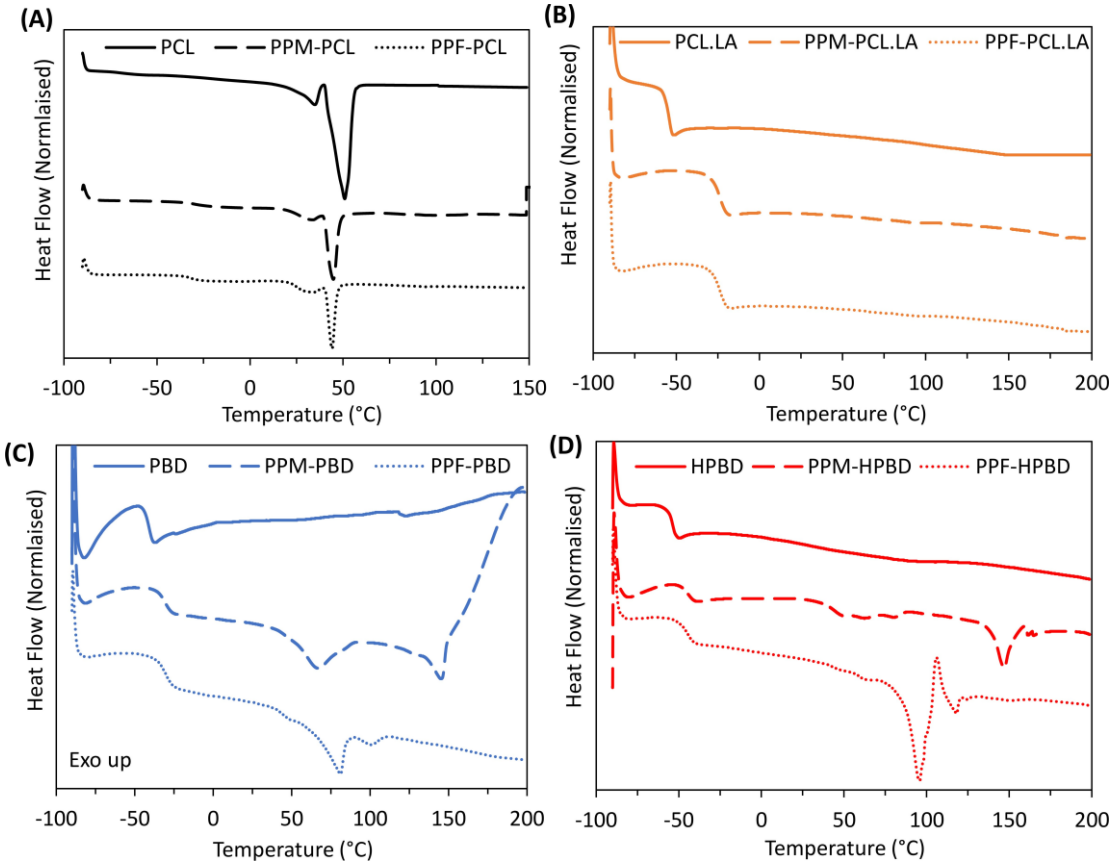

Figure 2.6 *DSC thermograms (1st heating cycles) of* ***(A)*** *PCL,* ***(B)*** *PCL.LA,* ***(C)*** *PBD and* ***(D)*** *HPBD polyols compared to corresponding* ***PPM-X*** *and* ***PPF-X*** *prepolymers. Exo up. Heating rate of 10 °C.min^{-1}.*

Table 2.3 *DSC thermal data obtained for polyols and corresponding* ***PPM-X*** *and* ***PPF-X*** *prepolymers.*

Material	T_g [a] (°C)	T_{mPCL} [a] (°C)	T_{mHS} [a] (°C)	ΔH_{mPCL} [a] (J.g^{-1})	ΔH_{mHS} [a] (J.g^{-1})
PCL	-67	53	-	83	-
PPM-PCL	-30	32/45	-	35	-
PPF-PCL	-32	32/44	-	27	-
PCL.LA	-55	-	-	-	-
PPM-PCL.LA	-24				
PPF-PCL.LA	-25	-	-	-	-
PBD	-42	-	-	-	-
PPM-PBD	-31	-	66/146	-	9.0/5.4
PPF-PBD	-30	-	81-100	-	8.6
HPBD	-54	-	-	-	-
PPM-HPBD	-45	-	36-90/148	-	4.2/5.0
PPF-HPBD	-46	-	96/118	-	11.8/3.3

[a] determined by DSC analysis using the 1st heating cycle at a heating rate of 10 °C.min^{-1}.

2.2.2 Synthesis and characterisation of ***DA-X*** *copolymers.*

Linear DA-TPUs (**DA-X**) comprising different SS backbones were synthesised by copolymerising the corresponding **PPF-X** and **PPM-X** prepolymers at ambient temperature (***Scheme 2.1, Step 3***). Since the M_n of all SS backbones is approximately 2000 g.mol^{-1} the DA-TPUs attained similar f_g values (0.32-0.37 mol.kg^{-1}) and thus concentrations of DA-cycloadducts at room temperature (***Table 2.4***).

Table 2.4 *f_g values and compositions of* ***DA-X*** *TPU copolymers.*

DA-X	f_g (mol.kg^{-1})	PPM-X	PPF-X
DA-PCL	0.37	PPM-PCL	PPF-PCL
DA-PCL.LA	0.37	PPM-PCL.LA	PPF-PCL.LA
DA-PBD	0.35	PPM-PBD	PPF-PBD
DA-HPBD	0.32	PPM-HPBD	PPF-HPBD

The f_g of each **DA-TPU** was calculated using the equation below:

$$f_{g\,(mol.kg^{-1})} = \left(\frac{(Mass\ fraction_{fm} \times 1000)}{Molecular\ weight_{fm}}\right) \times functionality\ of\ molecule$$

whereby f_m represents the telechelic bismaleimide or bisfuran functional molecule.

Copolymerisation was achieved *via* solvent casting in CH_2Cl_2, ensuring a 1 : 1 stoichiometry of furan : maleimide functional groups. Solvent was then removed, and the materials were subsequently compression moulded to give 1 mm thick elastomeric sheets which were conditioned at ambient

temperature to allow copolymerisation of furan and maleimide groups. ATR-FTIR spectroscopy was employed to assess the forward DA-reaction over time in the **DA-X** copolymers, after conditioning at 25 and 60 °C post compression moulding. This was achieved by monitoring the decrease in the relative absorbance at ν_{max} = 696 cm^{-1} (which represents free maleimide) (***Figure 2.7***).[28] At ambient temperature the relative absorbance at 696 cm^{-1} decreased quickly in all **DA-X** copolymers over the first four days before plateauing after 7 days whereby maximum DA-cycloadduct formation was achieved, with a final DA conversion between 85-90%. The overlayed ATR-FTIR spectra of **DA-PCL** obtained after specific time intervals at 25 °C demonstrated this decrease in the absorbance peak at ν_{max} = 696 cm^{-1} (***Figure 2.8***). Conditioning the same materials at 60 °C overtime led to a plateau in the relative absorbance at ν_{max} = 696 cm^{-1} after just 2-3 days, indicating that mild heating assists faster DA-cycloadduct formation.

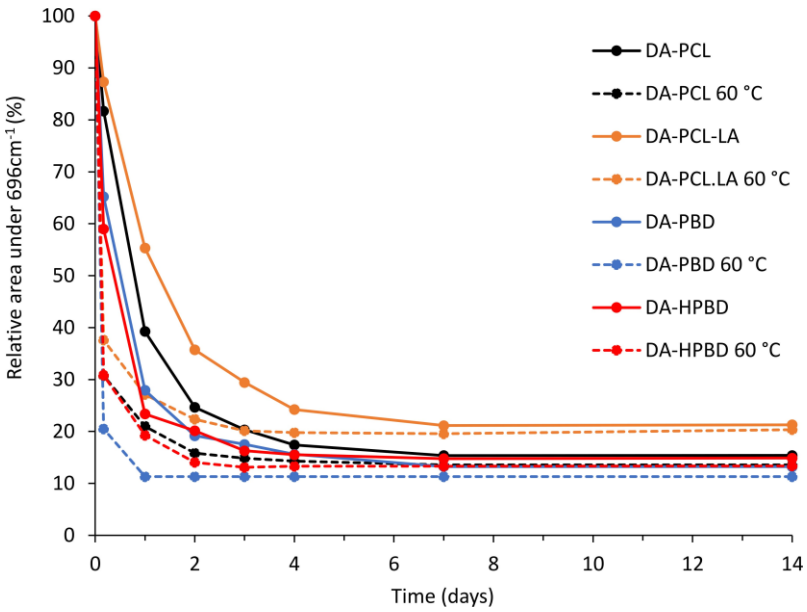

Figure 2.7 *Decrease in relative absorbance of FTIR band at ν_{max} = 696 cm^{-1} against time for **DA-X** copolymers after conditioning at 25 °C (solid lines) and 60 °C (dashed lines). Time = 0 is set as 100 %.*

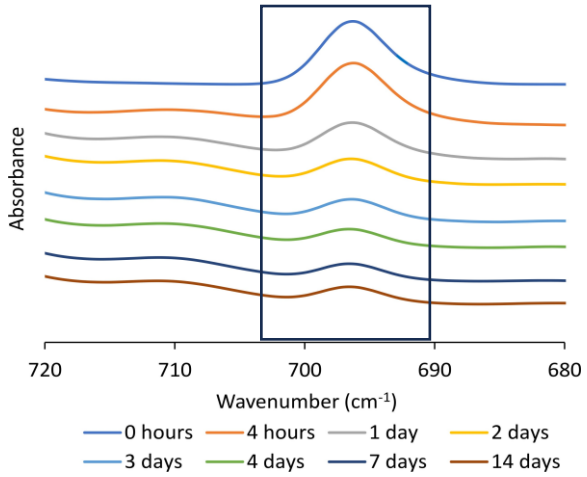

Figure 2.8 *Change in ATR-FTIR absorbance of band at ν_{max} = 696 cm^{-1} in* ***DA-PCL*** *over time at ambient temperature. Peak highlighted by black box.*

^{1}H NMR spectroscopy of the **DA-X** copolymers confirmed the presence of DA-cycloadducts, using **DA-PCL** as an example (***Figure 2.9***). The furan and maleimide end-group resonances from the **PPF-PCL** and **PPM-PCL** prepolymers almost disappeared, whilst new resonances at δ = 5.31, 3.03 and 2.89 ppm emerged, corresponding to the -C***H***(O)(CH)(CH)- protons on the DA-cycloadducts (**a**) and the two protons either side of the N atom in the DA-cycloadducts (**d** and **e** -C***H***(CH)C=O-, respectively).[29] These resonances were present in all **DA-X** copolymers.

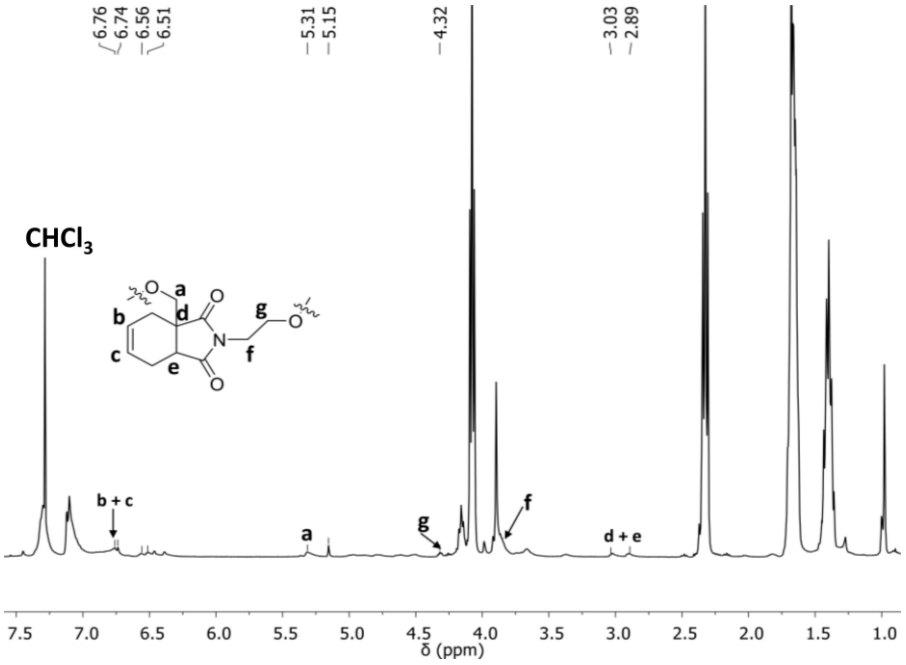

Figure 2.9 *^{1}H NMR spectrum of* ***DA-PCL*** *with resonances associated with the DA cycloadduct labelled. All other resonances correspond to the PCL-MDI backbone. (400 MHz, $CDCl_3$, 298 K).*

SEC analysis of the **DA-X** copolymers after conditioning for 7 days at ambient temperature revealed that copolymerisation of **PPM-X** and **PPF-X** prepolymers resulted in a substantial increase in apparent molecular weight (***Table 2.5***). This demonstrates the successful formation of linear TPU copolymers through DA-cycloaddition.

Table 2.5 *SEC analysis of* ***DA-X*** *copolymers. Obtained after 7 days at ambient temperature.*

Copolymer	M_n [a] (g.mol^{-1})	M_w [a] (g.mol^{-1})	$Đ_M$ [a]
DA-PCL	36,800	99,700	2.71
DA-PCL.LA	26,200	58,100	2.22
DA-PBD	37,000	93,200	2.52
DA-HPBD	28,300	57,200	2.02

[a] *Determined against PMMA standards using $CHCl_3$ as eluent.*

2.2.3 Thermal reversibility of DA-cycloadducts

The thermal reversibility of DA-cycloadducts in **DA-PCL** was demonstrated *via* SEC analysis after conditioning the material for specific time periods at different temperatures (***Figure* 2.10** *and* ***Table 2.6***). The M_n of **DA-PCL** reached 36,800 g.mol^{-1} after 7 days at 25 °C due to the formation of DA-cycloadducts between the **PPM-PCL** and **PPF-PCL** prepolymers. When **DA-PCL** was then heated to 120 °C for 15 minutes, the M_n decreased to 12,500 g.mol^{-1} (towards the original prepolymer M_n) due to the rDA reaction and breakdown of DA-cycloadducts. Subsequently, after conditioning **DA-PCL** at 60 °C for 24 hours, the M_n increased back up to 25,700 g.mol^{-1} through the reformation of DA-cycloadducts. This demonstrates proof of concept for the reversibility of DA-TPU molecular weight with temperature, which cannot be achieved in traditional TPUs.

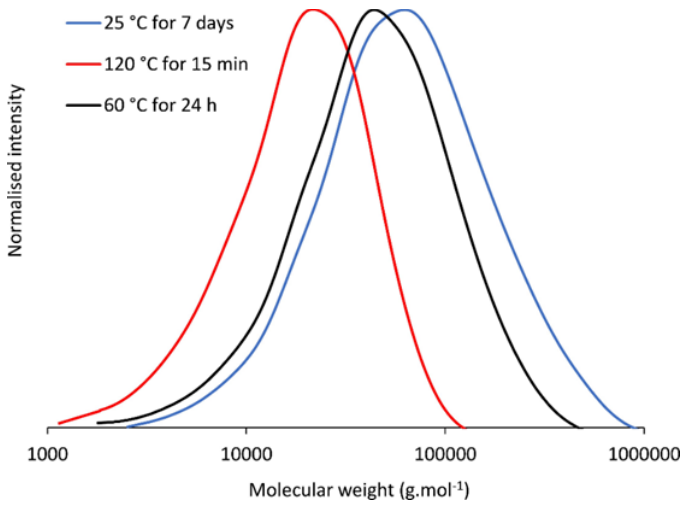

Figure 2.10 *SEC chromatograms of* ***DA-PCL*** *obtained after different heating conditions. Molecular weights determined against PMMA standards.*

Table 2.6 *SEC analysis of* ***DA-PCL*** *after different heating conditions.*

Condition	M_n [a] (g.mol^{-1})	M_w [a] (g.mol^{-1})	$Đ_M$ [a]
25 °C (7 days)	36,800	99,700	2.71
120 °C (15 min)	12,500	24,200	1.94
60 °C (24 h)	25,700	63,900	2.49

[a] *Molecular weights determined against PMMA standards using $CHCl_3$ eluent.*

The thermal reversibility of DA-cycloadducts in **DA-PCL** was further demonstrated *via* a sol-gel transition (***Figure 2.11***). This was accomplished by dissolving a known weight of a 250 µm film of **DA-PCL** in 20 wt.% dimethylformamide (DMF). Heating this solution to 120 °C for 5 minutes resulted in a low viscosity fluid with improved flow due to the rDA reaction and the resulting decrease in molecular weight as the TPU chains are broken down into smaller segments. When **DA-PCL** was subsequently held at 60 °C for 120 minutes it formed a gel with minimal flow due to the reformation of DA-cycloadducts and a corresponding increase in molecular weight. This sol-gel transition could be repeated several times, demonstrating the excellent thermally reversibility of the DA-adducts in **DA-PCL**.

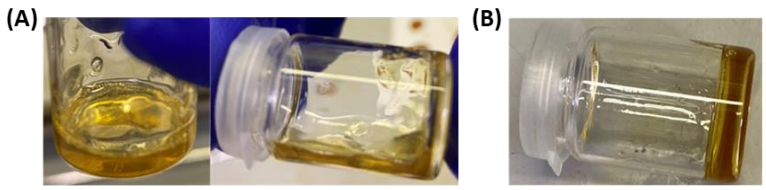

Figure 2.11 *Sol-gel-transformation of* ***DA-PCL*** *showing* ***(A)*** *transition to a low viscosity liquid after heating at 120 °C for 5 minutes and* ***(B)*** *formation of a gel after heating at 60 °C for 120 minutes.*

2.2.4 Thermal properties

The **DA-X** copolymers were analysed by DSC to determine their thermal properties after 7 days at 25 °C (***Figure 2.12*** and ***Table 2.7***). The DSC thermograms of all **DA-X** TPUs exhibited a broad double endotherm from 114 to 148 °C (T_{rDA}), representing the absorption of energy required to break both *endo*- and *exo*- DA-cycloadducts and induce the rDA reaction (ΔH_{rDA}).[30] The lower temperature minima occurring between 113 to 117 °C represent the energy required to break the kinetically favoured *endo* DA-cycloadducts whilst the higher temperature minima from 140 to 148 °C represent the energy required to break the more thermodynamically stable *exo* DA cycloadducts.[31] All **DA-X** copolymers displayed similar ΔH_{rDA} values between 7.1 and 11.5 $J.g^{-1}$, as they contain similar DA-cycloadduct concentrations. Moreover, all DA-TPUs displayed sub-ambient T_g values between -12 and -45 °C, depending on the flexibility of the SS backbone. **DA-PBD** also presented an upper T_g at 53 °C, likely a result of microphase separation between polar HSs and non-polar SSs. **DA-PCL** displayed an additional endotherm between 35 and 43 °C (T_{mPCL}) for the melting of semi-crystalline PCL segments (ΔH_{mPCL}).

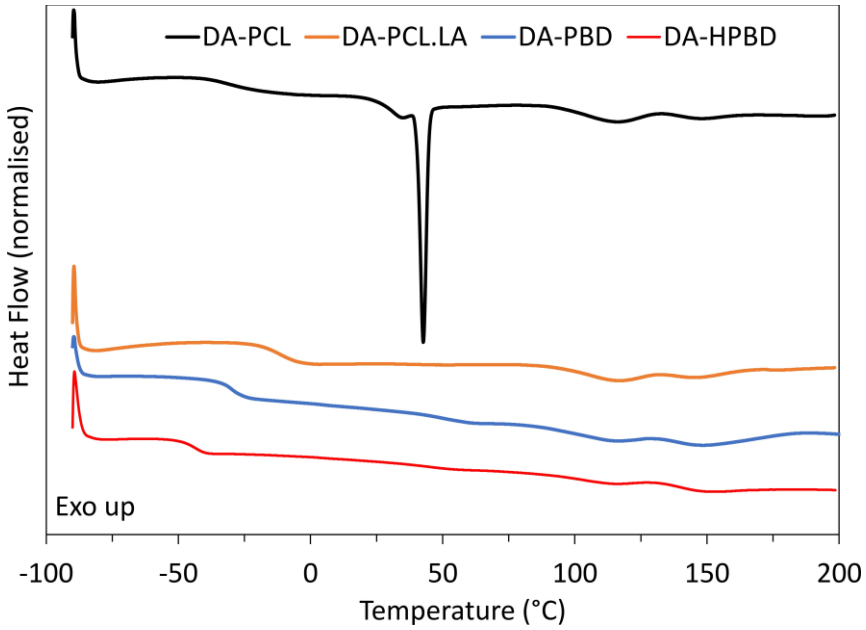

Figure 2.12 *DSC thermograms (1st heating cycles) of* ***DA-X*** *copolymers. Heating rate of 10 °C.min-1. Exo up.*

Table 2.7 *DSC thermal data for* ***DA-X*** *copolymers.*

Copolymer	T_g [a] (°C)	T_{mPCL} [a] (°C)	ΔH_{mPCL} [a] (J.g^{-1})	T_{rDA} [a] (J.g^{-1})	ΔH_{rDA} [a] (J.g^{-1})
DA-PCL	-32	35 & 43	17.0	117 & 145	8.9
DA-PCL.LA	-12	-	-	116 & 146	11.5
DA-PBD	-30	-	-	114 & 148	11.4
DA-HPBD	-45	-	-	113 & 149	7.1

[a] *obtained via DSC analysis using the 1st heating cycle after 7 days at ambient temperature.*

DSC was employed as another tool to monitor the forward DA-reaction overtime in the **DA-X** copolymers by measuring the rDA enthalpy (ΔH_{rDA}) after heating the samples to 120 °C for 1 hour then conditioning at 25 and 60 °C (***Figure 2.13***). In all materials conditioned at ambient temperature, ΔH_{rDA} gradually increased up to 7 days, before plateauing, indicating that an equilibrium state had been established between the forward and reverse DA reactions, in agreement with ATR-FTIR data. In the first 4 days at ambient there is a steep increase in ΔH_{rDA} as there is lots of free maleimide/furan groups and lower molecular weight prepolymer chains present. Between 4-7 days the growth in ΔH_{rDA} decelerates as less free diene and dienophile groups are available for cycloaddition and the polymer chain mobility is hindered by an increase in molecular weight. At the plateau after 7 days maximum

DA-cycloadduct conversion (85-90%) is achieved suggesting there is no longer enough free functional groups available for cycloaddition/not enough chain mobility. Conditioning **DA-X** copolymers at 60 °C allowed the ΔH_{rDA} values to plateau after 2-3 days, agreeing with the previous ATR-FTIR data, by showing that the forward DA reaction can be accelerated with mild heating. The speed of the DA cure is relatively slow, even at 60 °C, implying that the diffusion of maleimide/furan functional polymer chains is slow.

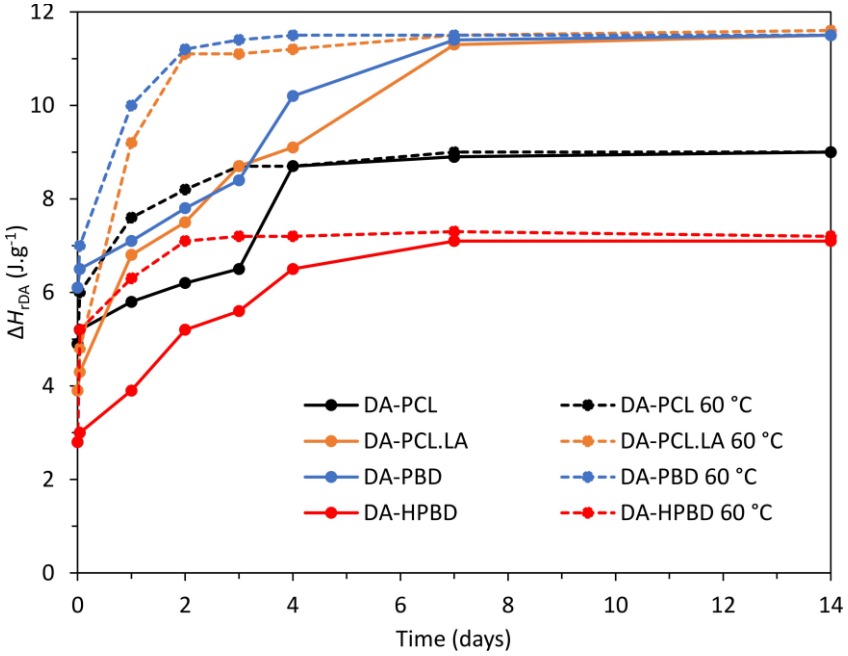

Figure 2.13 *Measured ΔH_{rDA} values in **DA-X** copolymers against time after conditioning samples at 25 °C and 60 °C post heating to 120 °C. Determined from DSC analysis using 1st heating cycle and 10 °C.min^{-1} heating rate.*

Time-dependant DSC measurements of **DA-PCL** after heating to 120 °C for 1 hour then conditioned at ambient temperature demonstrated changes in thermal properties (***Figure 2.14*** and ***Table 2.8***). The PCL melting endotherm (ΔH_{mPCL}) between 35 and 43 °C was not present in measurements until after 4 days suggesting that DA-cycloadducts supress the kinetics of PCL crystallisation (***Figure 2.14 (A)***). This is likely due to the rapid reformation of strong covalent DA-bonds between furan and maleimide terminated prepolymers post heating, which restricts PCL chain mobility and hinders the speed of chain packing to form lamellar crystals. ΔH_{mPCL} continued to increase over time until after 14 days

where it remained constant, demonstrating equilibrium was achieved for the PCL crystalline phase. Immediately after heating to 120 °C (0 days), **DA-PCL** displayed a prominent rDA endotherm at T_{rDA} = 146 °C, with a small shoulder appearing at T_{rDA} = 118 °C, indicating that the majority of reformed DA-cycloadducts were the more thermodynamically stable *exo* isomer (**Figure 2.14 *(B)***). This *exo* endotherm was caused by the *exo* DA-cycloadducts which form during the thermal window between the 120°C heat and cooling to ambient, where sufficient thermal energy is available for this conformation to preferentially form. Conditioning further at ambient temperature, however, does not provide enough thermal energy for the *exo* product to form at an observable rate, so the *exo* endotherm (T_{exo}) remained constant. On the other hand, the endotherm for the kinetic *endo* DA-cycloadducts, with the lower T_{rDA} (T_{endo}) grew in magnitude overtime, indicating the preferential formation of *endo* adducts, so much so that after 28 days there were more *endo* than *exo* DA-cycloadducts present. It is important to note that this increase in the *endo* isomer over time was a consequence of the DA reaction between unreacted furan and maleimide moieties, and not a rearrangement from the *exo* product.

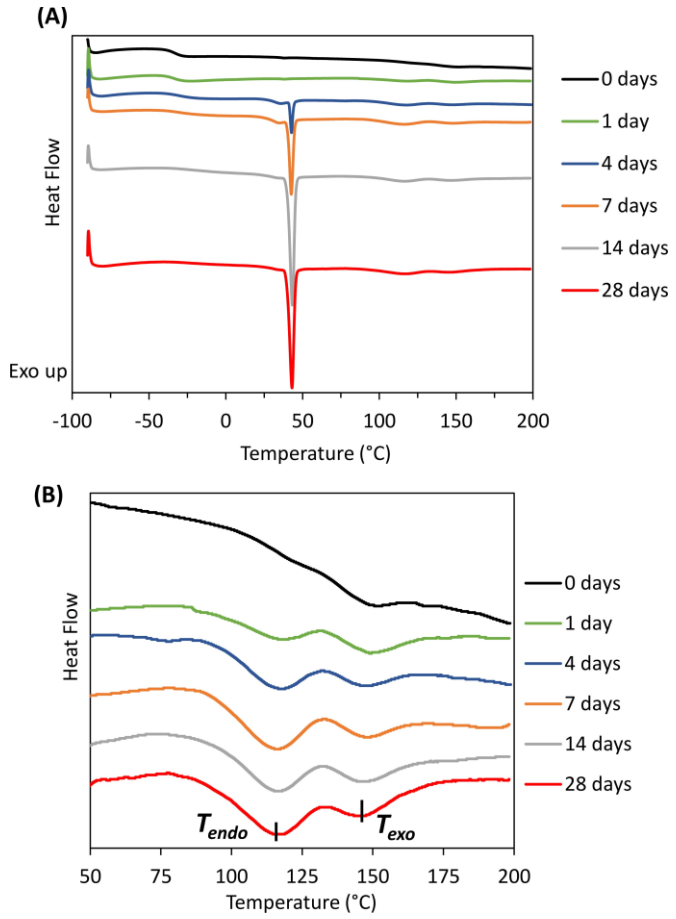

Figure 2.14 *DSC thermograms (1st heating cycles) of* ***DA-PCL*** *from* ***(A)*** *-90 to 200 °C and* ***(B)*** *50 to 200 °C overtime at ambient temperature. Heating rate of 10 °C.min^{-1}. Exo up.*

Table 2.8 *DSC thermal data of* ***DA-PCL*** *measured over 28 days at ambient temperature post isothermal to rDA temperature.*

Time (Days)	T_g [a] (°C)	T_{mPCL} [a] (°C)	ΔH_{mPCL} [a] (J.g^{-1})	T_{rDA} [a] (J.g^{-1})	ΔH_{rDA} [a] (J.g^{-1})
0	-32	-	-	146	4.9
1	-34	34 & 43	-	119 & 149	5.8
4	-32	35 & 43	7.3	117 & 148	6.3
7	-30	43	17	117 & 145	8.9
14	-23	43	28	116 & 147	9.1
28	-29	43	27	117 & 145	9.0

[a] determined by DSC analysis of 1st heating cycle using heating rate of 10 °C.min^{-1}.

To evidence this, **DA-PCL** was conditioned at 60 °C overtime post heating to the rDA temperature (120 °C) for 1 hour, a temperature at which it can overcome the larger energy barrier to preferentially form the thermodynamically favoured *exo* adducts (***Figure 2.15***). This demonstrated that the *exo* rDA

endotherm at T_{rDA} = 146 °C grew preferentially over the *endo* rDA endotherm at T_{rDA} = 118 °C, since there was enough energy to favour the formation of the more thermodynamically stable *exo* DA cycloadducts. These findings demonstrate that in the scope of DA elastomers curing at 60 °C would be beneficial since it accelerates the DA-reaction and preferentially forms the *exo* isomer which is more thermodynamically stable and therefore resistant to heat.

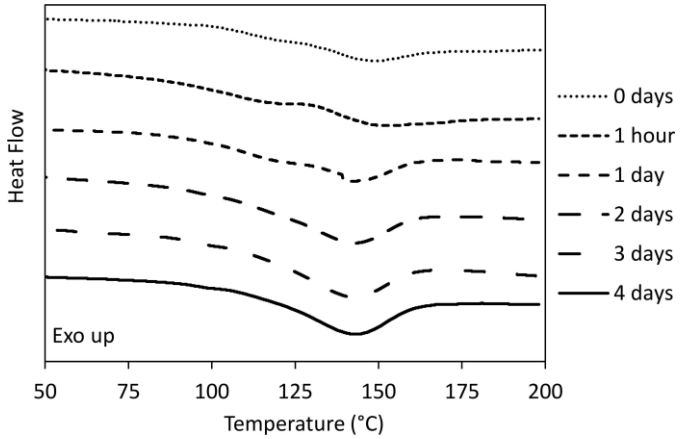

Figure 2.15 *DSC thermograms (1st heating cycles) of* ***DA-PCL*** *acquired overtime at 60 °C post a 1-hour heat to 120 °C . Exo up. 10 °C.min-1 heating rate.*

Thermogravimetric analysis (TGA) of the **DA-X** copolymers revealed high thermally stability above 200 °C with no mass loss, confirmed by the temperature of 5% weight loss ($T_{5\%}$) values (***Figure 2.16*** and ***Table 2.9***). All copolymers displayed a decomposition around 350 °C, which can be attributed to the thermal decomposition of urethane bonds in the DA-TPUs.[32] The TGA curves of **DA-PCL** and **DA-PCL.LA** were shifted to lower temperatures than **DA-PBD** and **DA-HPBD**, as their polyol backbones contain ester bonds, which thermally degrade at lower temperatures than hydrocarbon backbones.

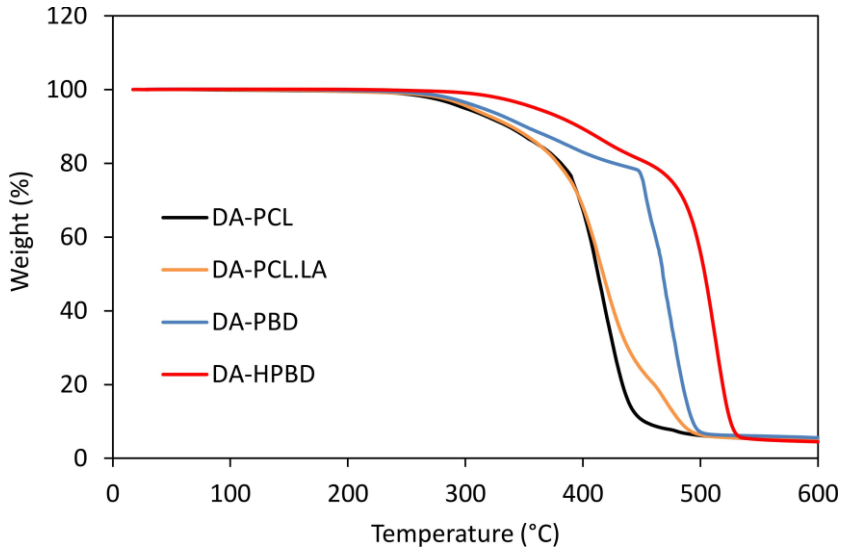

Figure 2.16 *TGA curves of* ***DA-X*** *copolymers.*

Table 2.9 *$T_{5\%}$ values of* ***DA-X*** *copolymers.*

Copolymer	$T_{5\%}$ (°C)[a]
DA-PCL	299
DA-PCL.LA	318
DA-PBD	314
DA-HPBD	360

[a] *Obtained from TGA analysis using a heating rate of 10 °C.min^{-1}.*

The **DA-X** copolymers were subjected to dynamic mechanical analysis (DMA) to determine their viscoelastic behaviour between -80 and 120 °C (***Figure 2.17*** and ***Table 2.10***). All copolymers displayed an initial drop in storage modulus (*E'*) when passing through the T_g due to an increase in co-operative mobility.[33] Approaching the T_g also caused a distinctive peak in the loss factor (tan *δ*) as more energy is dissipated from the larger segments of polymer that can move cooperatively. Tan *δ* can thus be used as an assessment of the ability of energy dissipation of elastomers.[34] **DA-HPBD** displayed the lowest T_g at -27 °C with the highest tan *δ* peak due to its highly flexible hydrocarbon SS backbone, followed by **DA-PBD** which was slightly less flexible on account of restriction of rotation around C=C double bonds. **DA-PCL.LA** displayed a higher T_g at 4 °C, suggesting that ester bonds restrict segmental chain motion more than carbon-carbon bonds. **DA-PCL** displayed the highest T_g at 25 °C accompanied by a significantly smaller tan δ peak due to its semi-crystalline nature, which restricts chain motion and

reduces damping ability. **DAPCL** displayed a further step change in *E'* with an associated softening event in tan δ at 40 °C, attributable to the melting of semi-crystalline PCL segments (T_{mPCL}). **DA-PCL** also exhibited a significantly higher *E'* at 20 °C than the amorphous **DA-X** copolymers due to physical reinforcement from these semi-crystalline segments.

After passing through the T_g or T_m, the moduli of the **DA-X** copolymers slowly reduced in the range of 40 -80 °C due to the rDA reaction becoming more favoured. At higher temperatures, *E'* decreased rapidly whilst tan δ accelerated through unity, demonstrating the transition point between a solid and a liquid where tan δ = 1 and viscous flow occurs. This is a direct consequence of the rDA reaction and the temperature-dependant DA equilibrium shifting towards the lower molecular weight prepolymers. The temperature of viscous flow (T_f) varied with DA-TPU polyol SS. **DA-PCL.LA** displayed the lowest T_f at 85 °C, followed by **DA-PCL** at 92 °C, whilst **DA-HPBD** and **DA-PBD** displayed higher T_f values at 97 and 107 °C , respectively. **DA-PBD** and **DA-HPBD** also exhibited more stable, extensive rubbery plateaus and wider service temperature windows than **DA-PCL.LA** and **DA-PCL**, which would enable good mechanical properties over a wider temperature range in industrial applications. This additional thermal stability is likely caused by microphase separation in the PBD and HPBD-based **DA-X** copolymers, leading to a higher dergree of physical interactions, such as strong interuethane H-bonding within the HS, which can synergistically reinforce the thermally reversible DA covalent bonds.

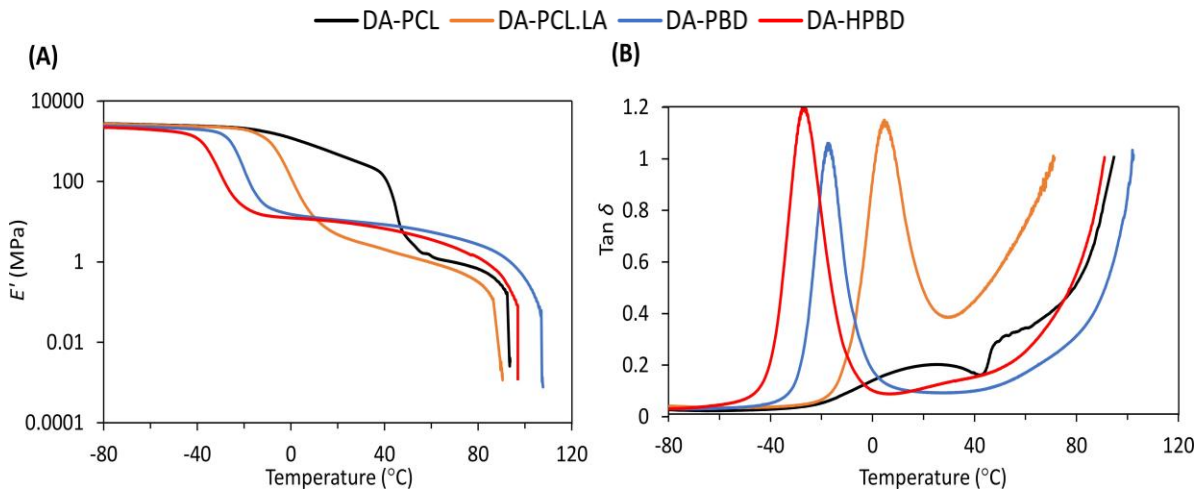

Figure 2.17 *The variation of DMA* ***(A)*** *storage modulus (E') and* ***(B)*** *tan δ with temperature for* ***DA-X*** *copolymers. Heating rate of 3 °C.min^{-1}.*

Table 2.10 *DMA thermal data for* ***DA-X*** *copolymers using a 3 °C.min^{-1}.heating rate.*

Copolymer	E' ($T < T_g$) [a] (MPa)	T_g [b] (°C)	E' ($T > T_g$) [c] (MPa)	T_{mPCL} [d] (°C)	T_f [e] (°C)
DA-PCL	2340	25.0	470	40.0	92.0
DA-PCL.LA	2500	4.0	5.0	-	85.0
DA-PBD	2260	-16.0	11.0	-	107.0
DA-HPBD	1960	-27.0	10.0	-	97.0

[a] Storage modulus measured at -60 °C. [b] Measured as peak in tan δ. [c] Storage modulus measured at 20 °C. [d] Measured as the onset of modulus reduction. [e] Measured as onset of viscous flow.

2.2.5 Solid state frequency sweeps

Solid state frequency sweep experiments were performed on **DA-PBD** and **DA-HPBD** using an Anton Paar MCR502 rheometer, within the frequency range of 0.01 to 10 Hz (***Figure 2.18***). A shear strain of 0.01% was applied across three temperatures: 23, 50, and 75 °C. Both **DA-X** copolymers displayed elastic dominant behaviour within the frequency range where storage modulus > loss modulus (*G'* > *G''*). Steep modulus gradients were observed in both DA-TPUs once the shear frequency reached 1 Hz, likely caused by instrument inertia effects, whereby the steep modulus gradient is an experimental artefact caused by the unsteady motion of the instrument accelerating, a common occurrence in commercial rheometers.[35] **DA-PBD** exhibited higher *G'* than **DA-HPBD** across all temperatures showing that **DA-PBD** displayed a greater shear strength (resistance to shear-induced deformation). This is

because the **DA-PBD** contains C=C double bonds which restrict bond rotation and polymer chain mobility, indicated by higher T_g via thermal analysis. For both **DA-PBD** and **DA-HPBD** *G'* decreased with increasing temperature. This is a result of the thermally reversible DA-equilibrium shifting towards the lower molecular weight prepolymers as the rDA reaction becomes more favoured. Both DA-TPUs displayed a bigger relative drop in *G'* as the temperature increased from 50 to 75 °C, indicating that a higher proportion of DA-cycloadducts dissociate as the temperature approaches closer to the rDA temperature.

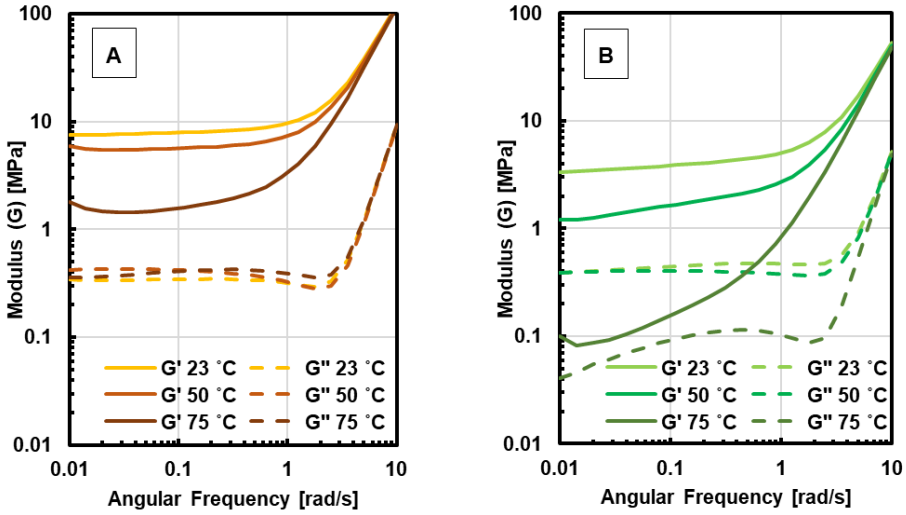

Figure 2.18 *Solid state frequency sweeps of* ***(A) DA-PBD*** *and* ***(B) DA-HPBD*** *at 23, 50 and 75 °C using 0.01% shear strain and a frequency range of 0.01–10 Hz.*

2.2.6 Mechanical properties

The mechanical properties of the **DA-X** copolymers were examined by uniaxial tensometry, using a 10 mm.min^{-1} extension rate. The Young's modulus (E_y) (linear regression in the 0-2% strain interval), ultimate tensile strength (σ_b), elongation at break (ε_b) and tensile toughness (U_T), (the total area under the stress-strain curve) were calculated from the resulting stress-strain curves (***Figure 2.19*** and ***Table 2.11***). The stress-strain curves of all DA-TPUs were typical of elastomeric materials, displaying high elongations. The stress-strain curve of **DA-PCL** exhibited a yield point, signifying the onset of plastic deformation of the crystalline PCL regions. This yielding meant that **DA-PCL** displayed a significantly higher E_y (150 MPa) compared to the amorphous **DA-X** copolymers (≤.6.4 MPa). The tensile curve of

DA-PCL also displayed a significant upturn at high elongations, indicating a phenomenon known as strain-induced crystallisation, whereby amorphous PCL chains transform into highly orientated and aligned crystalline domains in the direction of the applied stress, on account on disentanglement.[36] This remarkably reinforced **DA-PCL**, leading to a high tensile strength (13.6 MPa) and toughness (8029 MPa).[37] **DA-PCL.LA** was a highly extendible (ε_b =1270%) yet weak material (σ_b = 0.3 MPa), losing strength with elongation, leading to a low toughness of 200 MPa, over 45 times smaller than **DA-PCL**. This demonstrates the substantial effect of PCL SS backbone crystallinity on DA-TPU mechanical performance. **DA-PBD** and **DA-HPBD** exhibited typical stress-strain behaviour of amorphous elastomers, displaying strain-hardening leading to higher strength and toughness values than **DA-PCL.LA**. This could be a result of a higher degree of H-bonding within the HSs, resulting from enhanced microphase separation between the non-polar PBD or HPBD SSs and the polar HSs, as shown earlier by ATR-FTIR spectroscopy. **DA-PBD** displayed a tensile strength over three times greater than **DA-HPBD** (11.7 versus 3.6 MPa), perhaps because the polymer chains in **DA-PBD** are less flexible (indicated by a higher T_g) due to the presence of C=C double bonds, meaning that there is greater resistance to polymer chain alignment at higher strains in **DA-PBD**, causing a more pronounced strain-hardening effect.

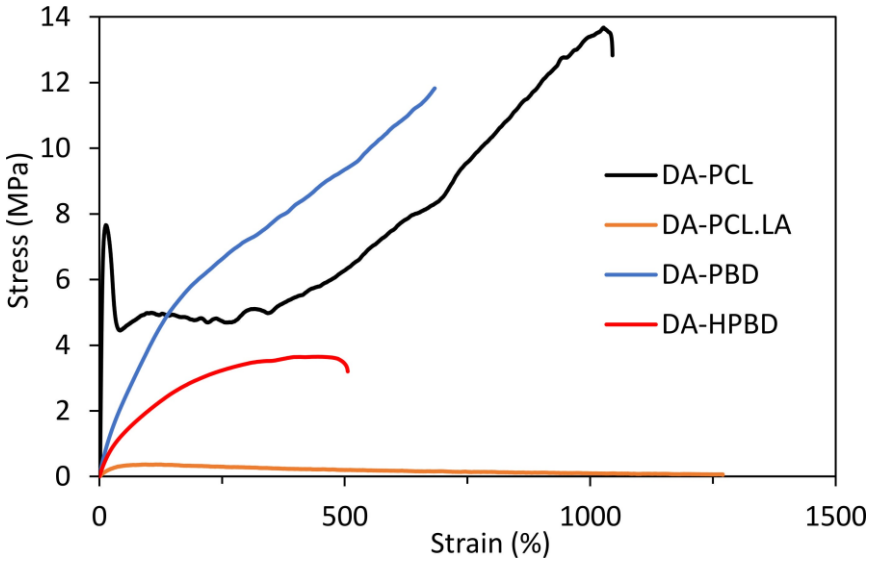

Figure 2.19 *Representative stress-strain curves of* ***DA-X*** *copolymers. Obtained from uniaxial tensile testing (10 mm.min^{-1} extension rate)*

Table 2.11 *Mechanical data of* ***DA*-X** *copolymers.*

Copolymer	E_y [a] (MPa)	σ_b [a] (MPa)	U_T [a] (MPa)	ε_b [a] (%)
DA-PCL	150 ± 4.0	13.6 ± 0.4	8030 ± 301	1030 ± 43
DA-PCL.LA	1.4 ± 0.2	0.3 ± 0.1	200 ± 25	1270 ± 55
DA-PBD	6.4 ± 0.4	11.7 ± 0.4	4980 ± 250	680 ± 32
DA-HPBD	4.3 ± 0.2	3.6 ± 0.3	1430 ± 106	500 ± 24

[a] *determined by uniaxial tensometry (10 mm.min^{-1} extension rate). Mean values ± standard deviation from measurements conducted independently on 5 specimens.*

To better assess the elasticity of the **DA-X** TPUs, uniaxial cyclic tensile testing was conducted at room temperature (***Figure 2.20***). Dumbbell samples were stretched to 200% strain and relaxed at a rate of 10 mm.min^{-1}, a process repeated over 10 hysteresis cycles. The first elastic cycle of all **DA-X** copolymers differed from subsequent ones; which can be attributed to stress-induced rearrangements in the polymer microstructure, indicating initial energy loss due the disentanglement of PCL or PBD chains.[38,39] The first elastic cycle of **DA-PCL** displayed a clear yield point, associated with a deformation mechanism involving orientation and destruction of micron to colloidal state semi-crystalline morphologies, explaining why the yield point is subsequently lost in the following elastic cycles (***Figure 2.20*** **(A)**).[40]

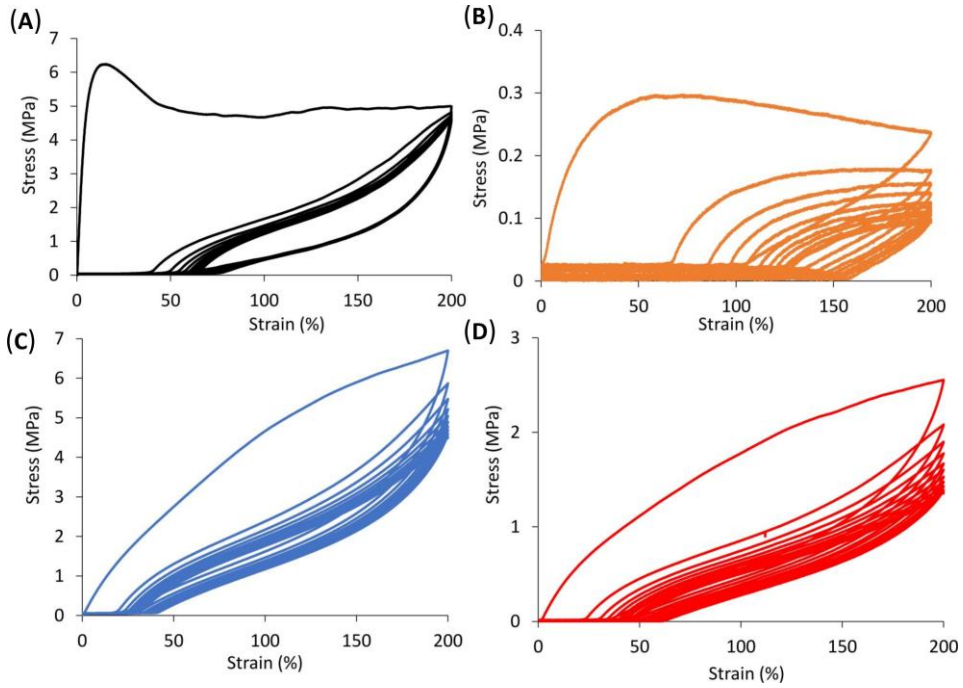

Figure 2.20 *Representative hysteresis curves for* ***(A) DA-PCL***, ***(B) DA-PCL.LA***, ***(C) DA-PBD*** *and* ***(D) DA-HPBD*** *copolymers up to 200% strain over 10 cycles obtained from cyclic tensile testing (10 mm.min^{-1} extension rate).*

Elastic recovery [defined as $(\varepsilon_{max} - \varepsilon_{min}/\varepsilon_{max}) \times 100$], resilience [defined as $(E_R/(E_L + E_R)) \times 100$], and residual strain ($\varepsilon_R$) were calculated over the 10 elastic cycles from the corresponding hysteresis curves, where E_L is energy loss, E_R is energy recovery, ε_{max} is maximum strain, ε_{min} is minimum strain and ε_R is residual strain. (***Figure 2.21***).[41]

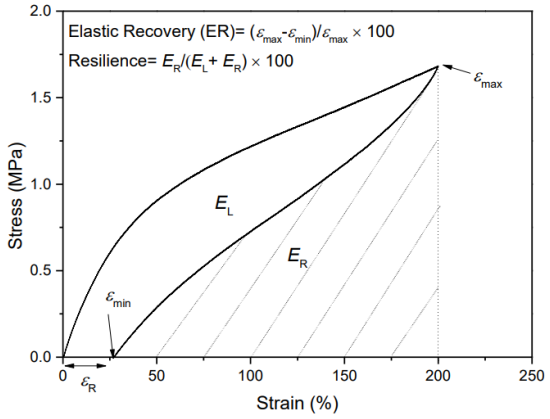

Figure 2.21 *Schematic of parameters measured during cyclic tensile test. Calculation of elastic recovery and resilience. Reprinted with permission from C. Tang and coworkers, ACS. Maro. Lett.,* ***2016****, 5, 220-223. Copyright 2024 American Chemical Society.*[41]

DA-PBD and **DA-HPBD** maintained the highest elastic recovery (80 and 70%) and resilience (74 and 70%), with low residual strain (10 and 17%), respectively, after the 10 hysteresis cycles demonstrating excellent elasticity (***Figure 2.22***). These DA-TPU copolymers displayed the lowest T_g values *via* thermal analysis, indicating that they contain the highest degree of polymer chain mobility for immediate elastic recovery to occur.[42] These findings suggest that such materials would be better suited than **DA-PCL** and **DA-PCL.LA** to applications which require durability and long fatigue life, where they are subjected to repeated stretching or loading. **DA-PCL** exhibited slightly lower elastic recovery and resilience (63%) and low residual strain (14%) after the 10 elastic cycles. The lower elastic recovery and resilience of **DA-PCL** could be a result of its lower chain mobility which results in a higher T_g of 25 °C (similar to ambient temperature) and reduces the ability of the material to dissipate elastic energy between hysteresis cycles and return to its original shape after being stretched under cyclic tensile loads. **DA-PCL.LA** displayed significantly lower elastic recovery (20%) and resilience (3%), along with higher residual strain (36%) across the 10 hysteresis cycles compared to the other **DA-X** copolymers. This is likely a result of interchain friction and permanent deformation which increase energy loss during stretching and recovery.[43]

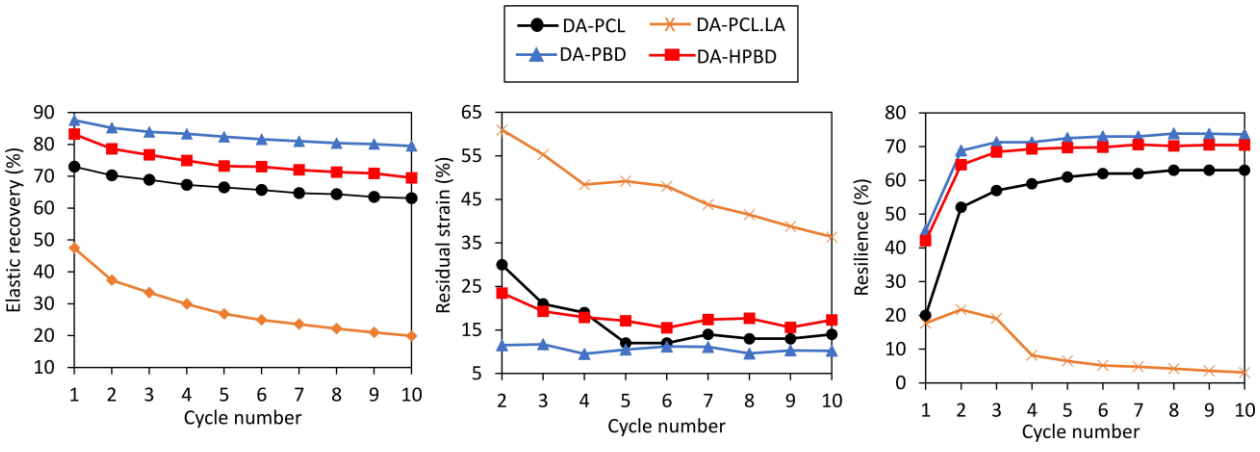

Figure 2.22 *Cyclic tensile testing parameters as a function of cycle number; elastic recovery (left), residual strain (middle) and resilience (right).*

2.2.7 Shore A hardness

Shore hardness A values of the **DA-X** elastomers were obtained according to ASTM D2240 using a durometer to measure the depth of indentation created in the materials (***Table 2.12***). The Shore A values of the DA-TPUs ranged from 58 to 80, depending on TPU SS backbone. The data agreed with mechanical data from tensile testing, *i.e* the stronger copolymers with higher stress values provided higher hardness values, demonstrating a greater ability to resist deformation, indentation, and scratching. Comparing the measured values to a commercial Shore A hardness scale demonstrates that **DA-PCL** is as hard as a leather belt whilst **DA-PCL.LA** is almost as soft as a pencil eraser, demonstrating how changing the polyol backbone can vastly affect the potential industrial applications of the DA-TPUs (***Figure 2.23***).

Table 2.12 *Shore A hardness values of* ***DA-X*** *copolymers.*

Copolymer	*Shore A hardness* [a]
DA-PCL	80 ± 2.5
DA-PCL.LA	58 ± 2.1
DA-PBD	72 ± 2.1
DA-HPBD	67 ± 2.4

[a] *Measured as an average of five repeats ± standard deviation values.*

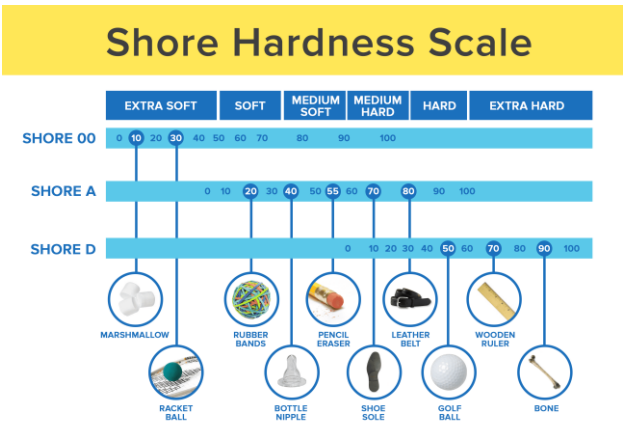

Figure 2.23 *Shore hardness scales. Reprinted with permission from Aeromarine products website.*[44]

2.2.8 Morphology

Morphology of the **DA-X** copolymers was investigated using small-angle X-ray scattering (SAXS) and wide-angle X-ray scattering (WAXS) measurements conducted at room temperature (***Figure 2.24***). The Lorentz-corrected (Iq^2) SAXS plots of **DA-PBD** and **DA-HPBD** displayed pronounced scattering peaks at similar positions of the maximum peak intensity (q_{max}) values. This suggests the formation of a two-phase morphology, resulting from nanoscale phase separation between non-polar PBD or HPBD SSs and polar HSs comprising DA-cycloadducts. These scattering peaks originate from the difference in electron density between these microphase separated hard and soft domains. The corresponding d-spacing values of 66 and 63 Å, respectively, can be interpretated as the interdomain distances between hard and soft segment within the DA-TPUs (***Table 2.13***).[45] **DA-PBD** and **DA-HPBD** exhibited another broad scattering feature at lower q_{max} values, indicating aggregates of hard domains with a larger d-spacing of 274 Å. SAXS patterns with similar low q_{max} features have been observed before by Hayes *et al.* in HPBD based supramolecular PUs.[46] **DA-PCL** produced a low intensity scattering feature with a d-spacing of 185 Å, where microphase separation results from PCL crystallisation rather than microphase separation. The SAXS pattern of **DA-PCL.LA** did not contain any pronounced scattering features, since PCL.LA polyol is a polar, amorphous SS which is likely be compatible with the polar DA-TPU HS.

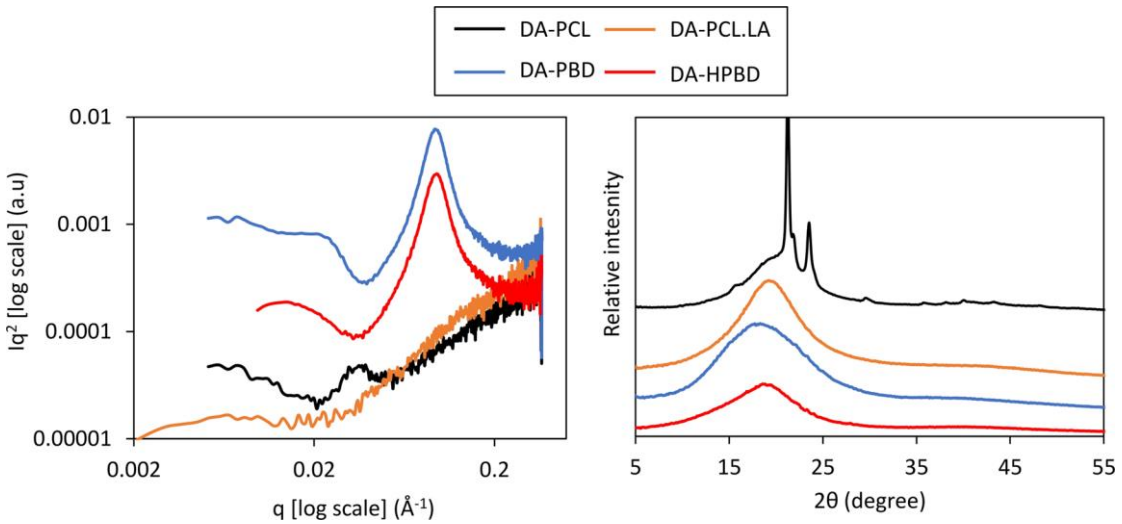

Figure 2.24 *Lorentz-corrected SAXS plots (left) and wide-angle X-ray scattering (WAXS) profiles (right) of DA-X copolymers obtained at room temperature.*

Table 2.13 *d-spacing values of obtained from main peaks in SAXS plots of* ***DA-X*** *copolymers.*

Copolymer	[a] d-spacing (Å)
DA-PCL	185
DA-PCL.LA	-
DA-PBD	66
DA-HPBD	63

[a] determined from q_{max} values in Lorentz-corrected SAXS plots.

The WAXS profiles of all **DA-X** copolymers displayed a broad amorphous peak between 2θ = 5-30°, representing the distribution of distances between chains in amorphous regions. **DA-PCL** also presented sharp diffraction peaks with Bragg angles of 2θ = 21.2°, 21.8° and 23.5°, corresponding to orthorhombic unit cell reflections with Miller indices of 110, 111 and 200, respectively, which are consistent with previously reported crystalline PCL.[47,48]

2.2.9 Recycling and self-healing

To confirm that the **DA-X** TPU elastomers are mechanically recyclable the samples were reprocessed by compression moulding using mild conditions (100 °C at 3 MPa for 10 minutes) and conditioned for 7 days at 25 °C before remeasurement of tensile properties (R1, ***Figure 2.25***). The process was repeated a further two times with the same samples (R2, R3) to determine any change in mechanical properties. All materials maintained very good mechanical properties with high stress-recovery ratios (typically > 80%) after 3 reprocessing cycles (***Table 2.14***).

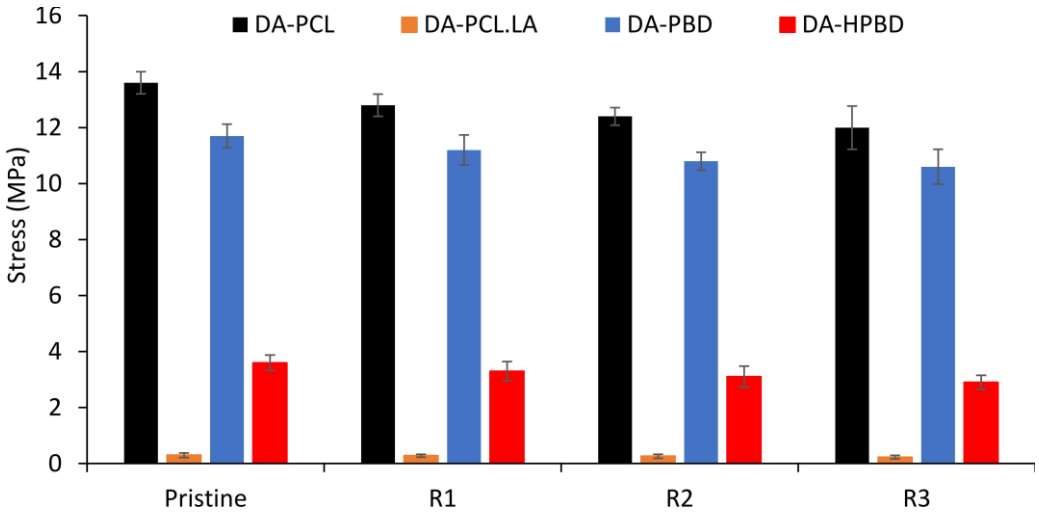

Figure 2.25 *Mean stress values for* ***DA-X*** *copolymers obtained via tensile testing for pristine samples and after 3 reprocessing cycles ± standard deviation from measurements conducted independently on 5 specimens. Samples were left at ambient for 7 days before tensile testing after each cycle.*

Table 2.14 *Stress recovery efficiency values of the* ***DA-X*** *copolymers after reprocessing cycles.*

Copolymer	Recovery ratio R1 (%) [a]	Recovery ratio R2 (%) [a]	Recovery ratio R3 (%) [a]
DA-PCL	94	91	88
DA-PCL.LA	93	87	77
DA-PBD	96	92	91
DA-HPBD	92	86	81

[a] *calculated as a percentage based on the ratio of the average stress at break before and after each reprocessing cycle, obtained via tensile testing.*

Optical micrographs of **DA-PBD** confirmed that a 50 µm width scratch could be completely healed by heating the material to 130 °C for 5 minutes. This demonstrates the excellent self-healing capability of **DA-PBD**, which can be attributed to the fast dissociation of the DA-cycloadducts at the rDA temperature, leading to a reduction in DA-TPU molecular weight and thus improved mobility (***Figure 2.26***).

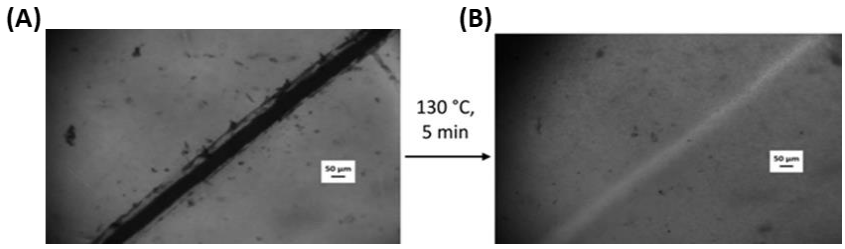

Figure 2.26 *Optical microscopy images of* ***(A) DA-PBD*** *at room temperature with a 50 µm scratch and* ***(B) DA-PBD*** *with a completely healed scratch after heating to 130 °C for 5 min.*

Moreover, optical micrographs of **DA-PCL** showed that the sample becomes transparent after 60 seconds at 60 °C due to melting of the crystalline PCL segments and a 20 µm width scratch could be subsequently healed by heating the same material to 80 °C for a further 90 seconds (***Figure 2.27***). This demonstrates that **DA-PCL** can rapidly heal scratches at relatively mild temperatures. Such excellent self-healing capabilities can again be attributed to the rDA-reaction in the DA-TPU copolymers causing a decrease in molecular weight and melt viscosity.

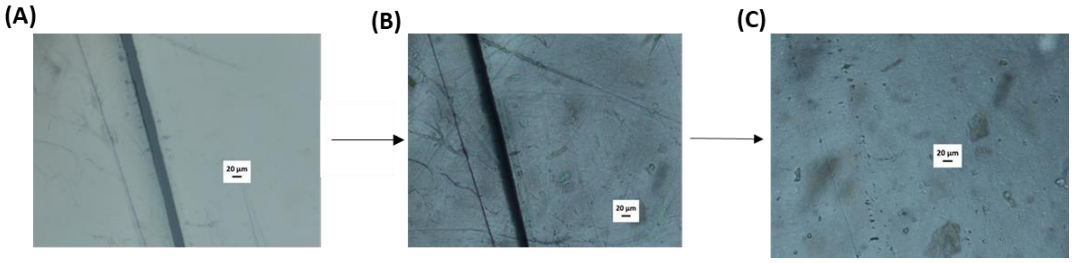

Figure 2.27 *Optical microscopy images of* ***(A) DA-PCL*** *at room temperature with a 20 µm scratch.* ***(B) DA-PCL*** *after heating to 60 °C for 60 seconds and* ***(C) DA-PCL*** *with a completely healed scratch after heating to 80 °C for a further 90 seconds.*

2.3 Conclusions

Maleimide and furan telechelic prepolymers (**PPM-X** and **PPF-X**) were synthesised by end-group modification of NCO terminated intermediates made from **PCL**, **PCL.LA**, **PBD** or **HPBD** polyol backbones of M_n = 2000 gmol^{-1} . FTIR spectroscopy confirmed successful reaction *via* the disappearance of NCO peak at ν_{max} = 2260 cm^{-1} whilst peaks at 696 and 733 cm^{-1} appeared, indicating the incorporation of maleimide and furan functional groups. ^{1}H NMR spectroscopy of the prepolymers showed aromatic urethane and furan/maleimide-end groups. SEC analysis confirmed an increase in apparent molecular weight over the starting polyols. ATR-FTIR analysis revealed that the PBD-based prepolymers displayed stronger H-bonding between urethane carbonyl groups than the PCL-based materials. DSC analysis showed that all prepolymers displayed sub-ambient T_g values. **PPM-PCL** and **PPF-PCL** also exhibited melting endotherms around 40 °C for the melting of semi-crystalline PCL segments whilst the **PBD** and **HPBD**-based prepolymers displayed hard segment melting endotherms between 60 and 100 °C suggesting microphase separation between non-polar SSs and polar HSs.

The corresponding **PPM-X** and **PPF-X** prepolymers were copolymerised at 25 °C to give four **DA-X** copolymers, (**DA-PCL**, **DA-PCL.LA**, **DA-PBD** and **DA-HPBD**). SEC analysis of the **DA-X** copolymers demonstrated a significant increase in apparent molecular weight over the prepolymers, indicating successful copolymerisation to form DA-cycloadducts. ^{1}H NMR spectroscopy revealed resonances confirming the presence of DA-cycloadducts. DSC analysis of all **DA-X** copolymers revealed a broad double endotherm between 117 and 148 °C, confirming the rDA reaction. **DA-PCL** also displayed a ΔH_{mPCL} melting endotherm indicating its semi-crystalline nature. **DA-PBD** displayed a hard segment T_g at 53 °C indicating microphase separation. By monitoring the increase in ΔH_{rDA} *via* DSC analysis and relative decrease in absorbance at ν_{max} = 696 cm^{-1} *via* FTIR analysis over time it was determined that DA-cycloadduct conversion plateaued after 7 days at 25 °C or 2-3 at 60 °C. The thermal reversibility **DA-PCL** was demonstrated *via* SEC analysis and sol-gel transitions showing reversible changes in molecular weight with temperature.

TGA analysis revealed that all **DA-X** copolymers displayed high thermal stability up to 200 °C. DMA analysis showed that all DA-TPUs displayed a steep drop in *E'* at high temperatures where viscous flow occurred due to dissociation of DA-cycloadducts. **DA-PBD** and **DA-HPBD** displayed wider service temperature windows and more stable rubbery plateaus than the PCL-based copolymers, likely due to microphase separation and synergistic reinforcement of the thermally reversible DA-cycloadducts. **DA-PCL** exhibited a significantly higher *E'* at 20 °C than the amorphous **DA-X** copolymers and a steep drop in *E'* around 40 °C due semi-crystalline PCL segments. Such structure-property relationships could be utilised to meet specific requirements for various industrial applications and reprocessing techniques.

Mechanical properties of DA-TPUs were highly tuneable with polyol backbone structure. **DA-PCL.LA** was very stretchy but very weak. **DA-PCL** was stretchy and strong providing a U_T value almost 45 times greater than **DA-PCL.LA**, demonstrating the significant benefit of crystallinity on mechanical performance. **DA-PBD** displayed more pronounced strain hardening than **DA-HPBD** resulting in a fracture stress over 3 times greater. Cyclic tensile testing showed that **DA-PBD** and **DA-HPBD** maintained the highest elastic recovery and resilience over 10 hysteresis cycles due to their backbones having the highest degree of flexibility. Indentation experiments showed that the **DA-X** copolymers displayed Shore A hardness values between 58 and 80. Morphology of the DA-TPUs varied with polyol SS. SAXS experiments showed that **DA-PBD** and **DA-HPBD** produced prominent scattering peaks at similar q_{max} values, suggesting lamellar morphologies due to nanoscale phase separation. **DA-PCL** presented a lower intensity scattering peak at a lower q_{max} value where phase separation resulted from crystallinity. No noticeable scattering peak observed for **DA-PCL.LA** due its lack of crystallinity and phase separation. WAXS experiments revealed that all **DA-X** copolymers exhibited broad diffraction peaks between 2θ = 5-30°, whilst **DA-PCL** also displayed sharp diffraction peaks at Bragg angles of 2θ = 21.2° and 23.5°, consistent crystalline PCL segments.

All **DA-X** copolymers could be thermally reprocessed under mild conditions, achieving high stress recovery ratios (> 80%) after 3 reprocessing cycles. **DA-PBD** and **DA-PCL** also demonstrated excellent

self-healing capability *via* optical microscopy. The work outlined in this chapter demonstrates how the incorporation of thermally reversible DA-cycloadducts into high molecular weight TPUs can be employed to improve processability by lowering melt viscosity for facile end-of-life recycling and extension of elastomer lifespan. This work also provides a deeper insight into how the thermomechanical and morphological properties of DA-TPUs such as T_g, degree of crystallinity, T_{rDA}, tensile strength, flexibility and toughness can be varied by changing TPU SS backbone.

2.4 Experimental

2.4.1 Materials

Capa® 2200J (OH value = 56.38 mg.KOH/g) and Capa® 8025D (OH value = 56.92 mg.KOH/g) were supplied by Ingevity. Krasol® LBH P 2000 (OH value = 53.53 mg.KOH/g) and Krasol® HLBH P 2000 (OH value = 46.56 mgKOH/g) were provided by Cray Valley. 4,4'-methylene bis(phenyl isocyanate) (MDI, 98 %), furfuryl alcohol (FA), dichloromethane (DCM), and deuterated chloroform ($CDCl_3$, 99.8 atom % D) were purchased from Sigma-Aldrich. 2-Hydroxyl ethyl maleimide (HEMI) was provided by Henkel Corporation. All materials were used as supplied.

2.4.2 Synthesis of PPF-X and PPM-X prepolymers.

All furan (**PPF-X**) and maleimide (**PPM-X**) terminated PU prepolymers were synthesised in a similar manner, a typical procedure is as follows: Polyol (77.96 g, 0.039 mol) was loaded into a 4-necked 250 mL flange flask, equipped with an overhead mechanical stirrer, gas inlet and digital thermometer. Vacuum was applied for 1 hour at 90 °C with a stirring rate of 90 rpm. Vacuum was removed and MDI (19.52 g, 0.078 mol) was added at 110 °C under nitrogen flow with stirring increased to 180 rpm. After 15 minutes the vacuum was reapplied for 1 hour to allow MDI to react with hydroxy groups. Vacuum was again removed and either **FA** (8.53 g, 0.087 mol) for **PPF-X** or **HEMI** (12.28 g, 0.087 mol) for **PPM-X** was added at 110 °C to react with terminal isocyanate groups. ATR-IR spectroscopy showed disappearance of the isocyanate band after approximately 1.5-2 hours. The reaction was then switched off and the mixture was decanted while hot to give quantitative yields.

PPF-PCL: **SEC** ($CHCl_3$): M_n = 7.2 kDa, M_w = 14.4 kDa, $Đ_M$ = 2.0. **^{1}H NMR** (400 MHz, 298 K, $CDCl_3$): δ = 7.43 (s, CH=C*H*O (FA)), 7.30 (m, Ar), 7.10 (d, $^3J_{H\text{-}H}$ = 7.8 Hz, Ar), 6.69 (s, N*H*), 6.60 (s, N*H*), 6.47 (d, $^3J_{H\text{-}H}$ = 2.9 Hz, CHC*H*=CHO (FA)), 6.37 (s, CC*H*CH (FA)), 5.14 (s, OC*H*C (FA)), 4.14 (t, $^3J_{H\text{-}H}$ = 6.4 Hz, CH_2OC=O), 4.06 (t, $^3J_{H\text{-}H}$ = 6.7 Hz, CH_2OC=O), 4.00 (s, MDI CH_2Ar), 3.89 (s, NPG CH_2O), 2.30 (t, $^3J_{H\text{-}H}$ = 7.5 Hz, CH_2C=OO), 0.98 (d, $^3J_{H\text{-}H}$ = 9.4 Hz, NPG CH_3), 1.65 and 1.38 (all remaining protons) ppm. **ATR-FTIR**: ν_{max} = 3338 (N-H), 2944 – 2865 (C-H), 1722 (C=O), 1597 (C-N), 1528 (Ar C=C), 1295 and 1163 (C-O) cm^{-1}.

PPM-PCL: **SEC** ($CHCl_3$): M_n = 8.0 kDa, M_w = 16.2 kDa, $Đ_M$ = 2.0. **^{1}H NMR** (400 MHz, 298 K, $CDCl_3$): δ =7.30 (m, Ar), 7.10 (d, $^3J_{H\text{-}H}$ = 8.3 Hz, Ar),6.71 (s, C=OC*H*CH (HEMI)), 6.62 (s, N*H*), 6.58 (s, N*H*), 4.32 (t, $^3J_{H\text{-}H}$ = 5.2 Hz, NCH_2CH_2O (HEMI)), 4.14 (t, $^3J_{H\text{-}H}$ = 6.4 Hz, CH_2OC=O), 4.06 (t, $^3J_{H\text{-}H}$ = 6.7 Hz, CH_2OC=O), 3.89 (s, MDI CH_2Ar), 3.89 (s, NPG CH_2O), 3.85 (t, $^3J_{H\text{-}H}$ = 5.2 Hz, NC$H_2$$CH_2$O (HEMI)), 2.30 (t, $^3J_{H\text{-}H}$ = 7.5 Hz, CH_2C=OO), 0.98 (d, $^3J_{H\text{-}H}$= 9.4 Hz, NPG CH_3), 1.65 and 1.38 (all remaining protons) ppm. **ATR-FTIR**: ν_{max} = 3341 (N-H), 2944- 2865 (C-H), 1722 and 1709 (C=O), 1597 (C-N), 1532 (Ar C=C), 1295 and 1164 (C-O) cm^{-1} .

PPF-PCL.LA: **SEC** ($CHCl_3$): M_n = 6.4 kDa, M_w = 13.6 kDa, $Đ_M$ = 2.1. **^{1}H NMR** (400 MHz, 298 K, $CDCl_3$): δ = 7.45 (s, CH=C*H*O (FA)), 7.30 (m, Ar), 7.11 (d, $^3J_{H\text{-}H}$ = 8.3 Hz Ar), 6.76 (s, N*H*), 6.69 (s, N*H*), 6.46 (d, $^3J_{H\text{-}H}$ = 3.2 Hz, CHC*H*=CHO (FA-CL)), 6.38 (m, CC*H*CH (FA-CL)), 6.36 (m, CHC*H*=CHO (FA-LA)), 6.31 (d, $^3J_{H\text{-}H}$ = 3.1 Hz, CC*H*CH (FA-LA)), 5.15 (s, OC*H*C (FA)), 5.19, 5.10, 4.16, 4.08, 3.89, 2.41, 2.31, 1.64, 1.58, 1.51, 1.40 and 0.99 (all remaining protons) ppm. **ATIR-FTIR** ν_{max} = 3343 (N-H), 2942 – 2866 (C-H), 1729 (C=O), 1598 (C-N), 1532 (Ar C=C), 1309 & 1160 (C-O) and 733 (FA C-H) cm^{-1}.

PPM-PCL.LA: **SEC** ($CHCl_3$): M_n = 6.4 kDa, M_w = 12.7 kDa, $Đ_M$ =2.0. **^{1}H NMR** (400 MHz, 298 K, $CDCl_3$): δ = 7.31 (d, $^3J_{H\text{-}H}$ = 7.3 Hz, Ar), 7.11 (d, $^3J_{H\text{-}H}$ = 6.7 Hz, Ar), 6.76 (d, $^3J_{H\text{-}H}$ = 2.7 Hz, C=OC*H*CH (HEMI)), 6.73 (s, C=OC*H*CH (HEMI)), 6.64 (s, N*H*), 6.59 (s, N*H*), 4.32 (t, $^3J_{H\text{-}H}$ = 5.0 Hz, NCH_2CH_2O (HEMI)), 3.85 (t, $^3J_{H\text{-}H}$ = 5.1 Hz, NC$H_2$$CH_2$O (HEMI)), 5.12, 4.17, 4.08, 3.97, 3.88, 3.81, 3.76, 2.41, 2.32, 1.65, 1.58, 1.53, 1.49, 1.40, 0.99 (all remaining protons) ppm. **ATR-FTIR**: ν_{max} = 3344 (N-H), 2942 – 2866 (C-H), 1729 and 1713 (C=O), 1598 (C-N), 1532 (Ar C=C), 1310 & 1160 (C-O) and 696 (HEMI C=C B_1) cm^{-1}.

PPF-PBD: **SEC** ($CHCl_3$): M_n = 7.6 kDa, M_w = 13.4 kDa, $Đ_M$ = 1.8. **^{1}H NMR** (400 MHz, 298 K, $CDCl_3$): δ = 7.43 (s, C*H*=CHO (FA)), 7.30 (m, Ar), 7.10 (d, $^3J_{H\text{-}H}$ = 7.8 Hz, Ar), 6.56 (s, N*H*), 6.50 (s, N*H*), 6.44 (d, $^3J_{H\text{-}H}$ = 2.9 Hz, CHC*H*=CHO (FA)), 6.37 (s, CC*H*CH (FA)), 5.8-5.3 (m, -C*H*=(1,2) and -C*H*=C*H*-(1,4), 5.12 (s, OC*H*C (FA)), 5.1-4.8 (m, =CH_2(1,2)), 4.25-3.9 (m, -CH_2-O), 3.86 (s, MDI CH_2Ar), 2.25-1.7 (m, -CH_2-(1,4) and -C*H*-(1,2)), 1.7-1 (m, -CH_2-(1,2)). **ATR-FTIR**: ν_{max} = 3332 (N-H), 3070 (C=C $_{stretch\ 1,2}$), 3050-2780 (C-H), 1702 (C=O), 1595 (C-N), 1521 (Ar C=C), 995 (C=C $_{bending\ 1,2}$), 965 (C=C $_{bending\ 1,4\ trans}$), 907 (C=C $_{bending\ 1,2}$) and 733 (FA C-H).cm^{-1}.

PPM-PBD: **SEC** ($CHCl_3$): M_n = 7.4 kDa, M_w = 12.4 kDa, $Đ_M$ = 1.7. **^{1}H NMR** (400 MHz, 298 K, $CDCl_3$): δ = 7.30 (m, Ar), 7.10 (d, $^3J_{H\text{-}H}$ = 7.8 Hz, Ar), 6.71 (s, C=OC*H*CH (HEMI)), 6.50 (s, N*H*), 5.8-5.3 (m, -C*H*=(1,2) and -C*H*=C*H*-(1,4)), 5.1-4.8 (m, =CH_2(1,2)), 4.32 (t,$^3J_{H\text{-}H}$ = 5.2 Hz, NCH$_2$CH_2O (HEMI)), 4.25-3.9 (m, -CH_2-O), 3.88 (s, MDI CH_2Ar), 3.83 (t, $^3J_{H\text{-}H}$ = 5.2 Hz, NCH_2CH$_2$O (HEMI)), 2.25-1.7 (m, -CH_2-(1,4) and -C*H*-(1,2)), 1.7-1 (m, -CH_2-(1,2)). **ATR-FTIR**: ν_{max} = 3332 (N-H), 3070 (C=C $_{stretch\ 1,2}$), 3050-2780 (C-H), 1702 (C=O), 1595 (C-N), 1521 (Ar C=C), 995 (C=C $_{bending\ 1,2}$), 965 (C=C $_{bending\ 1,4\ trans}$), 907 (C=C $_{bending\ 1,2}$) and 696 (C=C B_1) cm^{-1}.

PPF-HPBD: **SEC** ($CHCl_3$): M_n = 7.3 kDa, M_w = 14.4 kDa, $Đ_M$ = 2.0. **^{1}H NMR** (400 MHz, 298 K, $CDCl_3$): δ = 7.43 (s, C*H*=CHO (FA)), 7.30 (m, Ar), 7.10 (d, $^3J_{H\text{-}H}$ = 7.8 Hz, Ar), 6.58 (s, N*H*), 6.50 (s, N*H*), 6.45 (d, $^3J_{H\text{-}H}$ = 2.9 Hz, CHC*H*=CHO (FA)), 6.38 (s, CC*H*CH (FA)), 5.14 (s, OC*H*C (FA)), 4.16 (m, -CH_2-O HPBD), 3.86 (s, MDI CH_2Ar), 2.25-1.7 (m, -CH_2-(1,4) and -C*H*-(1,2) HPBD), 1.7-1 (m, -CH_2-(1,2) HPBD). 0.92 -0.75 (all remaining protons) ppm. **ATR-FTIR**: ν_{max} = 3344 (N-H), 2998-2830 (C-H), 1704 (C=O), 1598 (C-N), 1532 (Ar C=C), 738 (FA C-H).

PPM-HPBD: **SEC** ($CHCl_3$): M_n = 7.9 kDa, M_w = 15.0 kDa, $Đ_M$ = 1.9. **^{1}H NMR** (400 MHz, 298 K, $CDCl_3$): δ = 7.30 (m, Ar), 7.10 (d, $^3J_{H\text{-}H}$ = 7.8 Hz, Ar), 6.71 (s, C=OC*H*CH (HEMI)), 6.53 (s, N*H*), 4.31 (t,$^3J_{H\text{-}H}$ = 5.2 Hz, NCH$_2$CH_2O (HEMI)), 4.16 (m, -CH_2-O HPBD), 3.88 (s, MDI CH_2Ar), 3.84 (t, ^{3} $J_{H\text{-}H}$ = 5.2 Hz, N**C**H_2CH$_2$O (HEMI)), 2.25-1.7 (m, -CH_2-(1,4) and -C*H*-(1,2) HPBD), 1.7-1 (m, -CH_2-(1,2) HPBD). 0.92 -0.75 (all

remaining protons) ppm. **ATR-FTIR**: ν_{max} = 3344 (N-H), 2998-2830 (C-H), 1704 (C=O), 1598 (C-N), 1532 (Ar C=C), 696 (HEMI C=C B_1) cm^{-1}.

2.4.3 Synthesis of DA-X TPU copolymers

All **DA-X** copolymers were synthesised using a similar method, a typical procedure is as follows using the synthesis of **DA-PCL** as an example: **PPF-PCL** (13.39 g, 5 mmol) and **PPM-PCL** (13.82 g, 5 mmol) were added to a 50 mL glass vial and dissolved in approximately 20 mL of CH_2Cl_2, with continuous stirring until a homogenous solution formed. The solution was then cast into a PTFE-lined petri dish and left in the fume hood overnight for most of the solvent to evaporate. Residual CH_2Cl_2 was removed in a vacuum oven at 40 °C overnight. **DA-PCL** was then reprocessed *via* compression moulding for 10 minutes at 100 °C under 3 MPa of pressure to produce a 1 mm thick elastomeric sheet which was conditioned at 25 °C for 7 days before testing. Note masses required to achieve a 1 : 1 stoichiometry of furan : maleimide functional groups were calculated using the theoretical molar masses for each prepolymer. Theoretical prepolymer molar masses were calculated using OH values to determine the calculated molar mass of polyol + the molar mass of two MDI units + the molar mass of two FA or two HEMI end units, where **PPM-PCL** =2764 $g.mol^{-1}$, **PPF-PCL** = 2678 $g.mol^{-1}$, **PPM-PCL.LA** = 2753 $g.mol^{-1}$, **PPF-PCL.LA** = 2667 $g.mol^{-1}$, **PPM-PBD** = 2879 $g.mol^{-1}$, **PPF-PBD** = 2793 $g.mol^{-1}$, **PPM-HPBD** = 3193 $g.mol^{-1}$, and **PPF-HPBD** = 3107 $g.mol^{-1}$.

DA-PCL: **SEC** ($CHCl_3$): M_n = 36.8 kDa, M_w = 99.7 kDa, $Đ_M$ = 2.7. **^{1}H NMR** (400 MHz, 298 K, $CDCl_3$): δ = 7.30 (d, $^3J_{H\text{-}H}$ = 8.3 Hz, Ar), 7.08 (d, $^3J_{H\text{-}H}$ = 7.3 Hz, Ar), 6.77 (s, C(C)HC*H*=CH (DA)), 6.74 (s, C(C)HCH=C*H* (DA)), 6.57 (s, N*H*), 6.51 (s, N*H*), 5.30 (s, C*H*(O)(CH)(CH) (DA)), 5.13 (s, OC*H*C (FA)), 4.30 (t, $^3J_{H\text{-}H}$ = 5.2 Hz, NCH_2CH_2O (HEMI)), 4.14 (t, $^3J_{H\text{-}H}$ = 6.4 Hz, CH_2OC=O), 4.06 (t, $^3J_{H\text{-}H}$ = 6.7 Hz, CH_2OC=O), 3.96 (s, MDI CH_2Ar), 3.87 (s, NPG CH_2O), 3.03 (s, C*H*(CH)C=O (DA)), 2.90 (s, C*H*(CH)C=O (DA)), 2.30 (t, $^3J_{H\text{-}H}$ = 7.5 Hz, CH_2C=OO), 0.98 (d, $^3J_{H\text{-}H}$= 9.4 Hz, NPG CH_3), 1.65 and 1.38 (all remaining protons) ppm. **ATR-FTIR**: ν_{max} = 3339 (N-H), 2944 – 2865 (C-H), 1721 (C=O), 1598 (C-N), 1531 (Ar C=C) and 1188 (C-O) cm^{-1}

DA-PCL.LA: **SEC** ($CHCl_3$): M_n = 18.6 kDa, M_w = 38.0 kDa, $Đ_M$ = 2.4. **^{1}H NMR** (400 MHz, 298 K, $CDCl_3$): δ = 7.30 (m, Ar), 7.11 (d, $^3J_{H-H}$ = 8.0 Hz, Ar), 6.76 (s, C(C)HC*H*=CH (DA)), 6.73 (s, C(C)HCH=C*H* (DA)), 6.56 (s, N*H*), 6.51 (m, N*H*), 5.31 (s, C*H*(O)(CH)(CH) (DA)), 5.13 (s, OC*H*C (FA)), 4.30 (t, $^3J_{H-H}$ = 5.2 Hz, NCH_2CH_2O (HEMI)), 3.96 (s, MDI CH_2Ar), 3.02 (s, CH(CH)C=O (DA)), 2.90 (s, CH(CH)C=O (DA)), 5.13, 4.15, 4.08, 3.90, 3.88, 3.67, 2.41, 2.31, 1.65, 1.57, 1.53, 1.50, 1.40, 0.99 (all remaining protons) ppm. **ATR-FTIR**: ν_{max} = 3341 (N-H), 2942 – 2866 (C-H), 1729 (C=O), 1599 (C-N), 1532 (Ar C=C), 1310 and 1160 (C-O) cm^{-1}.

DA-PBD: **SEC** ($CHCl_3$): M_n = 37.0 kDa, M_w = 90.0 kDa, $Đ_M$ = 2.4. **^{1}H NMR** (400 MHz, 298 K, $CDCl_3$): δ = 7.30 (m, Ar), 7.10 (d, $^3J_{H-H}$ = 7.8 Hz, Ar), , 6.77 (s, C(C)HC*H*=CH (DA)), 6.74 (s, C(C)HCH=C*H* (DA)),6.50 (s, N*H*), 5.8-5.3 (m, -C*H*=(1,2) and -C*H*=C*H*-(1,4)), 5.17 (s, OC*H*C (FA)), 5.1-4.8 (m, =CH_2(1,2)), 4.33 (t,$^3J_{H-H}$ = 5.2 Hz, NCH_2CH_2O (HEMI)), 4.25-4.0 (m, -CH_2-O), 3.91 (s, MDI CH_2Ar), 3.86 (t, $^3J_{H-H}$ = 5.2 Hz, NCH_2CH_2O (HEMI)), 3.02 (s, C*H*(CH)C=O (DA)), 2.89 (s, C*H*(CH)C=O (DA)), 2.25-1.7 (m, -CH_2-(1,4) and -C*H*-(1,2)), 1.7-1 (m, -CH_2-(1,2)). **ATR-FTIR**: ν_{max} = 3332 (N-H), 3070 (C=C $_{stretch\ 1,2}$), 3050-2780 (C-H), 1702 (C=O), 1595 (C-N), 1521 (Ar C=C), 995 (C=C $_{bending\ 1,2}$), 965 (C=C $_{bending\ 1,4\ trans}$), 907 (C=C $_{bending\ 1,2}$) cm^{-1}.

DA-HPBD: **SEC** ($CHCl_3$): M_n = 26.0 kDa, M_w = 51.0 kDa, $Đ_M$ = 2.1. **^{1}H NMR** (400 MHz, 298 K, $CDCl_3$): δ = 7.30 (m, Ar), 7.10 (d, $^3J_{H-H}$ = 7.8 Hz, Ar), 6.77 (s, C(C)HC*H*=CH (DA)), 6.74 (s, C(C)HCH=C*H* (DA)), 6.53 (s, N*H*), 5.17 (s, OC*H*C (FA)), 4.31 (t,$^3J_{H-H}$ = 5.2 Hz, NCH_2CH_2O (HEMI)), 4.16 (m, -CH_2-O HPBD), 3.88 (s, MDI CH_2Ar), 3.84 (t, ^{3} J_{H-H} = 5.2 Hz, NCH_2CH_2O (HEMI)), 3.02 (s, C*H*(CH)C=O (DA)), 2.89 (s, C*H*(CH)C=O (DA)), 2.25-1.7 (m, -CH_2-(1,4) and -C*H*-(1,2) HPBD), 1.7-1 (m, -CH_2-(1,2) HPBD). 0.92 -0.75 (all remaining protons) ppm. **ATR-FTIR**: ν_{max}= 3344 (N-H), 2998-2830 (C-H), 1704 (C=O), 1598 (C-N), 1532 (Ar C=C) cm^{-1}.

2.4.4 Instrumental methods

Proton (^{1}H) nuclear magnetic resonance (^{1}H NMR) spectra were recorded using a Bruker AV or AVIIIHD 400 MHz spectrometer with the sample fully dissolved in deuterated chloroform ($CDCl_3$). Chemical shifts were recorded in parts per million (ppm) relative to a reference peak of chloroform solvent at

δ = 7.26 ppm. Spectra were analysed on MestReNova v6.0.2. **Attenuated Total Reflectance Fourier Transform Infrared (ATR-FTIR)** spectra were collected on a PerkinElmer FT-Infra-red spectrometer equipped with a UATR Two accessory. Eight scans were taken in the range of 4000 – 400 cm^{-1}. All FTIR-spectra were analysed and automatically baselined corrected using PerkinElmer Spectrum software. **Size Exclusion Chromatography (SEC)** was performed using an Agilent Technologies 1260 Infinity II system equipped with a refractive index detector. Two Agilent PL gel 5 µm Mixed-C columns and a guard column were connected in series and maintained at 35 °C. Approximately 20 mg of sample was dissolved in HPLC grade chloroform eluent (2 mL) containing 0.25 %w/w triethylamine (NEt_3) and filtered through 0.45 µm PTFE filters. The flow rate was set at 1.0 $mL.min^{-1}$. RI and UV detectors were calibrated using a series of near-monodisperse poly(methyl methacrylate) standards. **Differential scanning calorimetry (DSC)** was performed using a TA instruments Discovery DSC 25. Less than 3 mg of sample was accurately weighed on a microbalance and loaded into a T_{zero} aluminium pan. Heating and cooling ramps (from -90 °C to 200 °C) were conducted under a N_2 flow (40 mL min^{-1}) at a standard rate of 10 °C min^{-1}. T_g was taken as the midpoint of inflexion. T_m and T_{rDA} were measured as the temperature at the minimum heat flow of the appropriate endotherms. Analysis was performed on TRIOS v5.1.1 software. For time dependent measurements, samples for 0 days measurements were loaded at 25 °C, heated to 120 °C, held for 1 hour, cooled to -90 °C then heated to 200 °C at a rate of 10 $°C.min^{-1}$. **Dynamic Mechanical Analysis (DMA)** was performed using a TA Instruments Q800 DMA using tensile clamps. Sample dimensions were typically (10 mm length by 5 mm width by 1 mm thickness). Samples were evaluated between -80 °C and 200 °C at a heating rate of 3 $°C.min^{-1}$. A deformation frequency of 1 Hz and a strain of 0.05% were used. **Thermogravimetric analysis (TGA)** was performed on a Pyris 1 TGA by PerkinElmer. Samples of approximately 5 mg were heated from 25 °C to 600 °C at a rate of 10 °C min^{-1} under a N_2 atmosphere. **Uniaxial extension experiments** were carried out on dumbbell specimens which were cut out using a Zwick Roell® knee manual cutting press ZCP 020 with cutting device for ISO 527-2 type 5B die attachment (Length= 35 mm, gauge length = 12 mm, width = 2 mm) on a Zwickiline tensometer according to ISO 527 (10 $mm.min^{-1}$ extension rate). 5

specimens were tested for each material. **Cyclic tensile tests** were conducted up to 200% strain at an extension rate of 10 mm.min^{-1} using 10 hysteresis cycles. 3 specimens were measured for each sample. **Small-Angle (SAXS) and Wide-Angle (WAXS) X-ray Scattering** were performed at ISIS Neutron and Muon Source, Rutherford Appleton Laboratory, Oxfordshire, United Kingdom on a Xenocs Nano-inxider using an X-ray wavelength = 1.541889 Å and an acquisition time = 10 min × 3. **Solid state frequency sweeps** were performed on an Anton Paar MCR502 TwinDrive rheometer, equipped with parallel plates (PP25/TG; d = 25mm) and a lower measuring plate (L-PP25/TG/CTD V2.0 ; 50 mm) using a 0.01% shear strain and a frequency range of 0.01–10 Hz. Temperatures were fixed at 25, 50 and 75 °C using a convection oven (CTD450TD). Polymer disk samples (diameter = 25.0mm and thickness = 1.0 mm) were prepared via vacuum compression moulding and left to cure in ambient conditions for a week before measurement.

2.4.5 Shore A Hardness

Shore A hardness values were measured on 1 mm thick compression moulded sheets using the median value from 5 measurements of the indentation depth at room temperature in compliance with ISO 48-4 or ASTM D2240.

2.5 References

[1] K. R. Albanese, J. R. Blankenship, T. Quah, A. Zhang, K. T. Delaney, G. H. Fredrickson, C. M. Bates and C. J. Hawker, *ACS Polymers Au*, 2023, **3**, 376-382.

[2] W. Wang, W. Lu, A. Goodwin, H. Wang, P. Yin, N.-G. Kang, K. Hong and J. W. Mays, *Prog. Polym. Sci.*, 2019, **95**, 1-31.

[3] S. S. Tallury, K. P. Mineart, S. Woloszczuk, D. N. Williams, R. B. Thompson, M. A. Pasquinelli, M. Banaszak and R. J. Spontak, *J. Chem. Phys.*, 2014, **141**.

[4] G. Holden, R.H. Kricheldorf and P.R. Quirk. *Thermoplastic Elastomers,* 3rd ed. Hanser & Hanser/Gardner - Cincinnati, 2004.

[5] E.H. Backes, S.V. Harb, L. A. Pinto *et al., J. Mater. Sci*, 2024, **59**, 1123-1152.

[6] J. Datta, P. Kasprzyk,.*Polym. Eng. Sci.* 2018, ***58***, E14-E35.

[7] M.S Sánchez–Adsuar, E. Papon and J-J. Villenave, *J. Appl. Polym. Sci,* 2000, ***76*** (10), 1596-1601.

[8] B. Claeys, A. Vervaeck, X. K. Hillewaere, S. Possemiers, L. Hansen, T. De Beer, J. P. Remon and C. Vervaet, *Eur. J. Pharm. Biopharm*., 2015, **90**, 44-52.

[9] H. Laita, S. Boufi and A. Gandini, *Eur. Polym. J*., 1997, **33**, 1203.

[10] L. Feng, Z. Yu, Y. Bian, J. Lu, X. Shi and C. Chai, *Polymer*, 2017, **124**, 48-59.

[11] D. H. Turkenburg, H. Bracht, B. Funke, M. Schmider, D. Janke and H. R. Fischer, *J. Appl. Polym. Sci.*, 2017, **134**.

[12] C. Lakatos, K. Czifrák, R. Papp, J. Karger-Kocsis, M. D. Zsuga and S. Kéki, *Express Polym. Lett*, 2016, **10**, 324-336.

[13] M. Xia, Y. Zhang, Q. Na, T. Guo, M. Zhang, Z. Qi, N. Liu, F. Yang, Y. Luo and W. Yang, *RSC Adv.*, 2021, **11**, 32369-32375.

[14] C. Wu, J. Wang, M. Lan, Z. Wang and Z. Wang, *Prog. Org. Coat.*, 2023, **177**, 107429.

[15] W.-K. Liu, Y. Zhao, R. Wang, F. Luo, J.-S. Li, J.-H. Li and H. Tan, *Chinese J. Polym. Sci*., 2018, **36**, 514-520.

[16] T. Woldbæk, P. Klaboe and C. J. Nielsen*, J. Mol. Struct*, 1975, **27**, 283-301.

[17] F. Orozco, J. Li, U. Ezekiel, Z. Niyazov, L. Floyd, G. M. R. Lima, et al., *Eur. Polym. J*, 2020, **135**,

109882.

[18] C. Tan, T. Tirri and C.-E. Wilen, *Polymers*, 2017, **9**, 184.

[19] A. Degirmenci, G. Yeter Bas, R. Sanyal and A. Sanyal, *Bioconjugate Chem.*, 2022, **33**, 1672-1684.

[20] W. Li, A. J. Ryan and I. K. Meier, *Macromolecules*, 2002, **35**, 6306-6312.

[21] E. Princi, S. Vicini, K. Castro, D. Capitani, N. Proietti, L. Mannina, *Chem. Phys*., 2009, 210, 879-889.
[22] E. Yılgör, İ. Yılgör and E. Yurtsever, *Polymer*, 2002, **43**, 6551-6559.

[23] A. G. Strikovsky, V. V. Zharkov and M. P. Letunovsky, *Macromol. Symp.*, 1995, **94**, 181-188.

[24] Z. Kong, Q. Tian, R. Zhang, J. Yin, L. Shi, W. B. Ying, H. Hu, C. Yao, K. Wang and J. Zhu, *Polymer*, 2019, **185**, 121943.

[25] J. E. Báez, Á. Marcos-Fernández, A. Martínez-Richa and P. Galindo-Iranzo, *Polym.- Plast. Technol*., 2017, **56**, 889-898

[26] S. Lee, P. H. Hong, J. Kim, K. Choi, G. Moon, J. Kang, S. Lee, J. B. Ahn, W. Eom and M. J. Ko, *Macromolecules*, 2020, **53**, 2279-2286.

[27] I. D. Cunningham, A. Brownhill, I. Hamerton and B. J. Howlin, *Tetrahedron*, 1997, **53**, 13473-13494.

[28] L. M. Sridhar, M. O. Oster, D. E. Herr, J. B. D. Gregg, J. A. Wilson, and A. T. Slark, *Green. Chem.*, 2020, **22**, 8669-8679.

[29] P. Du, X. Liu, Z. Zheng, X. Wang, T. Joncheray and Y. Zhang, *RSC Adv.*, 2013, **3**, 15475-15482.

[30] Q. Zhou, Z. Sang, K. K. Rajagopalan, Y. Sliozberg, F. Gardea and S. A. Sukhishvili, *Macromolecules*, 2021, **54**, 10510-10519.

[31] J. Canadell, H. Fischer, G. De With and R. A. T. M. van Benthem, *J. Polym. Sci A. Polym. Chem.*, 2010, **48**, 3456-3467.

[32] M. Dhara, N. Giri, A. Dutta, A. K. Patra, P. U. Sastry, M. S. Ingole and T. Jana, *Polymer*, 2020, **204**, 122807.

[33] S. Terryn, J. Brancart, E. Roels, R. Verhelle, A. Safaei, A. Cuvellier, B. Vanderborght and G. Van Assche, *Macromolecules*, 2022, **55**, 5497-5513.

[34] J. Jiang, Q. Tang, X. Pan, J. Li, L. Zhao, Z. Xi and W. Yuan, *Polymers,* 2021, **13**, 2645.

[35] R. H. Aguirresarobe, S. Nevejans, B. Reck, L. Irusta, H. Sardon, J. M. Asua and N. Ballard, *Prog. Polym. Sci*., 2021, **114**, 101362.

[36] Y. Meng, J. Jiang, and M. Anthamatten, *ACS Macro Lett*, 2015, **4**, 115-118.

[37] C. M. Hartquist, S. Lin, J. H. Zhang, S. Wang, M. Rubinstein and X. Zhao, *Sci. Adv.*, 2023, **9**.

[38] B. Erman and J. E. Mark, in *The Science and Technology of Rubber*, ed. J. E. Mark, B. Erman and C. M. Roland, 4th ed, Academic Press, Boston, 2013, pp. 167–192.

[39] G. L. Gregory and C. K. Williams, *Macromolecules*, 2022, **55**, 2290-2299.

[40] I. M. Ward, in *Mechanical properties of solid polymers* , 2nd ed, Wiley, New York, 1983.

[41] Z. Wang, L. Yuan, F. Jiang, Y. Zhang, Z. Wang, C. Tang, *ACS Macro Lett*., 2016, **5**, 220-223.

[42] L. Wang and X. Wang, in *Fatigue Failure of Textile Fibres*, ed. M. Miraftab, Woodhead Publishing, 2009, pp. 95-132, DOI: https://doi.org/10.1533/9781845695729.2.95.

[43] Z. Wang, L. Yuan, F. Jiang, Y. Zhang, Z. Wang and C. Tang, *ACS Macro Lett*., 2016, **5**, 220–223.

[44] Durometer Shore Hardness Scale Explained | AeroMarine (aeromarineproducts.com) (accessed July 2024).

[45] C. Li, S. L. Goodman, R. M. Albrecht and S. L. Cooper, *Macromolecules*, 1988, **21**, 2367-2375.

[46] A. Feula, X. Tang, I. Giannakopoulos, A. M. Chippindale, I. W. Hamley, F. Greco, C. Paul Buckley, C. R. Siviour and W. Hayes, *Chem. Sci.*, 2016, **7**, 4291-4300.

[47] Y. Chatani, Y. Okita, H. Tadokoro, and Y. Yamashita, *Polym. J,* 1970, **1**, 555-562.

[48] Y.-C. Chien, W.-T. Chuang, U. S. Jeng and S.-H. Hsu, *ACS Appl. Mater. Interfaces,* 2017, **9**, 5419-5429.

3. Structure-Property Relationships of TPUs Containing Diels-Alder Cycloadducts.

3.1 Introduction

The characterisation of structure-property relationships in polymer networks and linear polymers containing thermally reversible Diels-Alder (DA) cycloadducts is essential in order to understand how to access a broad range of material properties for various applications and reprocessing techniques. Three major design parameters have been defined in the literature for DA-containing polymers so far: the concentration of DA-cycloadducts, the degree of functionality of the reactive maleimide and furan groups on the monomers, and the stoichiometric ratio between these reactive groups.[1]

Joost and coworkers reviewed the individual influence of these parameters on the kinetics and the thermomechanical, rheological, and healing properties of amorphous covalent adaptable networks (CANs) based on furan-functionalised polyether amines and *N,N'*-(4,4'-methylene diphenyl) bismaleimide (BMI).[2] They discovered that changing DA-cycloadduct concentration changed the cross-linking density, whilst altering the maleimide-to-furan stoichiometric ratio changed the self-healing rate and properties. Additionally, they established that the temperature of the reversible gel transition could be adjusted by means of the functionality of the reactive groups of the monomers used. Dang *et al.* synthesised semi-crystalline CANs based on furan and maleimide telechelic poly(caprolactone thiourethane)s and a tris-furan cross-linker. They altered the concentration of DA cycloadducts by changing the BMI/furan PCL/tris-furan molar ratio or the PCL-diol molecular weight to achieve an optimised material with high tensile strength (36 MPa) and a healing efficiency of 87% at 70 °C.[3] Reversibly crosslinked poly(1,4-butadiene)s (PBDs) have also been studied, obtained from the reaction of furan telechelic PBDs with various chain lengths and BMI. They found that PBD chain length and cross-link density, (controlled by changing the amount of BMI compound) highly affected material properties.[4]

DA-cycloadducts have also been incorporated into linear polymers.[5] A study by Mayo and Adronov investigated four pairs of bismaleimide and bisfuran monomers prepared from diamines with different spacer chemistries.[6] They obtained films with impressive hardness and adhesion which were spacer

dependant, but all materials were brittle due to short spacer structures, limiting potential applications. Latakos *et al.* researched the effect of poly(ε-caprolactone) (PCL) molecular weight on the thermomechanical properties of thermoplastic polyurethanes (TPUs) containing DA cycloadducts using fufurylamine capped PU prepolymers with BMI, achieving tensile strengths from 6 to 25 MPa and elongations from 26 to 778%.[7] A further study by Yang and coworkers investigated the preparation and characterisation of self-healing furan terminated PBD based on the DA-reaction.[8] Hydroxyl-terminated PBD (HTPB) was copolymerised with excess isophorone diisocyanate (IPDI) to yield NCO terminated prepolymers which were then reacted with furfuryl amine to give the furan-terminated PBDs. These were then reacted with BMI to obtain self-healing binder films, whereby self-healing efficiency and mechanical properties were controlled by adjusting the ratio of -NCO/-OH during the preparation process and the resulting DA-adduct contents. Whilst DA chemistry within linear polymer systems has been studied at length, there has been little research specifically on structure-property relationships of semi-crystalline thermoplastic polyurethanes (TPUs) without the use of BMI as a monomer, which is highly toxic when liberated upon retro Diels-Alder (rDA) and unsuitable for industrial applications.[9]

The mechanical properties of HTPB-based TPUs are often relatively poor in comparison to polyester-based PU elastomers. This is usually a consequence of the poor miscibility of HTPB with polar hard segments, causing unfavourable early phase separations, which negatively influence the formation of segmented block copolymers.[10] Little phase mixing occurs between the hard and soft domains in HTPB-based TPUs typically causing low tensile strengths and elongations at break in the resulting elastomers.[11,12] Researchers have attempted to overcome this, for example Fink *et al.* capped HTPB with 30 and 60 wt.% ε-caprolactone to synthesise amphiphilic triblock copolymers.[13] They discovered that the ε-caprolactone capped PBD samples displayed a more fringed hard phase with better bonding to the continuous phase than the HTPB-based TPUs, which led to higher compatibility between monomers. This achieved a substantial improvement in mechanical properties with tensile strengths between 20-30 MPa and elongations between 400-550% compared to 10 MPa and 100% for the HTPB-

based elastomer. Furthermore, Cui *et al*. synthesised TPU elastomers with one-soft segment: HTPB-PU, polytetrahydrofuran (PTMG)-PU or PCL-PU and bi-soft segment with a mass percentage of 1 : 1 of either PCL : HTPB or PTMG : HTPB using 4,4- methylene diphenyl diisocyanate (MDI) and 1,4-butanediol as raw materials.[14] Their results showed that the incorporation of PCL into HTPB-based TPUs was better than PTMG for promoting microphase mixing and crystallisation, leading to significantly improved mechanical properties over HTPB-PU and similar mechanical properties to PCL-PU. Despite this, to our knowledge no literature study to date has investigated the use of DA-cycloadducts to copolymerise and compatibilise HTPB and PCL soft segments in TPUs. Only linear DA-TPUs with one type of soft segment have been reported up until now.

3.2 Results and discussion

3.2.1 Synthesis and characterisation of PCL XK-M and PCL XK-F PU prepolymers.

The first part of this chapter aims to gain an understanding on how changing PCL diol molecular weight in bismaleimide and bisfuran terminated poly(ester urethane) (PEU) prepolymers affects the thermomechanical and morphological properties of the corresponding TPUs containing DA-cycloadducts (DA-TPUs), specifically for use in recyclable, self-healing elastomer applications.

For this, three neopentyl glycol (NPG) initiated, PCL polyols were used as different length soft segments for DA-TPUs: Capa® 2100J (**PCL-1K**), Capa® 2200J (**PCL-2K**) and Capa® 2400J (**PCL-4K**), with M_n values of 1000, 2000 and 4000 $gmol^{-1}$, respectively. Maleimide (**PCL XK-M**) and furan (**PCL XK-F**) terminated PU prepolymers for each molecular weight PCL polyol (where X = 1, 2 or 4, representing the PCL molecular weight in kDa) were synthesised. Note that **PCL 2K-M** and **PCL 2K-F** were synthesised and characterised previously in chapter 2 named under **PPM-PCL** and **PPF-PCL** but will be included here for comparison purposes. The **PCL-1K** and **PCL-4K** based prepolymers were synthesised in a similar manner to those previously, whereby **PCL-1K** or **PCL-4K** polyol was copolymerised with a two-fold excess of MDI followed by reaction with monofunctional HEMI or FA to afford separate maleimide-

and furan- terminated prepolymers. SEC analysis of the prepolymers shows a modest increase in molecular weight over the starting polyols according to the reactant stoichiometry (***Table 3.1***).

Table 3.1 *SEC analysis of polyols and* ***PCL XK-M*** *and* ***PCL XK-F*** *prepolymers.*

Material	M_n [a] (g.mol^{-1})	M_w [a] (g.mol^{-1})	$Đ_M$ [a]
PCL-1K	1,700	2,600	1.6
PCL 1K-M	6800	13,300	2.0
PCL 1K-F	5600	10,700	1.9
PCL-2K	1,900	3,600	1.9
PCL 2K-M	8000	16,200	2.0
PCL 2K-F	7200	14,400	2.0
PCL-4K	5200	9,600	1.8
PCL 4K-M	13,600	28,500	2.1
PCL 4K-F	13,700	22,300	1.6

[a] *Determined against PMMA standards in $CHCl_3$.*

The HS weight percent ($HS_{wt\%}$) in each prepolymer can be calculated using the equation below adapted from the work of Tsou *et al.*[15]:

$$HS_{wt\%} = \frac{wt_{MDI} + wt_{CE}}{wt_{MDI} + wt_{CE} + wt_{PCL}} \times 100$$

where wt_X represents the mass of each reagent added to the reaction flask This demonstrates that the $HS_{wt\%}$ values decrease with increasing prepolymer molecular weight (***Table 3.2***).

Table 3.2 *$HS_{wt\%}$ values of* ***PCL XK-M*** *and* ***PCL XK-F*** *prepolymers.*

Prepolymer	$HS_{wt\%}$ [a]
PCL 1K-M	28.9
PCL 1K-F	26.4
PCL 2K-M	16.9
PCL 2K-F	15.2
PCL 4K-M	9.2
PCL 4K-F	8.2

[a] *calculated using equation (1).*

^{1}H NMR spectroscopy of the PU prepolymers revealed resonances associated with the aromatic urethane (**G-J**) and maleimide or furan (**L-N**) end-groups, using the ^{1}H NMR spectra of the **PCL-XKF** polymers as examples (***Figure 3.1***). ^{1}H NMR spectra of the and furan-terminated prepolymers also displayed resonances at or δ = 5.16 and 4.17 ppm (**K** and **F'**), corresponding to the methylene groups

of FA and PCL adjacent to a urethane group, showing covalent linkage of FA and PCL to MDI, respectively. The **PCL XK-M** prepolymers also presented resonances at δ = 4.32 and 4.16 ppm, representing covalent linkage of HEMI and PCL to MDI (***experimental***). As the molecular weight of the PCL soft segment (SS) in the **PCL XK-F** prepolymer series increases, the integration values of resonances associated with repeat methylene units of the PCL backbone (**C-F'**) increases, relative to the aromatic urethane and furan end-group integrals (**G-N**), due to a decrease in the $HS_{wt\%}$ values (***Figure 3.1***). The same trend was also obtained for the maleimide functional prepolymers.

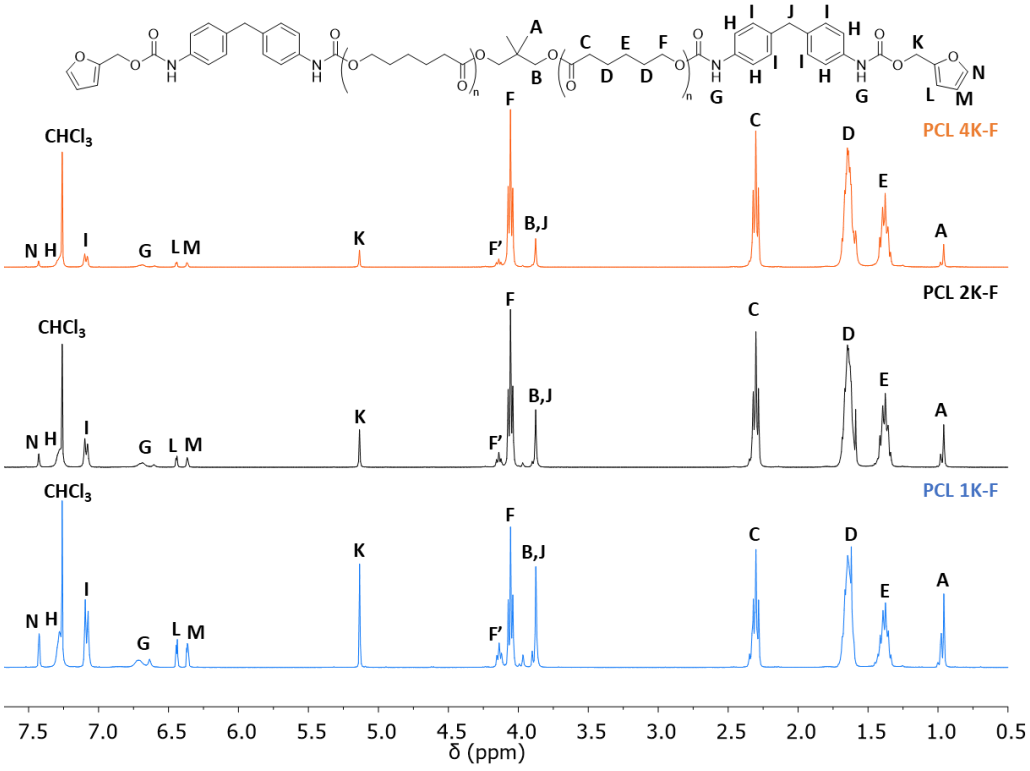

Figure 3.1 *^{1}H NMR spectra of **PCL 1K-F**, **PCL 2K-F** and **PCL 4K-F** (400 MHz, 298 K, $CDCl_3$). Integrals relative to NPG PCL initiator. PCL SS molecular weight increases from bottom to top.*

ATR-FTIR spectroscopy of the **PCL XK-M** and **PCL XK-F** prepolymers in the carbonyl region revealed several differences (***Figure 3.2***). In both prepolymer series the overall area under the FTIR curves increased with increasing PCL wt.% as the contribution of PCL ester carbonyl stretching to the absorbance at ν_{max} = 1720 cm^{-1} increases. As the PCL molecular weight in the **PCL XK-M** prepolymer series decreases, the ratio of maleimide-imide carbonyl stretching at ν_{max} = 1700 cm^{-1} to PCL ester carbonyl stretching at ν_{max} = 1720 cm^{-1} increases. For example, in **PCL 1K-M** the absorbance at ν_{max} =

1700 cm^{-1} dominates, indicating a higher concentration of maleimide functional groups (***Figure 3.2 (A)***). The carbonyl absorbance in the **PCL XK-F** prepolymer series shifted from a double-humped band in **PCL 1K-F** towards a broad single peak with a main absorption at ν_{max} = 1720 cm^{-1} in **PCL 4K-F**, as the amount of PCL ester carbonyls in the prepolymers increases (***Figure 3.2 (B)***).

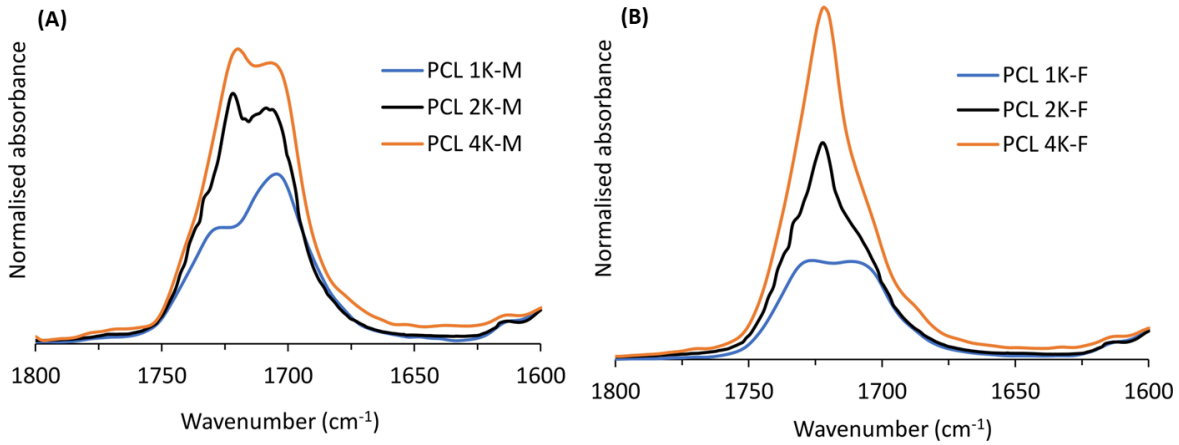

Figure 3.2 *Overlayed ATR-FTIR spectra of* ***(A) PCL XK-M*** *and* ***(B) PCL XK-F*** *prepolymers in the carbonyl region.*

The thermal properties of the **PCL-XK** polyols and the corresponding **PCL XK-F** and **PCL XK-M** PU prepolymers were analysed using DSC (***Figure 3.3*** and ***Table 3.3***). The thermal data showed that as the molecular weight of the **PCL-XK** polyols increased the enthalpy of the PCL melting endotherm (ΔH_{mPCL}) and T_g increased, indicating an increase in the degree of PCL crystallinity and a simultaneous decrease in polymer chain mobility. The DSC thermogram of **PCL-1K** displayed multiple PCL melting endotherms representing heterogeneous PCL order, whilst **PCL-2K** presented a double melting endotherm, with two T_{mPCL} values, implying there are two degrees of PCL order: a highly crystalline (T_{mPCL} > 44 °C) and less ordered PCL chains (T_{mPCL} < 44 °C).[16,17] However, **PCL-4K** only exhibited one T_{mPCL} at 53 °C suggesting a higher degree of PCL order.

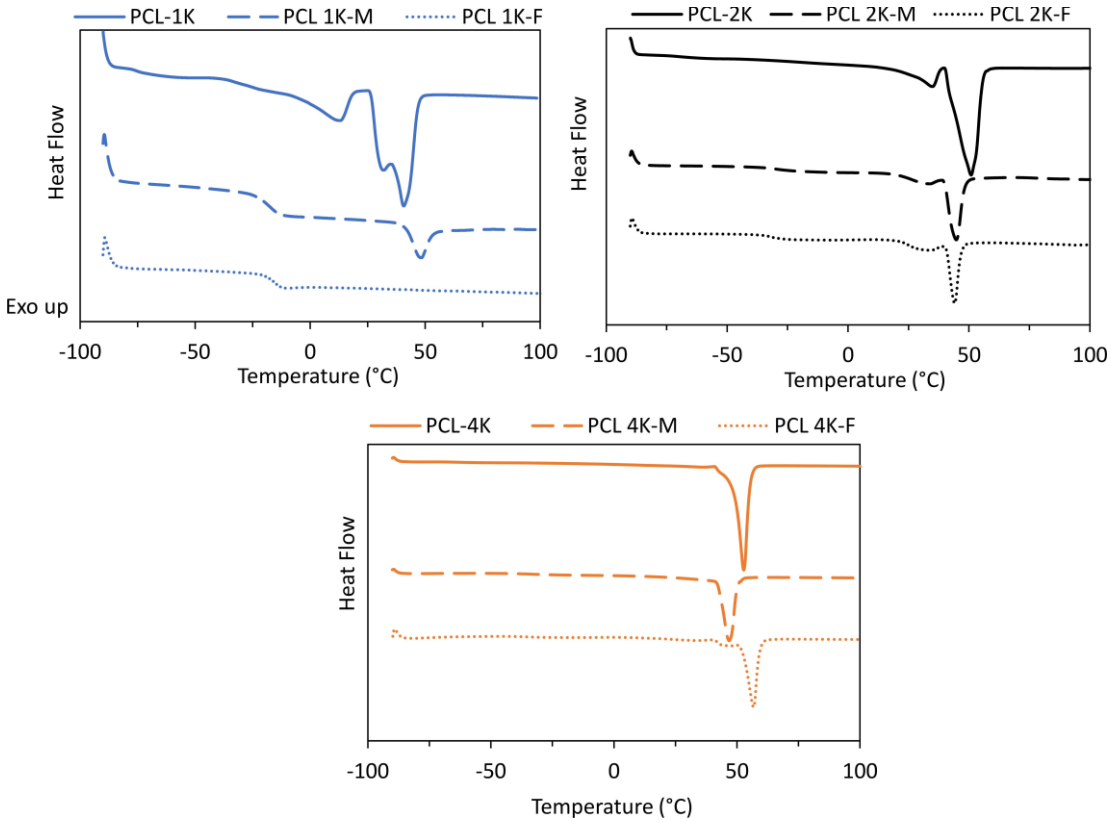

Figure 3.3 *DSC thermograms (1st heating cycles) of* ***PCL-XK*** *polyols compared to* ***PCL XK-M*** *and* ***PCL XK-F*** *prepolymers Exo up. Heating rate of 10 °C.min^{-1}.*

Table 3.3 *DSC thermal data of* ***PCL-XK*** *polyols and corresponding* ***PCL XK-M*** *and* ***PCL XK-F*** *prepolymers.*

Material	T_g [a] (°C)	T_{mPCL} [a] (°C)	ΔH_{mPCL} [a] (J.g^{-1})
PCL-1K	-76	13/31 & 41	67
PCL 1K-M	-18	48	8.8
PCL 1K-F	-17	-	-
PCL-2K	-67	35 & 51	83
PCL 2K-M	-30	32 &45	35
PCL 2K-F	-32	33 & 44	27
PCL-4K	-62	53	89
PCL 4K-M	-35	47	61
PCL 4K-F	-37	32/45 & 57	68

[a] determined from DSC analysis using 1st heating cycles and a 10 °C.min^{-1} heating rate.

DSC analysis revealed that after copolymerisation with MDI and subsequent reaction with monofunctional HEMI or FA the T_g of the **PCL-XK** polyols increased in the prepolymers due to interurethane H-bonding and π-π stacking between MDI phenyl rings which both hinder chain mobility. This relative increase in T_g was greatest for PCL 1K-M and PCL 1K-F, as they contain the highest $HS_{wt\%}$. The DSC thermal data also showed that the ΔH_{mPCL} values of the **PCL-XK** polyols decreased

significantly in the corresponding **PCL XK-M** and **PCL XK-F** prepolymers, revealing that MDI and maleimide or furan end-groups disrupt the order of PCL chains and reduce crystallinity. The relative decrease in ΔH_{mPCL} after copolymerisation increased with increasing $HS_{wt\%}$ and concentration of MDI. The DSC thermograms illustrated that **PCL 1K-F** was amorphous whilst **PCL 1K-M** only displayed a small PCL melting endotherm at 48 °C (ΔH_{mPCL} of 8.8 $J.g^{-1}$). **PCL 2K-M** and **PCL 2K-F** displayed melting endotherms with higher ΔH_{mPCL} values (27-35 $J.g^{-1}$), whilst the **PCL-4K** prepolymers presented the highest ΔH_{mPCL} values (61-68 $J.g^{-1}$), indicating that they contain the highest degree of crystallinity.

3.2.2 Synthesis and characterisation of DA-XKPCL copolymers.

The **DA-1KPCL** and **DA-4KPCL** DA-TPU copolymers were synthesised in a similar manner to **DA-2KPCL** (called DA-PCL in Chapter 2) *via* solvent casting equimolar ratios of the corresponding **PCL XK-M** and **PCL XK-F** prepolymers, followed by solvent removal and subsequent compression moulding to give 1mm thick elastomeric sheets. The sheets were then conditioned for 7 days at ambient temperature before testing to allow the forward DA reaction to equilibrate. **DA-2KPCL** was previously synthesised and characterised in chapter 2 but will be included here for comparison purposes. By altering the PCL SS molecular weight in the PU prepolymers, three **DA-XKPCL** copolymers with different equivalent concentrations of maleimide and furan functional groups (f_g) and thus concentrations of DA-cycloadducts at ambient temperature were obtained (***Table 3.4***).

Table 3.4 *f_g values of* ***DA-XKPCL*** *copolymers.*

Material	f_g (mol.kg^{-1})
DA-1KPCL	0.58
DA-2KPCL	0.37
DA-4KPCL	0.24

Similar to previous DA-TPUs, ^{1}H NMR spectroscopy of **DA-1K-PCL** and **DA-4KPCL** confirmed the presence of weak resonances at δ = 5.32 ppm, corresponding to the C*H*(O)(CH)(CH) protons on the DA cycloadducts (***experimental 3.4.3***). The ^{1}H NMR spectra also exhibited resonances at δ = 3.03 and 2.92 ppm, associated with the two protons C*H*(CH)C=O either side of the N atom from the DA cycloadducts, in line with the characterisation data from the previous chapter.

After conditioning for 7 days at 25 °C, SEC analysis of the **DA-XKPCL** copolymers demonstrated a significant increase in molecular weight over the **PCL XK-M** and **PCL XK-F** prepolymers, confirming successful copolymerisation *via* DA-cycloadduct formation to form linear DA-TPUs (***Table 3.5***).

Table 3.5 *SEC analysis of* ***DA-XKPCL*** *copolymers*.

Material	M_n [a] (g.mol^{-1})	M_w [a] (g.mol^{-1})	$Đ_M$ [a]
DA-1KPCL	34,200	88,400	2.58
DA-2KPCL	36,800	99,700	2.71
DA-4KPCL	39,100	108,500	2.77

[a] *Determined against PMMA standards using $CHCl_3$ as eluent.*

ATR-FTIR spectroscopy showed that after conditioning the **DA-XKPCL** copolymers for 7 days at 25 °C the FTIR band at ν_{max} = 696 cm^{-1} almost disappeared, implying successful maleimide-furan copolymerisation and simultaneous DA-cycloadduct formation (***Figure 3.4***). Comparative FTIR spectra also revealed that increasing the $HS_{wt\%}$ in the **DA-XPCL** copolymers caused an increase in the relative transmittance of FTIR bands at ν_{max} = 3336, 1598 and 1532 cm^{-1} relating to N-H, Ar C=C and C-N stretching in aromatic urethane. On the other hand, the relative transmittance of the PCL ester carbonyl stretching band at ν_{max} = 1720 cm^{-1} decreased with decreasing PCL molecular weight, due to a reduction in the amount of PCL ester carbonyl.

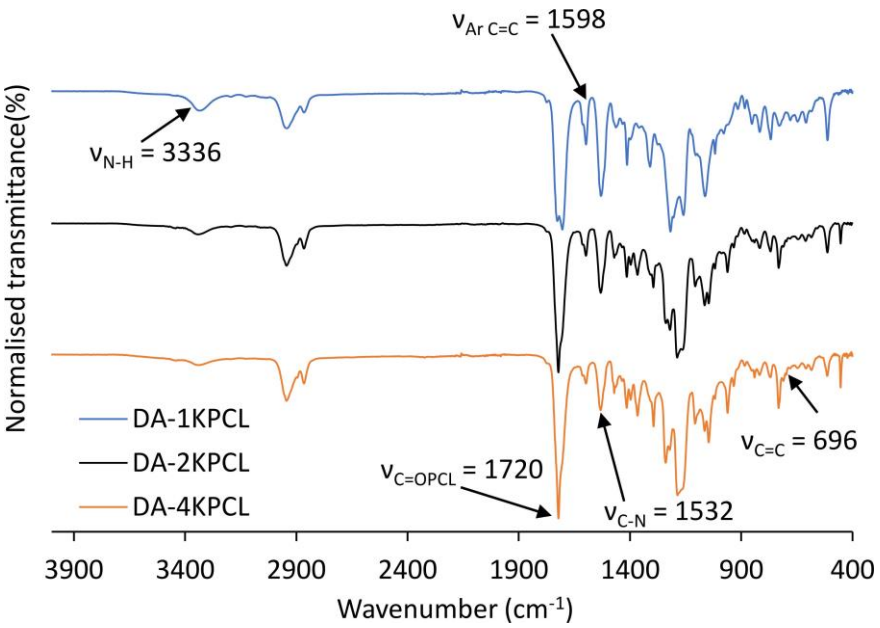

Figure 3.4 *Overlayed FTIR spectra of* ***DA-XKPCL*** *copolymers.*

The DSC thermograms of the **DA-XKPCL** copolymers obtained after conditioning the materials for 7 days at 25 °C revealed characteristic broad, double endotherms between 115 and 147 °C, representing the energy required to break the *endo* and *exo* DA-cycloadducts and induce the rDA reaction (***Figure 3.5***). The thermal data revealed that the T_g of the **DA-XKPCL** copolymers increased with f_g as the $HS_{wt\%}$ and concentration of rigid covalent DA-adducts increased, reducing chain mobility (***Table 3.6***).The ΔH_{rDA} values in the **DA-XKPCL** copolymers increased with increasing DA-TPU f_g, as more energy is required to dissociate the higher concentration of DA-cycloadducts. **DA-1KPCL** was amorphous whilst **DA-2KPCL** and **DA-4KPCL** were semi-crystalline, displaying endotherms for the melting of PCL crystalline segments (ΔH_{mPCL}). The ΔH_{mPCL} of **DA-4KPCL** was over triple that of **DA-2KPCL**, indicating that increasing concentration of DA-cycloadducts hinders the crystallisation of PCL segments.

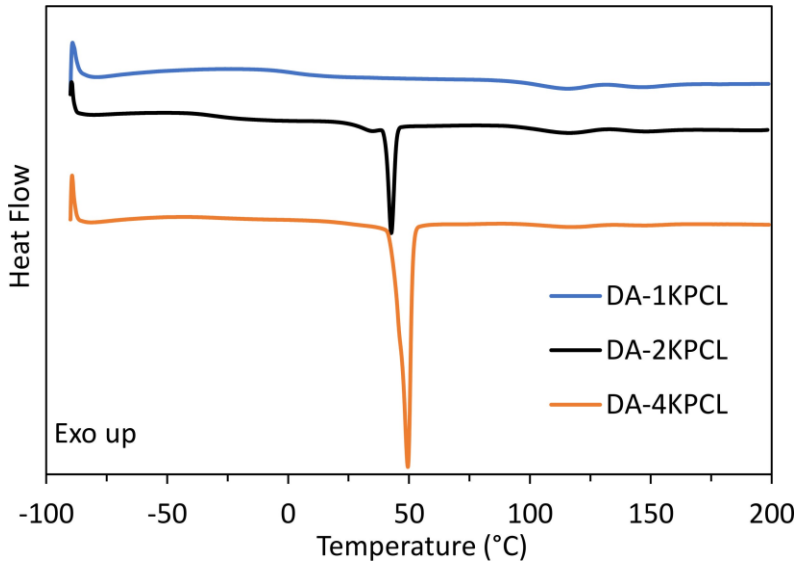

Figure 3.5 *DSC thermograms (1st heating cycles) of* ***DA-XKPCL*** *copolymers. Exo up. Heating rate of 10 °C.min^{-1}.*

Table 3.6 *Thermal data of* ***DA-XKPCL*** *copolymers obtained after 7 days at ambient temperature.*

Copolymer	f_g (mol.kg^{-1})	T_g [a] (°C)	T_{mPCL} [a] (°C)	ΔH_{mPCL} [a] (J.g^{-1})	T_{rDA} [a] (J.g^{-1})	ΔH_{rDA} [a] (J.g^{-1})
DA-1KPCL	0.58	0.8	-	-	115 & 147	16.0
DA-2KPCL	0.37	-32	43	17	117 & 145	8.9
DA-4KPCL	0.24	-38	50	58	115 & 147	4.2

[a]determined from DSC analysis using 1st heating cycles and heating rate of 10 °C.min^{-1}.

Time-dependant DSC experiments were performed on **DA-XKPCL** materials which had been conditioned at 25 °C over time after heating to the rDA temperature (120 °C) for 1 hour to monitor changes in thermal properties (***Table 3.7***).

Table 3.7 *DSC thermal data of all* ***DA-XPCL*** *copolymers obtained over 28 days at ambient.*

Copolymer	**Time** (days)	T_g [a] (°C)	ΔH_{mPCL} [a] (J.g^{-1})	ΔH_{rDA} [a] (J.g^{-1})
DA-1KPCL	0	-3.0	-	6.7
	1	-2.0	-	7.5
	4	-1.8	-	11.5
	7	0.6	-	15.9
	14	0.8	-	16.0
	28	0.7	-	15.8
DA-2KPCL	0	-32	-	4.9
	1	-34	-	5.8
	4	-32	7.3	6.3
	7	-30	17.0	8.9
	14	-23	28.0	9.1
	28	-29	27.0	9.0
DA-4KPCL	0	-36	47.0	0.9
	1	-35	58.4	2.0
	4	-37	58.6	3.6
	7	-36	58.7	4.5
	14	-36	58.5	4.4
	28	-37	58.4	4.6

[a] *obtained via DSC analysis using 1st heating cycles and heating rate of 10 °C.min^{-1}.*

The thermal data of the **DA-XPCL** copolymers showed that the T_g increased over time due to the formation of more rigid DA-cycloadducts, reducing the polymer chain mobility. For all copolymers the ΔH_{rDA} increased over time at ambient temperature until after 7 days, whereby a plateau occurred, showing that maximum DA-cycloadduct conversion was achieved, in line with data from previous chapters (***Figure 3.6***). The ΔH_{rDA} values in the **DA-XPCL** copolymers clearly increased with increasing f_g and DA-cycloadduct concentration.

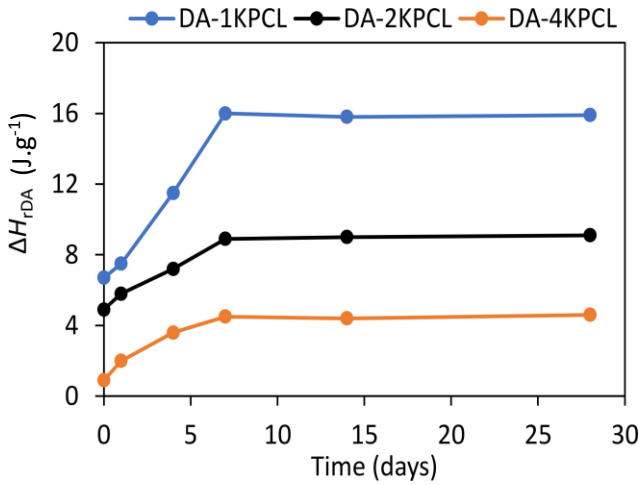

Figure 3.6 *ΔH_{rDA} values measured in* ***DA-XKPCL*** *copolymers against time at ambient temperature obtained from DSC analysis.*

Measuring ΔH_{mPCL} over time revealed that **DA-1KPCL** remained amorphous with no PCL melting endotherm (***Figure 3.7***). In **DA-2KPCL** a melting endotherm for crystalline PCL segments only appeared after 4 days at ambient temperature and it took 14 days for ΔH_{mPCL} to equilibrate, whilst in **DA-4KPCL** a crystalline PCL melting endotherm appeared immediately after heating to 120 °C for 1 hour (0 days) which equilibrated after 1 day at 25 °C. This indicates that **DA-4KPCL** exhibits much faster crystallisation kinetics than **DA-2KPCL**, suggesting that a higher concentration of DA-cycloadducts disrupts PCL crystallinity and suppress crystallisation kinetics.

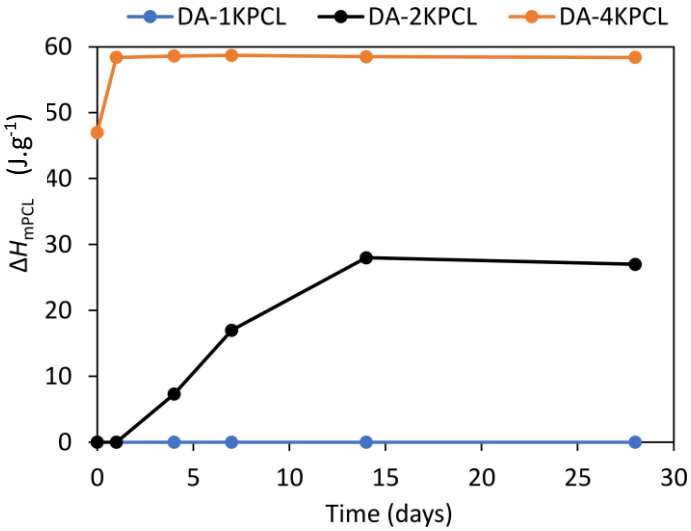

Figure 3.7 *ΔH_{mPCL} values measured in* ***DA-XKPCL*** *copolymers over time at ambient temperature obtained from DSC analysis.*

The **DA-XPCL** copolymers were subjected to DMA to determine their viscoelastic behaviour, where *E'* and tan *δ* were measured as a function of temperature (***Figure 3.8*** and ***Table 3.8***). As the temperature approached the T_g, all three copolymers displayed an initial drop in *E'* with an accompanying maximum in loss modulus (tan *δ*) due to an increase in co-operative mobility.[18] The T_g values of the **DA-XPCL** copolymers increased with increasing f_g and $HS_{wt\%}$, agreeing with DSC analysis. **DA-1KPCL** displayed a noticeably larger area under its tan *δ* curve than **DA-2KPCL** and **DA-4KPCL**, demonstrating that it exhibits superior damping ability, due to its amorphous nature and greater degree of molecular mobility. **DA-4KPCL** displayed the broadest tan *δ* peak.

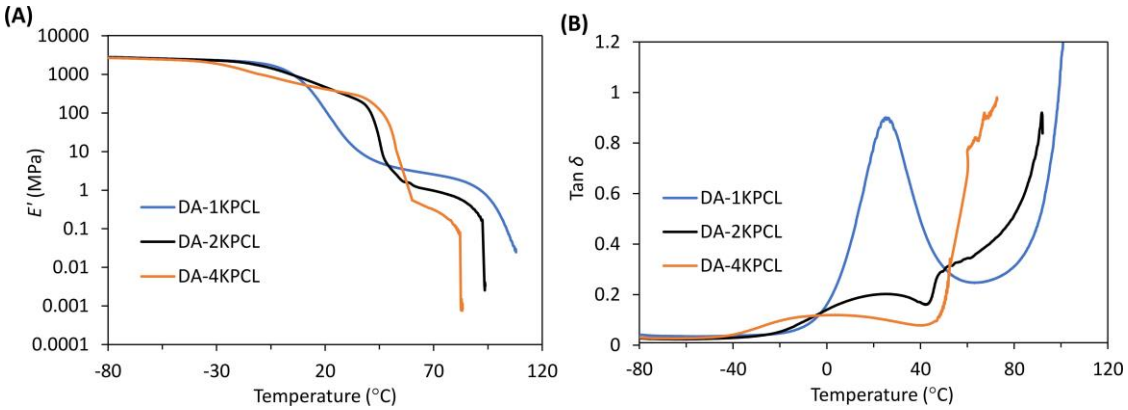

Figure 3.8 *The variation of* ***(A)*** *E' and* ***(B)*** *tan δ with temperature. Obtained via DMA with a heating rate of 3 °C.min^{-1}.*

Table 3.8 *DMA thermal data for* ***DA-XPCL*** *copolymers. Heating rate of 3 °C.min^{-1}.*

Copolymer	f_g (mol.kg^{-1})	*E'* at -60 °C [a] (MPa)	T_g [b] (°C)	*E'* at 20 °C [c] (MPa)	T_{mPCL} [d] (°C)	T_f [e] (°C)
DA-1KPCL	0.58	2640	26.0	116	-	108.0
DA-2KPCL	0.37	2340	25.0	470	40.0	92.0
DA-4KPCL	0.24	2500	3.6	416	48.0	81.0

[a] Storage modulus measured at -60 °C. [b] Measured as peak in tan δ. [c] Storage modulus measured at 20 °C. [d] Measured as the onset of modulus reduction. [e] Measured as onset of viscous flow.

DA-XPCL copolymers displayed similar *E'* values at -60 °C, however **DA-1KPCL** presented a significantly lower *E'* at 20 °C than **DA-2KPCL** and **DA-4KPCL** which contain PCL crystalline regions that can act as physical cross-linking points, making these DA-TPUs behave as though they are crosslinked networks. These crystalline regions also restrict molecular mobility and contribute to the stiffness of the

materials. **DA-2KPCL** and **DA-4KPCL** exhibited step changes in E' at 40 and 48 °C, respectively, representing the melting of semi-crystalline PCL segments (T_{mPCL}). **DA-4KPCL** displayed a higher T_{mPCL} than **DA-2KPCL** agreeing with DSC thermal data. After passing through the T_g or T_{mPCL}, the moduli all of DA copolymers decreased gradually with temperature. between 40-80 °C. The values of E' in this region increased with increasing f_g, demonstrating increased stiffness from the higher concentration of rigid DA-cycloadducts. At higher temperatures (> 80 °C) E' decreased rapidly and tan δ accelerated through unity, representing viscous flow due to the dissociation of DA-cycloadducts in the **DA-XPCL** copolymers and the resulting decreasing in molecular weight.[19] The temperature of viscous flow (T_f) in the **DA-XPCL** copolymers was inversely proportional to the PCL SS molecular weight. This could be a consequence of the higher concentration of DA-adducts together with the higher $HS_{wt\%}$ and degree of HS association *via* non-covalent interactions, synergistically reinforcing the covalent DA-cycloadducts.

The mechanical properties of the three **DA-XPCL** copolymers were evaluated by uniaxial tensile testing at room temperature, comparing the calculated Young's modulus (E_y) (linear regression in the 0-2% strain interval), ultimate tensile strength (σ_b), elongation at break (ε_b) and tensile toughness (U_T), (the total area under the stress-strain curve) (***Figure 3.9*** and ***Table 3.9***). All copolymers displayed stress-strain curves typical of elastomeric behaviour with pronounced strain-hardening at high elongations. **DA2K-PCL** and **DA-4KPCL** exhibited yield points at low strains due to their semi-crystalline nature, giving them significantly higher Young's modulus (E_y) values than **DA-1KPCL**. The tensile strength of the **DA-XPCL** copolymers increased with increasing PCL SS molecular weight, whilst elongation values only slightly reduced. Despite displaying the lowest f_g, **DA-4KPCL** displayed the highest tensile toughness (U_T of 14,200 MPa) nearly 3 times greater than **DA-1KPCL** (U_T of 4980 MPa). This indicates that that the mechanical performance of the DA copolymers was dominated by PCL molecular weight and the resulting degree of PCL crystallinity rather than the concentration of DA-cycloadducts.

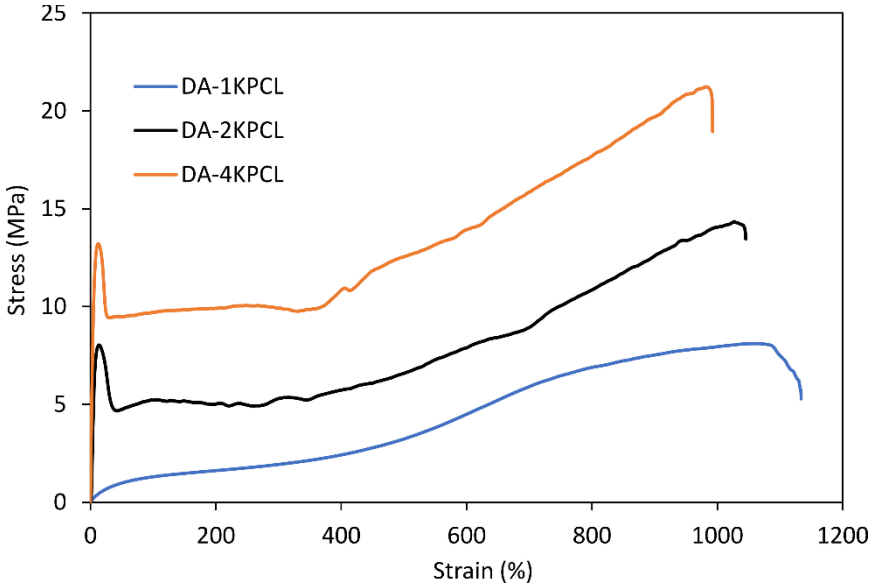

Figure 3.9 *Representative stress-strain curves of* ***DA-XPCL*** *copolymers (10 mm.min^{-1} extension rate).*

Table 3.9 *Mechanical data of* ***DA-X*** *copolymers.*

Copolymer	f_g (mol kg^{-1})	E_y [a] (MPa)	σ_{Max} [a] (MPa)	U_T [a] (MPa)	ε_b [a] (%)
DA-1KPCL	0.58	4.7 ± 0.3	8.0 ± 0.6	4980 ± 304	1130 ± 55
DA-2KPCL	0.37	150 ± 4.0	13.6 ± 0.4	8029 ± 610	1030 ± 43
DA-4KPCL	0.24	178 ± 8.0	20.1 ± 1.0	14,200 ± 1140	993 ± 38

[a] *Determined by uniaxial tensometry using a 10 mm.min^{-1} extension rate. Mean values ± standard deviation from measurements conducted independently on 5 specimens.*

To better assess elasticity, the **DA-XPCL** copolymers were subjected to cyclic tensile testing where each sample was stretched to 200% strain and relaxed at a rate of 10 mm.min^{-1} for 10 elastic cycles (***Figure 3.10***). The first elastic cycle of all DA-TPUs different to subsequent cycles, due to initial energy loss from stress-induced disentanglements of PCL chains. Moreover, the yield points present in the first elastic cycle of **DA-2KPCL** and DA-4KPCL disappeared in the following elastic cycles due to the destruction of the micron to colloidal state semi-crystalline morphologies. Elastic recovery and resilience were calculated as a function of elastic cycle number from the resulting hysteresis curves in the same manner as materials from the previous chapter (***Figure 3.11***). The elastic recovery of the **DA-XPCL** copolymers decreased with increasing PCL SS molecular weight, due to an in the degree of PCL crystallinity and a resulting increase in molecular mobility. The drop in elastic recovery from **DA-2KPCL** to DA-4KPCL is more significant, due to DA-4KPCL containing the highest degree of rigid PCL crystalline

phase. **DA-1KPCL** is amorphous, giving it the best damping properties and therefore the highest elastic recovery. Suprisingly, **DA-4KPCL** displayed the highest resilience *via* cyclic tensile testing, indicating that it has the greatest ability to absorb energy upon elastic deformation and release energy upon unloading. This could be because it contains the lowest cocentration of rigid DA-cycloadducts, leading to a lower T_g (3.6 °C from DMA) relative to **DA-2KPCL** and **DA-1KPCL** (25 and 26 °C, respectively). After the first elastic cycle in **DA-2KPCL** and **DA-4KPCL**, the resilience increased significantly due to the loss of the yield points in their hysteresis curves.

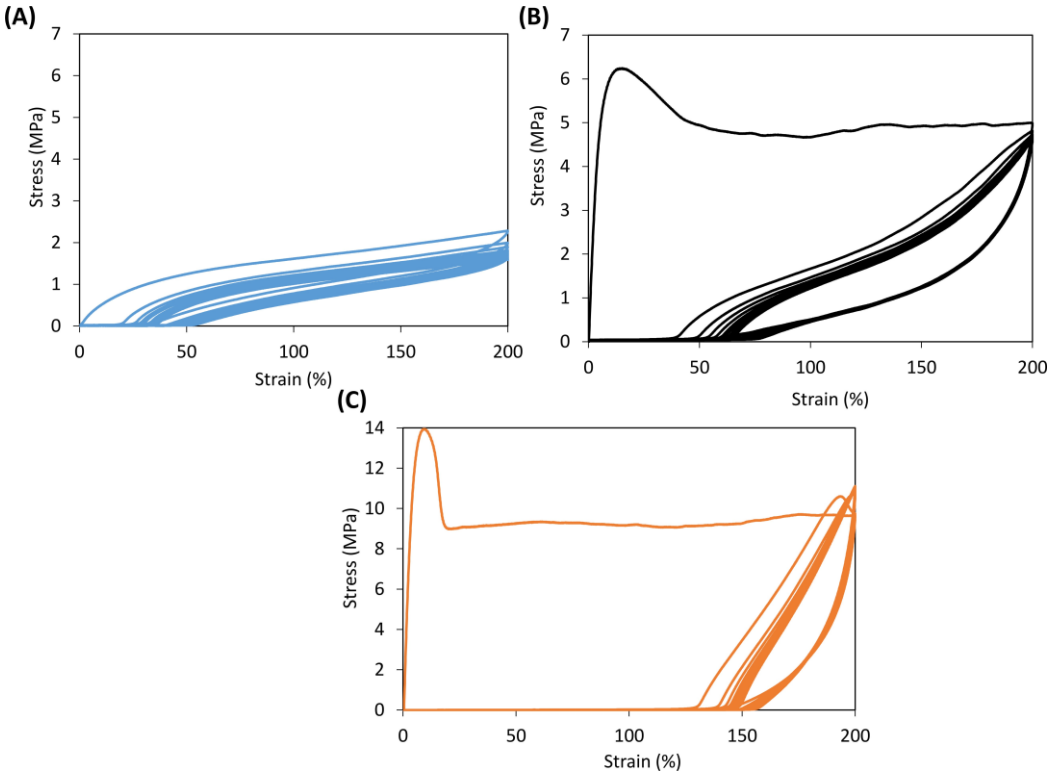

Figure 3.10 *Representative hysteresis curves for* ***(A) DA-1KPCL, (B) DA-2KPCL*** *and* ***(C) DA-4KPCL*** *copolymers up to 200% strain over 10 cycles (10 mm.min^{-1} extension rate).*

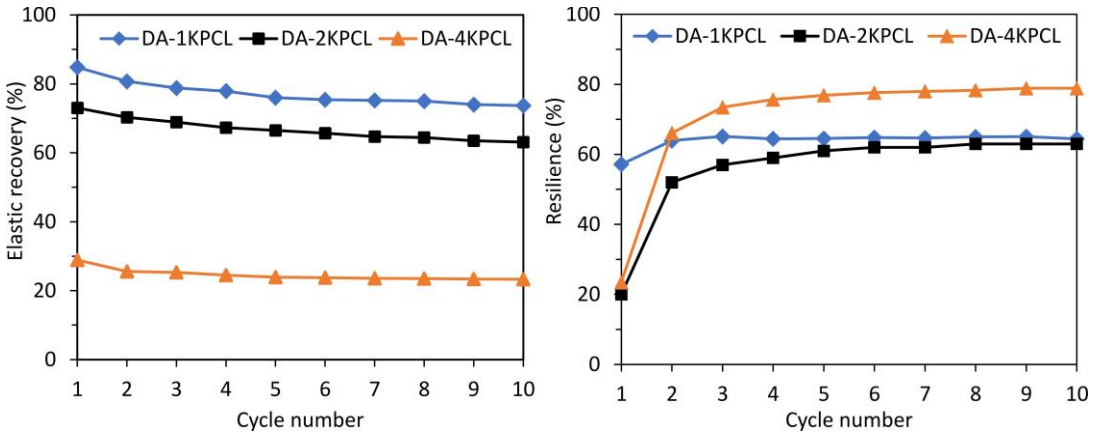

Figure 3.11 *Elastic recovery (left) and resilience (right) of DA-XPCL copolymers as a function of elastic cycle number.*

The morphology of the **DA-XPCL** copolymers was investigated *via* WAXS and SAXS experiments at room temperature (***Figure 3.12***). WAXS analysis showed that all **DA-XPCL** copolymers displayed a broad amorphous peak between 2θ = 10-30°, whilst **DA-2KPCL** and **DA-4KPCL** also presented superimposed sharp diffraction peaks at 2θ = 21.2° and 23.5°, ascribed to crystalline PCL regions.[20] The relative intensity of scattering for these sharp diffraction peaks increased from **DA-2KPCL** to **DA-4KPCL**, indicating an increase in PCL crystallinity with increasing SS molecular weight, in agreement with DSC results.

SAXS analysis demonstrated that **DA-2KPCL** and **DA-4KPCL** produced scattering peaks at similar q_{max} values, corresponding to d-spacings of 185 and 143 Å respectively, likely a result of phase separation from PCL crystallisation. This suggests that they display microdomain structures with a two-phase lamellar morphology- an alternating structure consisting of thin lamellar crystals and amorphous layers, by the crystallisation of PCL blocks.[21] The relative intensity (Iq^2) of this peak was greater for **DA-4KPCL**, confirming that it exhibits a higher degree of nanoscale phase separation from crystallinity than **DA-2KPCL**. **DA-1KPCL** did not display a noticeable scattering peak at similar q_{max} values, further implying that it is amorphous, agreeing with the thermomechanical and WAXS data.

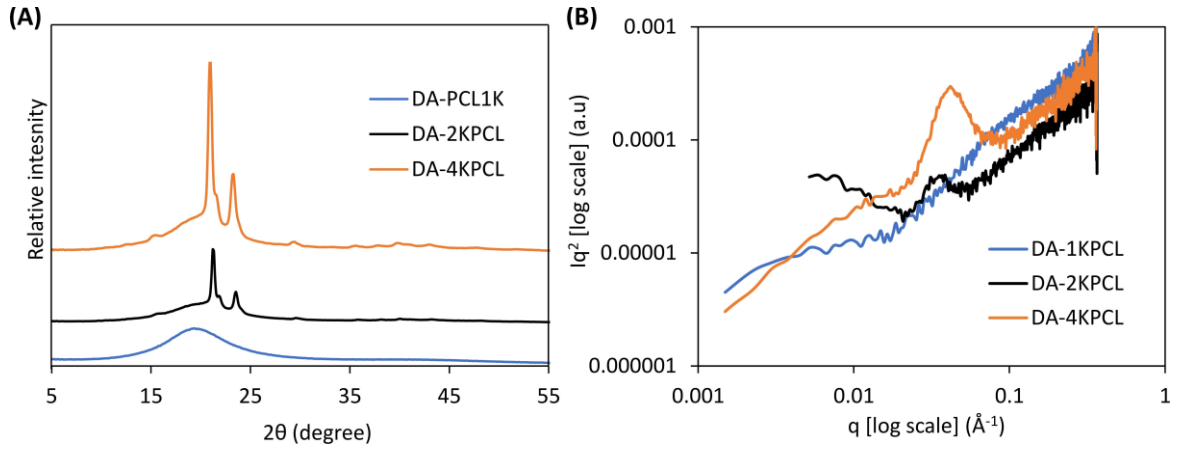

Figure 3.12 *Morphological properties of* ***DA-XPCL*** *copolymers at room temperature.* ***(A)*** *wide-angle X-ray scattering (WAXS) profiles and* ***(B)*** *Lorentz-corrected SAXS plots.*

To ensure that all **DA-XPCL** elastomers were thermally recyclable the samples were reprocessed *via* compression moulding using mild conditions (100 °C at 3 MPa for 10 minutes) and conditioned for 7 days at ambient temperature before remeasurement of tensile properties (R1, ***Figure 3.13***). The process was repeated a further two times with the same samples (R2, R3) to determine any change in mechanical properties. All materials maintained outstanding mechanical properties with high stress-recovery ratios (≥ 85%) after 3 reprocessing cycles.

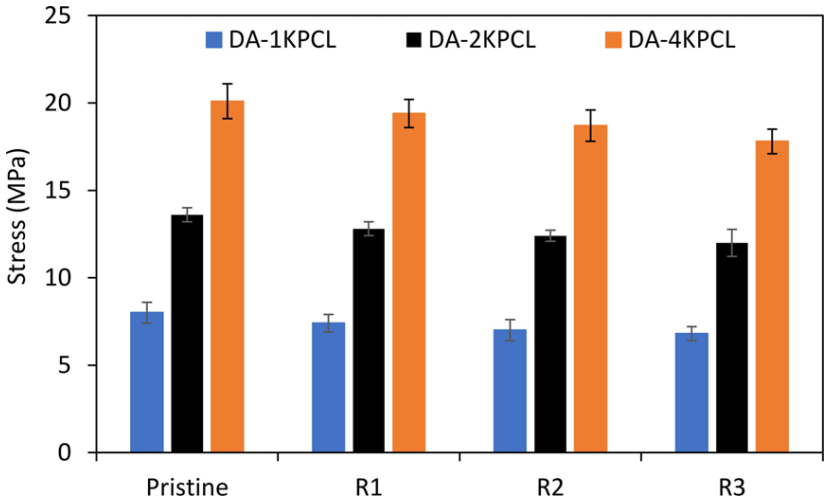

Figure 3.13 *Mean stress values for* ***DA-XPCL*** *copolymers obtained via tensile testing for pristine samples and after 3 reprocessing cycles ± standard deviation from measurements conducted independently on 5 specimens. Samples were left at ambient for 7 days before tensile testing after each cycle.*

3.2.3. Synthesis and characterisation of DA-(PBU-co-PEU) copolymers

Whilst research has been conducted on thermally reversible DA-TPUs containing one type of SS backbone, no literature to date has investigated DA-TPUs incorporating multiple SS backbones. After evaluation of the initial DA-TPUs from Chapter 2, it was determined that **DA-PCL** provided the strongest mechanical properties whilst **DA-PBD** displayed the greatest thermal stability. The second section of this chapter therefore aims to investigate **DA-(PBU-*co*-PEU)** copolymers containing both PBD and PCL SSs *via* copolymerising maleimide- and furan-terminated poly(ε-caprolactone urethane) (PEU) and poly(1,4-butadiene) (PBU) prepolymers. The effect of PBU : PEU composition on the thermomechanical properties of resulting DA-TPUs will be explored.

To achieve this, three **DA-(PBU-*co*-PEU)** copolymers were synthesised, comprising varying amounts of PBU and PEU backbones: **DA-(75PBU-*co*-25PEU)**, **DA-(50PBU-*co*-50PEU)** and **DA-(25PBU-*co*-75PEU)**, containing 75, 50 and 25 wt.% of PBU segments, respectively (***Table 3.10***). **DA-(PBU-*co*-PEU)** copolymers were prepared *via* copolymerisation of maleimide and furan-terminated PEU (**PPM-PCL** and **PPF-PCL**) and PBU (**PPM-PBD** and **PPF-PBD**) prepolymers in different ratios to alter the PBU : PEU composition, whilst maintaining stoichiometric equivalence of furan : maleimide groups. **DA-(PBU-*co*-PEU)** copolymers were compared against DA-TPUs containing 100 wt.% of either PBU or PEU backbone (**DA-100PBU** and **DA-100PEU**), previously referred to as **DA-PBD** and **DA-PCL** in Chapter 2.

Table 3.10 *Compositions of DA-TPU copolymers.*

DA polymer	Wt.% PPM-PBD	Wt.% PPF-PBD	Wt.% PPM-PCL	Wt.% PPF-PCL	Wt.% PBU	Wt.% PEU
DA-100PBU	50	50	0	0	100	0
DA-(75PBU-*co*-25PEU)	25	50	25	0	75	25
DA-(50PBU-*co*-50PEU)	0	50	50	0	50	50
DA-(25PBU-*co*-75PEU)	0	25	50	25	25	75
DA-100PEU	0	0	50	50	0	100

Similar to the previous DA-TPUs, ATR-FTIR spectroscopy of the **DA-(PBU-*co*-PEU)** copolymers after 7 days at ambient temperature revealed low absorption at 696 cm^{-1}, confirming that most maleimide functional groups had successfully copolymerised (***Figure 3.14***) ATR-FTIR spectroscopy also provided

evidence for the different amounts of PBD SS incorporated into the **DA-(PBU-*co*-PEU)** copolymers by analysing the bands appearing at 907, 995, and 3070 cm^{-1}, attributable to the C=C bending vibrations and stretching mode of 1,2-vinyl substitutes in PBD, respectively.[22] The weight % (wt.%) of PBD incorporated into each **DA-(PBU-*co*-PEU)** copolymer can be estimated by comparing the normalised transmittance values for each of these bands to the corresponding value for **DA-100PBU** (***Table 3.11***). This suggests that the average values of PBD incorporation (wt.% PBD_{Av}) calculated from FTIR analysis (70, 44 and 26 wt.%) are close to the corresponding targeted values (75, 50 and 25 wt.%, respectively). Despite this, as the amount of unreacted PBD hasn't been subtracted and cannot be accurately determined, the actual and targeted values should be the same, leading to a flaw in the calculation method.

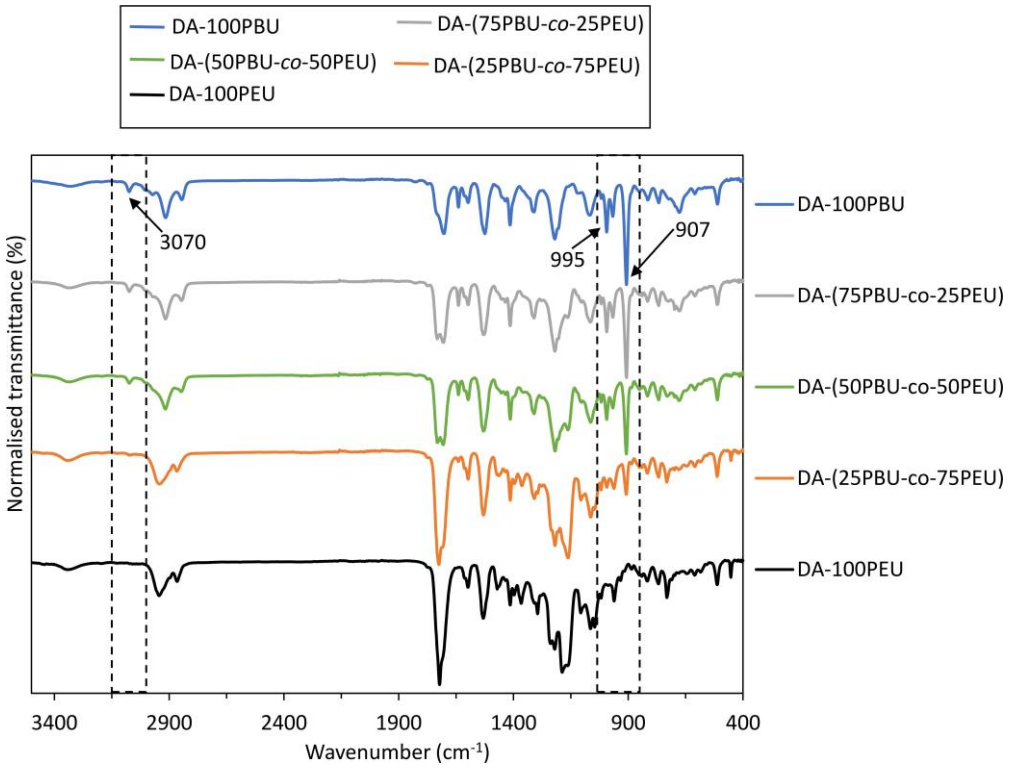

Figure 3.14 *ATR-FTIR spectra of DA copolymers. Peaks normalised against* v_{max} *= 1532* cm^{-1} *from C-N stretching of urethane bonds.*

Table 3.11 *Normalised transmittance values and corresponding wt.% values of PBD in DA polymers using FTIR bands at λ = 3070, 994 and 907 cm^{-1} and average wt.% values.*

DA polymer	T_{3070} [a] (%)	wt.% PBD_{3070}	T_{994} [a] (%)	wt.% PBD_{994}	T_{907} [a] (%)	wt.% PBD_{907}	wt.% PBD_{Av}
DA-100PBU	2.93	100	2.60	100	2.19	100	100
DA-(75PBU-*co*-25PEU)	2.14	73	1.82	70	1.47	67	70
DA-(50PBU-*co*-50PEU)	1.43	48	1.14	44	0.88	40	44
DA-(25PBU-*co*-75PEU)	0.86	29	0.61	23	0.56	26	26
DA-100PEU	0.00	0	0.00	0	0.00	0	0

[a] *Determined by ATR-FTIR spectroscopy, normalised against* λ = 1528 cm^{-1}.

ATR-FTIR spectroscopic analysis of the DA copolymers in the carbonyl region demonstrated that the absorption present at ν_{max} = 1740 cm^{-1} in **DA-100PBU**, representing free urethane carbonyl stretching narrowed and shifted towards ν_{max} = 1720 cm^{-1} as the concentration of PEU backbone and thus PCL ester carbonyls in the DA copolymers increased (***Figure 3.15***)

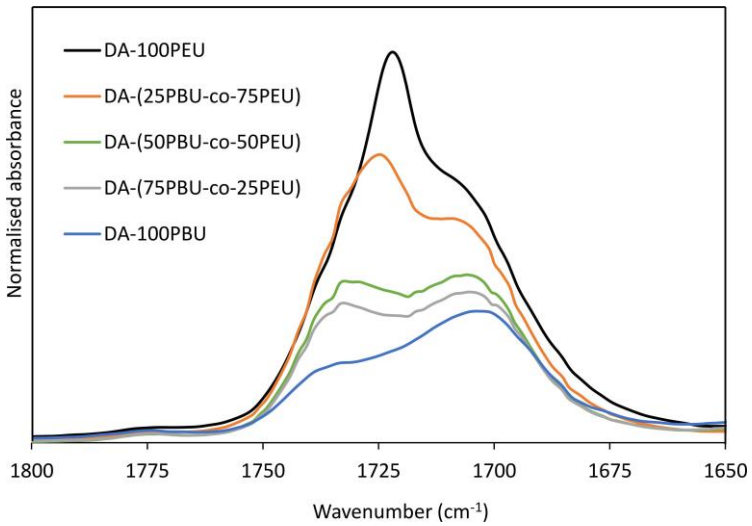

Figure 3.15 *ATR-FTIR spectra of DA copolymers in the carbonyl region. Peaks normalised against $V_{C\text{-}N}$ stretching band in urethane at 1532 cm^{-1}.*

Copolymerisation of maleimide and furan end-groups at ambient temperature resulted in a substantial increase in molecular weight compared to the PEU and PBU prepolymers due to the forward DA reaction and formation of DA-cycloadducts (***Table 3.12***). SEC analysis showed that the molecular weight distributions are remarkably similar for all DA copolymers independent of PBU : PEU composition, achieving high M_n values ranging from 34,000 to 42,000 g.mol^{-1} (***Figure 3.16***).

Table 3.12 *SEC analysis of DA copolymers.*

DA polymer	M_n [a] (g.mol^{-1})	M_w [a] (g.mol^{-1})	$Đ_M$ [a]
DA-100PBU	37,000	90,000	2.4
DA-(75PBU-*co*-25PEU)	38,000	88,500	2.3
DA-(50PBU-*co*-50PEU)	41,700	106,000	2.5
DA-(25PBU-*co*-75PEU)	34,400	118,000	3.4
DA-100PEU	36,800	99,700	2.7

[a] *Determined against PMMA standards using $CHCl_3$ as eluent.*

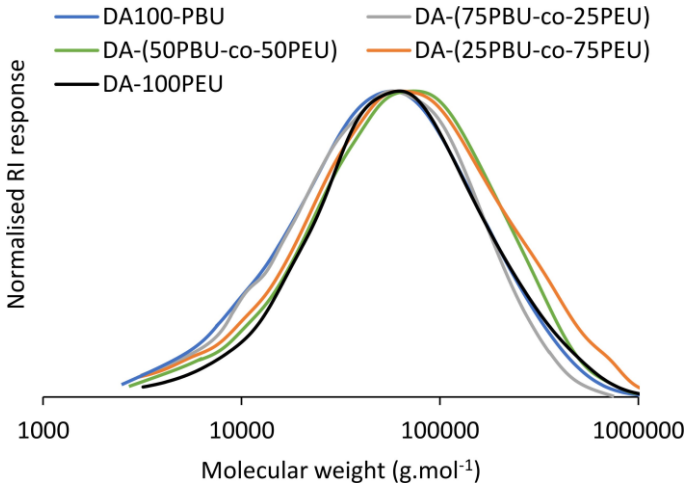

Figure 3.16 *SEC chromatograms of DA copolymers. Molecular weights determined against PMMA standards using $CHCl_3$ as eluent.*

^{1}H NMR spectroscopy of the **DA-(PBU-*co*-PEU)** copolymers revealed the appearance of resonances at δ = 3.03 (**d**) and 2.89 (**e**) ppm, corresponding to the protons either side of the N atom in the DA cycloadducts (-C*H*(CH)C=O-) (***Figure 3.17***). The ^{1}H NMR spectra of the **DA-(PBU-*co*-PEU)** copolymers also demonstrated the incorporation of different concentrations of PBD and PCL SSs.

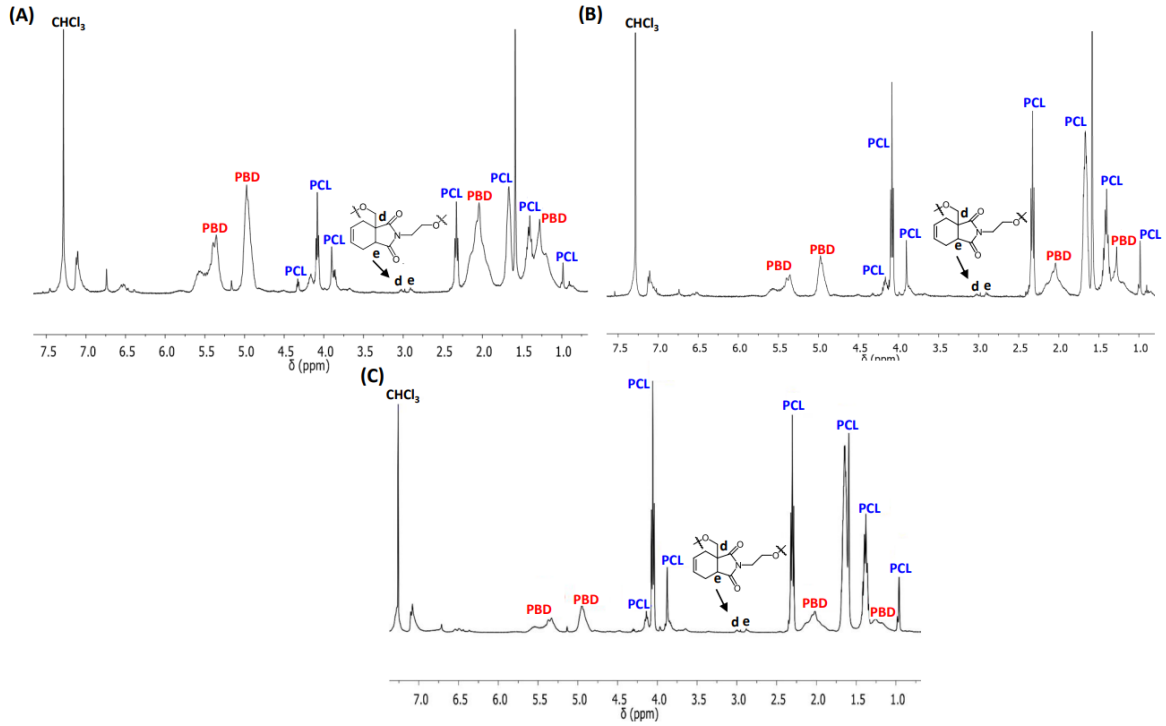

Figure 3.17 *^{1}H NMR spectra of* ***(A) DA-(75PBU-co-25PEU), (B) DA-(50PBU-co-50PEU)*** *and* ***(C) DA-(25PBU-co-75PEU)*** *with DA-cycloadduct and PBD and PCL backbone peaks labelled, (400 MHz, 298 K, $CDCl_3$).*

DSC, TGA and DMA were used to investigate the thermal properties of the **DA-(PBU-*co*-PEU)** copolymers compared to **DA-100PBU** and **DA-100PEU** (***Figure 3.18*** and ***Table 3.15***). DSC analysis revealed that all DA-TPU copolymers displayed low T_g values around -30 °C, whilst **DA-100PBU** also exhibited an upper T_g at 53 °C, likely a result of microphase separation (***Figure 3.18*** **(A)** and ***Table 3.13***). **DA-(25PBU-*co*-75PEU)** was the only **DA-(PBU-*co*-PEU)** copolymer to display a significant PCL melting endotherm at 43 °C, like **DA-100PEU**. At higher PBU contents, in **DA-(50PBU-*co*-50PEU)** and **DA-(75PBU-*co*-25PEU)** the size of the PCL melting endotherm and thus ΔH_{mPCL} decreased significantly. This phenomenon suggests that PBU segments restrict PCL crystallisation and as more PBU segments are incorporated in the **DA-(PBU-*co*-PEU)** copolymers, the SS crystallisation is restricted further.

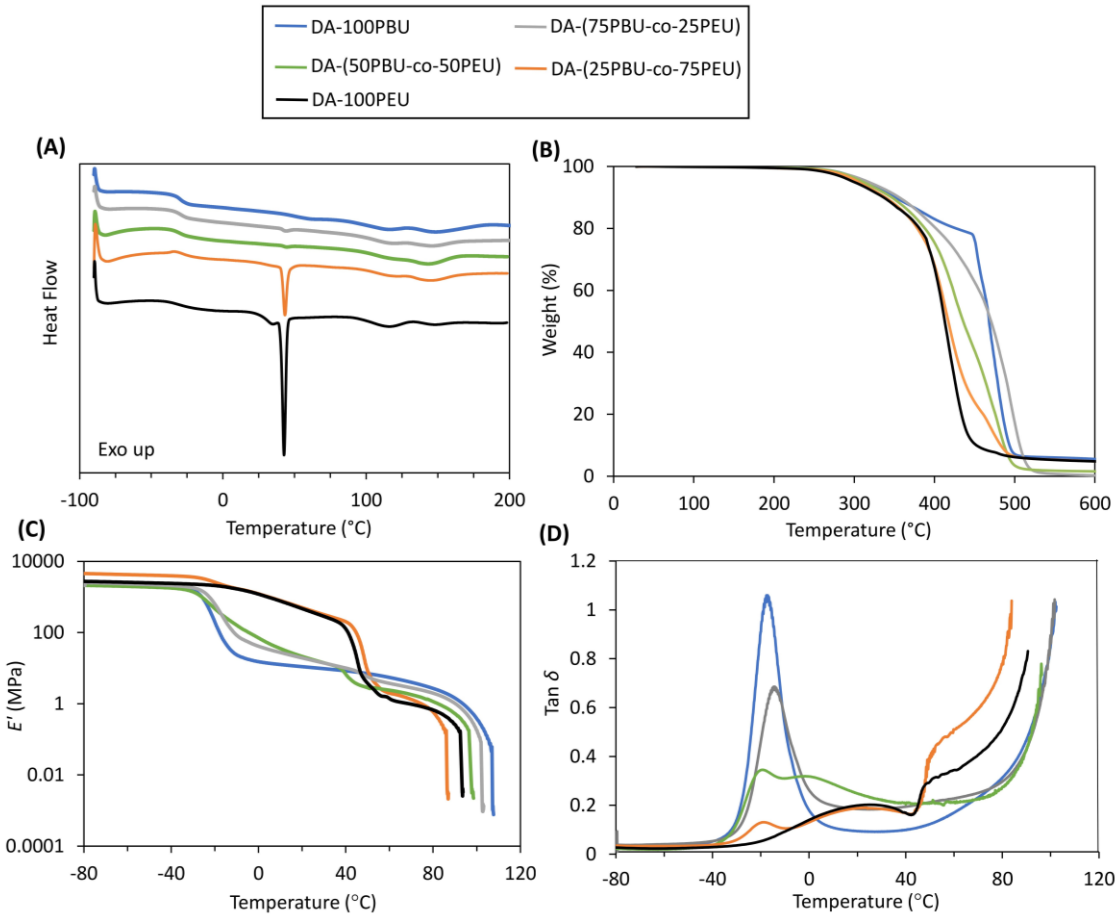

Figure 3.18 *Summary of thermal properties of DA copolymers measured after 7 days at ambient temperature.* ***(A)*** *DSC thermograms (1st heating cycles),* ***(B)*** *TGA curves,* ***(C)*** *E' against temperature DMA plots and* ***(D)*** *tan δ against temperature DMA plots.*

Table 3.13 *DSC thermal data of DA polymers obtained after 7 days at ambient temperature.*

DA polymer	T_g [a] (°C)	T_{mPCL} [a] (°C)	T_{rDA} [a] (°C)	ΔH_{mPCL} [a] (J.g^{-1})	ΔH_{rDA} [a] (J.g^{-1})
DA-100PBU	-30	-	114 & 148	-	11.4
DA-(75PBU-*co*-25PEU)	-30	43	117 & 140	0.1	10.0
DA-(50PBU-*co*-50PEU)	-30	43	118 & 143	0.2	11.0
DA-(25PBU-*co*-75PEU)	-31	43	118 & 143	7.7	11.5
DA-100PEU	-32	35 & 43	117 & 145	17.0	8.9

[a] *obtained via DSC analysis (1st heating cycles) using a heating rate of 10 C.min^{-1}.*

DSC analysis was used to estimate the weight fraction crystallinity of PCL ($X_{c\,PCL}$) in each DA copolymer from the calculated weight fractions (W_{PCL}) together with the experimental ΔH_{mPCL} values

(**experimental equations 1 and 2**). This data confirms that the only DA copolymers which displayed substantial $X_{c\ PCL}$ values were **DA-(25PBU-*co*-75PEU)** and **DA-100PEU** (***Table 3.14***).

Table 3.14 *Crystallinity- based parameters for DA polymers.*

DA Polymer	[a] ΔH_{mPCL} (J.g^{-1})	[b] W_{PCL}	[c] $X_{c\ PCL}$ (%)
DA-100PBU	0	0	0
DA-(75PBU-*co*-25PEU)	0.1	0.18	0.4
DA-(50PBU-*co*-50PEU)	0.2	0.36	0.4
DA-(25PBU-*co*-75PEU)	7.0	0.54	10.5
DA-100PEU	17	0.72	17.0

[a] Determined by DSC (1st heating cycle). [b] Calculated (Equation 2, experimental). [c] Calculated (Equation 1, experimental).

The DSC thermograms of all DA polymers exhibited broad double endotherms from 114 to 148 °C (T_{rDA}), representing the energy required to break the *endo*- and *exo*- DA cycloadducts and induce the rDA reaction. DA-TPU copolymers displayed similar rDA enthalpies (ΔH_{rDA}) between 8.9-11.5 J.g^{-1} as they contain similar concentrations of DA-cycloadducts.

The **DA-(PBU-*co*-PEU)** copolymers were subjected to DMA to compare their viscoelastic properties against **DA-100PBU** and **DA-100PEU** (***Figure 3.18 (B)*** & ***(C)*** and ***Table 3.15***). All DA copolymers displayed an initial drop in *E'* upon transitioning through the T_g as a consequence of increased co-operative mobility. This transition became more pronounced with increasing concentration of amorphous PBU segments, indicating a bigger increase in co-operative mobility. **DA-100PBU** displayed an extensive rubbery plateau above T_g until the temperature of viscous flow (T_f) where a sharp drop in *E'* was observed due to DA-cycloadduct dissociation. Incorporating PEU segments into the DA-TPUs led to a gradual decrease in *E'* above the T_g, until approximately 40 °C where a second drop in *E'* occurred due to the melting of semi-crystalline PCL segments (T_{mPCL}). This change in modulus was only significant in **DA-100PEU** and **DA-(25PBU-*co*-75PEU)**, agreeing with the DSC results. For these materials, the *E'* at 20 °C was high, further confirming that at least 75 wt.% of PEU segments are required for semi-crystalline behaviour to dominate. **DA-(50PBU-*co*-50PEU)** and **DA-(75PBU-*co*-25PEU)** behaved more like **DA-100PBU**, displaying low *E'* values at 20 °C. Above the T_{mPCL}, *E'* stabilised and slowly decreased as temperature increased from 40-80 °C. In this region, the value of *E'* increased with increasing

concentration of **PBU** segments, suggesting enhanced reinforcement from physical interactions associated with microphase separation. At higher temperatures (> 85 °C) the onset of viscous flow occurs as a consequence of the temperature-dependant DA equilibrium shifting towards lower molecular weight prepolymers. The T_f also generally increased with increasing concentration of PBU segments in the DA copolymers, demonstrating increased thermal stability.

The variation of tan δ with temperature indicates the phase behaviour in the materials (***Figure 3.18 (C)***). **DA-100PBU** and **DA-(75PBU-*co*-25PEU)** displayed one tan δ peak at -17 °C and -14 °C, respectively, whilst **DA-100PEU** presented a broad glass transition at 25 °C. **DA-(50PBU-*co*-50PEU)** and **DA-(25PBU-*co*-75PEU)** showed more complex behaviour. In particular, the data for **DA-(50PBU-*co*-50PEU)** suggests partial compatibility with a mixed phase occurring at 2 °C. The value of tan δ for the low temperature peak decreased with decreasing concentration of amorphous PBU segments in the DA copolymers indicating a reduction in damping ability.

Table 3.15 *Viscoelastic properties and T_5% values of DA polymers.*

DA polymer	$T_{g\ lower/upper}$ [a] (°C)	T_{mPCL} [a] (°C)	T_f [a] (°C)	*E' at 20 °C* [a] (MPa)	$T_{5\%}$ [b] (°C)
DA-100PBU	-17/-	-	107	11	314
DA-(75PBU-*co*-25PEU)	-14/-	44	102	19	318
DA-(50PBU-*co*-50PEU)	-19/2	38	97	21	311
DA-(25PBU-*co*-75PEU)	-19/24	43	86	498	305
DA-100PEU	-/25	40	92	470	299

[a] *Determined by DMA.* [b] *Determined by TGA.*

The peak in loss modulus (*E''*) against temperature broadened as the wt.% of PEU segments in the DA-TPU copolymers increases, indicating enhanced compatibility between the more polar SSs and polar HSs comprising MDI and DA-cycloadducts (***Figure 3.19***).

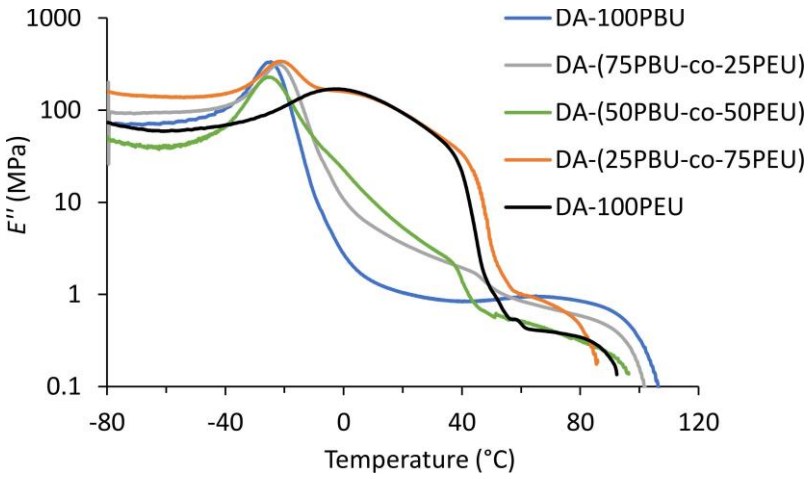

Figure 3.19 *Loss modulus against temperature plots for DA copolymers.*

The mechanical properties of the **DA-(PBU-*co*-PEU)** copolymers were evaluated by uniaxial tensile testing, comparing the calculated Young's modulus (E_y), stress at break (σ_b), strain at break (ε_b) and tensile toughness (U_T) values to the **DA-100PBU** and **DA-100PEU** copolymers (***Figure 3.20*** and ***Table 3.16***).

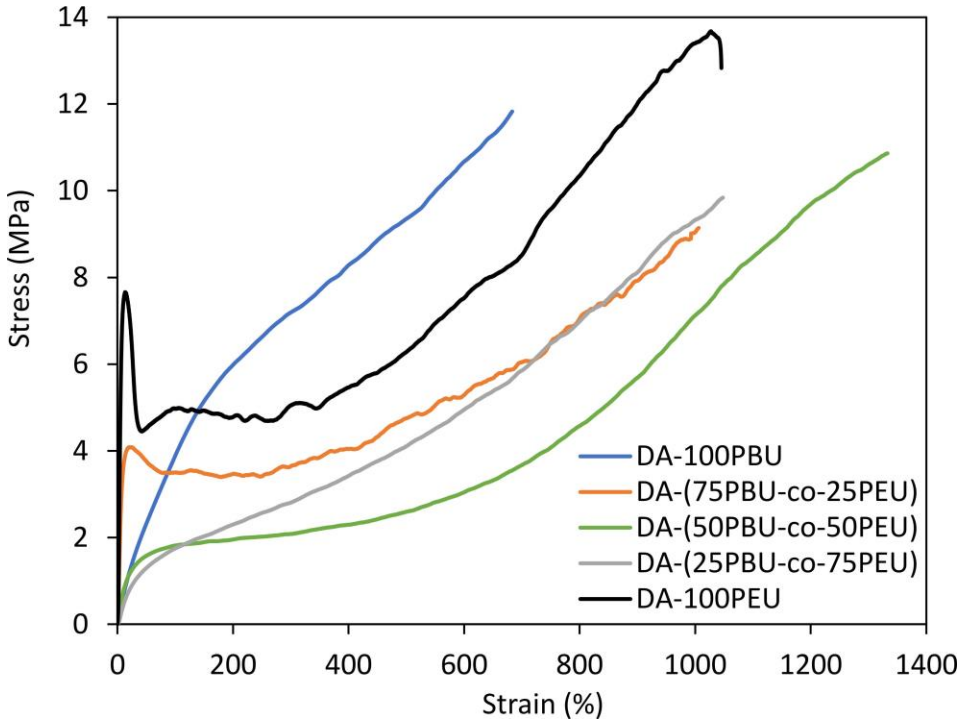

Figure 3.20 *Representative stress strain curves of DA copolymers (10 mm.min^{-1} extension rate).*

Table 3.16 *Mechanical data of DA polymers*

DA polymer	E_y [a] (MPa)	σ_b [a] (MPa)	ε_b [a] (%)	U_T [a] (MPa)
DA-100PBU	6.4 ± 0.4	11.7 ± 0.4	680 ± 32	4980 ± 250
DA-(75PBU-*co*-25PEU)	4.6 ± 0.7	9.8 ± 0.5	1070 ± 68	5190 ± 495
DA-(50PBU-*co*-50PEU)	14.0 ± 0.4	11.2 ± 0.3	1390 ± 83	6810 ± 382
DA-(25PBU-*co*-75PEU)	57.6 ± 3.5	9.5 ± 0.6	1060 ± 54	5880 ± 299
DA-100PEU	147 ± 6.2	13.6 ± 0.4	1030 ± 43	8030 ± 301

[a] *Determined by uniaxial tensometry (10 mm.min^{-1} extension rate). Mean values ± standard deviation from measurements conducted independently on 5 specimens.*

The tensile data revealed that all **DA-(PBU-*co*-PEU)** copolymers exhibited higher elongations at break and tensile toughness values than **DA-100PBU**, demonstrating how incorporating as little as 25 wt.% PEU segments can substantially improve elastomeric properties. **DA-(25PBU-*co*-75PEU)** and **DA-100PEU** displayed high E_y values due to yielding, characteristic of semi-crystalline polymers, whilst **DA-(50PBU-*co*-50PEU)** and **DA-(75PBU-*co*-25PEU)** exhibited low E_y values like **DA-100PBU**, in line with thermal data. There was over a 4-fold increase in E_y from **DA-(50PBU-*co*-50PEU)** to **DA-(25PBU-*co*-75PEU)**, showing that the rubbery PBU phase dominated in **DA-(50PBU-*co*-50PEU)**, whilst the rigid PCL phase dominated in **DA-(25PBU-*co*-75PEU)**. The elastomeric properties of **DA-(50PBU-*co*-50PEU)** were remarkable, displaying a higher σ_b (11.2 MPa), ε_b (1390%) and U_T (6808 MPa) than **DA-(75PBU-*co*-25PEU)** and **DA-(25PBU-*co*-75PEU)**. Moreover, the flexibility of **DA-(50PBU-*co*-50PEU)** was over twice the value of **DA-100PBU** and almost 40% higher than **DA-100PEU**, demonstrating a pronounced synergistic effect. **DA-(75PBU-*co*-25PEU)** and **DA-(25PBU-*co*-75PEU)** displayed similar stress and elongation at break values despite showing very different E_y values. All materials sustained very high tensile strains and displayed strain-induced crystallisation at high elongations, arising from the alignment of polymer chains as the samples are being stretched. This behaviour was most pronounced in **DA-(50PBU-*co*-50PEU)** from 500-1200% strain. *In situ* polarised light microscopy of **DA-(50PBU-*co*-50PEU)** showed initial birefringence, followed by whitening during stretching due to the likely formation of crystallites (***Figure 3.21***)

Figure 3.21 *In situ polarised optical microscopy images of* ***DA-(50PBU-co-50PEU)*** *during stretching showing* ***(A)*** *initial birefringence and* ***(B)*** *whitening.*

To investigate how the PBU : PEU composition effects elasticity, the DA-TPU elastomers were subjected to cyclic tensile testing, where each sample was stretched to 200% strain and relaxed at a rate of 10 $mm.min^{-1}$ over 10 hysteresis cycles (***Figure 3.22***). Elastic recovery, resilience, and residual strain were calculated from the resulting hysteresis curves of each material as a function of cycle number (***Figure* 3.23**). The first elastic cycles differed from subsequent cycles, indicating initial energy loss owing to stress-induced PCL or PBD chain disentanglement. The first elastic cycles of **DA-100PEU** and **DA-(25PBU-co-75PEU)** also exhibited yield points, which were lost in the following elastic cycles, due to plastic deformation of the semi-crystalline PCL segments. **DA-100PBU**, **DA-(75PBU-co-25PEU)** and **DA-(50PBU-co-50PEU)** demonstrated the highest elastic recovery (> 76%) and resilience (> 68%) after the 10 hysteresis cycles as they contain sufficient amorphous PBU segments to improve chain mobility for immediate elastic recovery to occur. Elastic recovery reduced significantly in **DA-(25PBU-co-75PEU)**, confirming that when 75 wt.% of PEU was incorporated, the rigid PCL phase dominated material behaviour, reducing chain mobility.

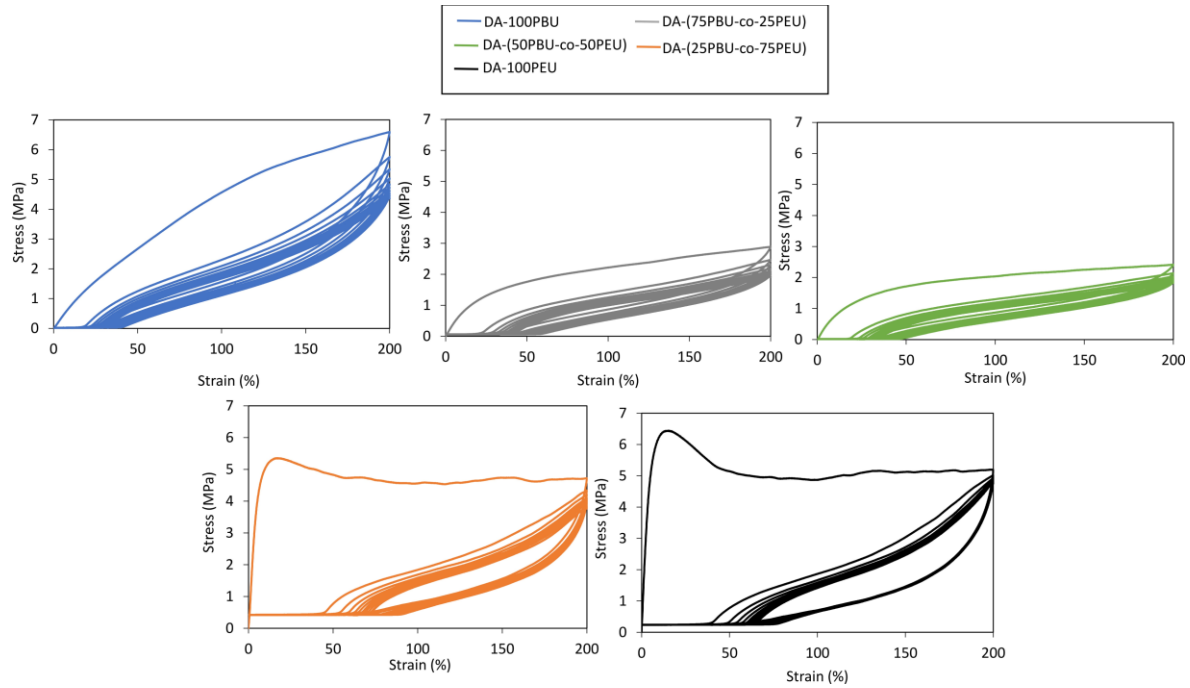

Figure 3.22 *Representative hysteresis curves for DA copolymers up to 200% strain over 10 cycles (10 mm.min^{-1} extension rate).*

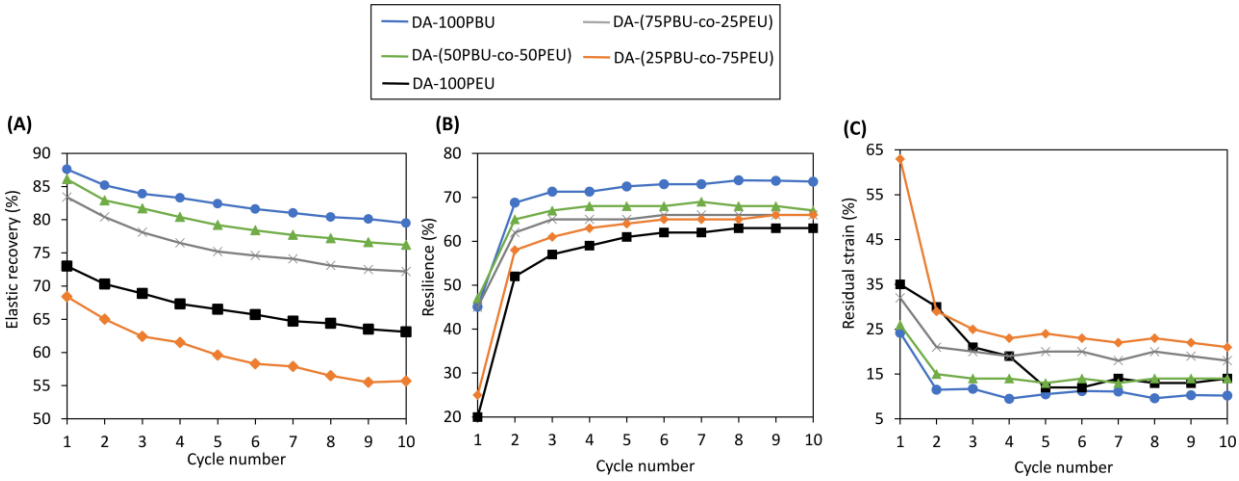

Figure 3.23 *Cyclic tensile testing parameters of DA copolymers as a function of cycle number:* ***(A)*** *elastic recovery,* ***(B)*** *resilience and* ***(C)*** *residual strain.*

To confirm that the DA copolymer elastomers were recyclable, the samples were thermally reprocessed *via* compression moulding using mild conditions (100 °C at 3 MPa for 10 minutes) and subsequently conditioned for 7 days at ambient before remeasurement of the tensile properties (R1, ***Figure 3.24***). The process was repeated a further two times (R2, R3) with the same samples to determine any change in mechanical properties. The results show that all materials maintained excellent mechanical properties with high stress-recovery ratios (> 85%) after 3 reprocessing cycles.

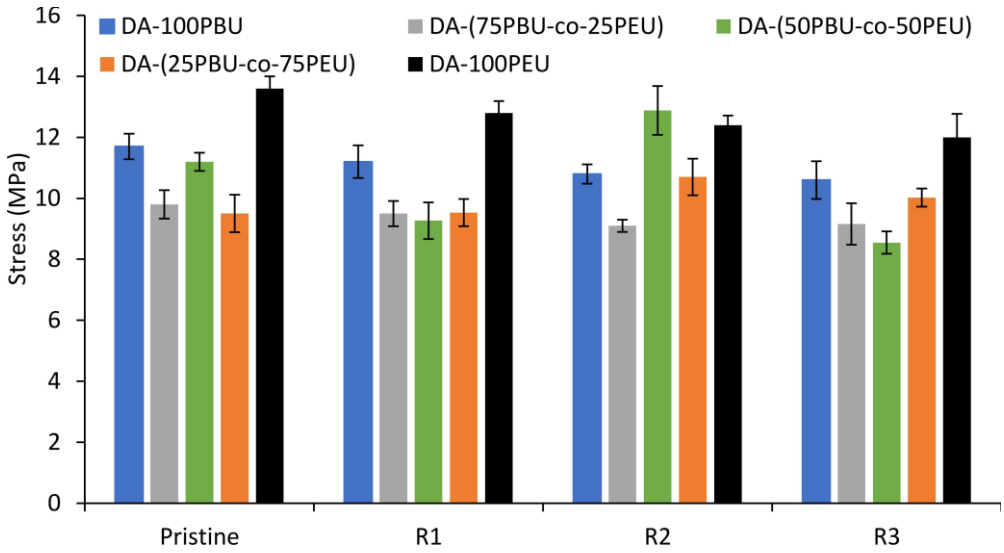

Figure 3.24 *Mean stress values for DA linear polymers obtained via tensile testing for pristine samples and after 3 reprocessing cycles ± standard deviation from measurements conducted independently on 5 specimens. Samples were left at ambient for 7 days before tensile testing after each cycle.*

The further understand the tensile behaviour of the **DA-(PBU-*co*-PEU)** copolymers wide-angle X-ray scattering (WAXS) and small-angle X-ray scattering (SAXS) measurements were carried out at room temperature to characterise the morphology of the materials (***Figure 3.25***).

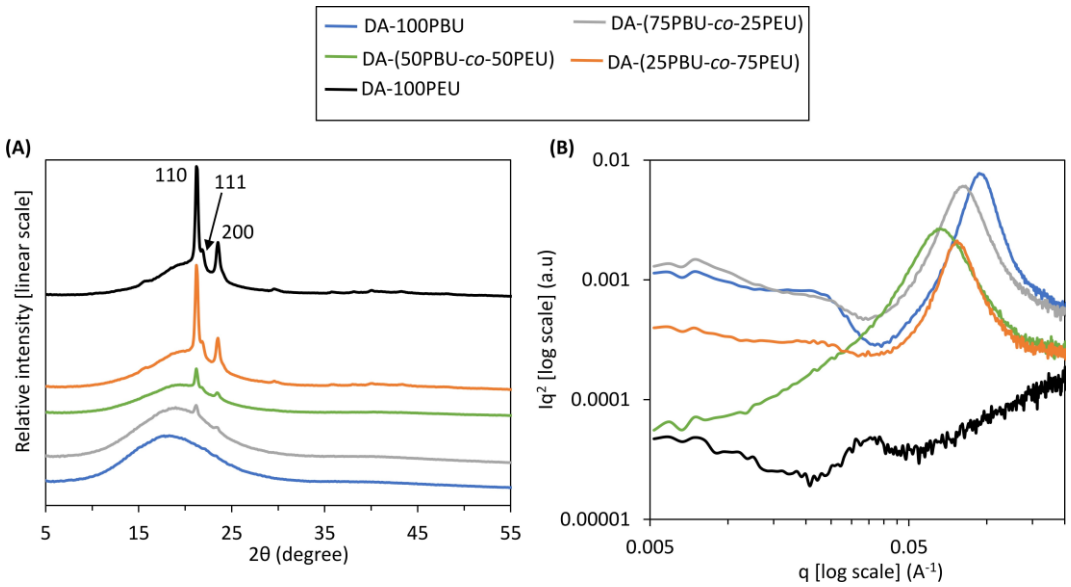

Figure 3.25 (A) *WAXS profiles and* ***(B)*** *Lorentz-corrected SAXS plots of DA copolymers obtained at room temperature.*

All DA copolymers exhibited broad diffraction peaks between 2θ = 10-30° in the WAXS region, corresponding to the mixture of the ordered structure of the HS and the disordered structure of the amorphous phase of the TPUs.[23] When PEU segments were incorporated into the DA copolymers sharp diffraction peaks with Bragg angles of 2θ = 21.2° and 23.5° also appeared, representing the diffraction of the 110 and the 200 lattice planes of semi-crystalline PCL, respectively.[24] The diffraction patterns of the **DA-(PBU-*co*-PEU)** copolymers corresponded to the sum of the patterns for **DA-100PBU** and **DA-100PEU**, demonstrating the existence of PCL crystalline regions in the blends. The intensity of these sharp diffraction peaks and therefore degree of PCL crystallinity can be systematically varied with PBU : PEU composition. The sharp diffraction peaks were only prominent in **DA-100PEU** and **DA-(25PBU-*co*-75PEU)**, supporting the thermomechanical data, by indicating that a critical concentration of 75 wt.% PEU is required for the semi-crystalline nature to dominate in the **DA-(PBU-*co*-PEU)** copolymers. There was no obvious peak shift for the PCL component with PBU : PEU composition, indicating that the interval of lamellar crystals and orientation of the PCL crystal plane was not affected by composition. Similar X-ray diffraction patterns were observed by Turng and coworkers in polyether TPU/PCL blends which were melt compounded *via* a twin-screw extruder and injection moulded at the same ratios used in this work.[25] SAXS analysis demonstrated that all materials apart from **DA-100PEU** produced pronounced scattering peaks, suggesting the formation of a two-phase, lamellar morphology as a result of nanoscale phase separation between non-polar PBD SSs and polar HSs comprising DA cycloadducts. Position of the maximum peak intensity (q_{max}) measured from the Lorentz-corrected one-dimensional SAXS profiles showed that the d-spacing values varied from 66 to 185 Å, depending on PBU : PEU composition (***Table 3.17***).

Table 3.17 *SAXS d-spacing values of DA copolymers.*

DA polymer	[a] d-spacing (Å)
DA-100PBU	66
DA-(75PBU-*co*-25PEU)	77
DA-(50PBU-*co*-50PEU)	95
DA-(25PBU-*co*-75PEU)	81
DA-100PEU	185

[a] *determined from q_{max} values Lorentz-corrected SAXS plots.*

From **DA-100PBU** to **DA-(75PBU-*co*-25PEU)** and then to **DA-(50PBU-*co*-50PEU)**, an increase d-spacing was observed, indicating an increase in the interlamellar distance between TPU hard domains. A reverse trend was found with a further increase in PEU content from **DA-(50PBU-*co*-50PEU)** to **DA-(25PBU-*co*-75PEU)**. The d-spacing was highest in **DA-100 PEU**, where phase separation resulted from PCL crystallisation. **DA-(50PBU-*co*-50PEU)** showed optimal compatibility, with the greatest distance between HS domains *via* SAXS and low PCL crystallinity from WAXS, which may explain why it displays the best elastomeric properties. **DA-(25PBU-*co*-75PEU)** and **DA-(75PBU-*co*-25PEU)** exhibited similar domain sizes (81 and 77 Å, respectively) with comparable distances between hard domains from phase separation, which could explain why the two materials showed similar σ_b, ε_b and U_T values *via* tensile testing despite a large difference in E_y values. Some DA-TPU copolymers displayed additional broad scattering peaks at lower q_{max} values, indicating the presence of HS aggregates with a much larger size (approximately 274 Å) in **DA-100PBU** where the effect is most prominent. Overall, the SAXS and WAXS data show that the tensile behaviour of the **DA-(PBU-*co*-PEU)** copolymers can be attributed to their phase morphology and crystal structure.

3.3 Conclusions

In the first part of this chapter, **DA-XPCL** copolymers comprising PCL SSs with M_n values of 1, 2 and 4 kDA were synthesised *via* the copolymerisation of the corresponding maleimide and furan- terminated PU prepolymers (**PCL X-M** and **PCL X-F**). All **DA-XPCL** copolymers achieved high molecular weights through DA-cycloaddition with M_n values between 35-39 kDa. As PCL SS molecular weight in the **DA-XPCL** copolymers decreased, the f_g (concentration of DA-cycloadducts) and $HS_{wt\%}$ increased, causing an increase in T_g and ΔH_{rDA}, whilst ΔH_{mPCL} decreased. DSC, WAXS and SAXS confirmed that **DA-1KPCL** was amorphous whilst **DA-2KPCL** and **DA-4KPCL** were semi-crystalline, with **DA-4KPCL** displaying a higher degree of PCL crystallinity. DMA revealed that the T_f, crucial for processing, and the damping ability of the **DA-XPCL** copolymers could be increased by increasing the concentration of DA-cycloadducts. All materials exhibited strong mechanical properties with Young's moduli of 4.7-178 MPa, maximum stresses of 8.0-20.1 MPa, ultimate strains of 993-1130% and tensile toughness of

4980-14,200 MPa. PCL crystallinity dominated overall mechanical performance more than DA-cycloadduct concentration. The elastic recovery of the **DA-XPCL** copolymers decreased with increased PCL molecular weight and crystallinity. All materials were mechanically reprocessable using mild conditions *via* compression moulding maintaining strong mechanical properties. This work demonstrates how changing PCL SS molecular weight in DA-TPUs can achieve a broad range of thermomechanical, and morphological properties, meeting specific requirements imposed by different elastomer applications.

For the second part of this chapter, maleimide and furan telechelic prepolymers were prepared by end-group modification of NCO terminated intermediates made from polyols of PBD and PCL. These prepolymers were copolymerised at ambient temperature to produce DA-TPUs, comprising different concentrations of PBU and PEU segments (0, 25, 50, 75 and 100 wt%). The molecular weights of the DA-TPUs obtained were relatively high (37 to 42 KDa) and independent of composition. Copolymerisation was confirmed by the presence of DA-cycloadducts and depolymerisation *via* dissociation was confirmed above 100 °C by a rDA DSC endotherm, reduction in molecular weight and an increase in flow. DA copolymers comprising 75-100% PEU segments exhibited predominately semi-crystalline polymer behaviour. Copolymerisation reduced crystallinity *via* compatibility between the PBD and PCL segments, with compositions comprising 50-100% PBU segments displaying amorphous polymer behaviour. All compositions displayed strain-hardening, whereas Young's modulus decreased with PBU segment concentration. Elastic recovery and resilience were high, especially for compositions comprising at least 50% PBU segments. **DA-(50PBU-co-50PEU)** provided a synergistic effect, combining very high toughness and elongation (compared to **DA-100PBU**) with excellent elastic recovery and resilience (compared to **DA-100PCL**). X-ray scattering indicated that this composition confers optimal compatibility with low crystallinity from WAXS and a long distance between HS domains *via* SAXS. All DA-TPUs could be thermally reprocessed in a facile manner to afford materials with similar mechanical properties. Although the starting PBD and PCL polyols are immiscible, functionalisation and copolymerisation *via* DA cycloadducts enabled compatibilisation resulting in improved mechanical

properties. This facile methodology provides a simple means to provide access to a broad range of material properties from immiscible components, reducing the need to invent new polymers.

3.4 Experimental

3.4.1 Materials.

Polycaprolactone (PCL) diols [Capa® 2100J, Capa® 2200J and Capa® 2400J] with OH values of 113.43, 56.38 and 27.94 mgKOH/g, respectively, were supplied by Ingevity. Poly1,4-butadiene (PBD) diol, [Krasol® LBH-P 2000 (LBH-p)], OH value = 53.53 mgKOH/g was provided by Cray Valley. 4,4'-methylene bis(phenyl isocyanate) (MDI, 98 %), furfuryl alcohol (FA), dichloromethane (DCM), and deuterated chloroform ($CDCl_3$, 99.8 atom % D) were purchased from Sigma-Aldrich. 2-Hydroxyl ethyl maleimide (HEMI) was provided by Henkel Corporation. All materials were used as supplied.

3.4.2 Synthesis of PCL-1K and PCL-4K maleimide or furan-terminated prepolymers.

Polyol (Capa® 2100J for **PCL 1K-M** and **PCL 1K-F** or Capa® 2400J for **PCL 4K-M** and **PCL 4K-F**) (0.039 mol) was loaded into a 4-necked 250 mL flange flask, equipped with an overhead mechanical stirrer, gas inlet and digital thermometer. Vacuum was applied for 1 hour at 90 °C with a stirring rate of 90 rpm. Vacuum was removed and MDI (0.078 mol) was subsequently added at 110 °C under N_2 flow with stirring increased to 180 rpm. After 15 minutes the vacuum was reapplied for 1 hour to allow MDI to react with hydroxy groups. Vacuum was again removed and either FA (0.087 mol) or HEMI (0.087 mol) was added at 120 °C to react with terminal NCO groups. ATR-FTIR spectroscopy showed disappearance of the NCO band after approximately 1.5 hours. The reaction was then switched off and the mixture was decanted while hot to give quantitative yields. Note **PCL 2K-F** and **PCL 2K-M** were previously synthesised and characterised in Chapter 2, named as **PPM-PCL** and **PPF-PCL**.

PCL 1K-F: SEC ($CHCl_3$): M_n = 5.6 kDa, M_w = 10.7 kDa, $Đ_M$ = 1.9.

PCL 4K-F: SEC ($CHCl_3$): M_n = 13.7 kDa, M_w = 22.3 kDa, $Đ_M$ = 1.6.

All PCL XK-F: **^{1}H NMR** (400 MHz, 298 K, $CDCl_3$): δ = 7.43 (s, CH=C*H*O (FA)), 7.30 (m, Ar), 7.10 (d, $^3J_{H\text{-}H}$ = 7.8 Hz, Ar), 6.69 (s, N*H*), 6.60 (s, N*H*), 6.47 (d, $^3J_{H\text{-}H}$ = 2.9 Hz, CHC*H*=CHO (FA)), 6.37 (s, CC*H*CH (FA)), 5.14

(s, ArCH_2O (FA)), 4.14 (t, $^3J_{H\text{-}H}$ = 6.4 Hz, CH_2OC=O), 4.06 (t, $^3J_{H\text{-}H}$ = 6.7 Hz, CH_2OC=O), 3.89 (s, MDI CH_2Ar), 3.89 (s, NPG CH_2O), 2.30 (t, $^3J_{H\text{-}H}$ = 7.5 Hz, CH_2C=OO), 0.98 (d, $^3J_{H\text{-}H}$ = 9.4 Hz, NPG CH_3), 1.65 and 1.38 (all remaining protons) ppm. **ATR-FTIR**: ν_{max} = 3338 (N-H), 2944 – 2865 (C-H), 1722 (C=O), 1597 (C-N), 1528 (Ar C=C), 1295 and 1163 (C-O) cm^{-1}.

PCL 1K-M: SEC ($CHCl_3$): M_n = 6.8 kDa, M_w = 13.3 kDa, $Đ_M$ = 2.0.

PCL 4K-M: SEC ($CHCl_3$): M_n = 13.6 kDa, M_w = 28.5 kDa, $Đ_M$ = 2.1.

All PCL XK-M: **^{1}H NMR** (400 MHz, 298 K, $CDCl_3$): δ =7.30 (m, Ar), 7.10 (d, $^3J_{H\text{-}H}$ = 8.3 Hz, Ar),6.71 (s, C=OC*H*CH (HEMI)), 6.62 (s, N*H*), 6.58 (s, N*H*), 4.32 (t, $^3J_{H\text{-}H}$ = 5.2 Hz, 175 NCH$_2$CH_2O (HEMI)), 4.14 (t, $^3J_{H\text{-}H}$ = 6.4 Hz, CH_2OC=O), 4.06 (t, $^3J_{H\text{-}H}$ = 6.7 Hz, CH_2OC=O), 3.89 (s, MDI CH_2Ar), 3.89 (s, NPG CH$_2$O), 3.85 (t, $^3J_{H\text{-}H}$ = 5.2 Hz, NCH_2CH$_2$O (HEMI)), 2.30 (t, $^3J_{H\text{-}H}$ = 7.5 Hz, CH_2C=OO), 0.98 (d, $^3J_{H\text{-}H}$= 9.4 Hz, NPG CH_3), 1.65 and 1.38 (all remaining protons) ppm. **ATR-FTIR**: ν_{max} = 3341 (N-H), 2944 – 2865 (C-H), 1722 and 1709 (C=O), 1597 (C-N), 1532 (Ar C=C), 1295 and 1164 (C-O) cm^{-1}.

3.4.3 Synthesis of DA-1KPCL and DA-4KPCL copolymers.

For **DA-1KPCL**, **PCL 1K-F** (10.0 g, 5.93 mmol) was solvent casted with **PCL 1K-M** (10.50 g, 5.93 mmol), whilst for **DA-4KPCL**, **PCL 4K-F** (10.0 g, 2.13 mmol) was solvent casted with **PCL 4K-M** (10.18 g, 2.13 mmol) in CH_2Cl_2 at ambient temperature. Masses required to achieve a 1 : 1 stoichiometry of furan : maleimide functional groups were calculated using theoretical molar masses for each prepolymer, (using OH value to determine theoretical molar mass of polyol + the molar mass of two MDI units + the molar mass of two FA or two HEMI end units), where **PCL 1K-F** = 1686 $g.mol^{-1}$, **PCL 1K-M** = 1771 $g.mol^{-1}$, **PCL 4K-F** = 4687 $g.mol^{-1}$ and **PCL 4K-M** = 4773 $g.mol^{-1}$. The correct amounts of **PCL XK-M** and **PCL XK-F** prepolymers were combined in a 50 mL glass vial and dissolved in approximately 20 mL of CH_2Cl_2, with stirring at 25 °C until homogenous solutions formed. The solutions were then solvent cast into PTFE-lined petri dishes and left in the fume hood overnight for most of the CH_2Cl_2 to evaporate. Residual solvent was removed in a vacuum oven at 40 °C overnight. The bulk **DA-1KPCL** and **DA-4KPCL** materials were then reprocessed *via* compression moulding for 10 minutes at 100 °C using 3 MPa of

pressure to produce 1 mm thick elastomeric sheets which were conditioned for 7 days at 25 °C before testing to allow DA-cycloadduct formation.

DA-1KPCL: SEC ($CHCl_3$): M_n = 34.2 kDa, M_w = 88.4 kDa, $Đ_M$ = 2.6.

DA-4KPCL: SEC ($CHCl_3$): M_n = 39.1 kDa, M_w = 108.5 kDa, $Đ_M$ = 2.8.

All DA-XKPCL: ^{1}H NMR (400 MHz, 298 K, $CDCl_3$): δ = 7.30 (d, $^3J_{H\text{-}H}$ = 8.3 Hz, Ar), 7.08 (d, $^3J_{H\text{-}H}$ = 7.3 Hz, Ar), 6.77 (s, C(C)HC*H*=CH (DA)), 6.74 (s, C(C)HCH=C*H* (DA)), 6.57 (s, N*H*), 6.51 (s, N*H*), 5.30 (s, C*H*(O)(CH)(CH) (DA)), 5.13 (s, OC*H*C (FA)), 4.30 (t, $^3J_{H\text{-}H}$ = 5.2 Hz, NCH_2CH_2O (HEMI)), 4.14 (t, $^3J_{H\text{-}H}$ = 6.4 Hz, CH_2OC=O), 4.06 (t, $^3J_{H\text{-}H}$ = 6.7 Hz, CH_2OC=O), 3.96 (s, MDI CH_2Ar), 3.87 (s, NPG CH_2O), 3.03 (s, C*H*(CH)C=O (DA)), 2.90 (s, C*H*(CH)C=O (DA)), 2.30 (t, $^3J_{H\text{-}H}$ = 7.5 Hz, CH_2C=OO), 0.98 (d, $^3J_{H\text{-}H}$= 9.4 Hz, NPG CH_3), 1.65 and 1.38 (all remaining protons) ppm. **ATR-FTIR**: ν_{max} = 3339 (N-H), 2944 – 2865 (C-H), 1721 (C=O), 1598 (C-N), 1531 (Ar C=C) and 1188 (C-O) cm^{-1}.

3.4.4 Synthesis of DA-(PBU-co-PEU) copolymers.

DA-(75PBU-*co*-25PEU), **DA-(50PBU-*co*-50PEU)** and **DA-(25PBU-*co*-75PEU)** containing 75, 50 and 25 wt.% PBU backbone, respectively, were made *via* solvent casting different amounts of the corresponding furan and maleimide terminated PBU and PEU prepolymers in CH_2Cl_2 at ambient temperature whilst maintaining a 1 : 1 furan : maleimide stoichiometry. For **DA-(50PBU-*co*-50PEU)**, **PPM-PCL** (13.82 g, 5 mmol) was solvent casted with **PPF-PBD** (13.97 g, 5 mmol). For **DA-(75PBU-*co*-25PEU)**, **PPF-PBD** (13.96 g, 5 mmol) was solvent casted with **PPM-PBD** (7.20 g, 2.5 mmol) and **PPM-PCL** (6.91 g, 2.5 mmol). For **DA-(25PBU-*co*-75PEU)**, **PPF-PCL** (13.39 g, 5 mmol) was solvent casted with **PPM-PCL** (6.91 g, 2.5 mmol) and **PPM**-PBD (7.20 g, 2.5 mmol). The correct amounts of prepolymers were added to 50 mL vials, dissolved in 20 mL of CH_2Cl_2, and stirred at 25 °C until homogenous solutions formed. The solutions were then cast into PTFE-lined petri dishes and left in the fume hood overnight for most of the CH_2Cl_2 to evaporate. Residual solvent was removed in a vacuum oven at 40 °C overnight. The samples were then reprocessed *via* compression moulding (10 minutes, 100 °C, 3 MPa) to form elastomeric sheets which were conditioned for 7 days at 25 °C before testing.

DA-(75PBU-co-25PEU): SEC ($CHCl_3$): M_n = 38.0 kDa, M_w = 88.5 kDa, $Đ_M$ = 2.5.

DA-(50PBU-co-50PEU): SEC ($CHCl_3$): M_n = 41.7 kDa, M_w = 106.0 kDa, $Đ_M$ = 2.5.

DA-(25PBU-co-75PEU): SEC ($CHCl_3$): M_n = 34.4 kDa, M_w = 118.0 kDa, $Đ_M$ = 3.4.

All DA-(PBU-*co*-PEU): ^{1}H NMR (400 MHz, 298 K, $CDCl_3$): δ = 7.30 (d, $^3J_{H\text{-}H}$ = 8.3 Hz, Ar), 7.10 (d, $^3J_{H\text{-}H}$ = 7.3 Hz, Ar), 6.77 (s, C(C)HC*H*=CH (DA)), 6.74 (s, C(C)HCH=C*H* (DA)), 6.57 (s, N*H*), 6.51 (s, N*H*), 5.8-5.3 (m, -C*H*=(1,2) and -C*H*=C*H*-(1,4) PBD), 5.16 (s, OC*H*C (FA)), 5.1-4.8 (m, =CH_2(1,2) PBD), 4.32 (t,$^3J_{H\text{-}H}$ = 5.2 Hz, NCH$_2$CH_2O (HEMI)), 4.25-4.13 (m, -CH_2-O PBD), 4.08 (t, $^3J_{H\text{-}H}$ = 6.7 Hz, CH_2OC=O PCL), 3.90 (s, MDI CH_2Ar), 3.90 (s, NPG CH_2O), 3.03 (s, C*H*(CH)C=O (DA)), 2.90 (s, C*H*(CH)C=O (DA)), 2.33 (t, $^3J_{H\text{-}H}$ = 7.5 Hz, CH_2C=OO PCL), 2.25-1.7 (m, -CH_2-(1,4) and -C*H*-(1,2 PBD)), 1.7-1 (m, -CH_2-(1,2) PBD), 0.98 (d, $^3J_{H\text{-}H}$= 9.4 Hz, NPG CH_3), 1.65 and 1.38 (all remaining protons) ppm. **ATR-FTIR**= 3345 (N-H), 3070 (C=C $_{\text{stretch 1,2 PBD}}$), 2990 – 2842 (C-H), 1730 and 1702 (C=O), 1600 (C-N), 1524 (Ar C=C) and 1188 (C-O), 995 (C=C $_{\text{bending 1,2PBD}}$), 965 (C=C $_{\text{bending 1,4 trans PBD}}$), and 907 (C=C $_{\text{bending 1,2PBD}}$) cm^{-1}.

3.4.5 Instrumental methods.

Proton (^{1}H) nuclear magnetic resonance (^{1}H NMR) spectra were recorded using a Bruker AV or AVIIIHD 400 MHz spectrometer with the sample fully dissolved in deuterated chloroform ($CDCl_3$). Chemical shifts were recorded in parts per million (ppm) relative to a reference peak of chloroform solvent at δ = 7.26 ppm. Spectra were analysed on MestReNova v6.0.2. **Molecular weights and dipsersities** were determined *via* size-exclusion chromatography (SEC) using an Agilent Technologies 1260 Infinity II system equipped with a refractive index detector. Two Agilent PL gel 5 µm Mixed-C columns and a guard column were connected in series and maintained at 35 °C. Approximately 20 mg of sample was dissolved in HPLC grade chloroform eluent (2 mL) containing 0.25 %w/w triethylamine (NEt_3) and filtered through 0.45 µm PTFE filters. The flow rate was set at 1.0 $mL.min^{-1}$. RI and UV detectors were calibrated using a series of near-monodisperse poly(methyl methacrylate) standards. **Attenuated Total Reflectance Fourier Transform Infrared (ATR-FTIR)** spectra were collected on a PerkinElmer FT-Infrared spectrometer equipped with a UATR Two accessory. Eight scans were taken in the range of 4000 – 400 cm^{-1}. Analysis was performed on PerkinElmer Spectrum software. **Differential scanning**

calorimetry (DSC) was performed using a TA instruments Discovery DSC 25. Less than 3 mg of sample was accurately weighed on a microbalance and loaded into a T_{zero} aluminium pan. Heating and cooling ramps (from -90 °C to 200 °C) were conducted under a N_2 flow (40 mL min^{-1}) at a standard rate of 10 °C min^{-1}. T_g was taken as the midpoint of inflexion. T_m and T_{rDA} were measured as the temperature at the minimum heat flow of the appropriate endotherms. Analysis was performed on TRIOS v5.1.1 software. For time dependent measurements, samples for 0 days measurements were loaded at 25 °C, heated to 120 °C, held for 1 hour, cooled to -90 °C then heated to 200 °C at a rate of 10 °C.min^{-1}. **Dynamic Mechanical Analysis (DMA)** was performed using a TA Instruments Q800 DMA using tensile clamps. Sample dimensions were typically 10 mm length by 5 mm width by 1 mm thickness. Samples were evaluated between -80 °C and 200 °C at a heating rate of 3 °C min^{-1}. A deformation frequency of 1 Hz and a strain of 0.05% were used. **Thermogravimetric analysis (TGA)** was performed on a Pyris 1 TGA by PerkinElmer. Samples of approximately 5 mg were heated from 25 °C to 600 °C at a rate of 10 °C min^{-1} under a N_2 atmosphere. **Monotonic uniaxial extension experiments** were carried out on a Zwickiline tensometer according to ISO 527 (10 mm.min^{-1} extension rate). Dumbbell specimens were cut out of approximately 1 mm thick compression moulded sheets using a ZwickRoell® knee manual cutting press ZCP 020 with cutting device for ISO 527-2 type 5B die attachment. (Length= 35 mm, gauge length = 12 mm, width = 2 mm). Before testing, thickness of each specimen was measured using a digital calliper and recorded on the software. 5 specimens were tested for each material. Results were analysed on TestXpert II software. Cyclic tensile tests were conducted using an extension rate of 10 mm.min^{-1} up to 200% strain using 10 hysteresis cycles. 3 specimens were tested for each material. **Small-Angle (SAXS) and Wide-Angle (WAXS) X-ray Scattering** experiments were performed at ISIS Neutron and Muon Source, Rutherford Appleton Laboratory, Oxfordshire, United Kingdom on a Xenocs Nano-inxider using an X-ray wavelength = 1.541889 Å and an acquisition time = 10 min × 3.

3.4.6 Thermal reprocessing.

For thermal reprocessing pristine dumbbell samples which had been pulled apart *via* uniaxial tensile testing were recompression-moulded with the rest of the chopped up original sheet at 100 °C for 10

minutes using 3 MPa of pressure. This sheet was left for 7 days at ambient temperature before re-cutting of dumbbell specimens using a ZwickRoell® knee manual cutting press and remeasurement of tensile properties *via* uniaxial tensile testing (R1). This process was repeated a further two times (R2, R3) with the same samples to determine any change in mechanical properties.

3.4.7 DSC crystallinity calculations.

DSC was used to estimate the weight fraction crystallinity of PCL ($X_{c\ PCL}$) in each DA copolymer using the following equation:

$$X_{c\ PCL}\ (\%) = \frac{\Delta H_{mPCL}}{w_{PCL}\,\Delta H^{0}_{mPCL}} \text{ X } 100\%$$

Equation 1 *Calculation for weight fraction crystallinity of PCL in DA copolymers.*

where ΔH_{mPCL} is the experimental melting enthalpy of PCL for the DA copolymers, ΔH^{o}_{mPCL} is the enthalpy of melting of 100% crystalline PCL (136 J.g^{-1}) and w_{PCL} is the weight fraction of PCL in the DA copolymers.[26] For 100% PCL-based maleimide and furan- terminated prepolymers (**PPM-PCL** and **PPF-PCL**) the weight fraction of PCL (Wt.%$_{PCL}$) can be calculated ***Equation 2***:

$$\text{Wt.\%}_{PCL} = \frac{\text{Mass of PCL polyol}}{\text{Mass of PCL+Mass of MDI+ Mass of HEMI or FA chain extender}}$$

Equation 2 *Calculation for the weight fraction of PCL in **PPM-PCL** and **PPF-PCL** prepolymers.*

Wt.%$_{PCL}$ was calculated to be approximately 72% in both **PPM-PCL** and **PPF-PCL**. 0.72 was therefore used as the W_{PCL} value in ***Equation 1*** for **DA-100PEU** as it contains 100% PCL SS. To calculate the W_{PCL} in the **DA-(PBU-*co*-PEU)** copolymers, 0.72 was multiplied by the wt.% of **PEU** in each copolymer expressed as a decimal *i.e* for **DA-(25PBU-*co*-75PEU)** it will be 0.72 × 0.75 = 0.54.

3.5 References

[1] S. Terryn, J. Brancart, E. Roels, R. Verhelle, A. Safaei, A. Cuvellier, B. Vanderborght and G. Van Assche, *Macromolecules*, 2022, **55**, 5497-5513.

[2] L. Feng, Z. Yu, Y. Bian, J. Lu, X. Shi and C. Chai, *Polymer*, 2017, **124**, 48-59.

[3] H. H. Dang, T. T. Truong, A. D. S. Nguyen, L. M. T. Nguyen, H. T. Nguyen, T. Q. Nguyen, T. M. Huynh, N. N. Le, T. C. D. Doan, C. M. Dang, L. H. Sinh, N. D. Luong, S. Jukka and L.-T. T. Nguyen, *J. Mater. Sci,* 2022, **57**, 15651-15661.

[4] P. Berto, A. Pointet, C. Le Coz, S. Grelier and F. Peruch, *Macromolecules*, 2018, **51**, 651-659.

[5] J. Stille and L. Plummer, *J. Org. Chem*., 1961, **26**, 4026-4029.

[6] J. D. Mayo and A. Adronov, *J. Polym. Sci. A1*, 2013, 51, 5056-5066.

[7] C. Lakatos, K. Czifrák, R. Papp, J. Karger-Kocsis, M. D. Zsuga and S. Kéki, *Express Polym. Lett.*, 2016, **10**, 324-336.

[8] M. Xia, Y. Zhang, Q. Na, T. Guo, M. Zhang, Z. Qi, N. Liu, F. Yang, Y. Luo and W. Yang, *RSC Adv.*, 2021, **11**, 32369-32375.

[9] X. Liu, P. Du, L. Liu, Z. Zheng, X. Wang, T. Joncheray and Y. Zhang, *Polym. Bull*., 2013, **70**, 2319-2335.

[10] M. Spirkova, *J. Appl. Polym. Sci*. 2002, **85**, 84.

[11] N. S. Schneider, R. W. Matton, *Polym. Eng. Sci.*, 1979, **19**,1122.

[12] E. Yilgör, E. Burgaz, E. Yurtsever, I. Yilgör, *Polymer*, 2000,**41**, 849.

[13] I. Fink, B. Eling, E. Pöselt and G. A. Luinstra, *J. Polym. Sci. Part A: Polym. Chem*, 2018, **56**, 1162-1172.

[14] Y. Cui, H. Wang, H. Pan, T. Yan, and C. Zong, *J. Appl. Polym. Sci*, 2021, **138**, 51346.

[15] C.-H. Tsou, H.-T. Lee, H.-A. Tsai, H.-J. Cheng, and M.-C. Suen, *Polym. Degrad. Stab*, 2013, **98**, 643-650.

[16] P. Cebe and S.-D. Hong, *Polymer*, 1986, **27**, 1183-1192.

[17] D. C. Bassett, R. H. Olley and I. A. M. Al Raheil, *Polymer*, 1988, **29**, 1745-1754.

[18] E. A. Turi, in *Thermal Characterization of Polymeric Materials*, Academic Press, Brooklyn, New York, 2nd Edition, 1981, Volume I., P. 487.

[19] L. M. Sridhar, M. O. Oster, D. E. Herr, J. B. D. Gregg, J. A. Wilson, and A. T. Slark, *Green Chem.*, 2020, **22**, 8669-8679.

[20] Y. Chatani, Y. Okita, H. Tadokoro, and Y. Yamashita, *Polym. J,* 1970, **1**, 555-562.

[21] A. Rohadi, R. Endo, S. Tanimoto, S. Sasaki and S. Nojima, *Polymer*, 2000, **32**, 602-609.

[22] A. Pournaghshband Isfahani, M. Shahrooz, T. Yamamoto, A. Muchtar, M. M. Ito, D. Yamaguchi, M. Takenaka, E. Sivaniah and B. Ghalei, *RSC Adv.*, 2021, **11**, 15449-15456.

[23] K. M. Zia, I. A. Bhatti, M. Barikani, M. Zuber and H. N. Bhatti, *Carbohydr. Polym.*, 2009, **76**, 183-187.

[24] H.-Y. Mi, X. Jing, J. Peng, M. R. Salick, X.-F. Peng and L.-S. Turng, *Cellulose*, 2014, **21**, 2727-2741.

[25] X. Jing, H.-Y. Mi, H.-X. Huang and L.-S. Turng, *J. Mech. Behav. Biomed.*, 2016, **64**, 94-103.

[26] F. B. Khambatta, F. Warner, T. Russell and R. S. Stein, *J. Polym. Sci.: Polym. Phys. Ed.*, 1976, **14**, 1391-1424.

4. PU Covalent Adaptable Networks Comprising Multifunctional Cross-linkers

4.1 Introduction

Thermosets display thermomechanical robustness, in addition to superior chemical, solvent and creep resistance, for high-performance, light-weight applications.[1] Despite this, thermosets remain non-recyclable as they contain irreversible covalent cross-links between polymer chains, meaning they cannot be reprocessed with heat.[2] On the other hand, thermoplastics contain weak Van der Waal's forces between polymer chains, which can be overcome with heat, deeming them reprocessable. This does however mean that they lack dimensional stability.[3] Vulcanised natural rubber has been extensively used for tyres whilst poly(dimethylsiloxane) (PDMS) has been widely used for electrical insulation as they are very tough and solvent-resistant materials.[4-5] Over the past decade huge efforts have been made to bridge the gap between thermosets and thermoplastics, due to the strong incentive to make relevant industrial applications more sustainable.

Covalent adaptable networks (CANs) have become a popular solution within the literature, as they contain dynamic covalent bonds which can respond to stimuli, such as light or heat, to enable bond exchange or dissociation, when the stimulus is applied. This allows flow and facile reprocessing upon demand but in principle they can retain their thermomechanical stability and solvent resistance when the stimulus is removed, due to the reformation of covalent bonds or elimination of bond exchange.[6] This endows CANs with self-healing and recycling properties, making them a promising candidate for bridging the gap between thermosets and thermoplastics for use in various industrial applications.[7]

There are two types of CANs: associative CANs which undergo bond exchange under certain stimuli to enable network topology rearrangements but maintain the same cross-link density and dissociative CANs which undergo bond dissociation under exposure to a certain threshold level of a stimulus, causing a loss of network integrity and a sol-gel transition.[1,8] Diels-Alder (DA) chemistry has become a popular choice of dissociative CAN chemistry, specifically the furan-maleimide diene-dienophile pairing, which was pioneered by Fred Wudl and coworkers back in 2002.[9] Since then, extensive literature has been published on the use of DA-CANs in various applications, such as self-healing and

recyclable adhesives,[10-12] elastomers,[13-15] and composites.[16-18] Whilst the chemistry platform of CANs is well developed, a recent perspective has highlighted the need for better understanding of material behaviour, including structure-property relationships.[19]

Both industrial applications and reprocessing techniques impose specific requirements, which in principle could be met by the large tunability of material properties in DA-based networks. Understanding structure-property relationships of DA-polymers is therefore essential to achieve such material properties. Most structure-property relationship studies associated with DA-CANs published in the literature are incomplete or not systematic, with more than one variable changing at once. However, some thorough studies within DA CANs exist. For example, Brancart *et al.* investigated structure-property relationships of self-healing polymer networks based on DA chemistry, by reacting different molecular weight and functionality furan-functionalised polyether amines with *N,N'*-(4,4'-methylene diphenyl) bismaleimide (BMI). [20] They found that mechanical properties of DA-CANs could be altered by changing the DA-cycloadduct concentration, whilst self-healing speeds could be tuned *via* the stoichiometric ratio between maleimide and furan groups. Moreover, they discovered that the temperature of gelation (T_{gel}), crucial for processing, could be varied with the degree of functionality of the reactive maleimide and furan groups on the monomers. Furthermore, Raffa and coworkers synthesised a series of styrene and furfuryl methacrylate (FMA) copolymers with different molecular architectures and compositions and cross-linked these with a bismaleimide to synthesise DA-CANs with variable structures, molecular weight, and FMA/styrene ratio.[21] They discovered that gelation occurred faster for polymers with higher FMA/styrene ratios and molecular weights. They also found that the thermal stability and the cross-link density of the polymers increased with FMA/styrene ratio. Research has also been conducted into self-healing polysilsesquioxane based on DA-chemistry, where a series of copolymers with varying alkyl lengths were synthesised to examine the effect of chain mobility.[22] They discovered that whilst the chain mobility increased with increasing alkyl chain length, the DA-reaction became slower, due to a larger inter-chain distance. Despite this, scratch tests

revealed that all DA-cross-linked materials were able to be healed in less than 5 minutes, indicating that the retro-Diels Alder (rDA) reaction was not affected by alkyl chain length.

Some studies have examined synergistic effects in DA-polymers, for example Peterson *et al.* investigated the reinforcement of a reversible DA-network with nanocellulose.[23] The combined effect of the network and nanocellulose was an increase in storage modulus by a factor of 60 at 80 °C and a decrease in creep strain by a factor of 40 at the same temperature. A study on self-healing TPU elastomers based on synergistically thermoreversible DA bonds and quadruple hydrogen (H-) bonds has also been conducted.[24] Materials were based on isophorone diisocyanate (IPDI)-based PUs chain-extended with different ratios of furfuryl alcohol (FA) to 5-(2-hydroxyethyl)-6-methyl-2-aminouracil (UPy), which were then reacted with BMI to generate DA-bonds. The results showed that the mechanical properties of the DA-TPUs were tuneable with FA : UPy ratio, with the best elastomer displaying a tensile strength of 6.3 MPa, elongation of 1957% and toughness of 84.5 MJ/m^3.

In the context of above, this work aims to expand the fundamental knowledge and understanding of DA synergistic effects, by exploring hybrid DA-CANs which combine thermoreversible DA bonds and non-covalent H-bonds. To achieve this, a series of trifuran cross-linkers with different degrees of H-bonding will be incorporated into PU DA-networks to investigate the effect on resulting thermomechanical and morphological properties.

4.2 Results and discussion

4.2.1 Synthesis and characterisation of trifuran cross-linkers.

Three trifunctional (TF) furan cross-linkers with isocyanurate cores comprising either ester, urethane or urea functional groups in the backbone were synthesised: **TF-ester**, **TF-urethane,** and **TF-urea**, respectively (***Scheme 4.1***). **TF-ester** was synthesised *via* the reaction of tris[2-(acryloyloxy)ethyl] isocyanurate with furfuryl mercaptan using triethylamine (NEt_3) in dichloromethane (DCM), whilst **TF-urethane** and **TF-urea** were synthesised from the reaction between Desmodur® N 3300 (hexamethylene diisocyanate (HDI) trimer) and furfuryl alcohol (FA) or furfuryl amine (FAM),

respectively, in butyl acetate (BuOAc) using dibutyltin dilaurate (DBDTL) catalyst. The TF-cross-linkers had similar molar masses (766-799 g.mol^{-1}) so that the equivalent concentration of furan and maleimide functional groups (f_g) and therefore concentration of DA-cycloadducts in the resulting DA-CANs remained similar.

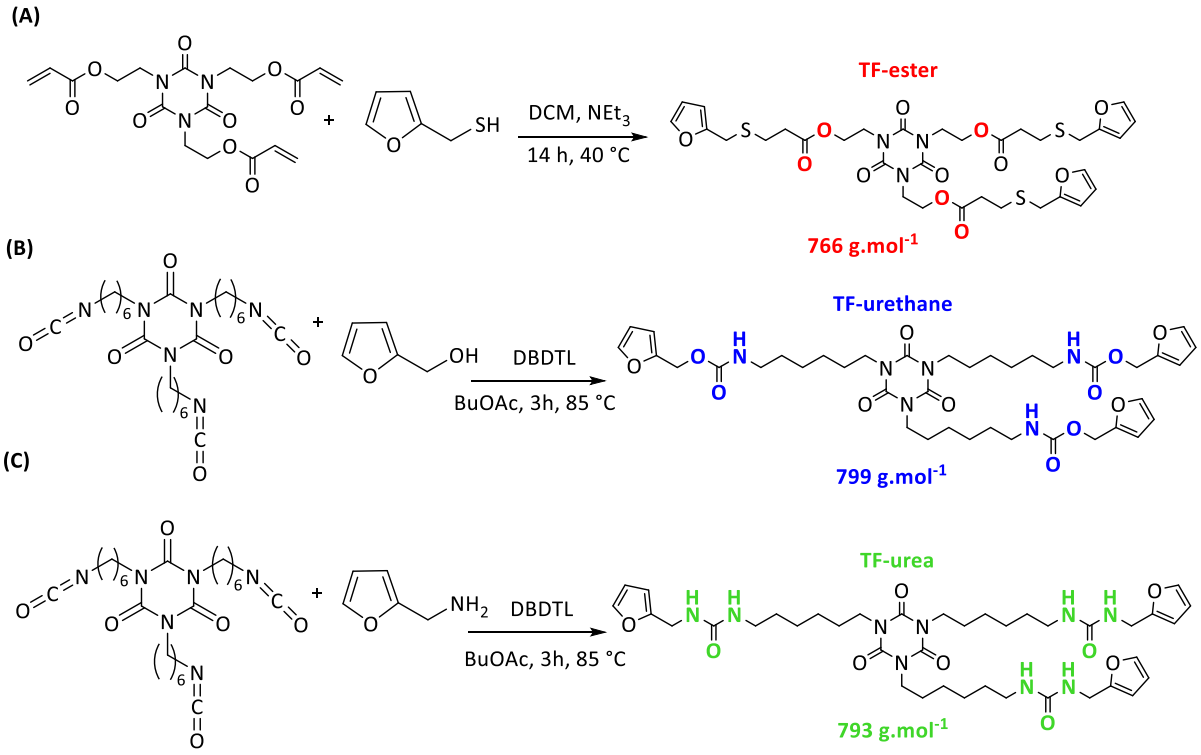

Scheme 4.1 *One step synthesis of* ***(A) TF-ester, (B) TF-urethane****, and* ***(C) TF-urea*** *trifunctional furans*

^{1}H NMR spectroscopy of the trifuran cross-linkers showed resonances between δ = 7.53-6.16 ppm, demonstrating successful incorporation of furan functional groups *via* facile quantitative reaction, in high yield (***Figure 4.1***). The ^{1}H NMR spectrum of **TF-ester** did not display a resonance at δ = 1.90 ppm, which represents the free SH protons in furfuryl mercaptan monomer (***Figure 4.1 (A)***). Additionally, the acrylate C=C proton resonances present in the ^{1}H NMR spectrum of tris[2-(acryloyloxy)ethyl] isocyanurate at δ = 5.85 and 6.08 ppm are replaced by resonances at δ = 4.32 and 4.15 ppm, confirming the thia-Michael addition of the S nucleophile in furfuryl mercaptan across the electron-deficient double bonds. Furthermore, the ^{1}H NMR spectra of **TF-urethane** and **TF-urea** exhibited resonances associated with the methylene units between the furan rings and either urethane or urea bonds at δ

= 5.03 and 4.16 ppm, respectively. The corresponding methylene protons in furfuryl alcohol and furfuryl amine appear at δ = 4.54 and 3.76 ppm, respectively in $CDCl_3$ and d_6-DMSO indicating that the resonances in the trifurans appear at higher chemical shifts due to the proton deshielding effect of urethane and urea bonds. The ^{1}H NMR spectra of **TF-urethane** and **TF-urea** also displayed resonances for urethane and urea protons at δ = 4.81 and 5.88 ppm, respectively (***Figure 4.1 (B)*** and ***(C)***). ^{13}C NMR spectroscopy of the trifuran cross-linkers confirmed the presence of ester carbonyl carbons at δ = 171 ppm in **TF-ester**, urethane carbonyl carbons at δ = 156 ppm in **TF-urethane** and urea carbonyl carbons at δ = 158 ppm in **TF-urea** (***experimental***). ^{13}C NMR spectra of the cross-linkers also presented resonances above δ = 100 ppm, associated with the furan-ring carbons.

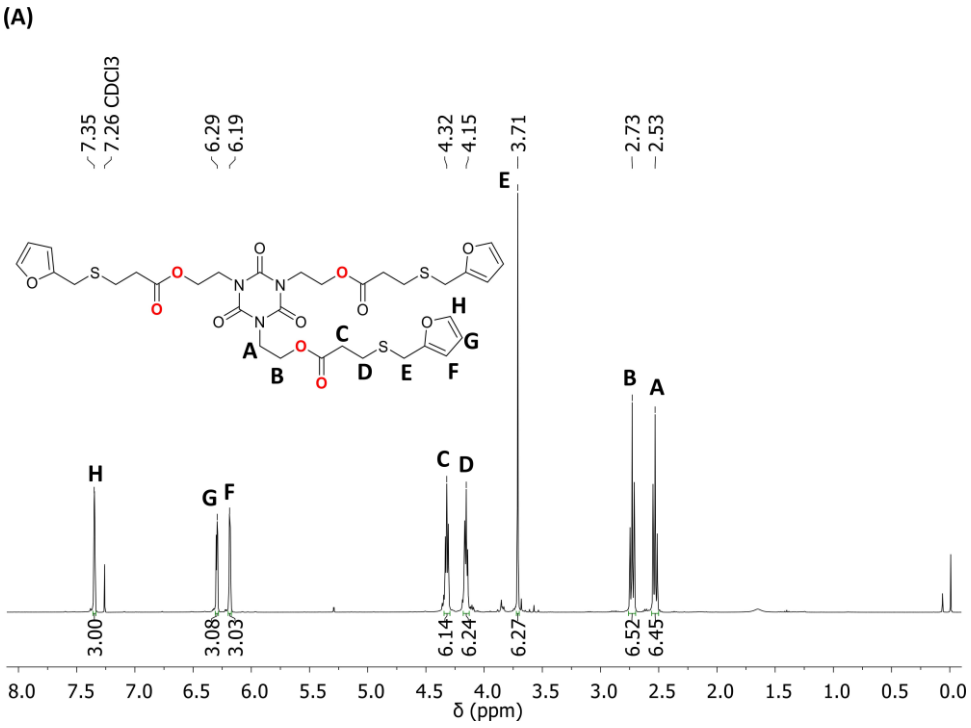

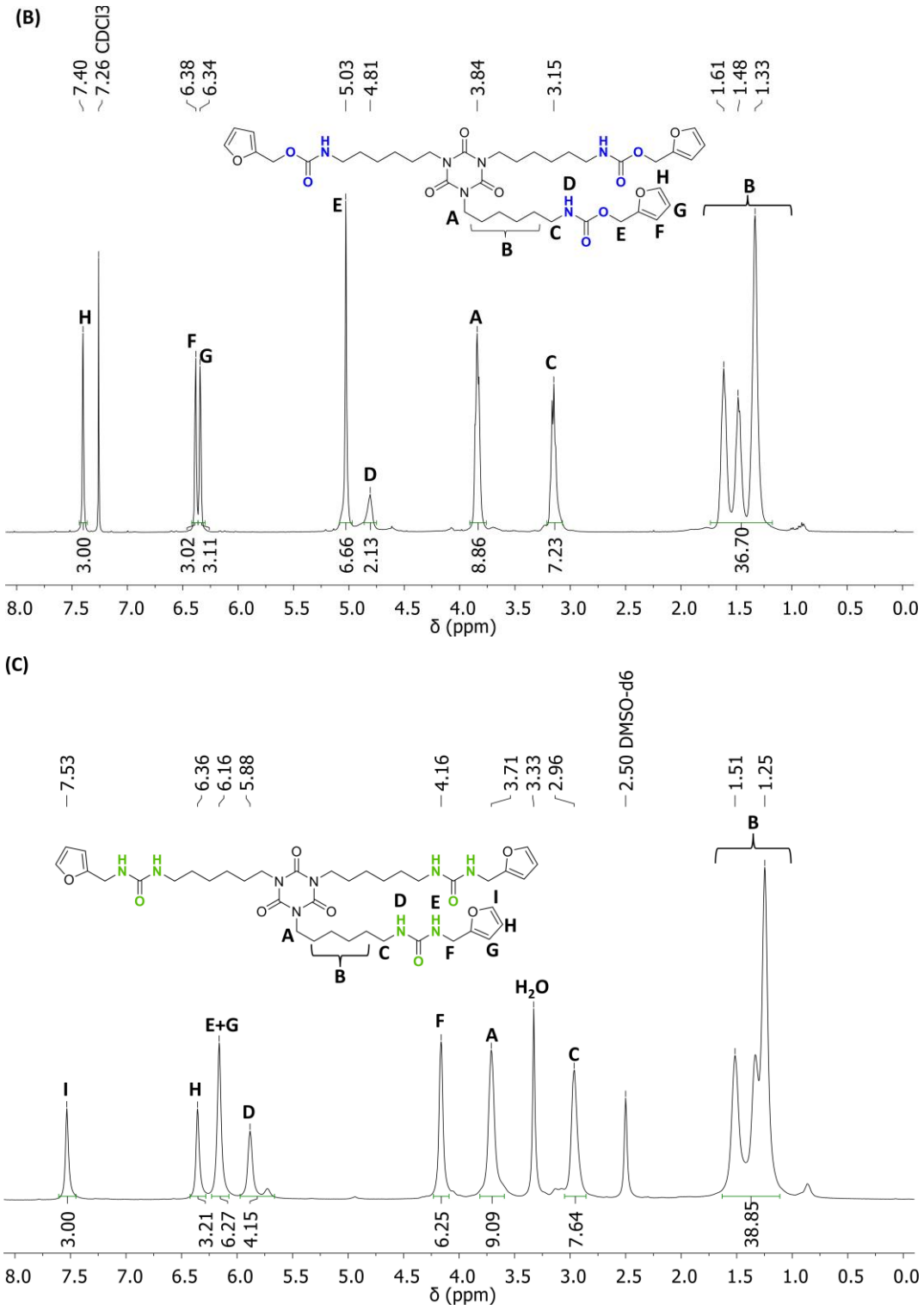

Figure 4.1 *^{1}H NMR spectra of* ***(A) TF-ester, (B) TF-urethane*** *(400 MHz, 298 K, $CDCl_3$) and* ***(C) TF-urea*** *cross-linkers (400 MHz, 298 K, DMSO-d_6). Chemical shifts labelled at the top and integration values at the bottom.*

ATR-FTIR spectroscopy was performed on the trifuran cross-linkers to investigate H-bonding and functionality differences (***Figure 4.2 (A)*** and ***(B)***). **TF-urethane** and **TF-urea** displayed FTIR bands at ν_{max}

= 3328 and 3320 cm^{-1}, representing N-H stretching from urethane and urea functional groups, respectively. **TF-ester** does not contain N-H groups and therefore did not display a FTIR band in this region. ATR-FTIR analysis of the carbonyl region revealed differences (***Figure 4.2 (B)***). **TF-ester** displayed two FTIR stretching vibrations in the carbonyl region: one at ν_{max} = 1730 cm^{-1} representing ester carbonyl stretching and one at ν_{max} = 1685 cm^{-1} for isocyanurate ring carbonyl stretching. **TF-urethane** presented a broad FTIR band at ν_{max} = 1685 cm^{-1}, resulting from the overlap of isocyanurate ring carbonyl and H-bonded urethane carbonyl stretching, with a small shoulder at ν_{max} = 1730 cm^{-1} from free urethane carbonyl stretching. **TF-urea** showed an FTIR band at ν_{max} = 1685 cm^{-1}, demonstrating isocyanurate ring carbonyl stretching with an additional band at ν_{max} = 1625 cm^{-1}, from H-bonded urea carbonyl stretching.

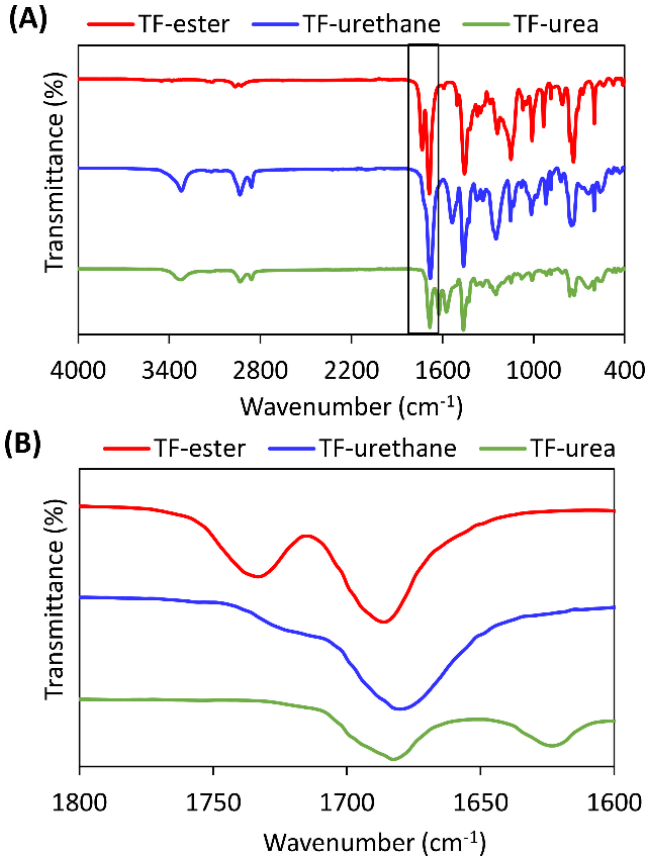

Figure 4.2 *ATR-FTIR spectra of TF-cross-linkers* ***(A)*** *from 4000 to 400 cm^{-1} and* ***(B)*** *zoomed into the carbonyl region (1800-1600 cm^{-1}).*

DSC analysis revealed that the glass transition temperature (T_g) of the trifuran cross-linkers increased significantly with degree of H-bonding, implying an increase in physical cohesion and rigidity, with a resulting decrease in segmental chain mobility (***Figure 4.3*** and ***Table 4.1***). **TF-ester** is an amorphous liquid with a sub-ambient T_g of -34 °C. Conversely, **TF-urethane** and **TF-urea** are semi-crystalline materials with higher T_g values of -1.4 and 71 °C and endotherms at 44 and 129/140 °C (T_m), respectively. These endotherms can be attributed to the melting of strong, physically H-bonded associations of urethane and urea bonds. This demonstrates how changing the degree of H-bonding within the trifuran cross-linkers vastly effects their physical and thermal properties.

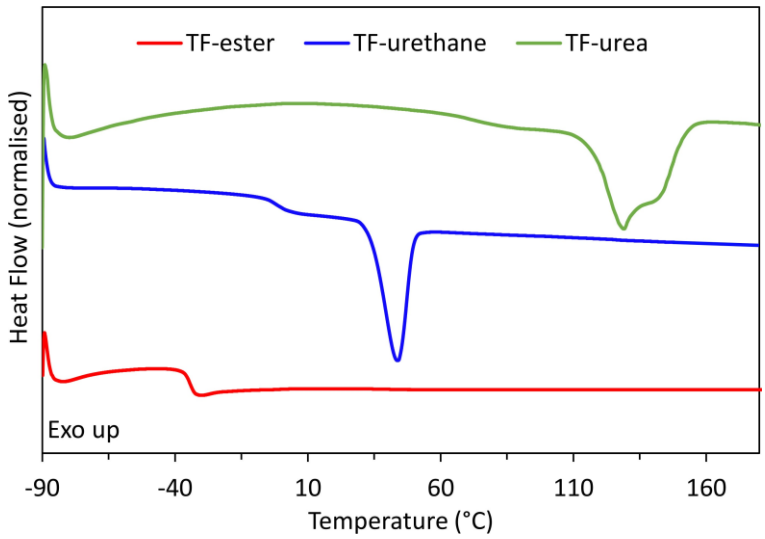

Figure 4.3 *DSC thermograms (1st heating cycles) of trifuran cross-linkers. Heating rate of 10 °C.min^{-1}. Exo up.*

Table 4.1 *DSC thermal data of trifunctional furan cross-linkers.*

Trifuran	T_g [a] (°C)	T_m [a] (°C)	ΔH_m [a] (J.g^{-1})
TF-ester	-34.0	-	-
TF-urethane	-1.4	44	25
TF-urea	71.0	129 & 140	46

[a] *Obtained from DSC analysis using 1st heating cycles. Heating rate of 10 °C.min^{-1}.*

4.2.2 Synthesis and characterisation of DA-PU CANs from telechelic bismaleimides and trifuran cross-linkers.

A series of 12 **DA-PU** CANs was produced *via* copolymerising the four telechelic bismaleimide PU prepolymers from Chapter 2 (**PPM-PCL**, **PPM-PCL.LA**, **PPM-PBD** and **PPM-HPBD**) separately with **TF-ester**, **TF-urethane**, or **TF-urea** (***Figure 4.4*** and ***Table 4.2***). All DA-networks displayed similar equivalent concentrations of maleimide and furan functional groups (f_g) and thus DA-cycloadduct concentrations, allowing the effect of cross-linker H-bonding or bismaleimide backbone on the thermomechanical properties to be independently determined. Copolymerisation was achieved *via* solvent casting in DCM for DA-CANs containing **TF-ester** or **TF-urethane** or in DMF for those containing **TF-urea**, ensuring a 1 : 1 furan : maleimide stoichiometric ratio. After solvent removal, 1 mm thick elastomeric sheets were made *via* compression moulding which were subsequently conditioned for 7 days at 25 °C to enable the DA-reaction to reach equilibrium prior to testing.

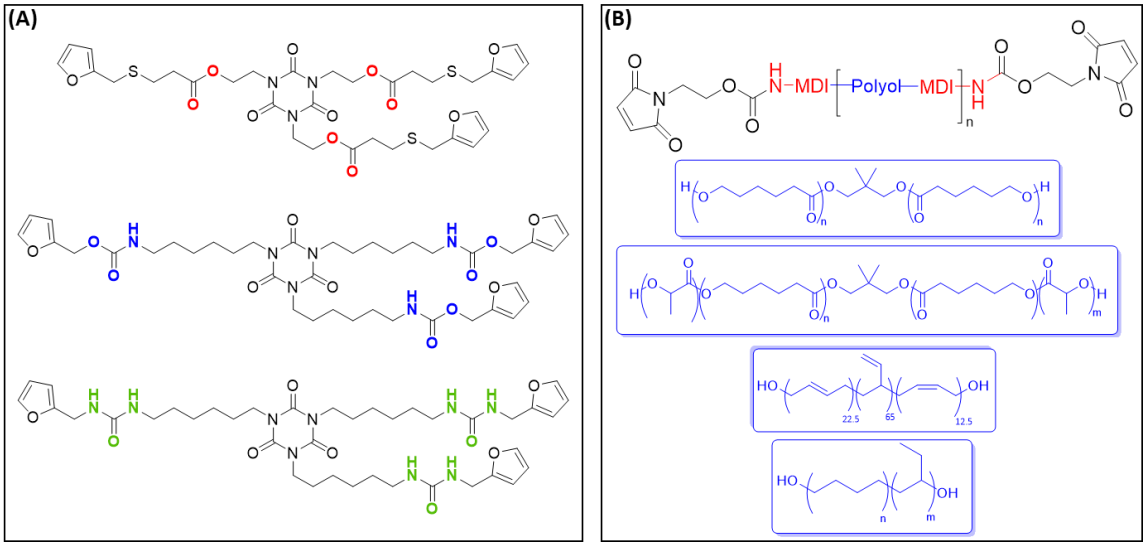

Figure 4.4 *Chemical structures of* ***(A)*** *trifuran cross-linkers:* ***TF-ester, TF-urethane****, and* ***TF-urea*** *and* ***(B)*** *generic structure of telechelic bismaleimide PU prepolymers based on* ***PCL, PCL.LA, PBD*** *and* ***HPBD*** *SS backbones.*

Table 4.2 *Compositions and f_g values of the 12* ***DA-PU*** *CANs.*

CAN	f_g (mol.kg^{-1})	Bismaleimide	TF-cross-linker
DAPCL-ester	0.61	PPM-PCL	TF-ester
DAPCL-urethane	0.61	PPM-PCL	TF-urethane
DAPCL-urea	0.61	PPM-PCL	TF-urea
DAPCL.LA-ester	0.61	PPM-PCL.LA	TF-ester
DAPCL.LA-urethane	0.61	PPM-PCL.LA	TF-urethane
DAPCL.LA-urea	0.61	PPM-PCL.LA	TF-urea
DAPBD-ester	0.59	PPM-PBD	TF-ester
DAPBD-urethane	0.59	PPM-PBD	TF-urethane
DAPBD-urea	0.59	PPM-PBD	TF-urea
DAHPBD-ester	0.54	PPM-HPBD	TF-ester
DAHPBD-urethane	0.54	PPM-HPBD	TF-urethane
DAPBD-urea	0.54	PPM-HPBD	TF-urea

The f_g of each **DA-PU** network was calculated using the equation below:

$$f_{g\,(mol.kg^{-1})} = \left(\frac{(Mass\ fraction_{fm} \times 1000)}{Molecular\ weight_{fm}}\right) \times functionality\ of\ molecule$$

whereby f_m represents the bismaleimide or TF-cross-linker functional molecule.

The degree of cross-linking in each **DA-PU** network was determined by running a 24-hour Soxhlet extraction in tetrahydrofuran (THF). Using this method, THF was continually passed through a sample of each material for a 24-hour period, washing away any non-cross-linked material uninvolved in the network (sol fraction). THF was chosen as the solvent as its boiling point is sufficiently lower than the typical retro DA (rDA) temperature (> 100 °C), so the networks should remain fully intact during the experiment. A comparison of the sample mass before and after the extraction enables the gel fractions of the **DA-PU** CANs to be calculated (***Table 4.3***).

Table 4.3 *Gel fractions of* ***DA-PU*** *CANs.*

CAN	Gel fraction [a] (%)
DAPCL-ester	95
DAPCL-urethane	95
DAPCL-urea	92
DA-PCL.LA-ester	92
DAPCL.LA-urethane	95
DA-PCL.LA-urea	94
DAPBD-ester	90
DAPBD-urethane	96
DAPBD-urea	97
DAHPBD-ester	91
DAHPBD-urethane	97
DAPBD-urea	93

[a] determined *via* Soxhlet extractions in THF after 24 hours.

All materials exhibited high gel fractions (≥ 90%), suggesting a high-degree of cross-linking and that most of the material had been successfully incorporated into the **DA-PU** networks.

ATIR-FTIR spectroscopy of all **DA-PU** CANs revealed low maleimide absorbance at ν_{max} = 696 cm^{-1} after conditioning for 7 days at 25 °C, confirming that most maleimide groups had successfully copolymerised to form DA-cycloadducts (***Figure 4.5***). This is similar to the linear DA-TPUs in the previous chapters, where high conversion was also obtained.

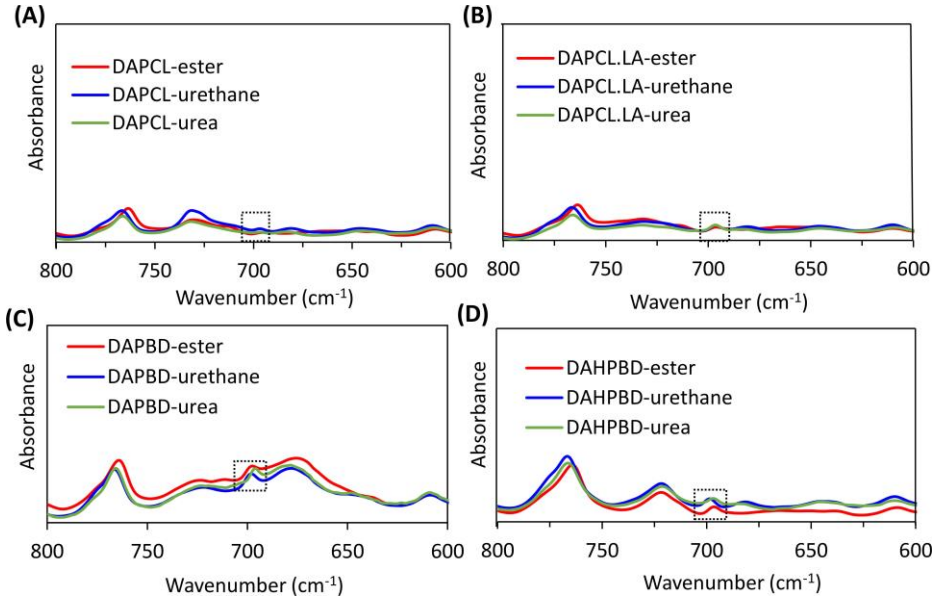

Figure 4.5 *ATR-FTIR spectra of* ***(A) DAPCL, (B) DAPCL.LA, (C) DAPBD*** *and* ***(D) DAHPBD****-PU CANs between 800-600* cm^{-1}*. Dashed boxes highlight low maleimide absorption at 696* cm^{-1}*.*

ATR-FTIR analysis of the carbonyl region within the **DA-PU** CANs revealed differences (***Figure 4.6***). The FTIR spectra of most **DA-PU** networks exhibited a small absorption at ν_{max} = 1775 cm^{-1}, which has been reported to indicate the presence of conjugated carbonyl groups in DA-cycloadducts.[25] However, this absorption was not observed in the FTIR spectra of the **DAPCL.LA** networks, due to overlap with a broad absorption for **PCL.LA** ester carbonyl stretching. The **DAPCL** and **DAPCL.LA**-PU CANs displayed strong absorptions between ν_{max} = 1730-1720 cm^{-1}, resulting from the overlap of PCL ester carbonyl and free urethane carbonyl stretching. **DAPCL-ester** and **DAPCL.LA-ester** also displayed narrow absorptions around ν_{max} = 1694 cm^{-1}, representing isocyanurate ring carbonyl stretching. This absorbance broadened and shifted to slightly higher wavenumbers (ν_{max} = 1702 cm^{-1}) in **DAPCL-urethane** and **DAPCL.LA-urethane**, suggesting they contain more H-bonded urethane carbonyl groups. **DAPCL-urea** and **DAPCL.LA-urea** displayed the broadest carbonyl FTIR absorptions from ν_{max} = 1710 to 1620 cm^{-1}, due to the additional presence of H-bonded urea carbonyl and N-H stretching vibrations. The **DAPBD** and **DAHPBD** networks displayed main absorptions at ν_{max} = 1695 cm^{-1}, resulting from the overlap of isocyanurate ring and H-bonded urethane carbonyl stretching which broadened with TF-urethane and TF-urea, as more H-bonded urethane and urea carbonyls were incorporated. **DAHPBD-ester** and **DAPBD-ester** exhibited more prominent absorptions at ν_{max} = 1730 cm^{-1} due the additional presence of ester carbonyls from the TF-ester trifuran cross-linker.

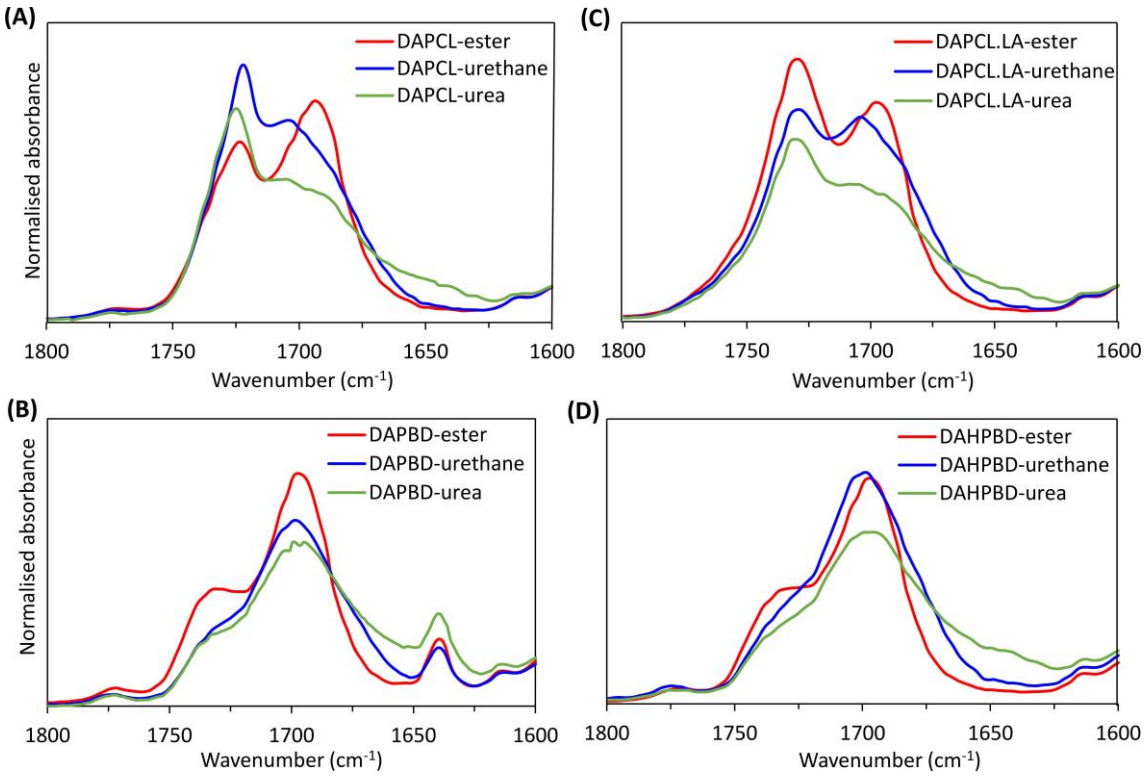

Figure 4.6 *ATR-FTIR spectra of* ***(A) DAPCL, (B) DAPCL.LA, (C) DAPBD*** *and* ***(D) DAHPBD*** *PU CANs with different TF-cross-linkers in the carbonyl region.*

The thermal properties of the **DA-PU** CANs were analysed *via* DSC after conditioning the materials for 7 days at 25 °C (***Figure 4.7*** and ***Table 4.4***). Dissociation of the DA-cycloadducts in the **DA-PU** networks was confirmed *via* the appearance of double endotherms between 107 and 146 °C, with ΔH_{rDA} values between 10-12 J.g^{-1}, due to similar DA-cycloadduct concentrations. It is important to note that after the rDA reaction (at temperatures above 150 °C) maleimide homopolymerisation starts to occur, resulting in an exothermic heat flow observed in DSC.[26] To minimise the influence of these side reactions at high temperatures, free-radical scavengers such as hydroquinone can be incorporated.[27] The PBD-based DA-networks exhibited steeper exothermic peaks, especially when **TF-urea** was incorporated, which could result from a combined effect of maleimide homopolymerisation and the Alder-ene reaction, mentioned previously. **DAPCL-urea** displayed a low T_g at -43 °C and a small endotherm (ΔH_{mPCL} of 6.1 J.g^{-1}) at 36-43 °C (T_{mPCL}) for the melting of semi-crystalline PCL segments. **DAPCL-ester** and **DAPCL-urethane** exhibited larger PCL melting endotherms at 44 °C with ΔH_{mPCL} values of 17.8 and 20.0 J.g^{-1}, respectively, meaning their T_g values could not be detected *via* DSC. This suggests

that the stronger H-bonding present in the **TF-urea** cross-linker suppresses the crystallisation of PCL. The **DAPBD** and **DAHPBD**-PU CANs exhibited two T_g transitions, a lower T_g for the PBD or HPBD SS at -29 °C and an upper T_g for the HS between 41 and 55 °C, indicative of microphase-separation.

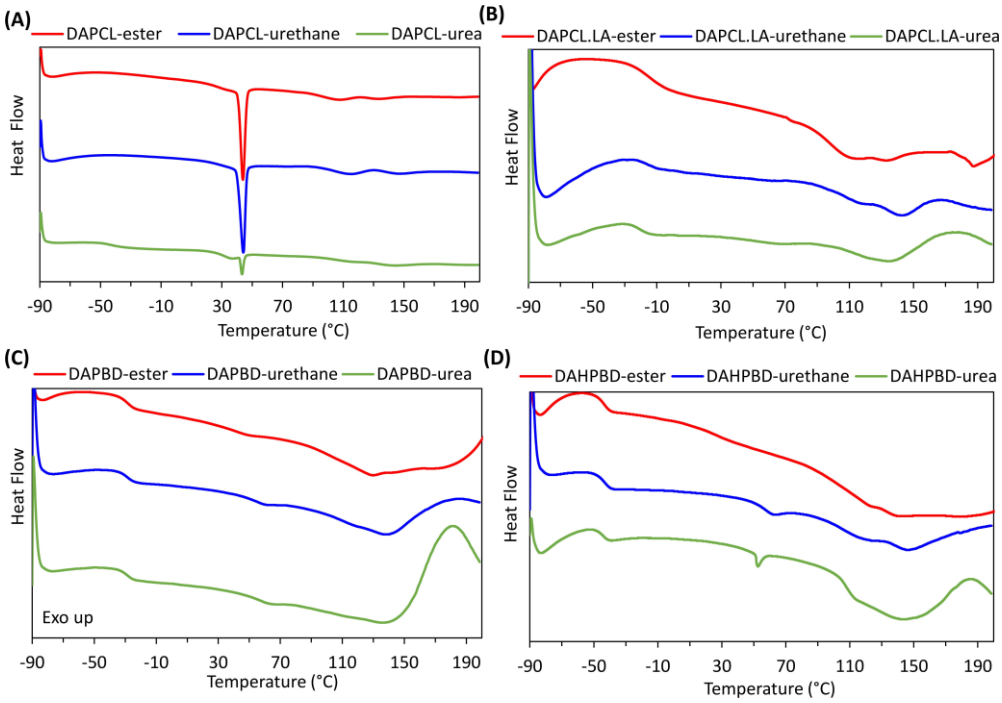

Figure 4.7 *DSC thermograms (1st heating cycles) of DA-PU CANs for* ***(A) DAPCL, (B) DAPCL.LA, (C) DAPBD*** *and* ***(D) DAHPBD*** *bismaleimide backbones with different TF-cross-linkers. Exo up. 10 °C.min^{-1} heating rate.*

Table 4.4 *DSC thermal data of* ***DA-PU*** *CANs.*

CAN	T_g [a] (°C)	T_{mPCL} [a] (°C)	ΔH_{mPCL} [a] (J.g^{-1})	T_{rDA} [a] (°C)	ΔH_{rDA} [a] (J.g^{-1})
DAPCL-ester	-	44.0	17.8	107 & 134	11.0
DAPCL-urethane	-	44.0	20.0	115 & 146	10.8
DAPCL-urea	-43	36 & 43	6.1	115 & 143	10.4
DA-PCL.LA-ester	-16	-	-	113 & 133	11.8
DAPCL.LA-urethane	-18	-	-	116 & 142	11.3
DA-PCL.LA-urea	-21	-	-	135	12.0
DAPBD-ester	-29 & 41	-	-	129	12.4
DAPBD-urethane	-29 & 54	-	-	137	11.2
DAPBD-urea	-29 & 55	-	-	136	9.6
DAHPBD-ester	-44	-	-	121 & 140	11.7
DAHPBD-urethane	-44/56	-	-	122 & 146	11.7
DAPBD-urea	-45	-	-	143	11.2

[a] *Determined via DSC analysis using 1st heating cycles and a 10 °C.min^{-1} heating rate.*

DMA was performed on the **DA-PU** networks to investigate viscoelastic properties as a function of temperature (***Figure 4.8***, ***Figure 4.9*** and ***Table 4.5***). All DA-networks exhibited an initial drop in storage modulus (*E'*) accompanied by a peak in tan δ upon heating through the T_g, due to an increase in cooperative mobility. The **DAPBD** and **DAHPBD**-PU CANs displayed narrow, high intensity tan δ peaks at low T_g values between -29 and -14 °C, due to their flexible, amorphous nature and high ability to dissipate energy. The **DAHPBD** networks exhibited lower T_g values than the corresponding **DAPBD** networks as HPBD does not contain C=C double bonds which restrict bond rotation and chain mobility. The tan delta δ curves of **DAPBD** and **DAHPBD**-PU CANs presented additional small, broad softening transitions between 30 and 90 °C, likely caused by strong physical interactions such as H-bonding within the microphase separated HSs. The tan δ curve of **DAPBD-ester** also displayed a small, broad peak at -51 °C, representing sub T_g molecular motions known as β-relaxations.[28] This yielding occurs due to molecular segments sliding past each other under stress, despite being brittle and constrained by cross-linking. The **DAPCL.LA** PU CANs displayed broader tan δ peaks at higher temperatures than the corresponding **DAPBD** or **DAHPBD** networks, indicating lower network flexibility and enhanced compatibility between the higher polarity PCL.LA SSs and polar HSs. In all of the amorphous DA-networks, the value of tan δ decreases with increased degree of TF-cross-linker H-bonding, demonstrating a decrease in flexibility and damping ability. The **DAPCL**-PU CANs exhibited the smallest tan δ peaks at the highest temperatures, due to the presence of semi-crystalline PCL segments which further decrease network flexibility. **DAPCL-urea** also presented a diffuse tan δ peak at -28 °C which could represent β-relaxation or a low temperature T_g.

After the T_g, **DAPCL**-PU CANs displayed another step change in *E'* at 45 °C, due to the melting of semi-crystalline PCL segments. In all DA-networks, heating above the T_g or T_m, causes a gradual decrease in *E'* as the DA cross-linking density slowly decreases until higher temperatures (> 90 °C) where a steep drop in *E'* and viscous flow occurs (T_f) due to the dynamic DA equilibrium shifting to lower molecular weight furan and maleimide precursors.[29-30] The DMA data shows that the T_f values increase systematically with degree of cross-linker H-bonding, independent of type of bismaleimide polymer

backbone. This demonstrates how non-covalent interactions can synergistically reinforce the thermoreversible DA-covalent bonds to enhance thermal stability and extend the service temperature windows of the materials. The rubbery plateau moduli ($E'_{rubbery}$) of the DA-networks also generally increased with degree of cross-linker H-bonding, whilst the cross-link density remained constant, indicating enhanced stiffness from the additional non-covalent interactions. Similar to the linear **DA-TPUs** from previous chapters, the **DAPBD** and **DAHPBD**-PU CANs displayed more stable, extensive rubbery plateaus and higher T_f values than the corresponding **DAPCL** and **DAPCL.LA** networks, indicating enhanced thermal stability, likely due to reinforcement of the polymer matrix *via* microphase separation.

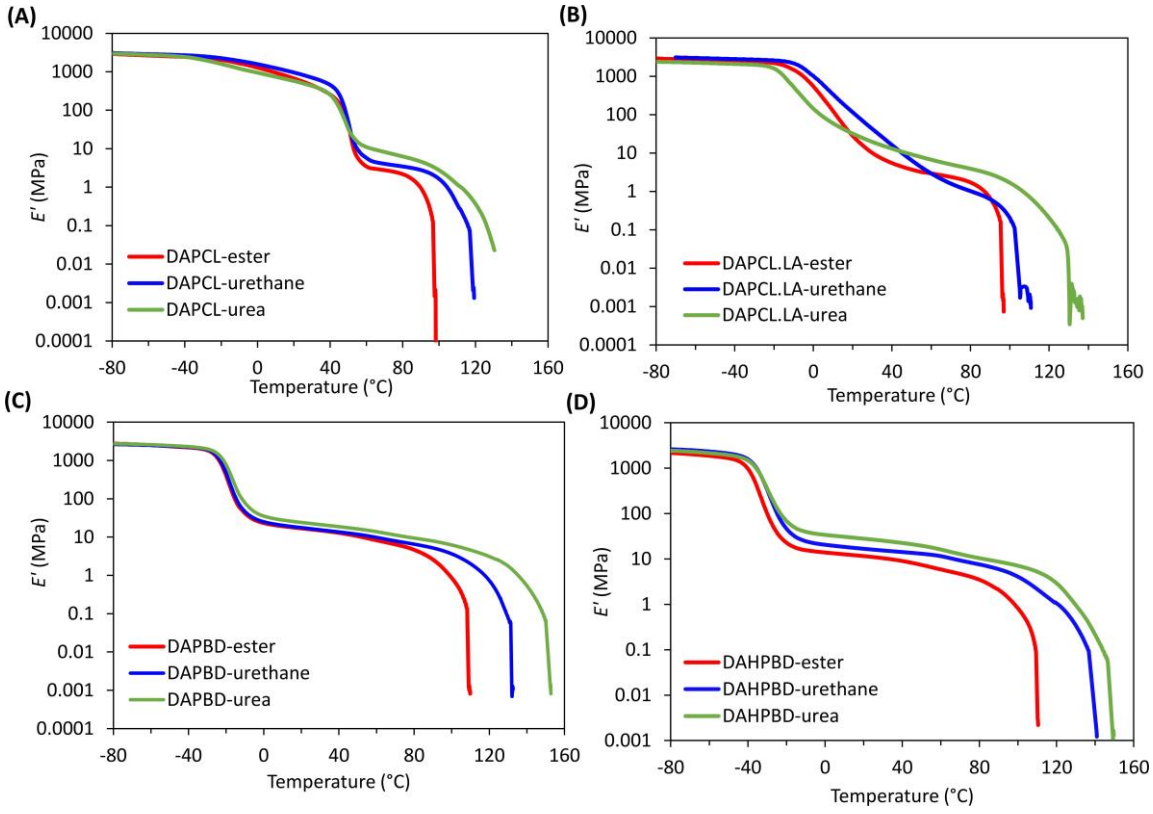

Figure 4.8 *Variation of E' with temperature for* ***(A) DAPCL***, ***(B) DAPCL.LA***, ***(C) DAPBD***, *and* ***(D) DAHPBD****-PU CANs with different TF-cross-linkers, obtained via DMA.*

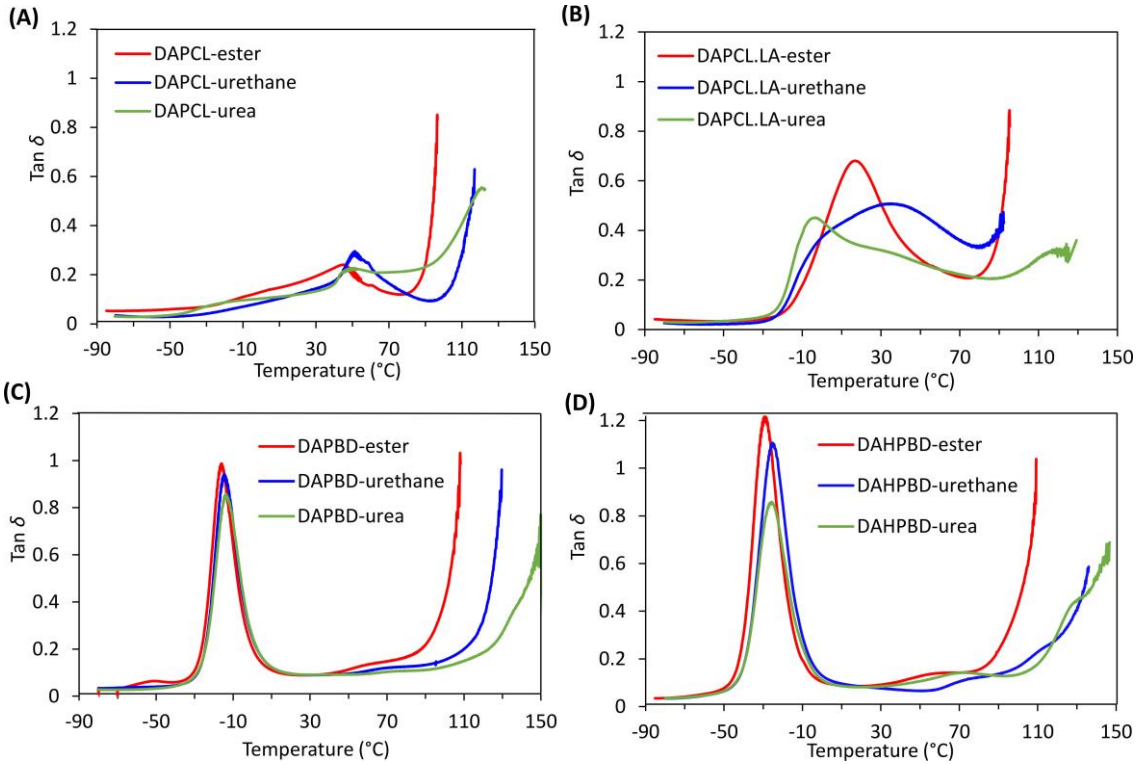

Figure 4.9 *Variation of tan δ with temperature for* ***(A) DAPCL, (B) DAPCL.LA, (C) DAPBD,*** *and* ***(D) DAHPBD****-PU CANs with different TF-cross-linkers, obtained via DMA.*

Table 4.5 *Thermal data for* ***DA-PU*** *CANs obtained via DMA using a heating rate of 3 °C.min^{-1}.*

CAN	E' ($T < T_g$) [a] (MPa)	T_g [b] (°C)	E' ($T > T_g$) [c] (MPa)	T_{mPCL} [d] (°C)	T_f [e] (°C)
DAPCL-ester	2633	44	671	45	96
DAPCL-urethane	2882	51	961	45	117
DAPCL-urea	2737	50	574	41	130
DAPCL.LA-ester	2724	17	28	-	95
DAPCL.LA-urethane	3038	34	116	-	102
DAPCL.LA-urea	2272	-2.6	32	-	129
DAPBD-ester	2530	-16	17	-	108
DAPBD-urethane	2473	-15	18	-	130
DAPBD-urea	2590	-14	24	-	150
DAHPBD-ester	1869	-29	12	-	109
DAHPBD-urethane	2339	-27	17	-	136
DAHPBD-urea	2164	-26	28	-	146

[a] Storage modulus measured at -60 °C. [b] Measured as peak in tan δ. [c] Storage modulus measured at 20 °C. [d] Measured as the onset of modulus reduction. [e] Measured as onset of viscous flow.

The influence of TF-cross-linker H-bonding on the mechanical properties at room temperature can also be illustrated *via* uniaxial tensile testing in strain-controlled experiments using a 10 mm.min^{-1} extension rate (***Figure 4.10***).

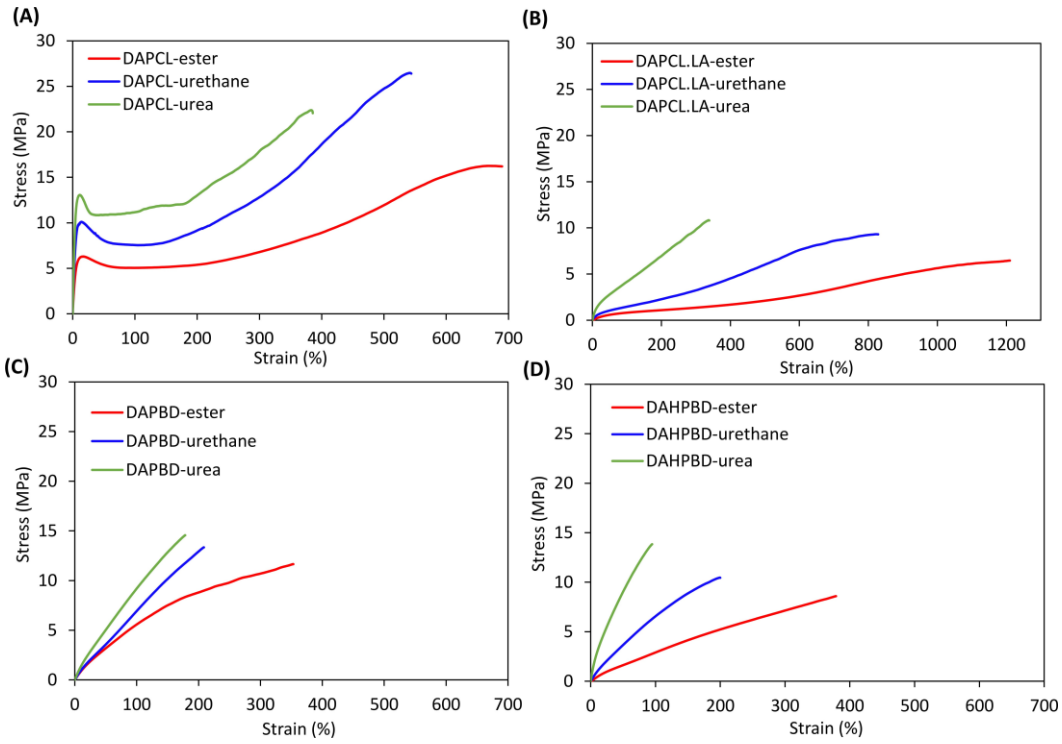

Figure 4.10 *Representative stress-strain curves of* ***(A) DAPCL, (B) DAPCL.LA, (C) DAPBD*** *and* ***(D) DAHPBD DA-PU*** *CANs. Obtained via tensile testing (10 mm.min^{-1} extension rate).*

From the resulting stress-strain curves, the Young's modulus (E_y) (linear regression in the 0-2% strain interval), stress at break (σ_b), strain at break (ε_b) and modulus of toughness (U_T, the total area under the stress-strain curve) can be calculated (***Table 4.6***).

Table 4.6 *Mechanical properties of* ***DA-PU*** *CANs.*

CAN	E_y [a] (MPa)	σ_b [a] (MPa)	ε_b [a] (%)	U_T [a] (MPa)
DAPCL-ester	136 ± 8	16.2 ± 0.4	690 ± 65	8060 ± 1230
DAPCL-urethane	219 ± 12	26.5 ± 1.1	540 ± 42	7570 ± 1035
DAPCL-urea	299 ± 10	22.1 ± 1.3	390 ± 40	5560 ± 982
DAPCL.LA-ester	1.1 ± 0.03	6.5 ± 0.3	1210 ± 88	3800 ± 750
DAPCL.LA-urethane	7.4 ± 1.2	9.3 ± 0.2	830 ± 72	4330 ± 801
DAPCL.LA-urea	17.1 ± 1.9	10.8 ± 0.8	340 ± 35	2060 ± 465
DAPBD-ester	8.8 ± 1.3	11.7 ± 0.5	350 ± 27	2620 ± 488
DAPBD-urethane	9.9 ± 1.0	13.3 ± 0.7	210 ± 40	1480 ± 303
DAPBD-urea	15.3 ± 0.9	14.6 ± 0.4	180 ± 42	1440 ± 292
DAHPBD-ester	1.9 ± 0.06	8.6 ± 0.2	380 ± 45	1810 ± 310
DAHPBD-urethane	10.5 ± 1.1	10.4 ± 0.8	200 ± 38	1230 ± 298
DAHPBD-urea	40.0 ± 2.4	13.8 ±1.0	90 ± 26	810 ± 235

[a]determined by uniaxial tensometry using an extension rate 10 mm.min^{-1}. Mean values ± standard deviation from measurements conducted independently on 5 specimens.

The mechanical data of the DA-CANs showed that the network strength and Young's modulus increased whilst the flexibility and toughness decreased with degree of trifuran cross-linker H-bonding. The increase in network strength and stiffness can be attributed to the higher amount of non-covalent H-bonds which need to be broken during stretching, whilst the large decrease in elongation can be attributed to a decrease in network flexibility, leading to the overall reduction in toughness.

The stress-strain properties of the DA-PU CANs also varied with the type of bismaleimide polymer backbone, for example the **DAPCL** and **DAPCL.LA**-PU networks displayed higher elongations and resulting toughness values than the corresponding **DAPBD** and **DAHPBD** networks. This is likely due to the higher stain-crystallisation ability of PCL SSs, in addition to the higher degree of polyol backbone H-bonding between ester carbonyls. The **DAPCL**-PU CANs exhibited yielding at low strains due to their semi-crystalline nature, which increased in ultimate stress with degree of TF-cross-linker H-bonding, demonstrating how non-covalent H-bonds can reinforce the semi-crystalline PCL segments. All **DAPCL**-PU networks exhibited pronounced strain-hardening beyond the yield point, with **DAPCL-urethane** displaying an impressive σ_b of 26.5 MPa and U_T of 7568 MPa. Additionally, **DAPCL-ester** showed superior flexibility to **DAPCL-urethane**, with only a small decrease in network strength to 16.2 MPa, giving it a higher U_T of 8055 MPa. **DAPCL.LA-ester** and **DAPCL.LA-urethane** also showed pronounced

strain-hardening leading to excellent elongation values (1210 and 828%) which exceeded **DAPCL-ester** and **DAPCL-urethane** (690 and 542%), respectively. This is likely due to amorphous nature of the **DAPCL.LA** PU networks enabling higher flexibilities than the more rigid, semi-crystalline **DAPCL**-PU networks. The **DAPBD** and **DAHPBD**-PU networks displayed similar stress-strains curves with lower elongations, but the **DAPBD**-PU CANs displayed slightly higher network strengths and toughness values due to the less flexible PBD chains which are more resistant to polymer chain alignment.

The **DA-PBD** and **DA-PCL**-PU CANs were subjected to hydrolytic stability testing according to ASTM D3137 – 81. Three repeat dog-bones (R1, R2 and R3) were suspended into separate 30 mL glass vials containing 20 mL of distilled water. Samples were placed into an oven for 96 hours at 85 °C then removed from the water, dried and conditioned at 25 °C for 7 days before remeasurement of tensile properties (***Figure 4.11***, ***Figure 4.12*** and ***Table 4.7***). Due to lack of thermal stability, **DAPCL-ester** was unable to be measured.

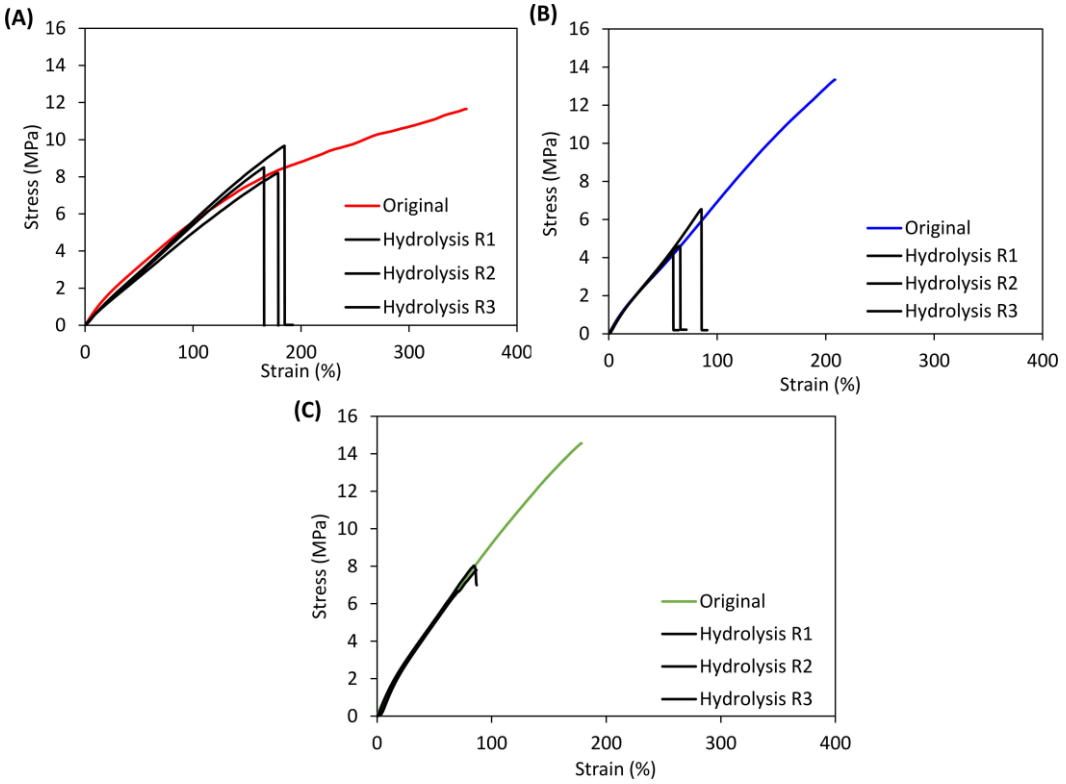

Figure 4.11 *Representative stress-strain curves of original* ***(A) DAPBD-ester, (B) DAPBD-urethane*** *and* ***(C) DAPBD-urea*** *dog-bones and repeat measurements of samples post hydrolysis for 4 days at 85 °C.*

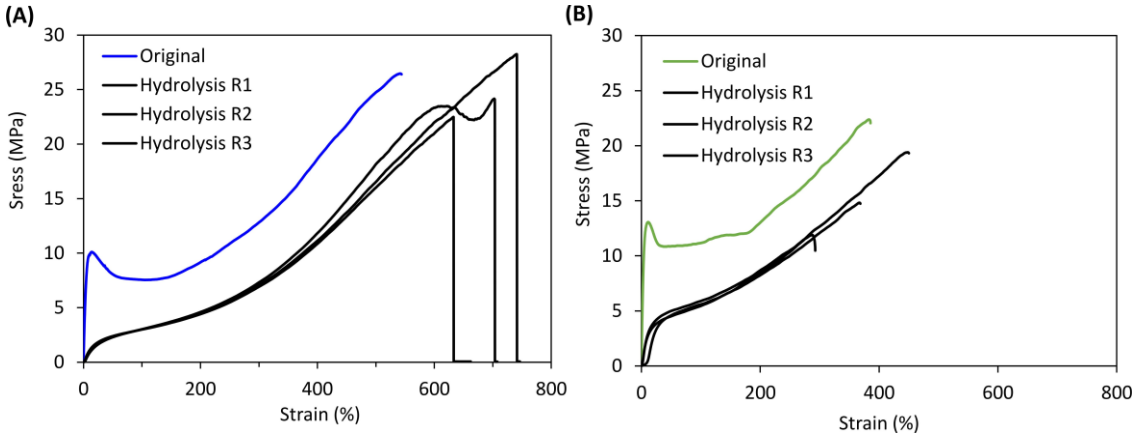

Figure 4.12 *Representative stress strain curves of original* ***(A) DAPCL-urethane*** *and* ***(B) DAPCL-urea*** *dog-bones and repeat measurements of samples after hydrolysis for 4 days at 85 °C, followed by conditioning for 7 days at ambient temperature.*

Table 4.7 *Average Young's modulus, stress at break and elongation at break values with corresponding recovery efficiency values for* ***DA-PBD*** *and* ***DA-PCL****-PU CANs pre and post hydrolytic stability testing.*

CAN	E_y [a] (MPa)	σ_b [a] (MPa)	ε_b [a] (%)
DAPBD-ester (original)	8.8 ± 1.3	11.6 ± 0.5	350 ± 27
Post hydrolysis	6.2 ± 1.4	8.8 ± 0.8	180 ± 9
Recovery efficiency	**70%**	**76%**	**50%**
DAPBD-urethane (original)	9.9 ± 1.0	13.0 ± 0.7	200 ± 40
Post hydrolysis	6.5 ± 2.4	5.1 ± 1.2	70 ±14
Recovery efficiency	**66%**	**39%**	**34%**
DAPBD-urea (original)	15.3 ± 0.9	14.6 ± 0.4	180 ± 42
Post hydrolysis	4.6 ± 4.9	7.5 ± 0.7	80 ± 8
Recovery efficiency	**30%**	**51%**	**44%**
DAPCL-urethane(Original)	219 ± 12.0	26.5 ± 1.1	540 ± 42
Post hydrolysis	3.2 ± 1.9	24.9 ± 2.5	690 ±55
Recovery efficiency	**1.5%**	**94%**	**127%**
DAPCL-urea (Original)	299 ± 10	22.1 ± 1.3	390 ± 40
Post hydrolysis	8.7 ±6.0	14.8 ± 2.6	350 ±59
Recovery efficiency	**2.9%**	**67%**	**91%**

[a] determined by uniaxial tensile testing after conditioning for 7 days at 25 °C. Average values ± standard deviations from 5 repeat measurements for original samples and 3 repeats measurements post hydrolysis samples.

DAPCL-urethane and **DAPCL-urea** displayed good recovery efficiency values of σ_b = 94 and 67% and ε_b = 127 and 91%, respectively, showing that the materials maintained high strength and flexibility post hydrolysis despite the loss of yield-points in their stress-strain curves, resulting in low E_y recovery

efficiently values of 1.5 and 2.9%, respectively. Pronounced strain-hardening still occurred, particularly in **DAPCL-urethane**, implying that the covalent DA-cross-links and the non-covalent cross-links (urethane and urea H-bonds) reformed or remained intact post-hydrolysis. Since PCL-segments melt around 60 °C but DA-cycloadducts don't dissociate until above 100 °C, the retention of the DA-covalent bonds may be suppressing or inhibiting PCL crystallisation kinetics, meaning 7 days isn't enough time for the recrystallisation of PCL segments to occur. Literature suggests that these hydrolysis conditions are not effective enough to hydrolyse the PCL aliphatic ester linkages due to the presence of five hydrophobic CH_2 groups in its repeat unit, meaning an acid or base would be required with a timescale much greater than 4 days to achieve higher degradation rates.[31,32] Surprisingly, the **DAPBD-urethane** and **DAPBD-urea** CANs exhibited lower σ_b and ε_b recovery efficiency values (between 39-51% and 34-44%, respectively) than the corresponding **DAPCL**-PU CANs. **DAPBD-ester** presented a higher σ_b recovery efficiency of 76% but still displayed a low ε_b recovery efficiency of 50%. One reason for this unexpected weaker hydrolysis resistance could be the greater incompatibility between the less polar PBD bismaleimide backbone and the polar cross-linkers, leading to a higher degree of microphase separation.

To confirm if the DA-networks were thermally reprocessable **DAPBD-urethane**, **DAPBD-urea**, **DAPCL-urethane**, and **DAPCL-urea** PU-CANs were subjected to mechanical reprocessing *via* compression moulding, using mild conditions (100-130 °C, 3 MPa for 10 minutes) and subsequently conditioned for 7 days at 25 °C before remeasurement of tensile properties (R1). This process was repeated another two times with the same materials (R2, R3) (***Figure 4.13*** and ***Figure 4.14***). The results showed that all four DA-PU networks maintained excellent mechanical properties with stress-recovery efficiencies above 80% after 3 recycles. This demonstrates the potential sustainability advantage of PU-CANs over current thermoset PU elastomers which are irreversibly cross-linked and therefore non-recyclable.

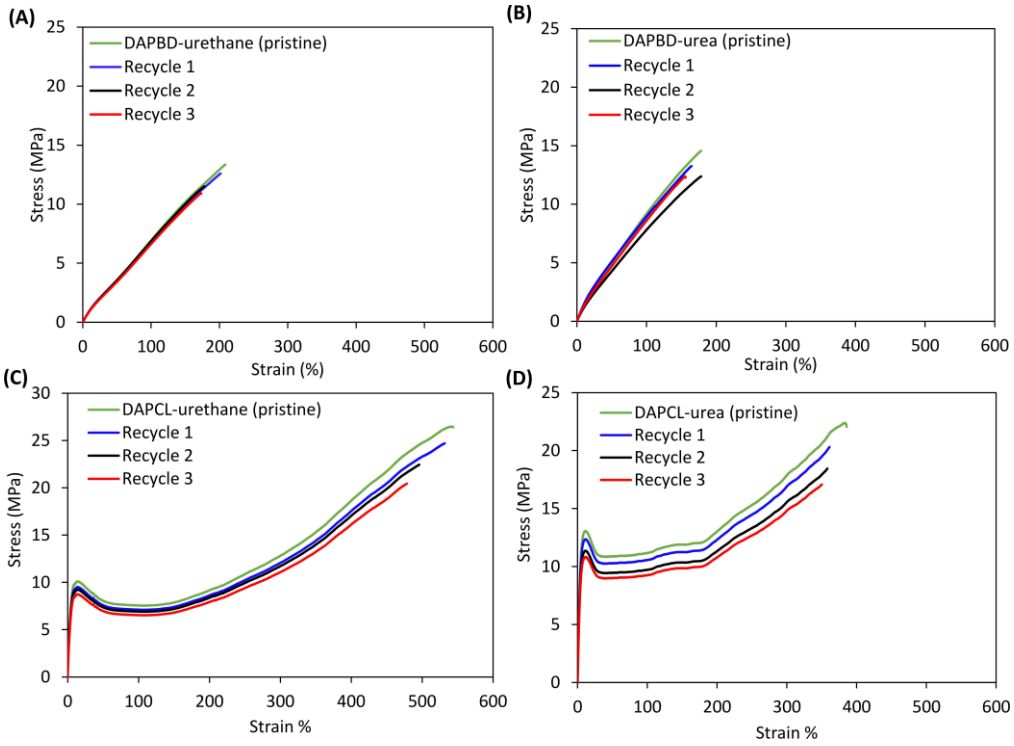

Figure 4.13 *Representative stress-strain curves of* ***(A) DAPBD-urethane****,* ***(B) DAPBD-urea****,* ***(C) DAPCL-urethane*** *and* ***(D) DAPCL-urea*** *PU CANs before recycling (pristine) and after 3 mechanical reprocessing cycles.*

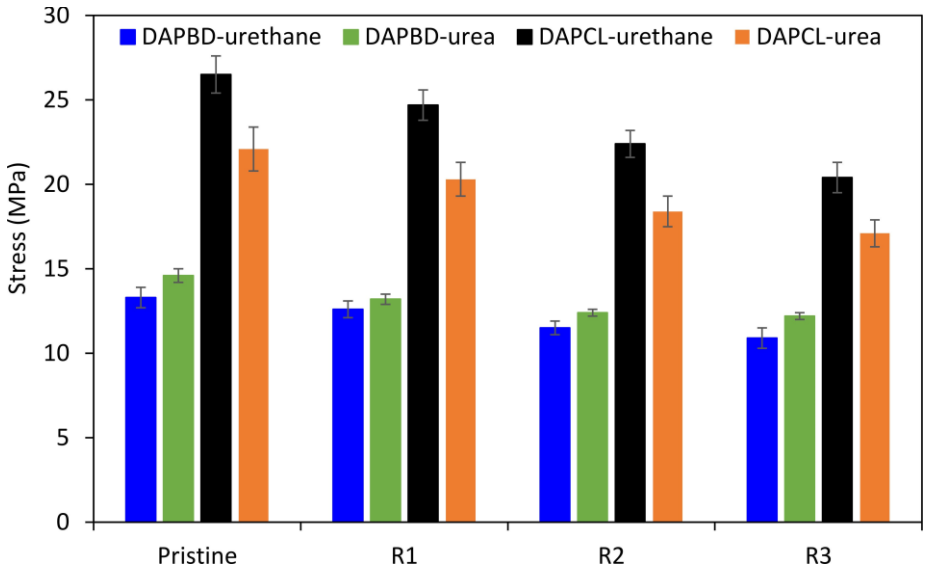

Figure 4.14 *Mean stress values for* ***DAPBD-urethane****,* ***DAPBD-urea****,* ***DAPCL-urethane,*** *and* ***DAPCL-urea*** *obtained via tensile testing for pristine samples and after 3 reprocessing cycles ± standard deviation from measurements conducted independently on 5 specimens.*

The morphology of the 12 **DA-PU** CANs was investigated *via* wide-angle x-ray scattering (WAXS) and small-angle x-ray scattering (SAXS) experiments conducted at room temperature (***Figure 4.15*** and ***Figure 4.16***). WAXS experiments revealed that all **DA-PU** CANs displayed broad, scattering features between 2θ = 5-30°, centred around 2θ = 20°, due to amorphous regions. The WAXS spectra of **DAPCL**-PU networks also contained superimposed sharp diffraction spikes at 2θ = 21.2°, 21.8° and 23.5°, characteristic of crystalline PCL segments.[33] All **DA-PU** CANs displayed another low intensity, diffuse scattering peak, centred at 2θ = 40°, which can be observed most clearly in the WAXS spectra of **DAPCL.LA**-PU CANs.

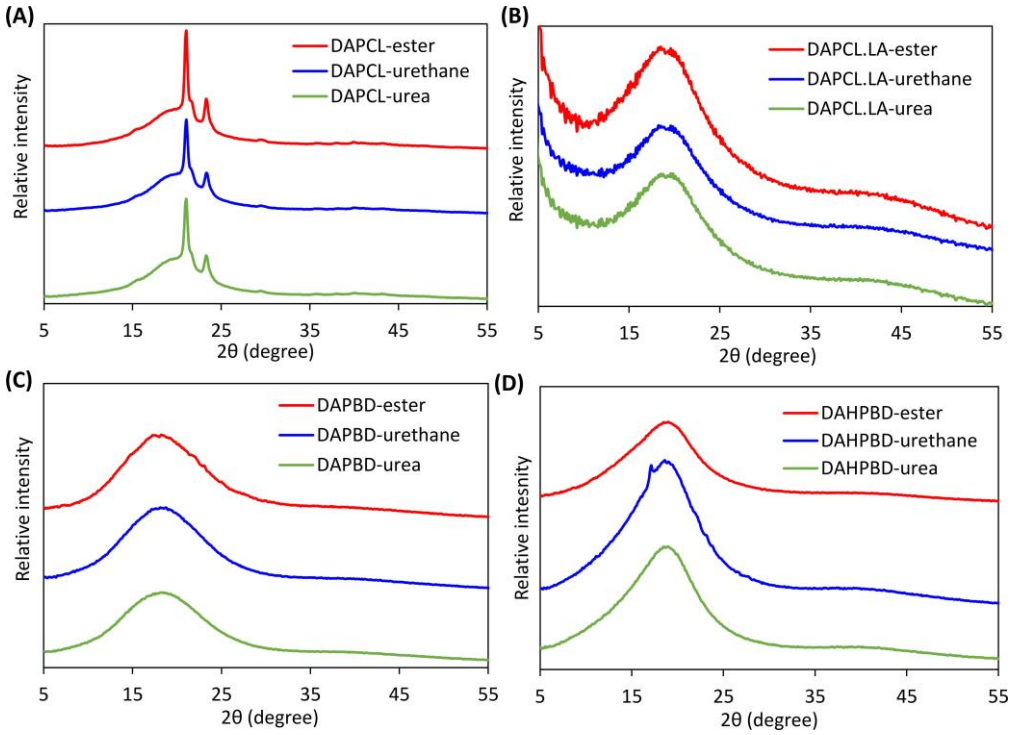

Figure 4.15 *WAXS profiles of* ***(A) DAPCL, (B) DAPCL.LA, (C) DAPBD*** *and* ***(D) DAHPBD****-PU CANs with different TF-cross-linkers.*

All materials showed SAXS patterns comprising a main scattering peak due to phase separated domains, whilst some materials were more complex with additional features. The Lorentz-corrected (Iq^2) SAXS plots of the **DAPCL** and **DAPCL.LA**-PU CANs displayed broad scattering features at q_{max} values between 0.05-0.08 $Å^{-1}$. The average interdomain spacing (d) can be calculated according to the Bragg equation: $d = 2\pi/q_{max}$, giving d-spacing values for these peaks between 7.9-12.5 nm. This periodic

scattering feature is likely caused predominantly by nanoscale phase separation of the polar TF-cross-linkers from the less polar **PCL** or **PCL.LA** polymer matrix. The SAXS profiles of the linear **DA-PCL** and **DA-PCL.LA** TPUs (from chapter 2) were overlayed for comparative purposes, demonstrating that without TF-cross-linker only a small or no scattering peak was observed, confirming that cross-linking is the driving force for microphase-separation. Similar SAXS patterns were observed by Wang *et.al.* when they incorporated quadruple H-bonds and boronic ester bond co-cross-links into styrene-butadiene elastomer vitrimers, revealing the formation of microphase-separated domains in the rubber matrix. [34]. **DAPCL-urea** and **DAPCL.LA-urea** display additional broad scattering peaks at lower q_{max} values with d-spacing values of 30.2 and 28.2 nm, respectively. These scattering features are likely caused by the aggregation of TF-urea cross-linkers *via* strong intramolecular urea bidentate H-bonding and π-π stacking of the furan aromatic rings, confining these bonding motifs to larger nanoscale hard domains within the soft PCL or PCL.LA matrix.[35] Sun *et al.,* observed similar results by exploiting hydrogen-bonding induced aggregation using dynamic covalent pyrazole-urea motifs to create phase-separated PDMS-based elastomers.[36]

The **DAPBD** and **DAHPBD-**PU CANs exhibited pronounced scattering maxima at q_{max} 0.054-0.066 $Å^{-1}$ corresponding to d-spacing values between 9.5-11.6 nm. These scattering peaks are more intense than the PCL materials, which may result from the higher electron density differences between the phases. Such features were also observed in the linear **DAPBD** and **DAHPBD** TPUs from chapter 2, indicating that they predominantly originate from microphase separation between the non-polar PBD or HPBD SSs and the polar HSs comprising MDI and DA-cycloadducts. The SAXS scattering features of the linear **DAPBD** and **DAHPBD** TPUs however exhibited higher q_{max} values corresponding to smaller d-spacings of 6.6 and 6.2 nm, respectively. This indicates that the **DAPBD** and **DAHPBD-**PU CANs displayed greater distances between hard domains, which could be attributed to extra microphase separation of the polar TF-cross-linkers from the non-polar PBD/HPBD matrix. The Lorentz-corrected SAXS plots of the **DAHPBD**-PU CANs displayed additional broad scattering peaks with lower q_{max} values between 0.0045-0.0067 $Å^{-1}$, suggesting the formation of larger HS aggregates with domain sizes between 94-140 nm.[37]

DAPBD-ester also showed a weaker, broad scattering feature at q_{max} = 0.018 Å^{-1} with a d-spacing of 35 nm, whilst **DAPBD-urethane** and **DAPBD-urea** revealed scattering shoulders at low q_{max} values, indicating further ordering but on a smaller scale than the **DAHPBD**-PU CANs.

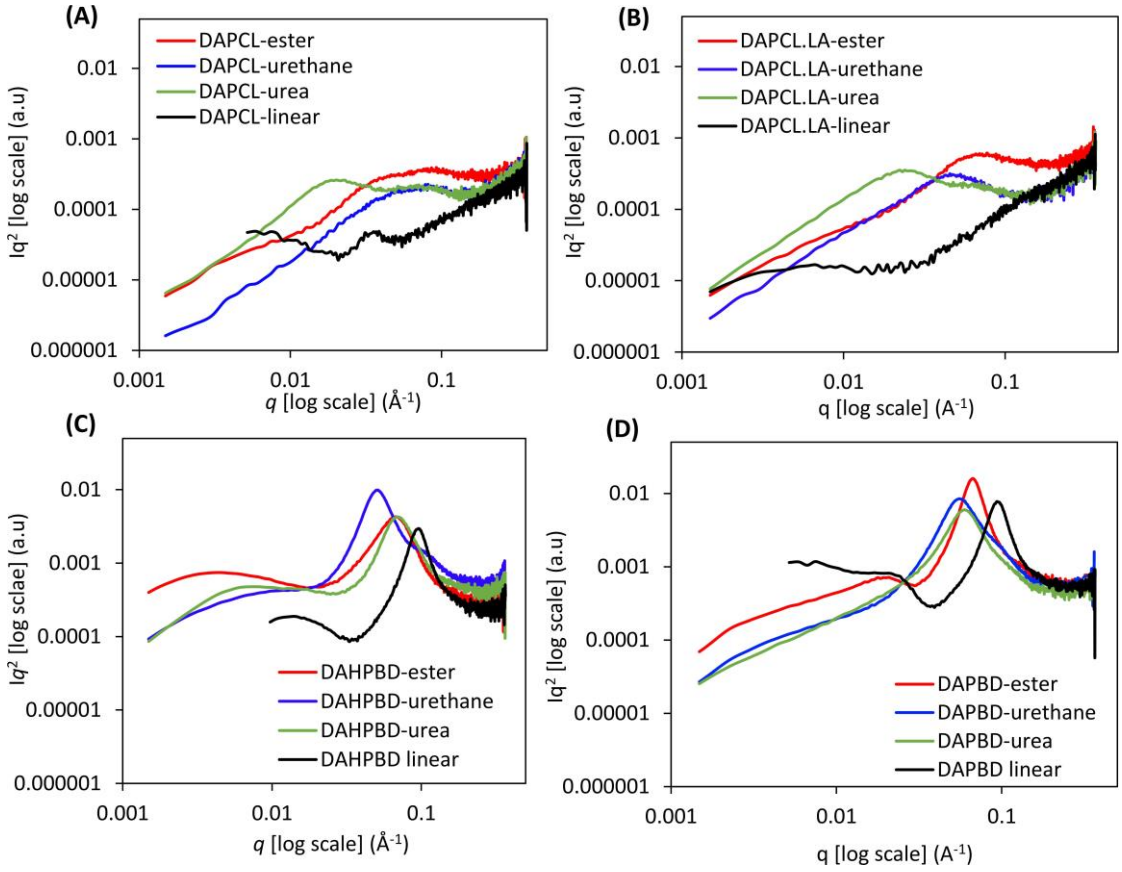

Figure 4.16 *Lorentz-corrected SAXS plots of* ***(A) DAPCL, (B) DAPCL.LA, (C) DAPBD*** *and* ***(D) DAHPBD****-PU CANs with different TF-cross-linkers compared to* ***linear*** *DA-TPUs at room temperature.*

4.2.3 Effect of cross-linking

Comparing the stress-strain curves of the **DA-PU** CANs to the corresponding linear **DA-TPUs** (Chapter 2) illustrates that cross-linking increases the tensile strength of the polymers as it creates a three-dimensional (3D) network which is more robust and resistant to deformation under stress (***Figure 4.17***). Moreover, the networks display higher f_g values meaning more DA-covalent bonds have to be broken during stretching. On the other hand, elongation at break and flexibility decrease upon cross-linking as the introduction of rigidity in the 3D network reduces the motion of polymer chains. The increase in tensile strength upon cross-linking is most pronounced when comparing **DAPCL.LA-linear**

(σ_b of 0.3 MPa) to **DAPCL.LA-ester** (6.5 MPa) whilst there is only a 60% decrease in elongation at break. On the other hand, **DAPCL**-linear and **DAPBD**-linear samples exhibited significantly enhanced elongations (1030 and 680%) over **DAPCL-ester** and **DAPBD-ester** (690 and 353%), respectively whilst displaying similar σ_b values.

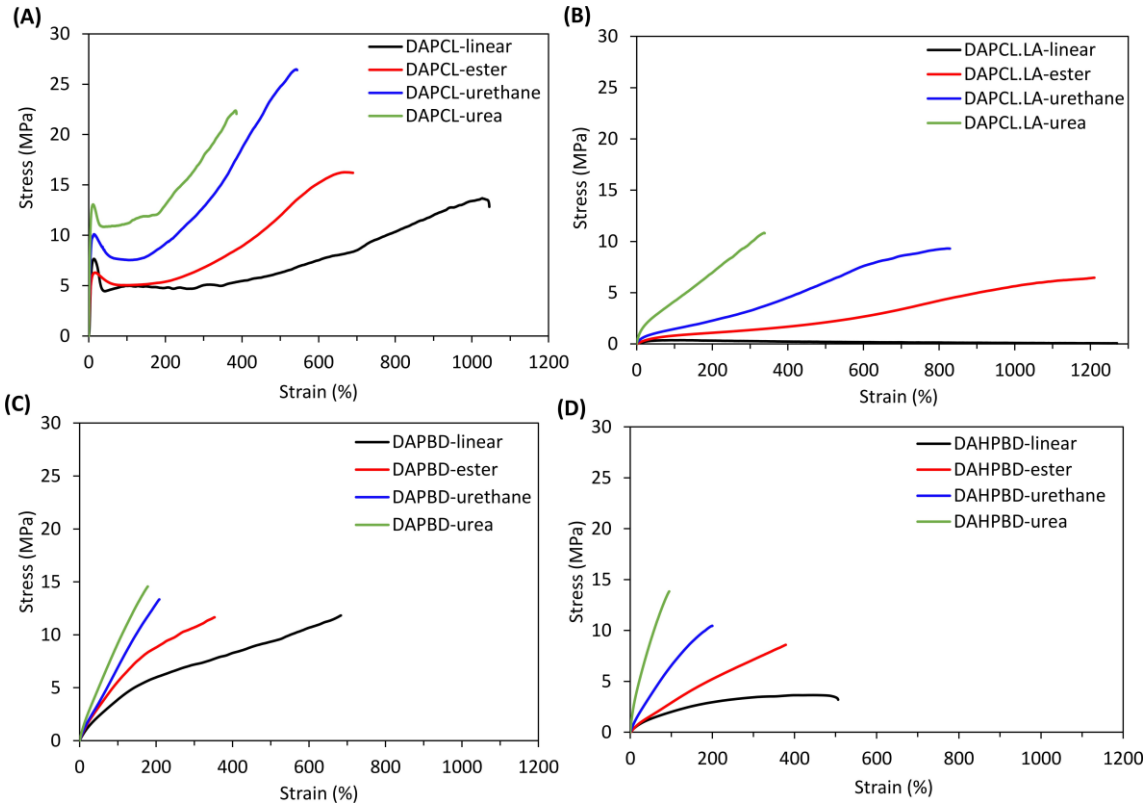

Figure 4.17 *Representative stress-strain curves of* ***(A) DA-PCL-linear*** *and* ***DAPCL-PU CANs, (B) DA-PCL.LA-linear*** *and* ***DAPCL.LA-PU CANs (C) DA-PBD-linear*** *and* ***DAPBD-PU CANs****, and* ***(D) DA-HPBD-linear*** *and* ***DAHPBD-PU*** *CANs obtained from tensile testing.*

The effect of cross-linking on the viscoelastic properties of the polymeric materials was also determined *via* DMA, by comparing the *E'* against temperature plots of the **DA-PU** CANs to the corresponding **DA-TPUs** (***Figure 4.18***). For all bismaleimide prepolymer backbones, the T_f increased upon cross-linking demonstrating increased thermal stability as more energy is required to dissociate the higher concentration of covalent DA-cycloadducts present in the **DA-PU** CAN networks. There is also a clear increase in the $E'_{rubbery}$ upon cross-linking for all polymer backbones, indicating that the **DA-PU** CANs display greater structural integrity than the **DA-TPUs**. This increase was more pronounced in the **DAPCL** and **DAPCL.LA**-PU CANs than in the **DAPBD** and **DAHPBD**-PU CANs, as the linear **DAPBD**

and **DAHPBD** TPUs exhibited synergistic reinforcement from physical interactions due to microphase separation. The PBD and HPBD DA-materials could be useful in elastomer applications such as recyclable tyres which require low temperature flexibility yet high temperature stability. On the other hand, the **DAPCL** and **DAPCL.LA** PU materials could be used in medical applications which require elastomers of high strength and elongation.

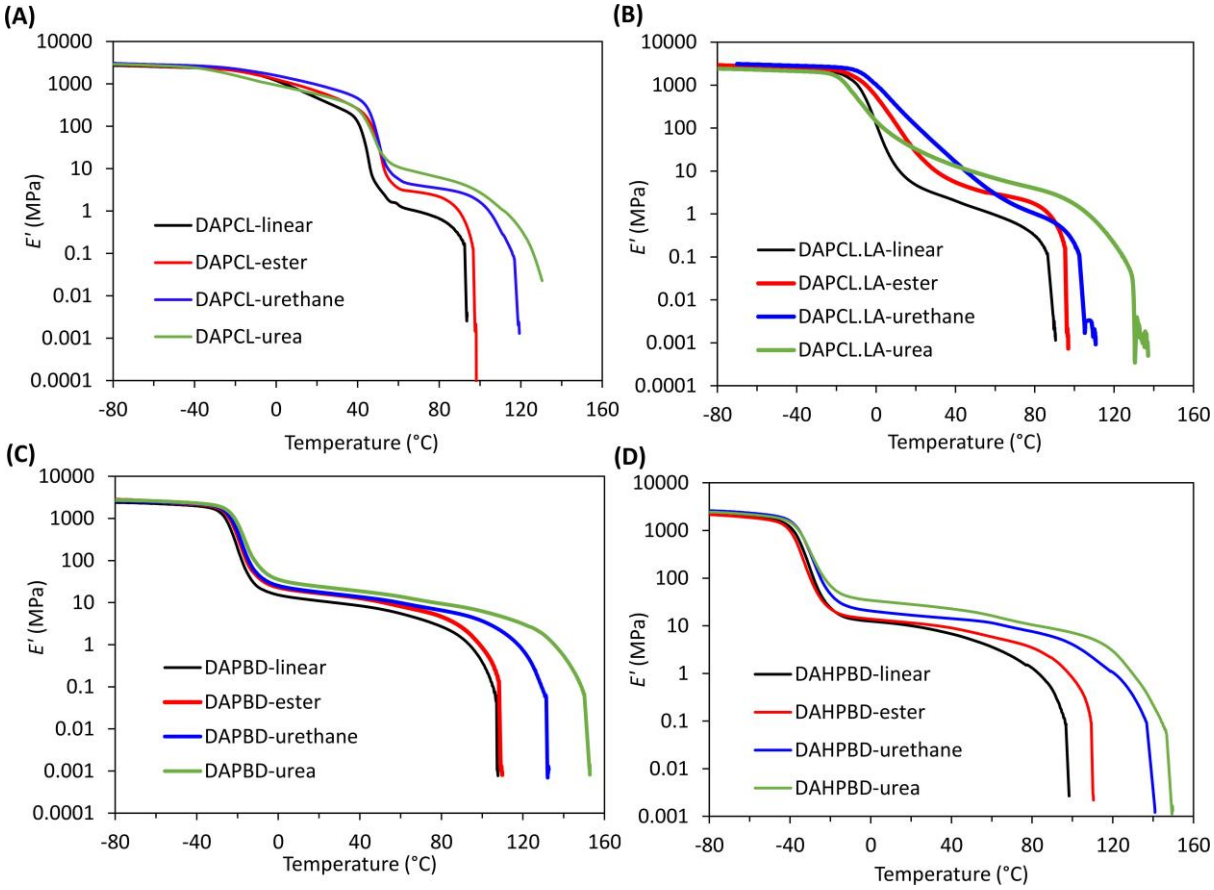

Figure 4.18 *E' against temperature DMA plots of* ***(A) DA-PCL****-linear and* ***DAPCL****-PU CANs,* ***(B) DA-PCL.LA****-linear and* ***DAPCL.LA****-PU CANs,* ***(C) DA-PBD-linear*** *and* ***DAPBD****-PU CANs, and* ***(D) DA-HPBD****-linear and* ***DAHPBD****-PU CANs.*

4.3 Conclusions

Three trifuran (TF) cross-linkers with isocyanurate cores and ester, urethane, or urea functional groups: TF-ester, TF-urethane, and TF-urea, respectively, were synthesised. ^{1}H NMR and ^{13}C NMR spectroscopy confirmed successful incorporation of furan functional groups *via* facile quantitative reaction, in high yield. ATR-FTIR spectroscopy and DSC analysis revealed differences in degree of cross-linker H-bonding and thermal properties. The TF cross-linkers were copolymerised with the four telechelic bismaleimide PU prepolymers from Chapter 2 (**PPM-PCL**, **PPM-PCL.LA**, **PPM-PBD** and **PPM-HPBD**), to produce 12 **DA-PU** CANs with f_g values between 0.54-0.61 mol.kg^{-1}. After conditioning for 7 days at ambient temperature, Soxhlet extraction experiments and ATR-FTIR spectroscopy demonstrated successful DA-network formation *via* high gel fractions (≥ 90%), and low maleimide absorptions at ν_{max} = 696cm^{-1}. **DA-PU** CANs exhibited double dissociation endotherms and sharp drops in *E'* between 100-146 °C *via* DSC and DMA, respectively, confirming the rDA reaction. DMA also demonstrated that the temperature of viscous flow (T_f), crucial for processing, could be increased by up to 40 °C through enhanced cross-linker H-bonding, meeting requirements imposed by different manufacturing techniques. Additionally, viscoelastic properties were tuneable with bismaleimide backbone, *i.e* **DAPBD** PU CANs displayed lower T_g yet higher T_f values, with more stable rubbery plateaus than the **DAPCL**-based PU CANS, providing improved thermal stability.

Network strength increased whilst flexibility significantly decreased with increasing degree of cross-linking H-bonding, leading to an overall decrease in tensile toughness. PU-CANs incorporating **DAPCL** and **DAPCL.LA** bismaleimide backbones exhibited superior flexibility to those containing **DAPBD** and **DAHPBD**. Unexpectedly, **DAPCL**-PU CANs demonstrated superior hydrolysis resistance to **DAPBD**-PU CANs. **DAPCL** and **DAPBD**-PU CANs could be thermally reprocessed using mild conditions, retaining excellent mechanical properties after 3 recycles, demonstrating a sustainability advantage over thermoset PU elastomers. Comparing the thermomechanical properties of linear **DA-TPUs** from Chapter 2 to the **DA-PU** CANs demonstrated that cross-linking increases tensile strength and decreases flexibility, whilst enhancing thermal stability of DA-polymers.

SAXS revealed that **DAPCL** and **DAPCL.LA**-PU CANs displayed broad scattering peaks between q_{max} 0.05-0.08 $Å^{-1}$, attributed to nanoscale phase separation of PCL polymer matrix from the TF-cross-linkers. **DAPCL** and **DAPCL.LA-**PU CANs containing **TF-urea** exhibited additional scattering peaks at lower q_{max} values, linked to the aggregation of **TF-urea** cross-linker *via* strong intramolecular forces. **DAPBD** and **DAHPBD-**PU CANs presented pronounced scattering peaks between q_{max} 0.054-0.066 $Å^{-1}$, predominantly originating form nanoscale phase separation between the non-polar PBD or HPBD SSs and the polar HSs comprising MDI and DA-cycloadducts.

This work describes the synthesis of a library of hybrid networks comprising both dynamic covalent and non-covalent thermally reversible bonds. The findings show how non-covalent H-bonds can be used to synergistically reinforce the thermally reversible DA-covalent bonds, providing tuneable thermomechanical and morphological properties with degree of H-bonding.

4.4 Experimental

4.4.1 Materials

Desmodur® N 3300 was supplied by Covestro. Butyl acetate (BuOAc), dibutyltin dilaurate (DBDTL), dichloromethane (DCM), dimethylformamide (DMF), deuterated chloroform ($CDCl_3$, 99.8 atom % D), deuterated dimethyl sulfoxide (DMSO-d_6, 99.5 atom % D), furfuryl amine (FAM), furfuryl alcohol (FA), fufuryl mercaptan (FM), tris[2-(acryloyloxy)ethyl] isocyanurate (TAEICN), and triethylamine (NEt_3) were all purchased from Sigma-Aldrich. The telechelic bismaleimide PU prepolymers (PPM-PCL, PPM-PCL.LA, PPM-PBD and PPM-HPBD) were made as described in chapter 2. All materials were used as supplied.

4.4.2 Synthesis of TF-ester cross-linker

Tris[2-(acryloyloxy)ethyl] isocyanurate (TAEICN, 3 g, 7.09 mmol) was dissolved in DCM (5.4 mL) in the presence of TEA (0.5 mL) in a 100 mL round bottom flask. Furfuryl mercaptan (FM, 2.55 g, 22.33 mmol) was added to the solution and the mixture was stirred in an ice bath for 1 h. The stirring was continued

for 14 h at 40 °C, followed by the removal of the solvent in vacuo. The excess FM was removed under high vacuum to produce a pale-yellow viscous liquid (TF-ester, 82% yield).

^{1}H NMR (400 MHz, $CDCl_3$, 298 K,): δ = 7.35 (d, $^{3}J^{H-H}$ = 1.2 Hz, 3H, OC*H*=CH-CH)), 6.30 (d, $^{3}J^{H-H}$ = 2.5 Hz, 3H, OCH=CH-C*H*), 6.19 (d, $^{3}J^{H-H}$ = 3.1 Hz, 3H, OCH=C*H*-CH), 4.32 (t, $^{3}J^{H-H}$ = 5.2 Hz, 6H, SCH_2CH_2COO), 4.15 (t, $^{3}J^{H-H}$ = 5.1 Hz, 6H, S-CH_2CH_2COO), 3.71 (s, 6H, $CH_2CH_2SCH_2C(O)=CH$), 2.73 (t, $^{3}J^{H-H}$ = 7.3 Hz, 6H, NCH_2CH_2OOC), 2.53 (t, $^{3}J^{H-H}$ = 7.3 Hz, 6H, NCH_2CH_2OOC) ppm. **^{13}C NMR** (125 MHz, $CDCl_3$, 298 K) δ = 171.7 (*C*=O), 151.3 (N-*C*=O), 148.9 (O-*C*=C), 142.2 (O-C=*C*), 110.6 (CH_2-C=*C*), 107.6 (CH_2-*C*=C), 61.2 (N-CH_2-*C*H_2), 42.0 (N-*C*H_2-CH_2), 34.2 (*C*H_2-CH_2-S), 28.3 (S-*C*H_2-), 26.3 (CH_2-*C*H_2-S) ppm. **ATR-FTIR***:* ν_{max} = 1730 (C(=O)-O), 1686 (N-C(=O)-N), 1504 (Ar C=C), 1237 and 1148 (C-O) and 737 (FA C-H) cm^{-1}.

4.4.3 Synthesis of TF-urethane cross-linker

In a 4-necked flask equipped with a mechanical stirrer, reflux condenser and nitrogen inlet, Desmodur N3300 (HDI trimer, 500 g, 2590 mmol isocyanate) was mixed with toluene (300 mL) and 4 drops of DBDTL and the mixture was stirred with a mechanical stirrer and heated to 85 °C in an oil bath. Furfuryl alcohol (FA, 254 g, 2592 mmol) was added dropwise with mechanical stirring and heated for 3 hours until infra-red spectroscopy indicated disappearance of the isocyanate band at 2200 cm^{-1}. Toluene was removed under vacuum using a rotary evaporator and residual solvent was evaporated using Kugelrohr distillation set up at 70 °C. The product was further dried in a vacuum oven overnight at 60 °C. This gave multifunctional furan TF-urethane as an off-white liquid which solidified upon cooling to room temperature.

^{1}H NMR (400 MHz, CDCl3, 298 K): δ = 7.40 (d, $^{3}J_{H-H}$ = 2.2 Hz, 3H, OCH=CH-CH), 6.38 (d, $^{3}J_{H-H}$ = 3.3 Hz, 3H, OCH=CH-CH), 6.34 (s, 3H, OCH=CH-CH), 5.03 (s, 6H, COOCH2 C(O)=CH), 4.81 (s, 3H, NH), 3.84 (m, 6H, NCH2), 3.15 (m, 6H, CH2 NH), 1.75-1.25 (m, 24H, CH2) ppm. **^{13}C NMR** (125 MHz, $CDCl_3$, 298 K): δ = 155.95 (O-*C*(=O)-NH), 150.02 (N-C(=O)-N), 148.90 (furfuryl C-O), 143.03 (furfuryl CH-O), 110.39 (CH=*C*H-CH), 110.19 (CH-*C*H=C), 58.26 (C-*C*H_2-O), 42.70 (NH-*C*H_2-CH_2), 40.79 (N-*C*H_2-CH_2), 29.61 (NH-

CH_2-*C*H_2), 27.56 (N-CH_2-*C*H_2) and (CH_2-*C*H_2-CH_2), 26.13 (CH_2-*C*H_2-CH_2) ppm. **ATR-FTIR** ν_{max} = 3328 (N-H), 2994 – 2835 (C-H), 1740-1610 (C(=O)-O) and (N-C(=O)-N), 1532 (Ar C=C), 1250 & 1153 (C-O) and 733 (FA C-H) cm^{-1}.

4.4.4 Synthesis of TF-urea cross-linker

In a 4-necked flask equipped with a mechanical stirrer, reflux condenser and nitrogen inlet, Desmodur N3300 (HDI trimer, 500 g, 2590 mmol isocyanate) was mixed with ethyl acetate (300 mL) and 4 drops of DBDTL and the mixture was stirred with a mechanical stirrer and heated to 80 °C in an oil bath. Furfuryl amine (FAM, 251.7 g, 2592 mmol) was added dropwise with mechanical stirring and heated for 3 hours until infra-red spectroscopy indicated disappearance of the isocyanate band at 2200 cm^{-1}. Toluene was removed under vacuum using a rotary evaporator and residual solvent was evaporated using Kugelrohr distillation set up at 70 °C. The product was further dried in a vacuum oven overnight at 60 °C. This gave multifunctional furan TF-urea as a yellow powder (90% yield).

^{1}H NMR (400 MHz, DMSO-d_6, 298 K): δ = 7.53 (s, 3H, OC*H*=CH-CH), 6.36 (d, $^3J_{H\text{-}H}$ = 3.3 Hz, 3H, OCH=CH-C*H*), 6.16 (dd, $^3J_{H\text{-}H}$ = 1.8 Hz, 3H, OCH=C*H*-CH and s, 3H, N*H*CH_2C(O)=CH), 5.73 (s, 3H, CH_2N*H*CONH), 4.16 (s, 6H, NHC*H*$_2$C(O)=CH), 3.71 (m, 6H, NC*H*$_2$), 3.32 (s, 2H, *H*$_2$O), 2.96 (s, 8H, C*H*$_2$NHCONH), 1.7-1.0 (m, 24H, C*H*$_2$) ppm. **^{13}C NMR** (125 MHz, DMSO-d_6, 298 K): δ = 158.18 (NH-*C*(=O)-NH), 154.26 (furfuryl *C*-O), 149.35 (N-C(=O)-N), 142.26 (furfuryl CH-O), 110.83 (CH=*C*H-CH), 106.53 (CH-*C*H=C), 42.60 (N-*C*H_2-CH_2), ~40.00 (NH-*C*H_2-CH_2), 36.81 (NH*C*H2C(O)=C), 30.35 (NH-CH_2-*C*H_2), 27.66 (N-CH_2-*C*H_2), 26.47 and 26.36 (CH_2-*C*H_2-CH_2) ppm. **ATIR-FTIR** ν_{max} = 3320 (N-H), 2976– 2810 (C-H), 1730-1620 (C(=O)-O) and (N-C(=O)-N), 1626 (NHC(=O)NH and NH urea) 1569 (Ar C=C), 1250 & 1150 (C-O) and 728 (FA C-H) cm^{-1}.

4.4.5 Synthesis of DA-PU CANs

DA-PU networks were synthesised *via* solvent casting four bismaleimide PU prepolymers based on different polyol backbones (**PPM-PCL**, **PPM-PCL.LA**, **PPM-PBD** and **PPM-HPBD**) separately with three

trifuran cross-linkers (**TF-ester**, **TF-urethane**, and **TF-urea**) to give 12 networks. TF-ester and TF-urethane cross-linkers were solvent casted in DCM whilst TF-urea cross-linker was solvent casted in DMF. The mass of reagents required to achieve 1 : 1 furan : maleimide stoichiometric ratio were calculated based on the molar masses of the cross-linkers (**TF-ester** = 766 $g.mol^{-1}$, **TF-urethane** = 799 $g.mol^{-1}$ and **TF-urea** = 793 $g.mol^{-1}$) and the theoretical molar masses of the bismaleimide PU prepolymers (using OH values to determine the theoretical molar mass of polyol + the molar mass of two MDI units + the molar mass of two FA or two HEMI end units), where **PPM-PCL** = 2764 $g.mol^{-1}$, **PPM-PCL.LA** = 2753 $g.mol^{-1}$, **PPM-PBD** = 2878 $g.mol^{-1}$ and **PPM-HPBD** = 3193 $g.mol^{-1}$. A typical procedure is as follows: **PPM-PCL** (10 g, 3.6 mmol) and **TF-ester** (1.85 g, 2.4 mmol) were added to a 50 mL glass vial followed by 20 mL of CH_2Cl_2 solvent. The components were stirred at room temperature until a homogenous solution formed after which the solution was cast into a PTFE-lined petri dish. The solvent casted network was left in the fume hood overnight so that most of the CH_2Cl_2 evaporated. Residual CH_2Cl_2 was removed in a vacuum oven at 40 °C overnight. After solvent removal the bulk PU network was compression moulded at 110 °C for 10 minutes using 3 MPa of pressure to produce a bubble-free, 1 mm elastomeric sheet which was left at 25 °C for 7 days prior to testing. For DAPU-networks containing **TF-urea** cross-linker a similar procedure was used but DMF and mild heating (60 °C) were required to fully solubilise the cross-linker to achieve a homogenous solution. Samples were also placed in a vacuum oven at 80 °C for 3 days to remove residual DMF. Moreover, compression moulding was typically carried out between 120-130 °C using 3 MPa of pressure for 20 minutes.

DAPCL-ester: **ATIR-FTIR**: ν_{max} = 3334 (N-H), 2997-2820 (C-H), 1775 (C=O DA), 1722 (PCL C(=O)-O and free NHC(=O)N), 1693 (N-C(=O)-N and H-bonded NHC(=O)N), 1597 (C-N),1531 (Ar C=C), 1216 & 1155 (C-O) and 725 (FA C-H) cm^{-1}. **DSC:** T_{mPCL} = 44 °C, ΔH_{mPCL} = 17.8 $J.g^{-1}$, T_{rDA} = 107 & 134 °C, and ΔH_{rDA} = 11.0 $J.g^{-1}$.

DAPCL-urethane: **ATIR-FTIR**: ν_{max} = 3334 (N-H), 2997-2820 (C-H), 1774 (C=O DA), 1722 (PCL C(=O)-O and free NHC(=O)N), 1695 (N-C(=O)-N and H-bonded NHC(=O)N), 1598 (C-N), 1532 (Ar C=C), 1224 &

1157 (C-O) and 734 (FA C-H) cm^{-1}. **DSC**: T_{mPCL} = 44 °C, ΔH_{mPCL} = 20.0 $J.g^{-1}$, T_{rDA} = 115 & 146 °C, and ΔH_{rDA} = 10.8 $J.g^{-1}$.

DAPCL-urea: **ATIR-FTIR**: ν_{max} = 3337 (N-H), 2997-2810 (C-H), 1771 (C=O DA), 1728 (PCL C(=O)-O and free NHC(=O)N), 1697-1630 1695 (N-C(=O)-N, H-bonded NHC(=O)N and H-bonded NHC(=O)NH), 1595 (C-N),1528 (Ar C=C), 1242 & 1156 (C-O) and 726 (FA C-H) cm^{-1}. **DSC**: T_g = -43 °C, T_{mPCL} = 36 & 43 °C, ΔH_{mPCL} = 6.1 $J.g^{-1}$, T_{rDA} = 115 & 143 °C, and ΔH_{rDA} = 10.4 $J.g^{-1}$.

DAPCL.LA-ester: **ATIR-FTIR**: ν_{max} = 3330 (N-H), 3020-2790 (C-H), 1732 (PCL C(=O)-O, LA C(=O)-O and free NHC(=O)N), 1694 (N-C(=O)-N and H-bonded NHC(=O)N), 1597 (C-N),1536 (Ar C=C), 1214 & 1165 (C-O) and 725 (FA C-H) cm^{-1}. **DSC**: T_g = -16 °C, T_{rDA} = 113 & 133°C, and ΔH_{rDA} = 11.8 $J.g^{-1}$.

DAPCL.LA-urethane: **ATIR-FTIR**: ν_{max} = 3329 (N-H), 3020-2790 (C-H), 1726 (PCL C(=O)-O, LA C(=O)-O and free NHC(=O)N), 1701 (N-C(=O)-N and H-bonded NHC(=O)N), 1596 (C-N),1535 (Ar C=C), 1216 & 1164 (C-O) and 722 (FA C-H) cm^{-1}. **DSC**: T_g = -18 °C, T_{rDA} = 116 & 142 °C, and ΔH_{rDA} = 11.3 $J.g^{-1}$.

DAPCL.LA-urea: **ATIR-FTIR**: ν_{max} = 3337 (N-H), 2997-2810 (C-H), 1771 (C=O DA), 1728 (PCL C(=O)-O, LA C(=O)-O and free NHC(=O)N), 1697-1630 (N-C(=O)-N, H-bonded NHC(=O)N and H-bonded NHC(=O)NH), 1595 (C-N),1528 (Ar C=C), 1242 & 1156 (C-O) and 726 (FA C-H) cm^{-1}. **DSC**: T_g = -21 °C, T_{rDA} = 135 °C, and ΔH_{rDA} = 12.0 $J.g^{-1}$.

DAPBD-ester: **ATIR-FTIR**: ν_{max} = 3328 (N-H), 3070 (C=C $_{stretch\ 1,2}$), 3050-2780 (C-H), 1775 (C=O DA), 1735 (TF-ester C(=O)-O and free NHC(=O)N), 1692 (N-C(=O)-N, H-bonded NHC(=O)N), 1640 (C=C $_{stretch}$) 1597 (C-N), 1528 (Ar C=C), 995 (C=C $_{bending\ 1,2}$), 965 (C=C $_{bending\ 1,4\ trans}$), and 907 (C=C $_{bending\ 1,2}$) cm^{-1}. **DSC**: $T_{g\ lower}$ = -29 °C, $T_{g\ upper}$ = 41 °C, T_{rDA} = 129 °C, and ΔH_{rDA} = 12.4 $J.g^{-1}$.

DAPBD-urethane: **ATIR-FTIR**: ν_{max} = 3327 (N-H), 3070 (C=C $_{stretch\ 1,2}$), 3050-2780 (C-H), 1775 (C=O DA), 1735 (free NHC(=O)N), 1700 1640 (C=C $_{stretch}$) 1597 (C-N), 1528 (Ar C=C), 995 (C=C $_{bending\ 1,2}$), 965 (C=C $_{bending\ 1,4\ trans}$), and 907 (C=C $_{bending\ 1,2}$) cm^{-1}. **DSC**: $T_{g\ lower}$ = -29 °C, $T_{g\ upper}$ = 54 °C, T_{rDA} = 137 °C, and ΔH_{rDA} = 11.2 $J.g^{-1}$.

DAPBD-urea: **ATIR-FTIR**: ν_{max} = 3327 (N-H), 3070 (C=C $_{stretch\ 1,2}$), 3050-2780 (C-H), 1775 (C=O DA), 1740 (free NHC(=O)N), 1700-1660 (N-C(=O)-N, H-bonded NHC(=O)N and H-bonded NHC(=O)NH), 1640 (C=C $_{stretch}$), 1597 (C-N), 1532 (Ar C=C), 995 (C=C $_{bending\ 1,2}$), 965 (C=C $_{bending\ 1,4\ trans}$), and 907 (C=C $_{bending\ 1,2}$) cm^{-1}. **DSC**: $T_{g\ lower}$ = -29 °C), $T_{g\ upper}$ = 55 °C, T_{rDA} = 136 °C, and ΔH_{rDA} = 9.6 $J.g^{-1}$.

DAHPBD-ester: **ATR-FTIR**: ν_{max}= 3334 (N-H), 2998-2760 (C-H), 1775 (C=O DA), 1727 (TF-ester C(=O)-O and free NHC(=O)N), 1693 (N-C(=O)-N, H-bonded NHC(=O)N), 1597 (C-N), 1527 (Ar C=C) cm^{-1}. **DSC**: T_g = -44 °C, T_{rDA} = 121 & 140 °C, and ΔH_{rDA} = 11.7 $J.g^{-1}$.

DAHPBD-urethane: **ATR-FTIR**: ν_{max}= 3340 (N-H), 2998-2760 (C-H), 1775 (C=O DA), 1739 (free NHC(=O)N), 1698 (N-C(=O)-N, H-bonded NHC(=O)N), 1597 (C-N), 1529 (Ar C=C) cm^{-1}. **DSC**: $T_{g\ lower}$ = -44 °C, $T_{g\ upper}$ = 56 °C, T_{rDA} = 122 & 146 °C, and ΔH_{rDA} = 11.7 $J.g^{-1}$.

DAHPBD-urea: **ATR-FTIR**: ν_{max}= 3338 (N-H), 2998-2760 (C-H), 1775 (C=O DA), 1739 free NHC(=O)N), 1697 (N-C(=O)-N, H-bonded NHC(=O)N), 1598 (C-N), 1529 (Ar C=C) cm^{-1}. **DSC:** $T_{g\ lower}$ = -45 °C, T_{mHS} = 52.6 °C, ΔH_{mHS} = 1.0 $J.g^{-1}$, T_{rDA} = 143 °C, and ΔH_{rDA} = 11.2 $J.g^{-1}$.

4.4.6 Instrumental methods.

Proton nuclear magnetic resonance (^{1}H NMR) spectra were recorded using a Bruker AV or AVIIIHD 400 MHz spectrometer at room temperature with ~ 10 mg of sample fully dissolved in deuterated chloroform ($CDCl_3$) or DMSO-d_6. Chemical shifts were recorded in parts per million (ppm) relative to the reference peak of chloroform solvent at δ = 7.26 ppm or dimethyl sulfoxide solvent at δ = 2.50 ppm. Spectra were analysed on MestReNova v6.0.2. **Carbon nuclear magnetic resonance (^{13}C NMR)** spectra were recorded at 125 MHz using ~ 40 mg of sample. Chemical shifts were recorded in parts per million (ppm) relative to a reference peak of chloroform solvent at δ = 77.16 ppm or DMSO solvent at δ = 39.51 ppm. **Attenuated Total Reflectance Fourier Transform Infrared (ATR-FTIR)** spectra were collected on a PerkinElmer FT-Infra-red spectrometer equipped with a UATR Two accessory. Eight scans were taken in the range of 4000 – 400 cm^{-1}. Analysis was performed on PerkinElmer Spectrum software. **Differential scanning calorimetry (DSC)** was performed using a TA instruments Discovery

DSC 25. Less than 3 mg of sample was accurately weighed on a microbalance and loaded into a T_{zero} aluminium pan. Heating and cooling ramps (from -90 °C to 200 °C) were conducted under a N_2 flow (40 mL.min^{-1}) at a standard rate of 10 °C.min^{-1}. T_g was taken as the midpoint of inflexion. T_m and T_{rDA} were measured as the temperature at the minimum heat flow of the appropriate endotherms. Analysis was performed on TRIOS v5.1.1 software. **Dynamic Mechanical Analysis (DMA)** was performed using a TA Instruments Q800 DMA using tensile clamps. Sample dimensions were typically 10 mm length by 5 mm width by 1 mm thickness. Samples were evaluated between -80 °C and 200 °C at a heating rate of 3 °C.min^{-1}. A deformation frequency of 1 Hz and a strain of 0.05% were used. **Monotonic uniaxial extension experiments** were carried out on a Zwickiline tensometer according to ISO 527 (10 mm.min^{-1} extension rate). Dumbbell specimens were cut out of approximately 1 mm thick compression moulded sheets using a ZwickRoell® knee manual cutting press ZCP 020 with cutting device for ISO 527-2 type 5B die attachment. (Length= 35 mm, gauge length = 12 mm, width = 2 mm). Before testing, thickness of each specimen was measured using a digital calliper and recorded on the software.5 specimens were tested for each material. Results were analysed on TestXpert II software. Cyclic tensile tests were conducted using an extension rate of 10 mm.min^{-1} up to 200% strain using 10 hysteresis cycles. 3 specimens were tested for each material. **Small-Angle (SAXS) and Wide-Angle (WAXS) X-ray Scattering** experiments were performed at ISIS Neutron and Muon Source, Rutherford Appleton Laboratory, Oxfordshire, United Kingdom on a Xenocs Nano-inxider using an X-ray wavelength = 1.541889 Å and an acquisition time = 10 min × 3.

4.4.7 Soxhlet experiments

Approximately 0.5 g of DA-PU CAN elastomeric sheet was accurately weighted and folded into a pre-weighed piece of filter paper. A repeat sample was made up *via* the same method. A folded piece of blank filter paper containing no sample was included as a control. Samples were inserted into a 250 mL Soxhlet extractor on top of a 500 mL round-bottom flask containing THF solvent (300 mL) with a reflux condenser attached above. The solvent was heated to reflux for 24 hours. The samples were

then removed and dried at 40 °C overnight in a vacuum oven to remove residual THF. Sample mass was recorded before and after extraction (dried).

The sample mass difference was used to calculate the gel fraction of the material. The gel fraction is defined as the weight ratio of dried network polymer (W_2) after extraction to that of the polymer before (W_1).

$[W_2 / W_1] \times 100\% = \text{Gel fraction, \%}$ (Equation 1).

4.4.8 Hydrolytic stability testing

Hydrolytic stability of the **DA-PU CAN** elastomers was performed according to ASTM D3137 – 81. Three repeat dog-bones (R1, R2 and R3) of each sample (Length= 35 mm, gauge length = 12 mm, width = 2 mm) were cut out of the same rubber sheet from which specimens were cut out for the original tensile strength using a ZwickRoell® knee manual cutting press ZCP 020 with cutting device for ISO 527-2 type 5B die attachment. The thickness of each specimen was measured, then the samples were suspended into separate 30 mL glass vials containing 20 mL of distilled water, using non-corrosive metal hooks soldered to the bottom of the container cap so that the samples were not in contact with the glass vials (***Figure 4.19***). The containers were capped loosely and placed into a circulating air oven for 96 hours at 85 °C. After 15 minutes the oven was opened briefly, and the container caps were secured tightly. At the end of the exposure period samples were removed from the oven and allowed to cool down to room temperature. Samples were then placed in the vacuum oven at 40 °C for 6 hours to remove residual water and conditioned at 25 °C for 7 days before remeasurement of tensile properties, using the original, unexposed thickness values.

Figure 4.19 *Experimental setup of dog-bones suspended in distilled water for hydrolytic stability testing.*

4.4.9 Compression moulding

5 g of each DA-PU network bulk material was cut into small pieces and spread evenly into a metal compression mould lined with a thin sheet of PTFE (***Figure 4.20***). Another PTFE sheet was placed on top followed by the metal mould lid. The metal mould was then placed between two preheated metal plates between 110-130 °C, depending on TF-cross-linker used. 3 MPa of pressure was applied for ten minutes to melt and spread the material into an even film. The mould was then removed from the heat and once cooled to room temperature, the material was removed.

Figure 4.20 *The compression moulding process.*

4.4.10 Thermal reprocessing

For thermal reprocessing pristine dumbbell samples which had been pulled apart *via* uniaxial tensile testing were combined with the rest of the original cuttings, so the total mass was 5 g, and the sample was evenly spaced into a metal compression mould lined with a thin sheet of PTFE. Another PTFE sheet was placed on top followed by the metal mould lid which was then placed between two preheated

metal plates at 110-130 °C. 3 MPa of pressure was applied for ten minutes to melt and spread the material into an even film. The mould was then removed from the heat and once cooled to room temperature, the material was carefully removed. Rubber sheets were conditioned for 7 days at ambient temperature before re-cutting of dumbbell specimens using the ZwickRoell® knee manual cutting press and remeasurement of tensile properties *via* uniaxial tensile testing (R1). This process was repeated a further two times (R2,R3) with the same samples to determine any change in mechanical properties.

4.5 References

[1] J. M. Winne, L. Leibler and F. E. Du Prez, *Polym. Chem.*, 2019, **10**, 6091-6108.

[2] T. Liu, C. Hao, L. Wang, Y. Li, W. Liu, J. Xin and J. Zhang, *Macromolecules*, 2017, **50**, 8588-8597.

[3] A. Bîrcă, O. Gherasim, V. Grumezescu and A. M. Grumezescu, in *Materials for Biomedical Engineering*, eds. V. Grumezescu and A. M. Grumezescu, Elsevier, **2019**, pp. 1-28.

[4] L. Imbernon, E. K. Oikonomou, S. Norvez and L. Leibler, *Polym. Chem.*, 2015, **6**, 4271-4278.

[5] W. Schmolke, N. Perner and S. Seiffert, *Macromolecules*, 2015, **48**, 8781-8788.

[6] W. Zou, J. H. Dong, Y. Luo, Q. Zhao and T. Xie, *Adv. Mater.*, 2017, **29**.

[7] W. Alabiso and S. Schlögl, *Polymers*, 2020, **12**, 1660.

[8] C. J. Kloxin and C. N. Bowman, *Chem. Soc. Rev*, 2013, **42**, 7161-7173.

[9] X. Chen, M. A. Dam, K. Ono, A. Mal, H. Shen, S. R. Nutt, K. Sheran and F. Wudl, *Science*, 2002, **295**, 1698-1702.

[10] L. M. Sridhar, M. O. Oster, D. E. Herr, J. B. D. Gregg, J. A. Wilson and A. T. Slark, *Green. Chem*, 2020, **22**, 8669-8679.

[11] J. H. Aubert, *J. Adhes.*, 2003, **79**, 609-616.

[12] A. A. Kavitha and N. K. Singha, *ACS Appl. Mater. Interfaces.*, 2009, **1**, 1427-1436.

[13] A. Safaei, J. Brancart, Z. Wang, S. Yazdani, B. Vanderborght, G. Van Assche and S. Terryn, *Polymers*, 2023, **15**, 3527.

[14] J. Zhao, R. Xu, G. Luo, J. Wu and H. Xia, *J. Mater. Chem. B.*, 2016, **4**, 982-989.

[15] P. Berto, A. Pointet, C. Le Coz, S. Grelier and F. Peruch, *Macromolecules*, 2018, **51**, 651-659.

[16] G. Griffini, B. Rigatelli and S. Turri, *Macromol. Mater. Eng.*, 2023, **308**, 2300133.

[17] Z. Jia, S. Zhu, Y. Chen, W. Zhang, B. Zhong and D. Jia, *Compos. Part A Appl. Sci. Manuf.*, 2020, **129**, 105709.

[18] Y. Heo, M. H. Malakooti and H. A. Sodano, *J. Mater. Chem. A*, 2016, **4**, 17403-1741.

[19] J. M. Winne, L. Leibler and F. E. Du Prez, *Polym. Chem*., 2019, **10**, 6091–6108.

[20] S. Terryn, J. Brancart, E. Roels, R. Verhelle, A. Safaei, A. Cuvellier, B. Vanderborght and G. Van Assche, *Macromolecules*, 2022, **55**, 5497-5513.

[21] P. Raffa, A. Kassi, J. Gosschalk, N. Migliore, L. M. Polgar and F. Picchioni, *Macromol. Mater. Eng.*, 2021, **306**, 2000755.

[22] Y. Y. Jo, A. S. Lee, K.-Y. Baek, H. Lee and S. S. Hwang, *Polymer*, 2017, **108**, 58-65.

[23] A. Peterson, M. Roy, J. Fagerlund, G. Lo Re and C. Müller, *Mater. Adv.*, 2021, **2**, 5171-5180.

[24] Y. Song, J. Li, G. Song, L. Zhang, Z. Liu, X. Jing, F. Luo, Y. Zhang, Y. Zhang and X. Li, *ACS Appl. Polym. Mater.*, 2023, **5**, 1302-1311.

[25] P. van den Tempel, F. Picchioni and R. K. Bose, *Macromol. Rapid. Commun.*, 2022, **43**, 2200023.

[26] Q. Zhou, Z. Sang, K. K. Rajagopalan, Y. Sliozberg, F. Gardea and S. A. Sukhishvili, *Macromolecules*, 2021, **54**, 10510-10519.

[27] B. T. McReynolds, K. D. Mojtabai, N. Penners, G. Kim, S. Lindholm, Y. Lee, J. D. McCoy and S. Chowdhury, *Polymers*, 2023, **15**, 1106.

[28] L. Q. Reyes, S. R. Swan, H. Gan, S. M. Seraji, J. Zhang and R. J. Varley, *Polym. Test*, 2021, **93**, 106873.

[29] G. Scheltjens, M. M. Diaz, J. Brancart, G. Van Assche and B. Van Mele, *React. Funct. Polym.*, 2013, **73**, 413-420.

[30] L. M. Polgar, M. van Duin, A. A. Broekhuis and F. Picchioni, *Macromolecules*, 2015, **48**, 7096-7105.

[31] M. Bartnikowski, T. R. Dargaville, S. Ivanovski and D. W. Hutmacher, *Prog. Polym. Sci*, 2019, **96**, 1-20.

[32] B. L. Dargaville and D. W. Hutmacher, *Trends. Chem.*, 2024, **6**, 5-13.

[33] Y. Chatani, Y. Okita, H. Tadokoro and Y. Yamashita, *Polym. J.*, 1970, **1**, 555-562.

[34] L. Wang, Y. Liu, Y. Qiao, Y. Wang, Z. Cui, S. Zhu, F. Dong, S. Fang, and A. Du, *Polym. Chem*, 2022, **13**, 4144-4153.

[35] S. Salimi, L. R. Hart, A. Feula, A. B. R. Toure´ and E. A. Kabova, *Eur. Polym. J.*, 2019, **118**, 88–96.

[36] S. Sun, G. Fei, X. Wang, M. Xie, Q. Guo, D. Fu, Z. Wang, H. Wang, G. Luo and H. Xia, *Chem. Eng. J.*, 2021, **412**, 128675.

[37] X. Tang, A. Feula, B. C. Baker, K. Melia, D. Hermida Merino, I. W. Hamley, C. P. Buckley, W. Hayes and C. R. Siviour, *Polymer*, 2017, **133**, 143-150.

5. Synthesis and Characterisation of Polyester DA-Networks

5.1 Introduction

Over the last decade, polyester covalent adaptable networks (CANs) have attracted significant interest in elastomer applications as they can provide a more sustainable alternative to conventional thermoset polyester networks. Unlike thermoset polyester elastomers, CANs can be reprocessed at elevated temperatures, yet provide similar mechanical, thermal and solvent robustness at room temperature, owing to the thermally reversible nature of the dynamic covalent bonds.[1] Research has started to shift towards polyester CANs as they are less toxic than PU CANs which use harmful isocyanates as monomers.[2]

As with most polymers, CANs are typically made from petroleum resources, but recently there has been a push towards using biobased and renewable feedstock, such as cellulose, natural rubber and their derivatives.[3] Biobased, Diels Alder (DA) dissociative CANs have been well documented within literature. Brande *et al*. developed self-healing bio-aromatic networks with lignin contents of up to 29 wt.% based on the thermally reversible DA reaction.[4] The networks were synthesised by reacting a furan-functionalised lignin and polyether with *N,N'*-(4,4'-methylene diphenyl) bismaleimide (BMI). Researchers have also incorporated DA-cross-links into natural rubber to obtain recyclable and self-healing properties in elastomers.[5] This was achieved by first reacting natural rubber with maleic anhydride, followed by grafting furan moieties onto the maleated rubber *via* reaction with furfuryl amine. The pendant furans were then further cross-linked with BMI. Moreover, in 2013 Zeng and coworkers reported the preparation of poly(2,5-furandimethylene succinate) *via* a condensation reaction between bio-based monomers (succinic acid and bis(hydroxymethyl)furan).[6] They produced self-healing polyester DA-CANs by cross-linking poly(2,5-furandimethylene succinate) with 1,8-bis(maleimido)triethylene glycol in different ratios to achieve a range of mechanical properties. Although the network could self-heal without external stimuli, it was more efficient when solvent or BMI solution was used, which is not environmentally friendly.

Whilst some research has been conducted on biobased polyester DA-CANs, most of the previous literature has only focussed on the synthesis of biobased furan components, reacting them with low molecular weight, toxic, non-biobased bismaleimides, such as BMI, which is not practical for consumer goods or industrial applications.[7] There has also been limited research into the structure-property relationships of such polyester DA-CANs.

This work aims to explore the synthesis of novel biobased furan-cross-linkers, made from the ring-opening addition of furfuryl glycidyl ether (FGE), with either furfuryl amine (FAM) or vegetable oil-derived dimer diamine, Priamine™ 1075 (P1075). FGE can be obtained by reaction of furfuryl alcohol with epichlorohydrin (ECO), where ECO is derived from glycerol and furfuryl alcohol from furfural. FAM can also be synthesised from furfural through reductive amination.[8,9] Bismaleimides obtained from the esterification of polyols (some with 100% biobased-content such as the vegetable oil Pripol™2033) with 6-maleimidocaproic acid (6-MCA) will also be investigated. 6-MCA can be considered as a biobased monomer as can be made from the reaction of maleic anhydride (which can be derived from vegetable feedstocks) with 6-aminocaproic acid, a natural derivative and analogue of the amino acid lysine.[10,11] The incorporation of such bio-based building blocks into polyester DA-CANs will be investigated as initial proof of concept. Note not all bismaleimides and furans are biobased. Network design parameters such as the effect of DA-cycloadduct concentration and furan backbone structure on the thermomechanical properties of the DA-networks will also be explored.

5.2 Results and discussion

5.2.1 Synthesis of bismaleimides from 6-maleimidocaproic acid

Five bismaleimides, containing different length hydrocarbon spacers were synthesised *via* Fischer esterification of the corresponding polyols with 2.1 molar equivalents 6-MCA (***Table 5.1***).

Table 5.1 *Summary of 6-MCA capped bismaleimides and calculated molar masses.*

Bismaleimide	Backbone	Molar mass [a] (g.mol^{-1})
6-MCA-1,12-DD	1,12-DD	589
6-MCA-C_{36}	C_{36} dimer diol	946
6-MCA-HPBD1000	HPBD	2044
6MCA-HPBD2000	HPBD	2695
6MCA-HPBD3000	HPBD	4310

The bismaleimide molar masses were calculated using the sum of the molar mass of the polyol (based on OH value) plus the molar mass of two 6-MCA units, minus the molar mass of two water molecules which form during the esterification and azeotrope with toluene in the dean-stark apparatus:

$$Molar\ mass\ (g.mol^{-1}) = molar\ mass\ of\ polyol + (2 \times 211.21\ g.mol^{-1}) - (2 \times 18\ g.mol^{-1})$$

The synthetic scheme of 1,12-dodecyl bismaleimidocaproate (**6-MCA-1,12-DD**) from 1,12-dodecanediol (1,12-DD) and 6-MCA is shown as an example (***Scheme 5.1***). Excess 6-MCA was subsequently removed *via* sodium bicarbonate washes or precipitation in cold methanol to purify the bismaleimides.

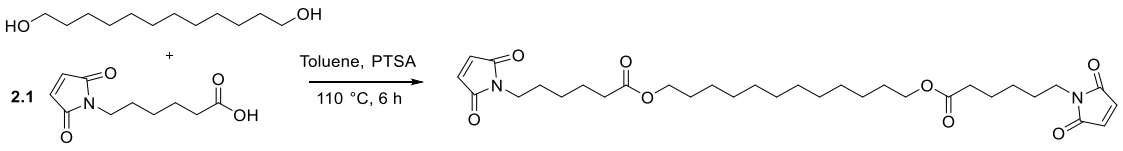

Scheme 5.1 *Synthesis of* ***6-MCA-1,12-DD*** *via Fischer esterification.*

Other commercial polyols which were esterified with 6-MCA include Pripol™ 2033 (a 100% biobased C_{36} fatty dimer diol), in addition to GI-1000, GI-2000, and GI-3000 (a series of hydroxyl-terminated hydrogenated poly(1,4-butadiene)s (HPBDs) with hydroxyl (OH) values of 67.7, 48.6 and 28.6 mgKOH.g^{-1} and calculated number-average molecular weights (M_n) of 1657, 2309 and 3923 g.mol^{-1}, respectively (***Figure 5.1***).

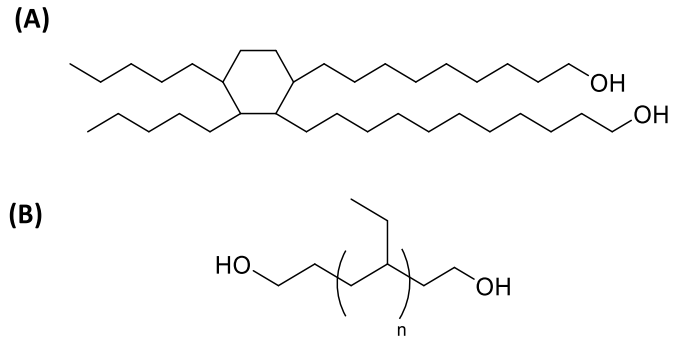

Figure 5.1 *Structures of* ***(A)*** *Pripol™ 2033-C_{36} fatty dimer diol and* ***(B)*** *GI-HPBDs where n varies with backbone molecular weight.*

^{1}H NMR spectroscopy demonstrated successful esterification of polyols with 6-MCA (***Figure 5.2***, ***Figure 5.3***, and ***Figure 5.4***). ^{1}H NMR spectra of the bismaleimides displayed resonances at δ = 4.04 ppm, representing the methylene units of the polyol backbones adjacent to the newly formed ester groups. These resonances presented higher chemical shifts than the corresponding methylene units next to the OH groups in the polyol reagents. For example, 1,12-DD showed the appearance of a resonance at δ = 3.63 ppm. All integrals were relative to the resonance at δ = 3.50 ppm (**B**), representing the methylene units adjacent to the maleimide-ring nitrogen atoms, which was set to 4.00. The corresponding integration values for the resonance at δ = 6.67 ppm (**A**), representing maleimide-ring protons, were divided by 4.00 and multiplied by 100 to determine the percentage of maleimide-end capping in each bismaleimide, giving high values between 86 and 94%. 100% maleimide functionality was not achieved, possibly due to side reactions during the Fischer esterification, such as the formation of Michael adducts from the self-addition of 6-MCA to the maleimide double bond.

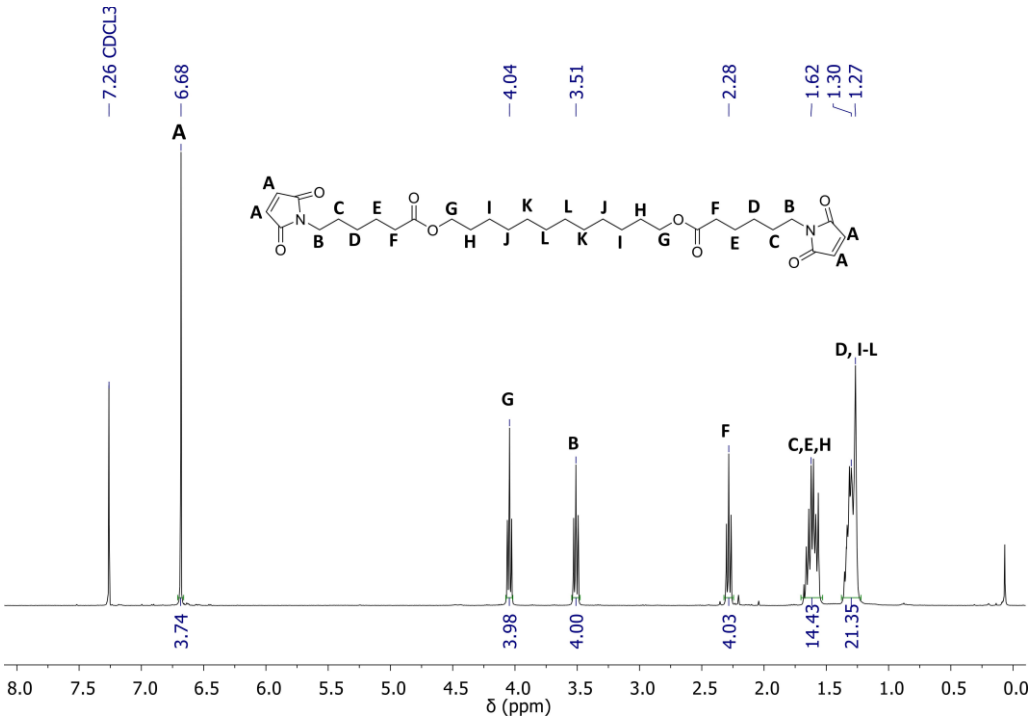

Figure 5.2 *^{1}H NMR spectrum of **6-MCA-1,12-DD**. Integrals relative to methylene units adjacent to maleimide-ring nitrogen atoms at δ = 3.51 ppm (**B**) (400 MHz, 298 K, $CDCl_3$). Chemical shifts denoted at the top and integration values denoted at the bottom.*

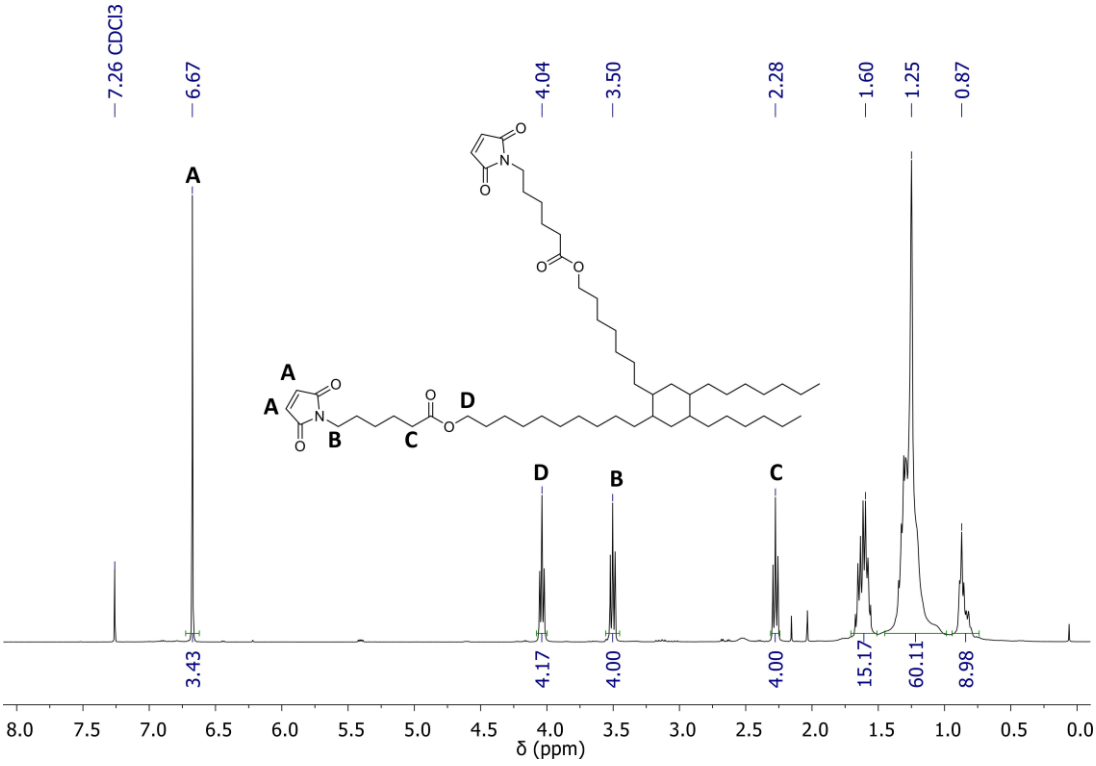

Figure 5.3 *^{1}H NMR spectrum of bismaleimidocaproyl C_{36} dimerate (**6-MCA-C_{36}**). Integrals relative to methylene units adjacent to the maleimide-ring nitrogen atoms at δ = 3.50 ppm (**B**) (400 MHz, 298 K, $CDCl_3$).*

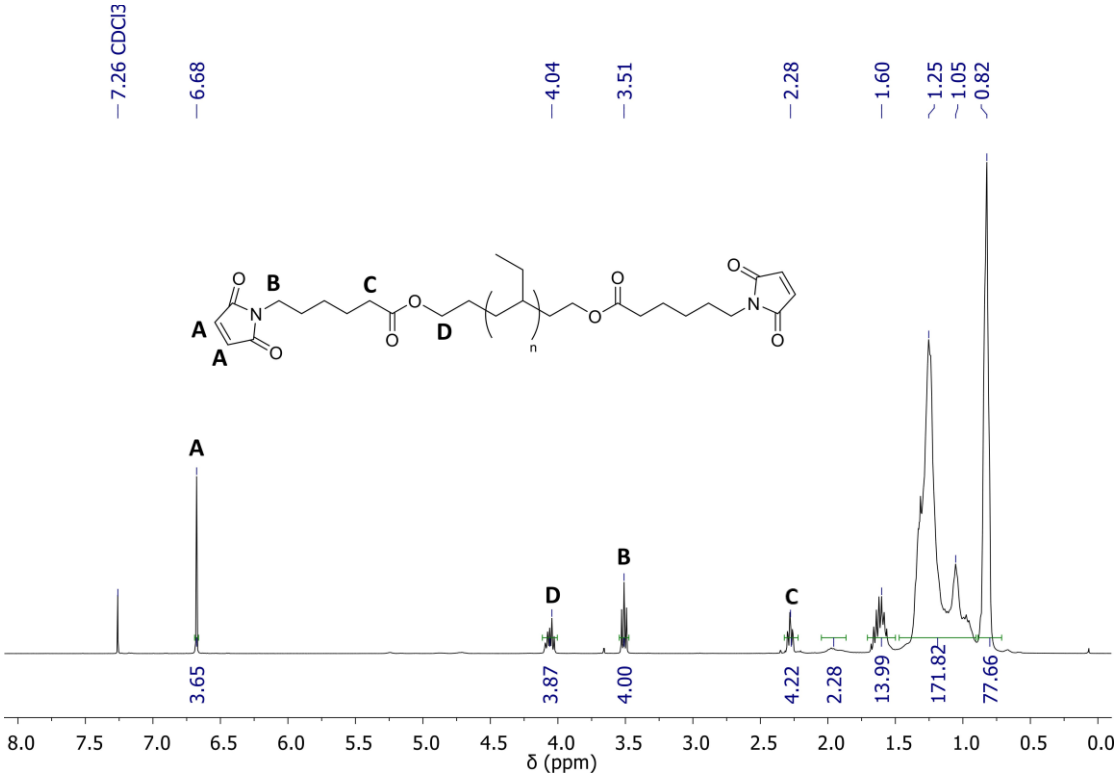

Figure 5.4 *^{1}H NMR spectrum **6-MCA-HPBD1000** as a representative example. Integrals relative to methylene units adjacent to the maleimide-ring nitrogen atoms at δ = 3.50 ppm (**B**) (400 MHz, 298 K, $CDCl_3$).*

Diffusion-ordered ^{1}H NMR spectroscopy (DOSY) was performed on the bismaleimides to determine if excess 6-MCA had been fully removed after the purification step, since it separates NMR resonances of distinct species according to their diffusion coefficient. The DOSY ^{1}H NMR spectra of all bismaleimides showed that the ^{1}H NMR signals produced a straight line on the diffusion coefficient axis, demonstrating that only one type species exists, and confirming successful removal of low molecular weight 6-MCA, using **6-MCA-HPBD1000** for demonstration (***Figure 5.5***).

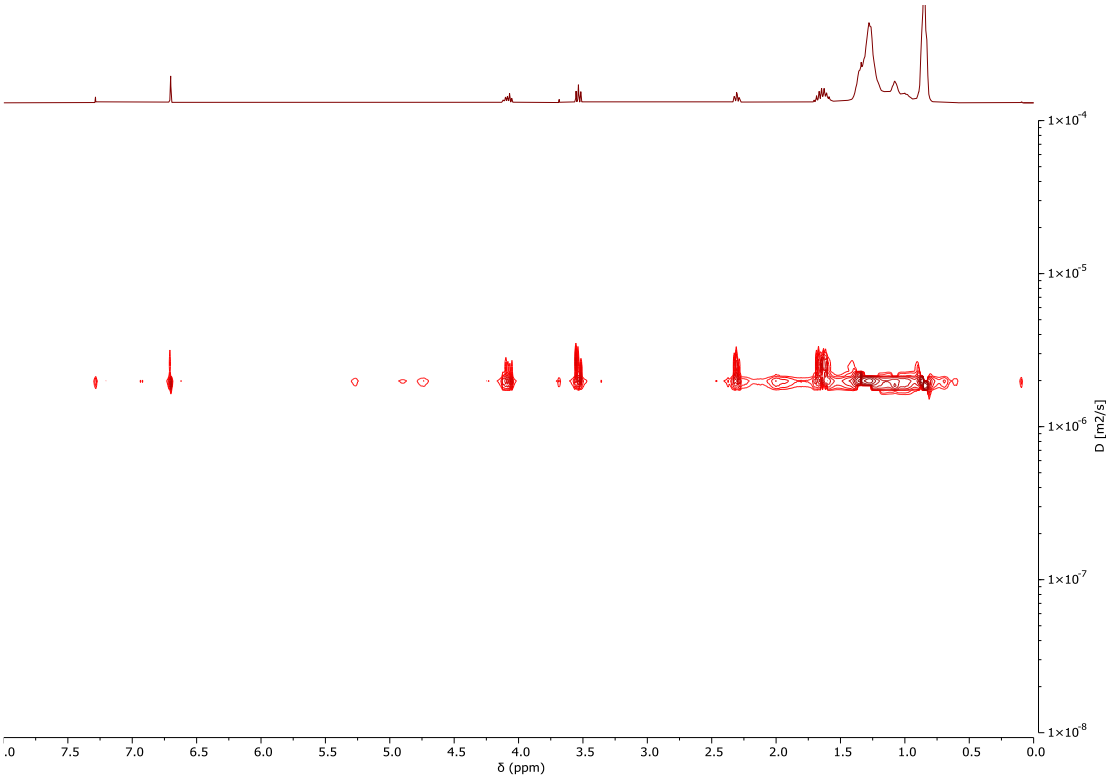

Figure 5.5 *DOSY ^{1}H NMR spectrum of* **6-MCA-HPBD1000** *as a representative example (400 MHz, 298 K, $CDCl_3$).*

Carbon (^{13}C) spectroscopy also confirmed the structures of the bismaleimides and identified characteristic carbons, using **6-MCA-1,12-DD** as an example (***Figure 5.6***). The ^{13}C NMR spectrum of **6-MCA-1,12-DD** displayed a resonance at δ = 171.05 ppm, corresponding to the carbonyl carbons of the newly formed esters (**8**). Moreover, resonances at δ = 173.67 and 134.29 ppm appeared, confirming the presence of imide carbonyl carbons (**2**) and double bond carbons (**1**) from maleimide end-groups, respectively. The ^{13}C NMR spectrum of **6-MCA-1,12-DD** also exhibited a resonance at δ = 64.74 ppm, representing the carbons of the methylene units adjacent to the newly formed ester bonds (**7,9**). All bismaleimides displayed resonances at similar chemical shifts, confirming the presence of both ester and maleimide functionality (***Experimental 5.4***).

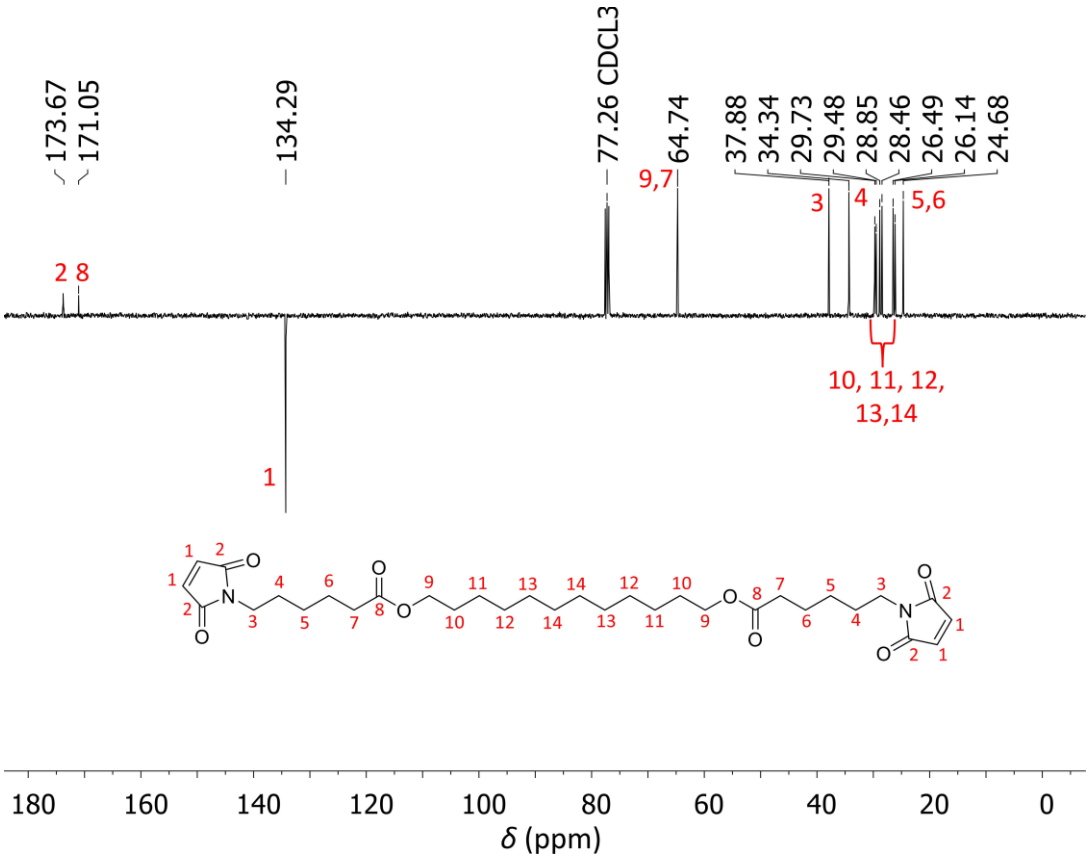

Figure 5.6 *^{13}C NMR spectrum of* ***6-MCA-1,12-DD*** *(125 MHz, 298 K, $CDCl_3$).*

ATR-FTIR spectroscopy also provided evidence of successful Fischer esterifications by comparing the FTIR-spectra of the reagents against the bismaleimide, using the synthesis of **6-MCA-1,12-DD** for representation (***Figure 5.7***). 1,12-DD displayed a broad O-H stretch at ν_{max} = 3500-3200 cm^{-1}, which disappeared in the FTIR spectrum of **6-MCA-1,12-DD**, indicating that all of the OH groups from the polyol had successfully reacted with **6-MCA**. **6-MCA** exhibited noticeable transmittance bands at ν_{max} = 1695 and 696 cm^{-1}, associated with maleimide-imide carbonyl stretching and the maleimide B1 antisymmetric ring deformation mode, respectively.[12] These bands also appeared in **6-MCA-1,12-DD**, confirming maleimide functionality. **6-MCA-1,12-DD** presented an additional FTIR carbonyl stretching band at ν_{max} = 1735 cm^{-1}, confirming the formation of ester carbonyls in the bismaleimide product.

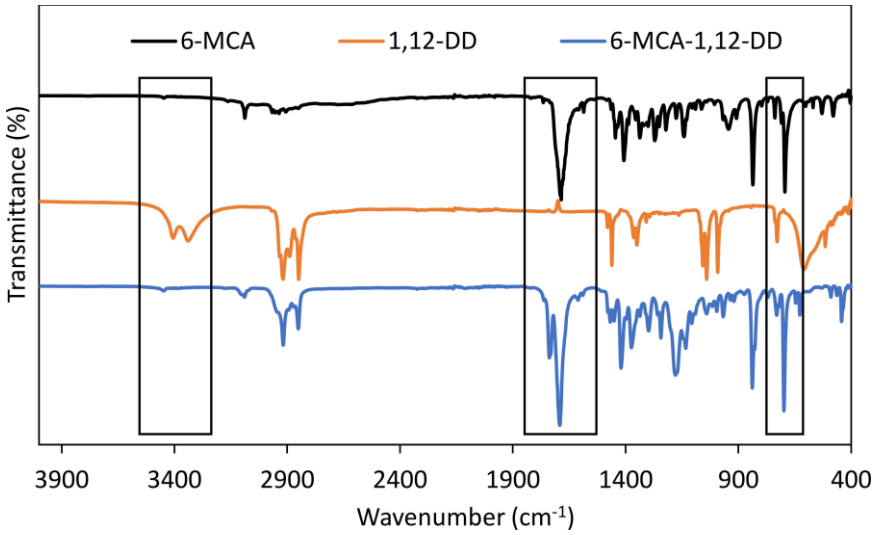

Figure 5.7 *ATR-FTIR spectra of* ***6-MCA***, ***1,12-DD*** *and* ***6-MCA-1,2-DD****. Significant regions highlighted with black boxes.*

ATR-FTIR analysis of the carbonyl and maleimide regions of the bismaleimides revealed that the normalised absorbance values for the bands at ν_{max} = 1740-1730 cm^{-1}, ν_{max} = 1715-1690 cm^{-1} and ν_{max} = 710-690 cm^{-1}, representing ester carbonyl, imide carbonyl and maleimide C=C stretching, respectively, increased as the molar mass of the hydrocarbon-spacer decreased, due to an increase in the concentration of maleimide and carbonyl functional groups (***Figure 5.8***). The wavenumber of the carbonyl stretching band also shifted to lower values, whilst the maleimide C=C stretching band broadened as the hydrocarbon-spacer molar mass decreases, indicating a higher degree of H-bonding between carbonyl groups.

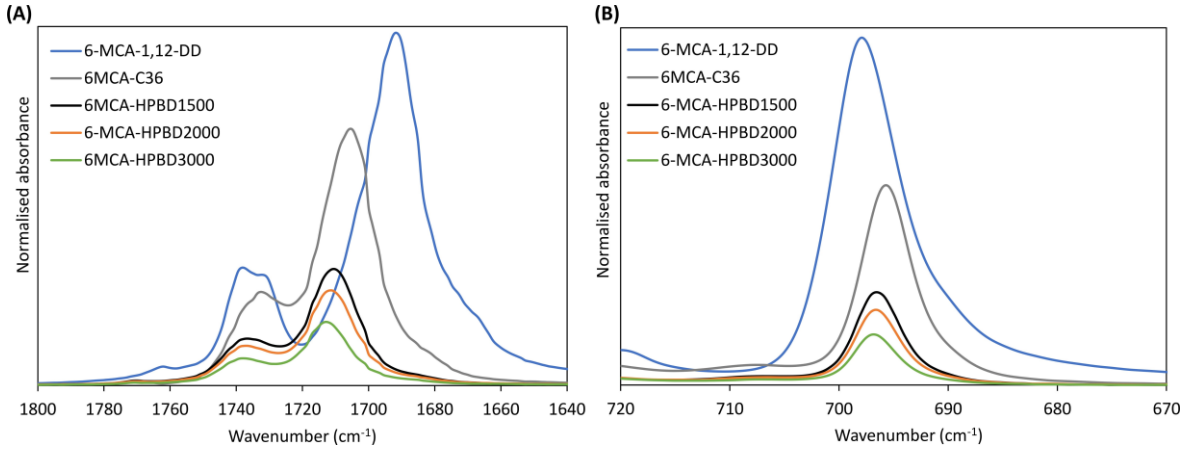

Figure 5.8 *ATR-FTIR spectra of hydrocarbon bismaleimides in* ***(A)*** *the carbonyl region and* ***(B)*** *the maleimide region.*

DSC analysis was performed on the bismaleimides to determine their thermal properties (***Figure 5.9*** and ***Table 5.2***). **6-MCA-1,12-DD** is semi-crystalline, displaying a large melting endotherm at 62.5 °C (T_m) with an enthalpy (ΔH_m) of 131.6 J.g^{-1}. The T_m was slightly lower than 1,12-DD (79-81 °C) suggesting that maleimide groups disrupt the ordering and packing of 1,12-DD chains. The glass transition temperature (T_g) of **6-MCA-1,12-DD** was too difficult to observe due to high crystallinity. All other bismaleimides are amorphous liquids with sub-ambient T_g values.

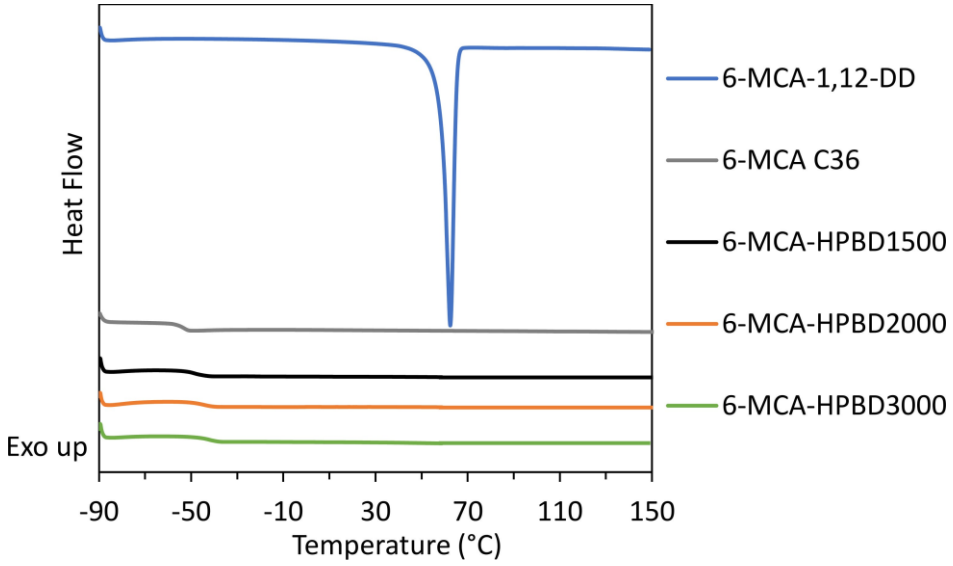

Figure 5.9 *DSC thermograms (1st heating cycles) of bismaleimides. Heating rate of 10 °C.min^{-1}.*

Table 5.2 *DSC thermal data for 6-MCA bismaleimides.*

Bismaleimide	T_g [a] (°C)	T_m [a] (°C)	ΔH_m [a] (J.g^{-1})
6-MCA-1,12-DD	-	62.5	131.6
6-MCA-C_{36}	-53.9	-	-
6-MCA-HPBD1500	-48.2	-	-
6-MCA-HPBD2000	-45.1	-	-
6-MCA-HPBD3000	-42.4	-	-

[a] *determined by DSC analysis using the 1st heating cycles at a heating rate of 10 °C.min^{-1}.*

5.2.2 Synthesis and characterisation of furfuryl glycidyl ether

Furfuryl glycidyl ether (FGE) was synthesised according to previous literature, *via* the reaction of epichlorohydrin (ECH) with furfuryl alcohol (FA), using tetrabutylammonium bromide (TBAB) in a 50 wt.% sodium hydroxide (NaOH) aqueous solution (***Scheme 5.2***).[13]

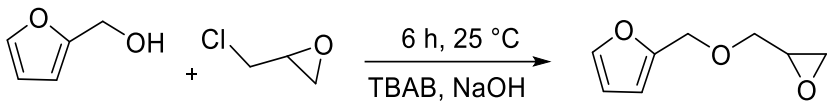

Scheme 5.2 *Synthetic route of FGE.*

^{1}H NMR spectroscopy of FGE confirmed the correct structure was achieved (***Figure 5.10***). The ^{1}H NMR spectrum of FGE contained resonances at δ = 7.41 and 6.34 ppm (**a-c**), confirming furan functionality and at δ = 3.16, 2.79 and 2.61 ppm (**f**, **g**), representing the protons on the epoxy-ring.

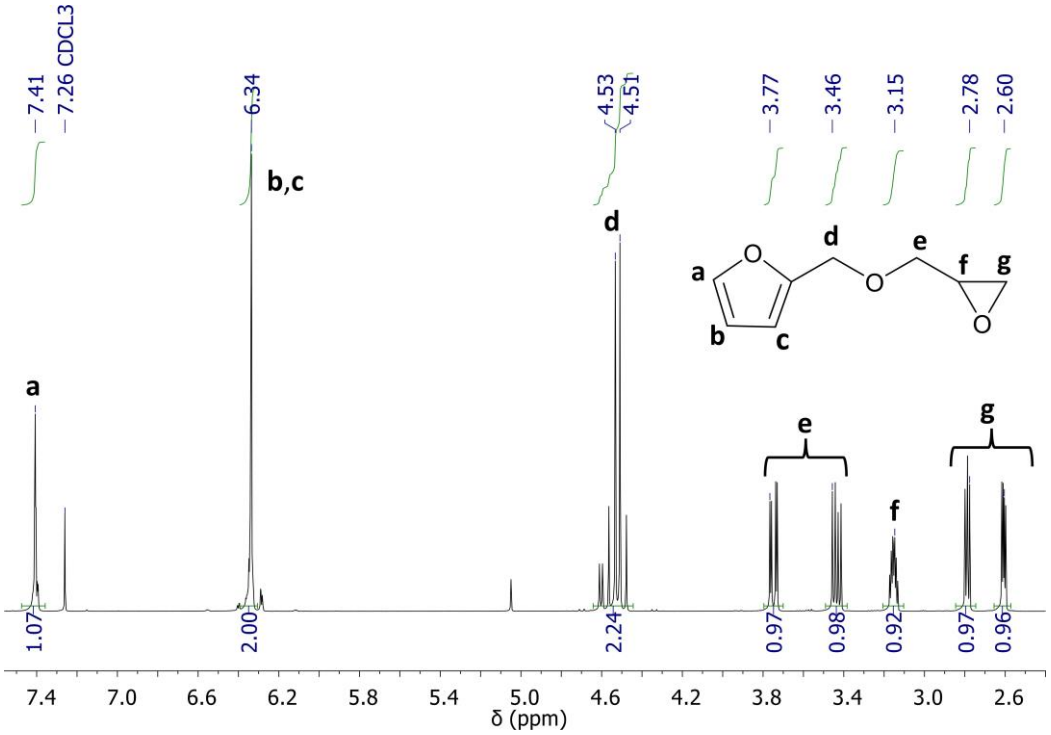

Figure 5.10 *^{1}H NMR spectrum of FGE (400 MHz, 298 K, $CDCl_3$).*

^{13}C NMR spectroscopy of FGE further confirmed its structure (***Figure 5.11***). The ^{13}C NMR spectrum of FGE displayed resonances at δ = 151.12 and 143.08 ppm, (**1** and **4**), corresponding to the carbons on the furan ring next to the oxygen. The spectrum also exhibited resonances at δ = 110.45 and 109.75 ppm (**2** and **3**) representing the two carbons in the furan ring adjacent to **1** and **4**, respectively. Additionally, resonances at δ = 50.87 and 44.44 ppm appeared, corresponding to the epoxy-ring carbons (**7** and **8**).

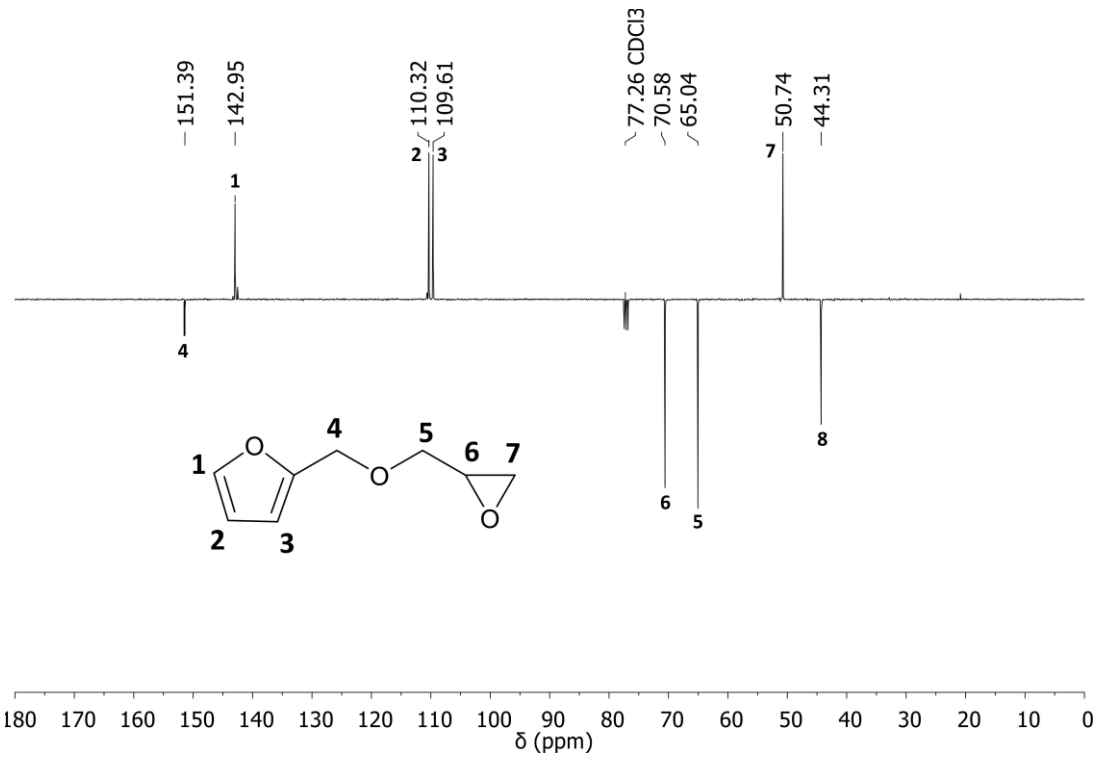

Figure 5.11 *^{13}C NMR spectrum of FGE (125 MHz, 298 K, $CDCl_3$).*

ATR-FTIR spectroscopy was performed on FGE to identify characteristic functional groups (***Figure 5.12***). The FTIR spectrum of FGE displayed absorptions at ν_{max} = 3146 and 3125 cm^{-1} for aromatic (=C-H) stretching. The FTIR spectrum also displayed an absorbance band at ν_{max} = 3062 cm^{-1} for (-C-H) stretching on the oxirane ring. An absorption at ν_{max} = 1504 cm^{-1} also appeared, representing aromatic (-C=C) stretching. Moreover, absorptions at ν_{max} = 1257, 918 and 850 cm^{-1}, representing (C-O-C) stretching on the epoxy-ring emerged. Absorptions at ν_{max} = 1217 and 1084 cm^{-1} were also observed representing (CH_2-O-CH_2) stretching. Bands at ν_{max} = 1150 and 1018 cm^{-1} appeared, corresponding to (C-O-C) stretching and (C-O-C) bending on the furan ring, respectively. An absorption was also observed at ν_{max} = 742 cm^{-1} for bending on the single-substituted furan ring.

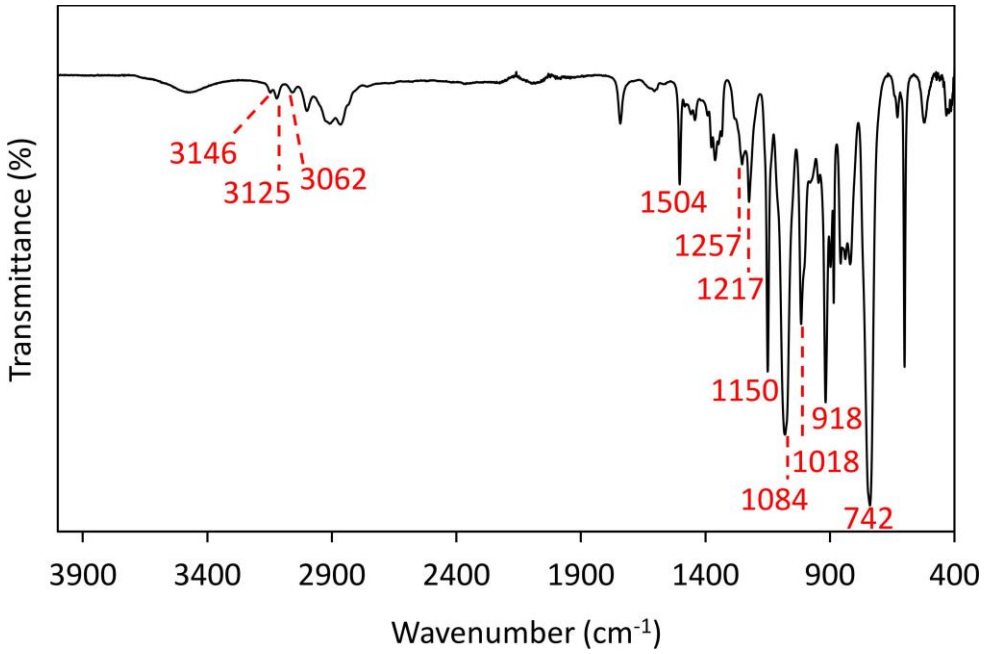

Figure 5.12 *ATR-FTIR spectrum of FGE, with significant functionalities highlighted in red.*

5.2.3 Synthesis and characterisation of FGE-FAM and FGE-P1075

Two multifunctional furan cross-linkers: trifunctional **FGE-FAM** (405.45 g.mol^{-1}) and tetrafunctional **FGE-P1075** (1151.66 g.mol^{-1}), were synthesised in bulk *via* the epoxy-amine ring-opening addition of FGE with stoichiometric amounts of FAM or vegetable-derived dimer diamine (Priamine^{TM} 1075, P1075), respectively (***Scheme 5.3***). All monomers can be derived from biomass, which is beneficial from a sustainability perspective.

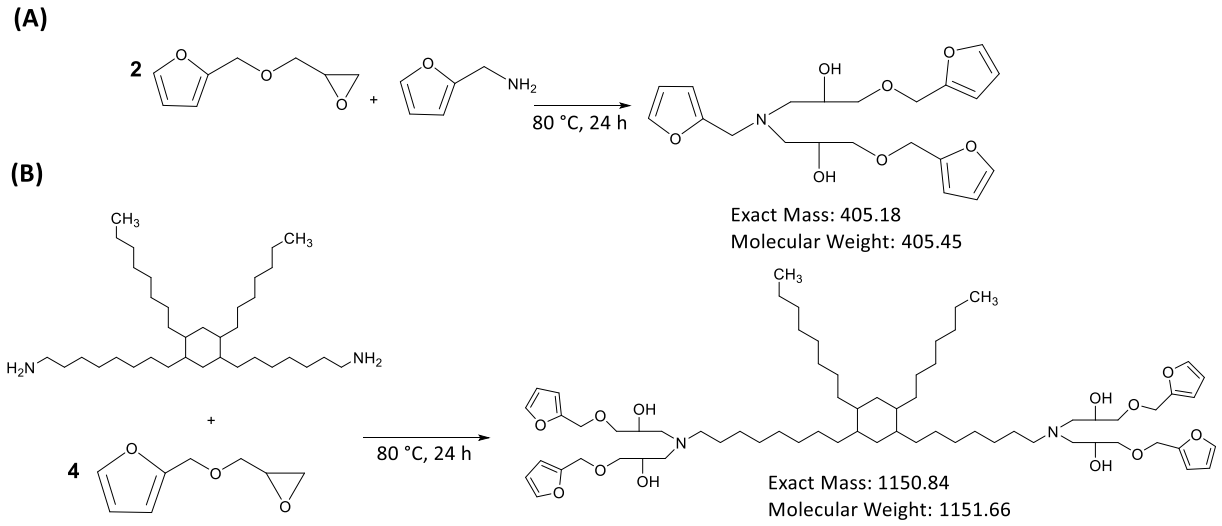

Scheme 5.3 *Synthesis of* ***(A) FGE-FAM*** *trifuran cross-linker and* ***(B) FGE-P1075*** *tetrafuran cross-linker.*

The structure of **FGE-FAM** was confirmed *via* ^{1}H NMR spectroscopy (***Figure 5.13***). Stacked ^{1}H NMR spectra illustrate that resonances at δ = 3.15, 2.78 and 2.60 ppm, corresponding to the epoxide protons in the **FGE** monomer (***Figure 5.10***) were replaced by a multiplet at δ = 2.67-2.54 ppm (**k**) in the ^{1}H NMR spectrum of **FGE-FAM**, confirming complete ring-opening addition (***Figure 5.14***). The ^{1}H NMR spectrum of **FGE-FAM** also displayed two broad singlets at δ = 3.11 and 3.03 ppm, representing the protons on the newly formed β-hydroxyls (**j**), formed *via* ring-opening addition. Moreover, resonances appeared at δ = 7.35 and 6.17 ppm in the **FGE-FAM** ^{1}H NMR spectrum, confirming the incorporation of furan protons from FAM (**b** and **f**).

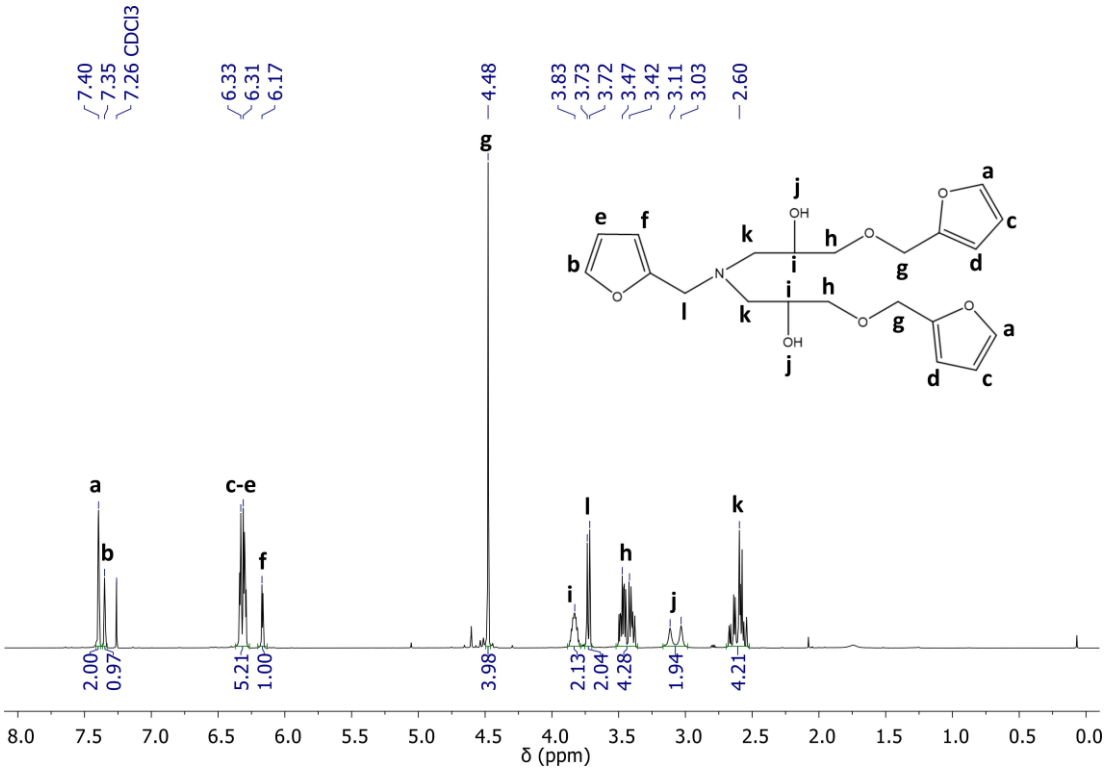

Figure 5.13 *^{1}H NMR spectrum of **FGE-FAM** cross-linker (400 MHz, 298 K, $CDCl_3$).*

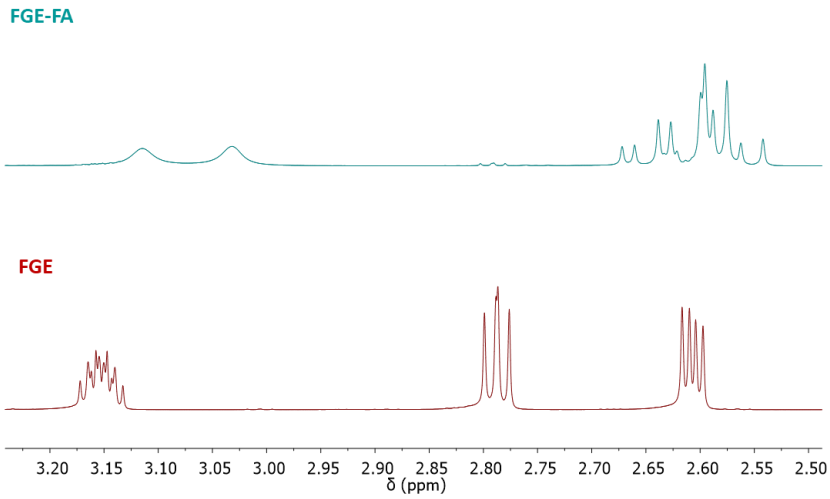

Figure 5.14 *Stacked ^{1}H NMR spectra of* ***FGE*** *monomer (bottom) and* ***FGE-FAM*** *cross-linker (top) from 3.25-2.50 ppm (400 MHz, 298 K, $CDCl_3$).*

^{13}C NMR spectroscopy also confirmed the structure of **FGE-FAM**, whilst illustrating the distinct types of carbon environments present (***Figure 5.15***). The resonances at δ = 50.87 and 44.44 ppm, representing the epoxy-ring carbons in the ^{13}C NMR spectrum of **FGE**, disappeared in the ^{13}C NMR spectrum of **FGE-FAM** demonstrating successful ring-opening addition. The ^{13}C NMR spectrum of **FGE-FAM** also exhibited resonances at δ = 68.45 and 68.07 ppm, corresponding to the carbons next to the newly formed β-hydroxy groups (**7**) *via* the ring-opening addition.

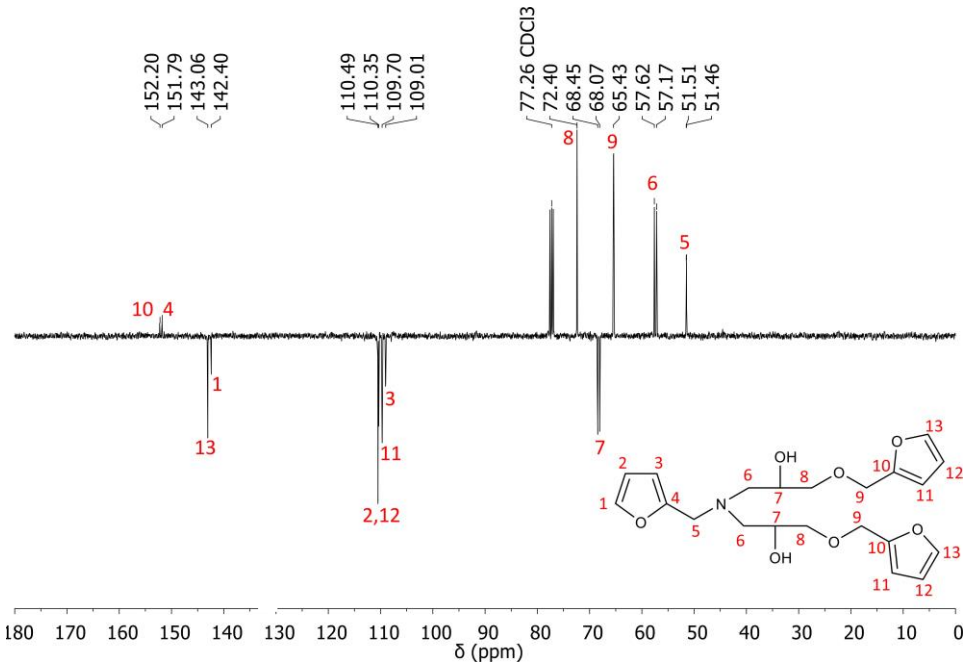

Figure 5.15 *^{13}C NMR spectrum of* ***FGE-FAM*** *(125 MHz, 298 K, $CDCl_3$).*

Electrospray ionisation mass spectroscopy (ESI-MS) was performed on **FGE-FAM** to determine whether molecular weight of the cross-linker matched the exact theoretical mass of 405.18 g.mol^{-1} (***Figure 5.16***). The time of flight (TOF) ESI mass spectrum of **FGE-FA** displayed a $[M + H]^+$ ion peak at 406.186 g.mol^{-1}, matching the exact mass of the cross-linker. Another small peak was present at 428.168 g.mol^{-1}, representing the $[M + Na]^+$ sodium adduct. This demonstrates that **FGE-FAM** was obtained in high purity.

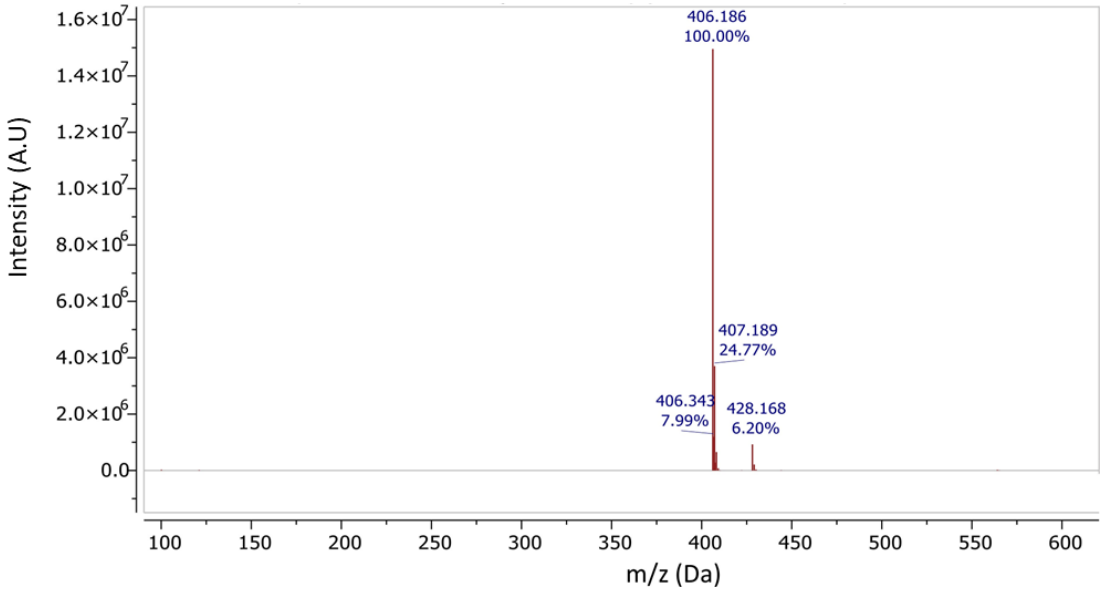

Figure 5.16 *ESI-TOF mass spectrum of* ***FGE-FAM*** *cross-linker.*

^{1}H NMR spectroscopy also confirmed the structure of **FGE-P1075**, with resonances appearing at δ = 7.40 and 6.32 ppm (**a** and **b**), indicating successful incorporation of the furan functional groups *via* facile quantitative reaction in high yield (***Figure 5.17***). The ^{1}H NMR spectrum of **FGE-P1075** also displayed a broad singlet at δ = 3.06 ppm (**f**), corresponding to the β-OH protons formed from the ring-opening addition of **FGE** epoxide-rings. A resonance was also observed at δ = 3.82 ppm (**e**), representing the four protons on the carbon atoms adjacent to the newly formed β-hydroxy groups.

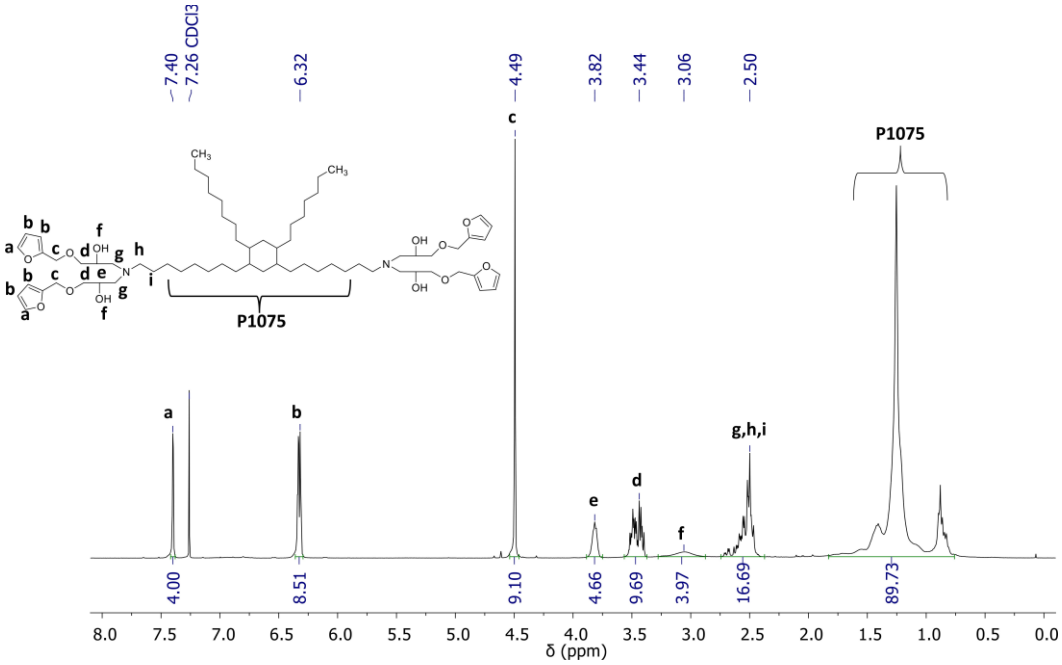

Figure 5.17 *^{1}H NMR spectrum of* ***FGE-P1075*** *cross-linker (400 MHz, 298 K, $CDCl_3$).*

The structure of **FGE-P1075** was also confirmed using ^{13}C NMR spectroscopy, with resonances between δ = 151.81-109.66 ppm, indicating the presence of furan-ring carbons (**11-14**) (***Figure 5.18***). The ^{13}C NMR spectrum also showed a resonance at δ = 65.40 ppm, representing the carbons of the methylene units next to the furan-rings (**10**). Moreover, resonances between δ = 68.93 -68.00 ppm were observed, correlating to the carbons adjacent to the β-hydroxy groups (**8**), formed from the ring-opening addition of **FGE** with **P1075**. Additionally, resonances at δ = 52.10, 50.09 and 32.15 ppm appeared for the cyclohexane carbons of the **P1075** backbone (**1-3**).

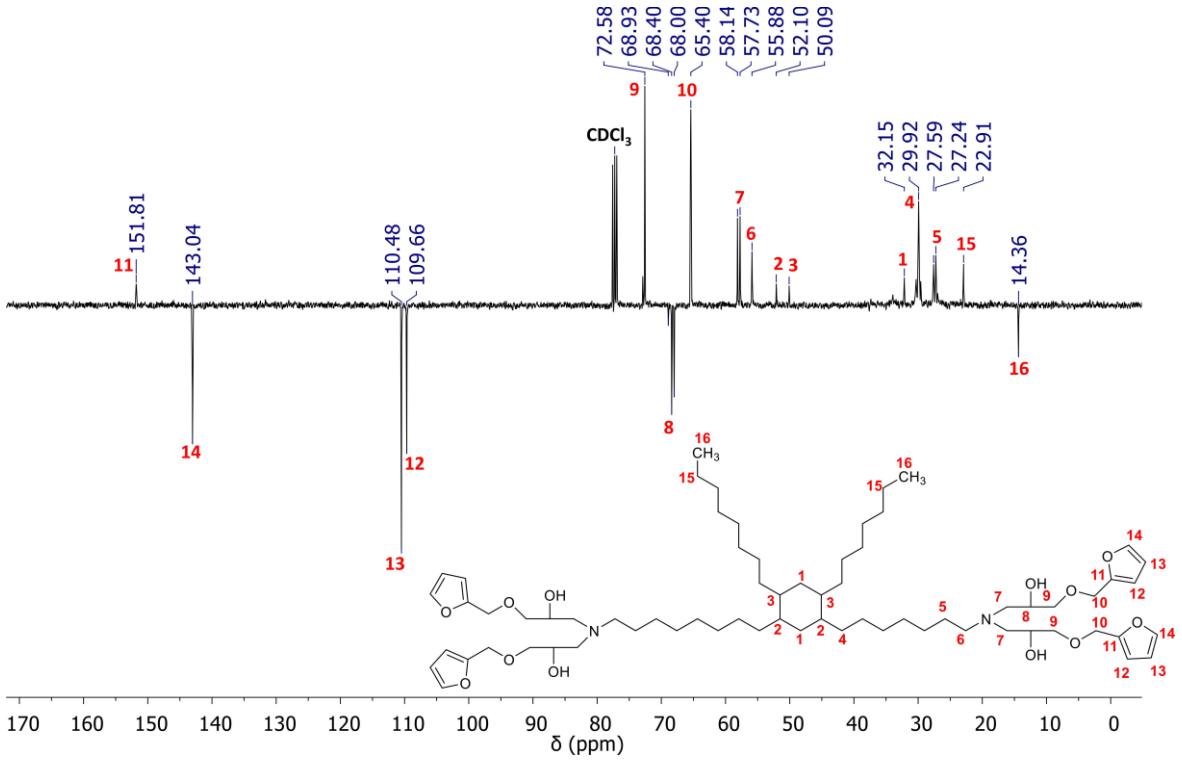

Figure 5.18 *^{13}C NMR spectrum of* ***FGE-P1075*** *(125 MHz, 298 K, $CDCl_3$).*

The ESI TOF mass spectrum of **FGE-P1075** exhibited a $[M + H]^+$ ion peak at 1151.84 g.mol^{-1}, matching the exact mass of the cross-linker (1150.84 g.mol^{-1}) (***Figure 5.19***). Another high intensity ion peak appeared at 997.675 g.mol^{-1} with an average difference in mass/charge (m/z) of 154.16 g.mol^{-1} from the $[M + H]^+$ peak. This difference in m/z is attributable to the mass of one **FGE** unit, indicating fragmentation has occurred where a ring-opened **FGE** unit is lost. Another low intensity ion peak emerged at 843.581 g.mol^{-1}, again with an average m/z difference of 154.16 g.mol^{-1} from 997.675 g.mol^{-1}, indicating further fragmentation, where two ring-opened **FGE** units are lost. Such fragmentations are likely due to facile cleavage at heteroatoms such as C-N bonds and C-O bonds.

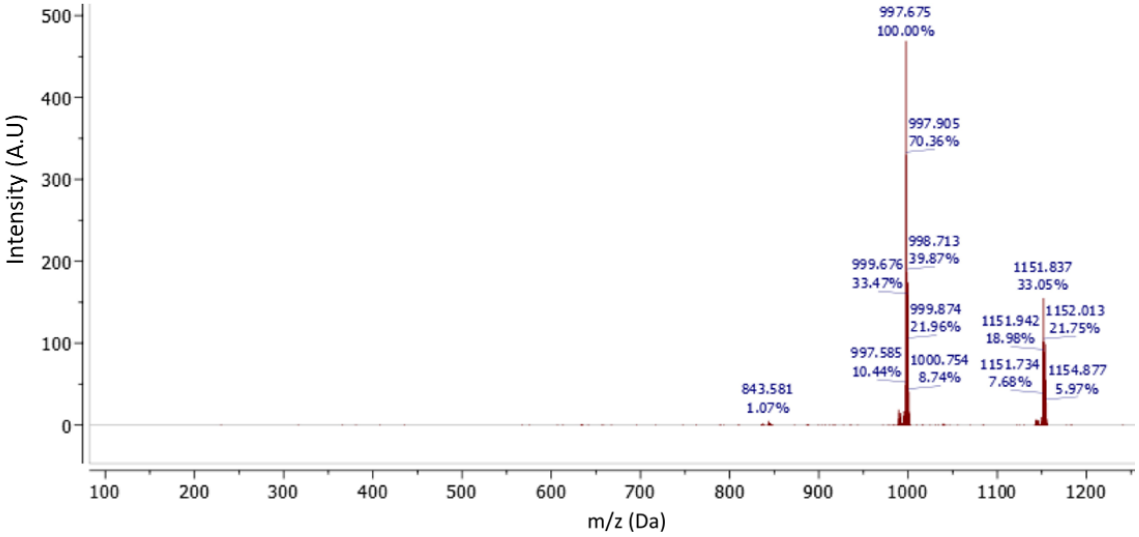

Figure 5.19 *ESI-TOF mass spectrum of* ***FGE-P1075*** *cross-linker.*

5.2.4 Synthesis and characterisation of 1,3,5-trifuryl benzoate

1,3,5-trifuryl benzoate (**TFBZ**) was synthesised *via* the reaction of 1,3,5-benzenetricarbonyl chloride with furfuryl alcohol, according to previous literature (***Scheme 5.4***).[7]

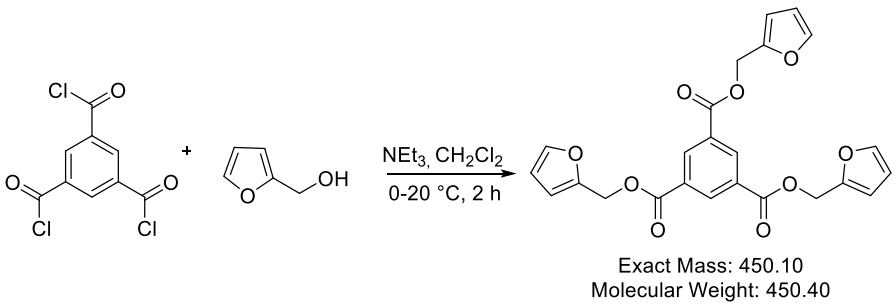

Scheme 5.4 *One-step synthesis of 1,3,5-trifuryl benzoate (**TFBZ**).*

The structure of **TFBZ** was confirmed *via* ^{1}H NMR spectroscopy, with resonances at δ =7.44 , 6.51 and 6.39 ppm (**C**-**E**), demonstrating successful covalent incorporation of furan groups *via* facile, quantitative reaction, in high yield (**Figure 5.20**). The ^{1}H NMR spectrum of **TFBZ** also displayed resonances at δ =8.85 and 5.34 ppm, representing the core benzene-ring protons (**A**) and methylene protons adjacent to the newly formed ester bonds (**B**), respectively.

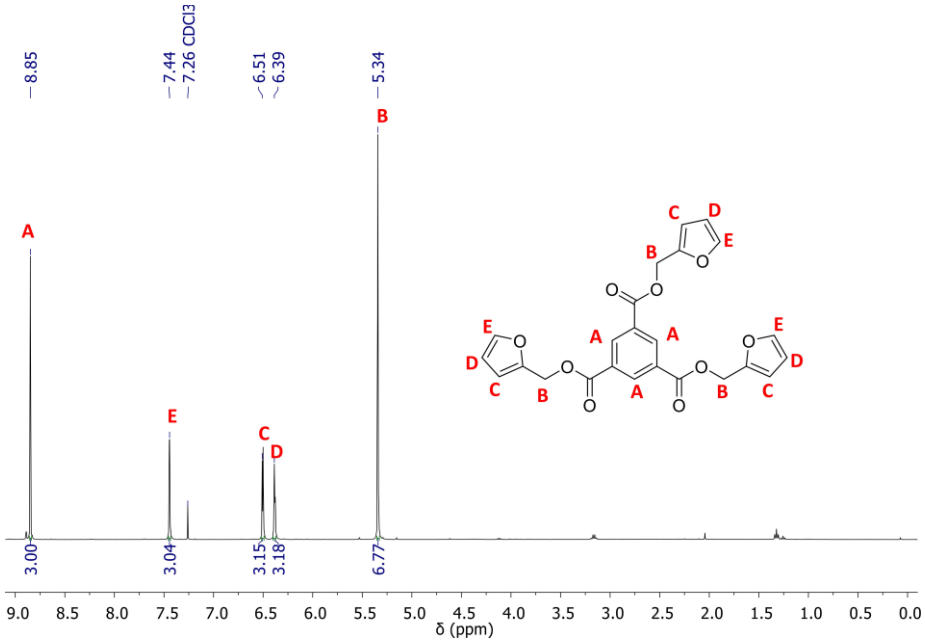

Figure 5.20 *^{1}H NMR spectrum of **TFBZ**. Integrals relative to benzene ring protons (400 MHz, 298 K, $CDCl_3$).*

^{13}C NMR spectroscopy of **TFBZ** revealed resonances associated with furan-ring carbons at δ = 149.17, 143.75, 111.57 and 110.89 ppm (**1**-**4**), demonstrating successful covalent incorporation of furan functionality (***Figure 5.21***). Moreover, the ^{13}C NMR spectrum of **TFBZ** displayed a resonance at δ = 164.84 ppm, representing the carbonyl carbons in the newly formed ester bonds (**6**). The presence of benzene aromatic carbons was also confirmed by the appearance of resonances at δ = 135.15 and 131.26 ppm (**7** and **8**).

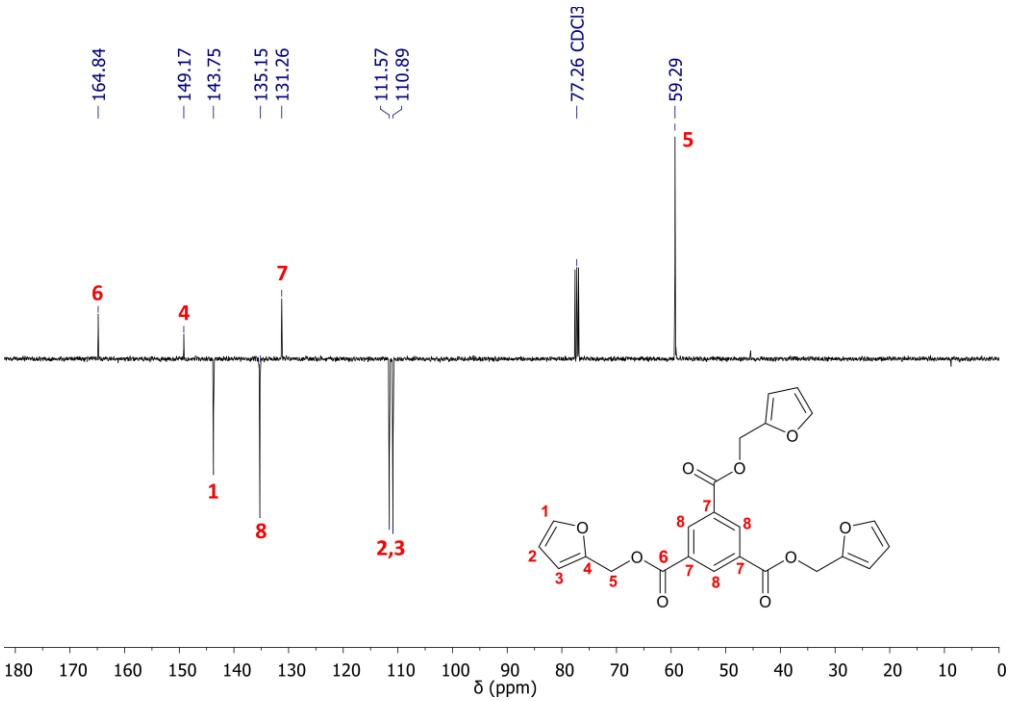

Figure 5.21 *^{13}C NMR spectrum of **TFBZ**. (125 MHz, 298 K, $CDCl_3$).*

ATIR-FTIR spectroscopy of **TFBZ** confirmed the presence of significant functional groups, for example the band present at ν_{max} = 1727 cm^{-1} represents (C=O) stretching in the newly formed ester bonds (***Figure 5.22***). Moreover, FTIR bands appeared at ν_{max} = 1150 and 1018 cm^{-1}, indicating (C-O-C) stretching and (C-O-C) bending on the furan rings, respectively. The FTIR spectrum of **TFBZ** also displayed a band at ν_{max} = 736 cm^{-1}, corresponding to bending on the single-substituted furan rings. Additionally, a band emerged at ν_{max} = 1609 cm^{-1}, representing aromatic (-C=C) stretching from the benzene core. A band was also apparated at ν_{max} = 1232 cm^{-1}, corresponding to (C-O-) stretching in the ester bonds.

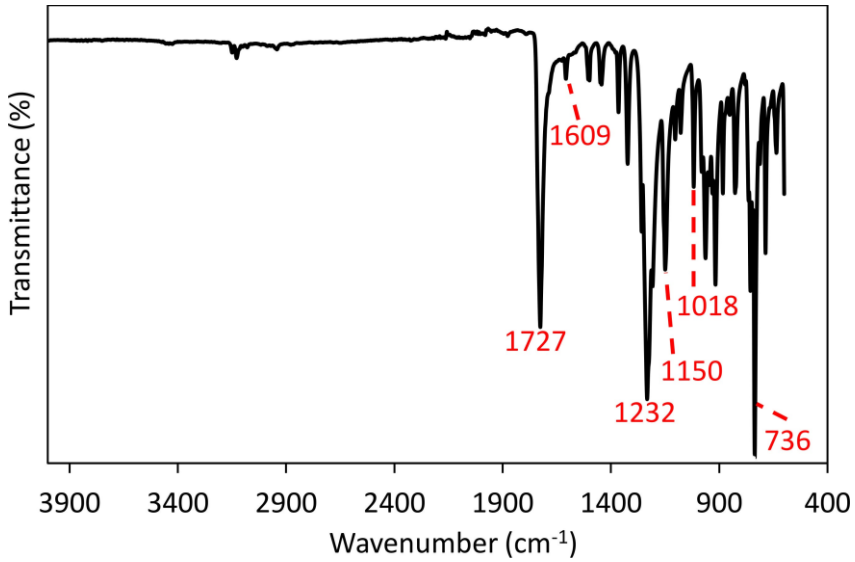

Figure 5.22 *ATR-FTIR spectrum of* ***TFBZ****.*

5.2.5 Comparison of furan cross-linkers

The functionalities and molar masses of the three multifunctional furan cross-linkers are summarised for comparison (***Table 5.3***).

Table 5.3 *Summary of multifunctional furan cross-linkers*

Cross-linker	**Functionality**	**Molar mass** (g.mol^{-1})
FGE-FAM	3	405.45
FGE-P1075	4	1151.66
TFBZ	3	450.40

The multifunctional furan cross-linkers were analysed by DSC to compare their thermal properties (***Figure 5.23***). **FGE-FAM** and **FGE-P1075** are amorphous liquids with low T_g values of -44.7 and -42.9 °C, respectively, whilst **TFBZ** is a highly crystalline compound, evident by the sharp endotherm at 102 °C (ΔH_m = of 79.8 J.g^{-1}), where the ordered structure melts.

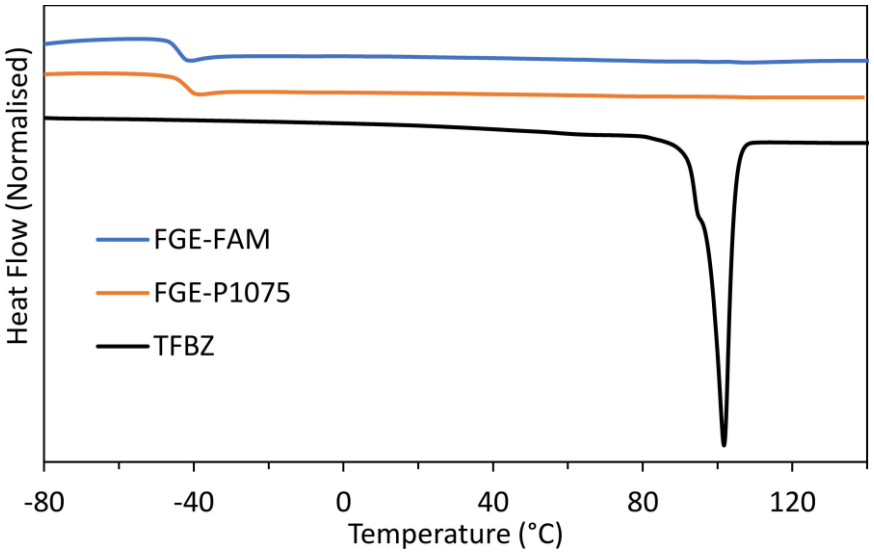

Figure 5.23 *DSC thermograms (1st heating cycles) of multifunctional furan cross-linkers using a heating rate of 10 °C.min^{-1}. Exo up.*

5.2.6 Synthesis and characterisation of FGE-FAM and TFBZ polyester DA-CANs

The influence of equivalent concentration of maleimide and furan functional groups (f_g) or trifuran cross-linker backbone on the thermomechanical properties of polyester DA-CANs, was investigated by copolymerising five different molar mass hydrocarbon bismaleimides separately with **FGE-FAM** or **TFBZ** (***Table 5.4***). Copolymerising **FGE-FAM** (405.45 g.mol^{-1}) or **TFBZ** (450.40 g.mol^{-1}) with the same bismaleimide resulted in DA-networks with similar f_g values and DA-adduct concentrations, allowing the effect of cross-linker backbone to be independently evaluated. Another direct comparison can be made whereby the same trifuran cross-linker (**FGE-FAM** or **TFBZ**) is used but the f_g and therefore DA-cycloadduct concentration at room temperature in the reversible networks is altered by changing the molar mass of the hydrocarbon bismaleimides. As the DA-cycloadducts are used as the reversible cross-links to form the networks the DA concentration is proportional to the cross-link density.

Table 5.4 *Compositions and f_g values of polyester DA-CANs.*

DA-CAN	Bismaleimide	Trifuran	f_g (mol.kg^{-1})
1,12-DD-FGE-FAM	1,12-DD	FGE-FAM	2.33
1,12-DD-TFBZ	1,12-DD	TFBZ	2.25
C_{36}-FGE-FAM	C_{36} dimer diol	FGE-FAM	1.67
C_{36}-TFBZ	C_{36} dimer diol	TFBZ	1.63
HPBD1000-FGE-FAM	HPBD1000	FGE-FAM	0.88
HPBD1000-TFBZ	HPBD1000	TFBZ	0.88
HPBD2000-FGE-FAM	HPBD2000	FGE-FAM	0.70
HPBD2000-TFBZ	HPBD2000	TFBZ	0.70
HPBD3000-FGE-FAM	HPBD3000	FGE-FAM	0.45
HPBD3000-TFBZ	HPBD3000	TFBZ	0.45

The polyester DA-networks were synthesised by copolymerising the corresponding bismaleimide and trifuran cross-linker in chloroform at ambient temperature with continuous mixing, using the synthetic scheme of **C_{36}-TFBZ** for representation (***Scheme 5.5***). The masses used were calculated to give an equimolar ratio of furan to maleimide. Once homogenous solutions were achieved, they were solvent cast into PTFE-lined petri-dishes and solvent was subsequently removed. The bulk DA-networks were then processed by compression moulding (3 MPa, 10 min, 100-120 °C) to produce approximately 1 mm thick elastomeric sheets. The compression-moulded sheets were cooled and conditioned at ambient temperature for 7 days to allow the forward DA-reaction to occur.

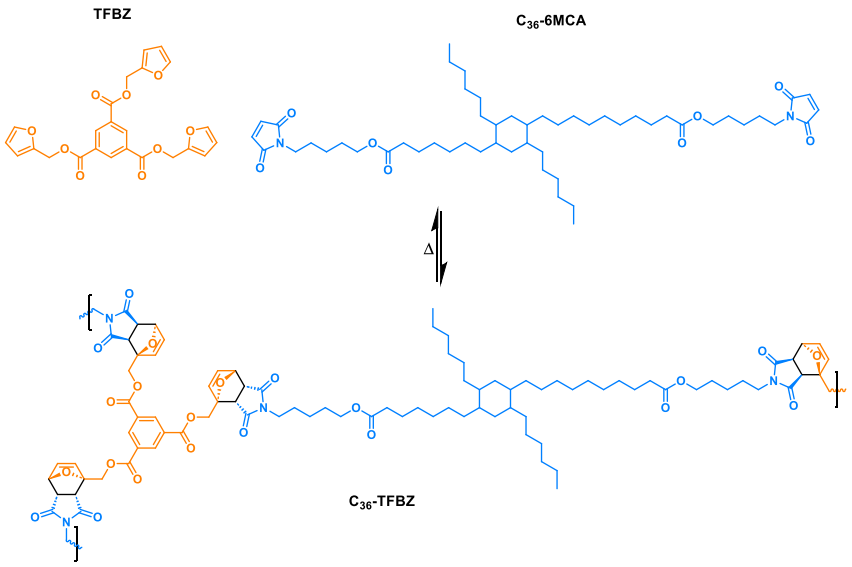

Scheme 5.5 *The copolymerisation of the trifunctional furan **TFBZ** and bismaleimide **C_{36}-6MCA** at ambient temperature to form the DA-network **C_{36}-TFBZ**.*

Soxhlet extractions were performed on all polyester DA-networks after conditioning materials at ambient temperature for 7 days, to determine their degree of cross-linking and solvent resistance. Using this method, THF was continually passed through a sample of each material for a 24-hour period, washing away any non-crosslinked material (sol fraction). A comparison of the sample masses before and after the extraction experiments allows for the gel fractions to be determined (***Table 5.5***).

Table 5.5 *Gel fractions of polyester DA-CANs.*

DA-CAN	Gel fraction [a](%)
1,12-DD-FGE-FAM	93
1,12-DD-TFBZ	94
C_{36}-FGE-FAM	89
C_{36}-TFBZ	93
HPBD1000-FGE-FAM	92
HPBD1000-TFBZ	94
HPBD2000-FGE-FAM	88
HPBD2000-TFBZ	91
HPBD3000-FGE-FAM	90
HPBD3000-TFBZ	89

[a] *determined via Soxhlet extractions in THF after 24 hours.*

All networks exhibited high gel fractions (≥ 88%), indicating that most material was successfully incorporated into the DA-CANs. Importantly, this shows that at temperatures below the rDA, all of the DA-CANs display high solvent resistance, similar to thermoset elastomers, which is beneficial for industrial applications.

ATR-FTIR spectroscopy of all polyester DA-CANs revealed low maleimide transmittance at ν_{max} = 696 cm^{-1}, after conditioning for 7 days at 25 °C, indicating that most of the maleimide functional groups had successfully copolymerised with furans to form DA-cycloadducts (***Figure 5.24 (A)*** and ***Figure 5.25***). The full FTIR spectra of the **FGE-FAM** and **TFBZ** polyester DA-CANs showed that the transmittance of bands at ν_{max} = 1695, 1150 and 727 cm^{-1}, representing maleimide-imide carbonyl stretching, (C-O-C) stretching on the furan rings, and bending on the single-substituted furan rings, respectively, increased with increasing network f_g (top to bottom), demonstrating an increase in equivalent concentration of maleimide and furan functional groups (***Figure 5.24 (B)*** and ***Figure 5.25***). The transmittance of FTIR-

bands at ν_{max} = 3445 and 1733 cm^{-1} also increased with network f_g, suggesting a higher concentration of β-hydroxy groups from **FGE-FAM** and ester carbonyls from bismaleimide backbones, respectively. Additionally, the transmittance of the FTIR band at ν_{max} = 1775 cm^{-1} increased as the network f_g of the DA-CANs increased, indicating an increase in DA-cycloadduct concentration.

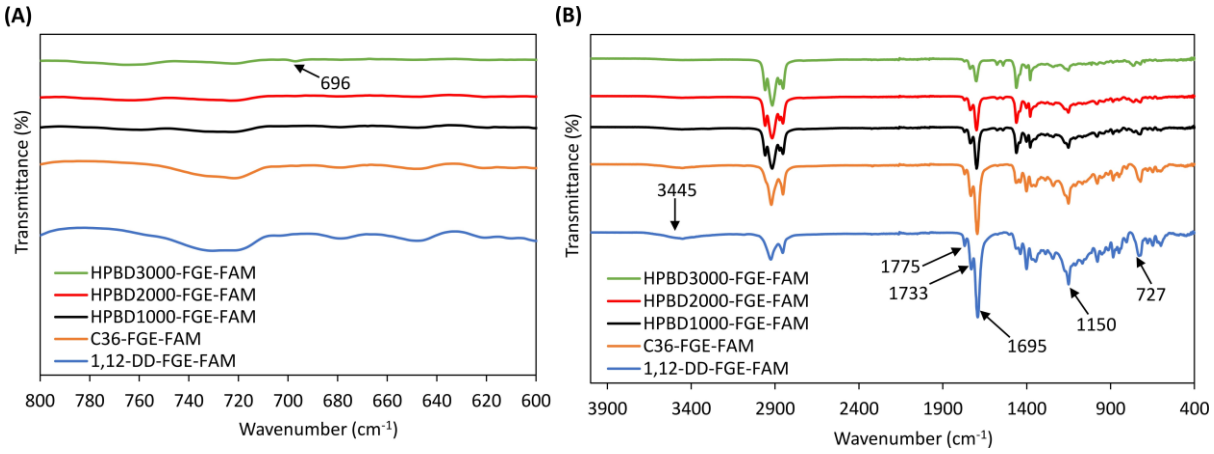

Figure 5.24 *ATR-FTIR spectra of* ***FGE-FAM*** *polyester DA-CANs comprising different bismaleimides after 7 days at 25 °C.* ***(A)*** *zoomed into maleimide fingerprint region (800-600 cm^{-1}) and* ***(B)*** *full ATR-FTIR spectra (4000-400 cm^{-1}) with significant functionalities labelled. Increasing network f_g from top to bottom.*

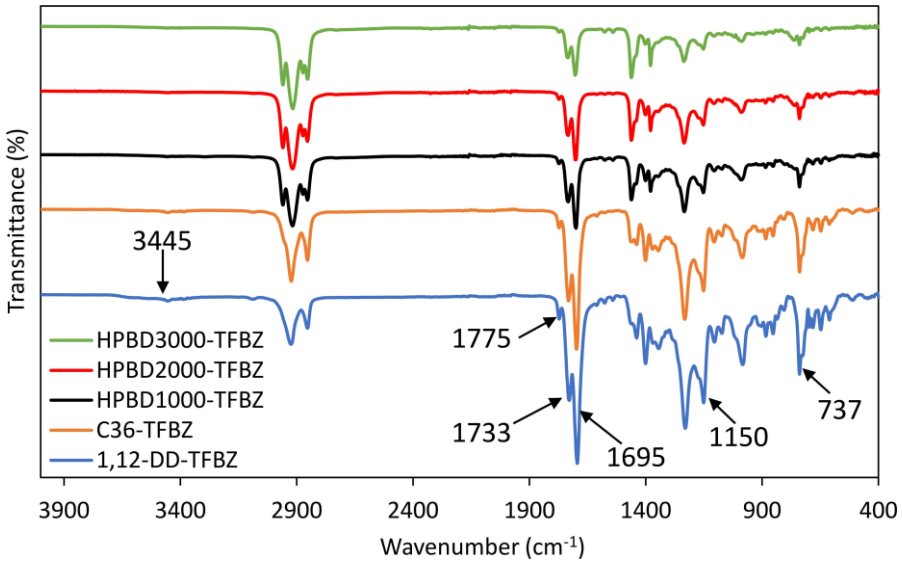

Figure 5.25 *ATR-FTIR spectra of the* ***TFBZ*** *polyester DA-CANs with containing different bismaleimides.*

The ATR-FTIR spectra of **1,12-DD-TFBZ** and **1,12-DD-FGE-FAM** were compared as an example to identify any functionality differences due to trifuran cross-linker backbone (***Figure 5.26***). The FTIR

spectrum of **1,12-DD-FGE-FAM** displayed a more prominent transmittance band than **1,12-DD-TFBZ** at ν_{max} = 3445 cm^{-1} due to the formation of β-hydroxy groups from the ring-opening addition of **FGE** with **FAM**. Moreover, the FTIR-spectrum of **1,12-DD-TFBZ** displayed a more prominent FTIR band at ν_{max} = 1730 cm^{-1} than **1,12-DD-FGE-FAM** due to the DA-network containing additional ester carbonyl groups from the trifuran **TFBZ** cross-linker. The ATR-FTIR spectra exhibited small but comparable size bands at ν_{max} = 1775 cm^{-1}, indicating that they contain similar concentrations of DA-cycloadducts.

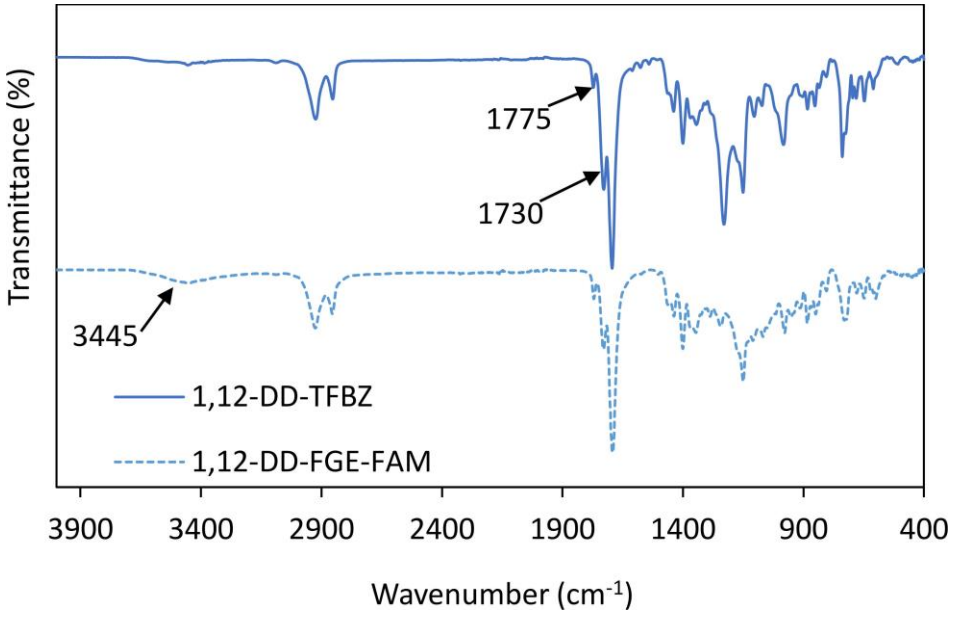

Figure 5.26 *ATR-FTIR spectra of* ***1,12-DD-TFBZ*** *and* ***1,12-DD-FGE-FAM*** *polyester DA-CANs, as a representative example.*

The thermal properties of the polyester DA-CANs were analysed using DSC, after conditioning materials for 7 days at ambient temperature (***Figure 5.27*** and ***Table 5.6***). The thermal data shows that an increase in network f_g, through the use of lower molecular weight bismaleimides, causes an increase in T_g due to an increase in the concentration of rigid DA cross-links, which reduce network mobility. This increase was only noticeable at high DA concentrations where f_g > 1. At lower DA concentrations, there was only a limited influence on T_g, as the flexibility of the connecting HPBD chains is the primary controlling parameter, leading to low T_g values between -31 and -33 °C.[14] The T_g of the **1,12-DD-TFBZ** network could not be detected *via* DSC, due to overlap with a small endotherm at 58 °C, from the melting of semi-crystalline segments, resulting from the highly crystalline nature of

the **TFBZ** and **6-MCA-1,12-DD** constituents. All DA-CANs exhibited broad double melting endotherms between 110 and 153 °C (T_{rDA}), representing the energy required for the dissociation of *endo* and *exo* DA-cycloadducts in the rDA reaction (ΔH_{rDA}). DA-networks with higher f_g values displayed more pronounced endothermic peaks with larger ΔH_{rDA} values, due to the greater heat absorption required to dissociate the higher concentration of DA-cycloadducts. An increased proportion of sterically hindered *endo* adducts are formed at higher DA cross-link densities. This has been reported to occur due to the extra restriction to the mobility of polymer chains in the DA-networks, which can hinder the rearrangements necessary for furan and maleimide groups to form the more thermodynamically stable *exo* adducts, in addition to decreasing their thermal stability. [15]

The **C_{36}-TFBZ** DA-network displayed a higher T_g than **C_{36}-FGE-FAM** at similar cross-link densities, due to the restricted cross-linker flexibility of **TFBZ**, reducing network flexibility. This effect was not observed in the **HPBD** DA-networks, where the flexibility of the HPBD chains was the main controlling parameter of T_g. The **TFBZ** polyester DA-CANs displayed higher T_{rDA} values than the corresponding **FGE-FAM** DA-CANs at similar cross-link densities, indicating higher thermal stability (***Table 5.6***). This is because the highly electron-withdrawing benzoate groups in **TFBZ** stabilise the *endo* and *exo* conformations of the DA-cycloadducts more than the hydrocarbon backbone of **FGE-FAM**.[16] In the **FGE-FAM** DA-networks the *endo* isomers were preferentially formed due to the Alder-*endo* rule (***Figure 5.27***).[17] This rule states that *endo* adducts are typically preferred as they lead to a more sterically crowded transition state (TS), allowing intermolecular forces to stabilise and lower the energy of the overall TS. On the other hand, the DSC thermograms of the **TFBZ** DA-CANs showed that the higher T_{rDA} endotherms representing the *exo* cycloadducts were more prominent. This is because the less sterically hindered TS of the *exo* cycloadducts is stabilised *via* the electron-withdrawing benzoate groups attached to the trifuran, lowering their activation energy barrier. Polyester DA-CANs incorporating **FGE-FAM** and **TBFZ** paired with the same bismaleimide resulted in similar ΔH_{rDA} values, as they contain similar DA-cycloadduct concentrations.

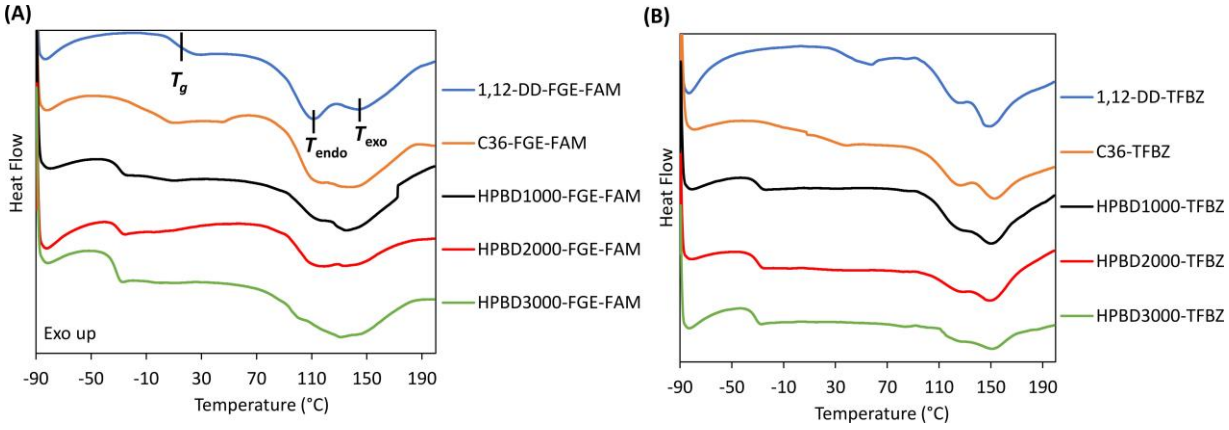

Figure 5.27 *DSC thermograms (1st heating cycles) of* ***(A) FGE-FAM*** *polyester DA-CANs with different bismaleimides and* ***(B) TFBZ*** *polyester DA-CANs with different bismaleimides. Exo up. Heating rate of 10 °C.min^{-1}.*

Table 5.6 *DSC thermal properties of polyester DA-CANs.*

DA-CAN	f_g (mol.kg^{-1})	T_g [a] (°C)	T_{rDA} [a] (°C)	ΔH_{rDA} [a] (J.g^{-1})
1,12-DD-FGE-FAM	2.33	12.4	110 & 143	52
1,12-DD-TFBZ	2.25	-	122 & 148	47
C_{36}-FGE-FAM	1.67	3.5	110 & 137	41
C_{36}-TFBZ	1.63	27	124 & 152	35
HPBD1000-FGE-FAM	0.88	-31	112 &137	33
HPBD1000-TFBZ	0.88	-31	123 & 153	32
HPBD2000-FGE-FAM	0.70	-31	116 & 136	18
HPBD2000-TFBZ	0.70	-31	124 & 149	16
HPBD3000-FGE-FAM	0.45	-33	132	16
HPBD3000-TFBZ	0.45	-33	123 & 150	12

[a] determined by DSC using 1st heating cycles, heating rate of 10 °C.min^{-1}.

The polyester DA-CANs were subjected to DMA to determine their viscoelastic properties as a function of temperature (***Figure 5.28*** and ***Table 5.7***). At the T_g the mechanical behaviour of the DA-CANs changed from stiff thermoset behaviour (energy elasticity) to flexible elastomeric behaviour (entropy elasticity), demonstrated by a drop in *E'* and a peak in tan *δ*. Networks with higher DA cross-link densities displayed higher T_g values, i.e the **C_{36}** and **1,12-DD** polyester DA-CANs displayed broad T_g values above 0 °C, whilst the **HPBD** polyester DA-CANs exhibited narrow, sub-ambient T_g values between -14 and -17 °C (***Figure 5.28 (C) and (D)***). This effect was only prominent at high DA cross-link densities (f_g > 1), due to a substantial reduction in segmental chain motion. The height of the tan *δ* peaks also decreased with increasing concentration of DA-crosslinks, indicating a reduction in damping

ability. The tan δ curves of the **HPBD** polyester DA-CANs presented additional transitions between 20-80 °C, which likely result from the softening of the polar **FGE-FAM** or **TFBZ** cross-linkers which phase separate from the non-polar HPBD polymer matrix. **1,12-DD-FGE-FAM** displayed two softening processes at 24 and 35 °C, which could represent two T_g values with overlap. The tan δ curve of **1,12-DD-TFBZ** exhibited complex behaviour with multiple softening events, such as T_g's and melting points (T_m) which overlap. **1,12-DD-TFBZ** also displayed a significantly higher E' at 20 °C (1375 MPa) compared to other DA-CANs as it contains semi-crystalline segments which reinforce the network through physical interactions. **C_{36}-FGE-FAM** displayed a broad softening region from -20 to 47 °C. For all DA-CANs, heating above T_g or T_m caused a gradual decrease in E' due to a decrease in DA cross-link density and a resulting increase in flexibility as the rDA becomes more favoured. The rubbery plateau E' ($E'_{rubbery}$) increased with increasing DA cross-link density. For crosslinked polymers, $E'_{rubbery}$ can be correlated to the molecular weight between cross-links (M_c) using equation **(2)**.[18]

$$M_c = \frac{3RTd}{E'_{rubbery}} \qquad (2)$$

where R is the universal gas constant, T is the absolute temperature and d is the density of the polymer. Since $E'_{rubbery}$ is inversely proportional to M_c, a larger $E'_{rubbery}$ indicates a shorter chain length between cross-links. **TFBZ** polyester DA-CANs displayed higher E' values at 20 °C than those containing **FGE-FAM**. This effect became more prominent as the wt.% of **TFBZ** cross-linker in the networks increased, suggesting that **TFBZ** provides more stiffness than **FGE-FAM** to the resulting DA-CANs. Upon heating through the delegation transition temperature (T_{gel}), a substantial number of DA cross-links dissociate, resulting in the loss of network integrity, evidenced by a sharp drop in E' towards zero where viscous flow occurs (T_f). The **TFBZ** polyester DA-CANs exhibited higher T_f values than those containing **FGE-FAM** at similar cross-linking densities, indicating enhanced thermal stability, in agreement with DSC results.

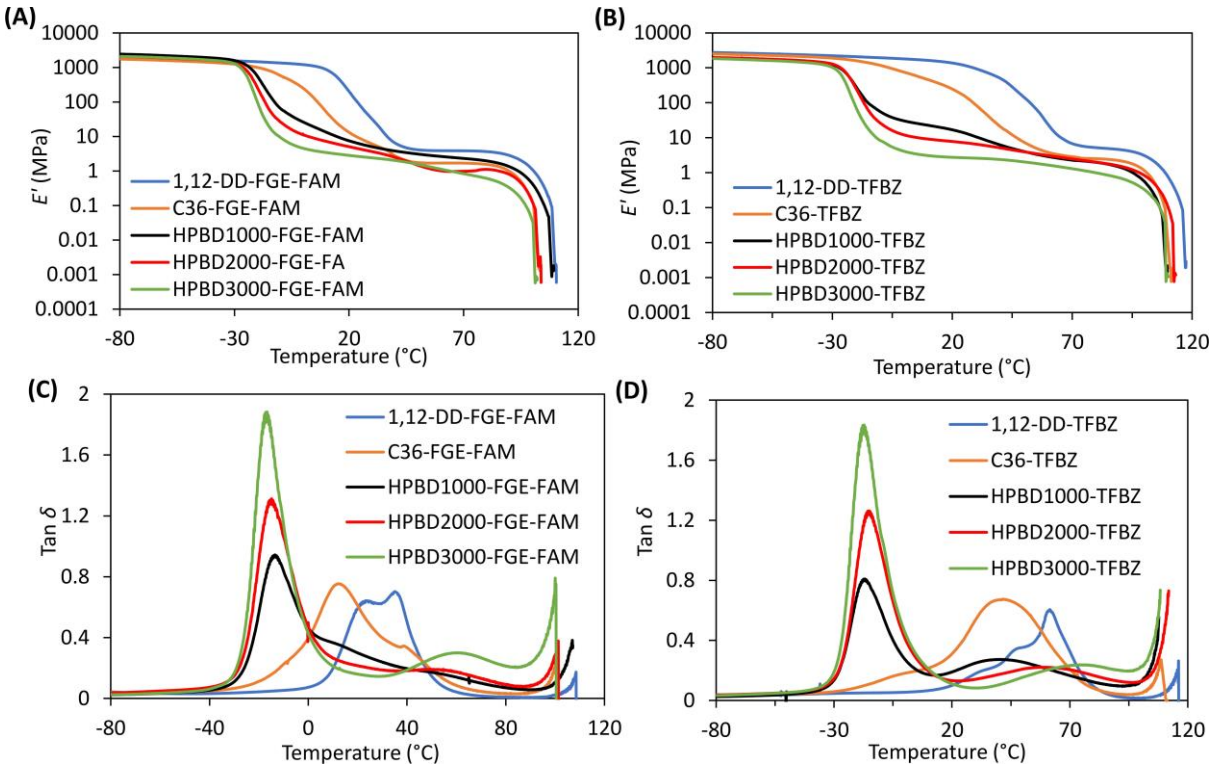

Figure 5.28 *Variation of E' with temperature for* ***(A) FGE-FAM*** *based DA-CANs with different bismaleimides, and* ***(B) TFBZ*** *based DA-CANs with different bismaleimides. Variation of tan δ with temperature for* ***(C) FGE-FAM*** *based DA-CANs with different bismaleimides and* ***(D) TFBZ*** *based DA-CANs with different bismaleimides.*

Table 5.7 *DMA thermal data of polyester DA-CANs using a heating rate of 3 °C.min^{-1}.*

DA-CAN	f_g (mol.kg^{-1})	E'^{a} ($T < T_g$) (MPa)	T_g [b] (°C)	E'^{c} ($T > T_g$) (MPa)	T_f [d] (°C)
1,12-DD-FGE-FAM	2.33	1796	24 & 35	204	108
1,12-DD-TFBZ	2.25	2568	21, 40 & 54	1374	116
C_{36}-FGE-FAM	1.67	1611	13	13	100
C_{36}-TFBZ	1.63	2311	42	248	109
HPBD1000-FGE-FAM	0.88	2224	-14	8	107
HPBD1000-TFBZ	0.88	1800	-17	17	108
HPBD2000-FGE-FAM	0.70	1888	-15	5	101
HPBD2000-TFBZ	0.70	1811	-15	8	112
HPBD3000-FGE-FAM	0.45	1921	-17	3	100
HPBD3000-TFBZ	0.45	1650	-17	3	109

[a] Storage modulus measured at -60 °C. [b] Measured as peak in tan δ. [c] Storage modulus measured at 20 °C. [d] Measured as onset of viscous flow.

The influence of the DA-cycloadduct concentration or trifuran cross-linker backbone on the mechanical properties at room temperature was investigated *via* uniaxial tensile testing in strain-controlled experiments using a 10 mm.min^{-1} extension rate (***Figure 5.29***).

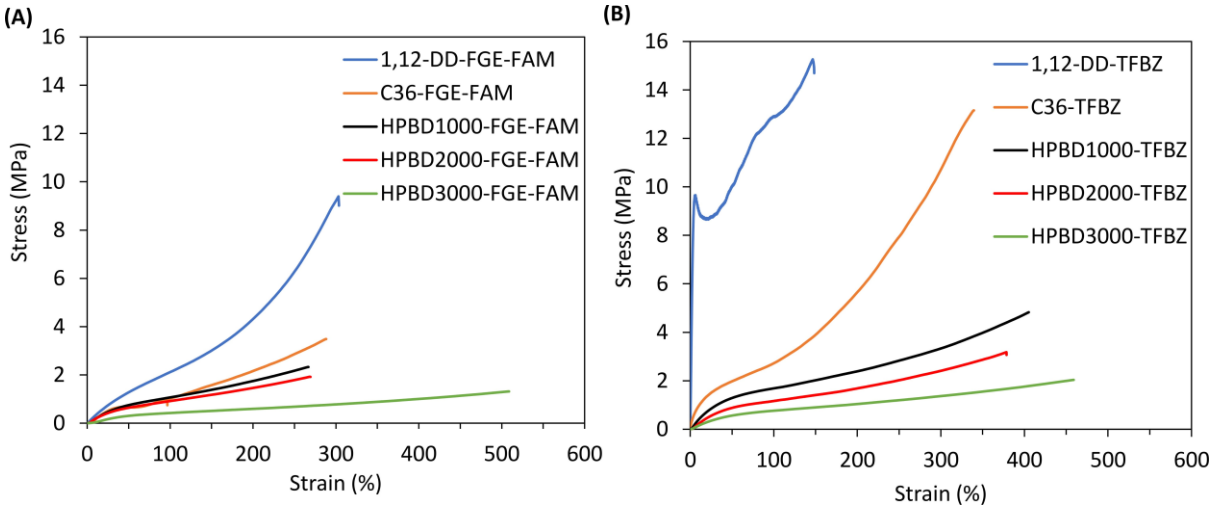

Figure 5.29 *Representative stress-strain curves of* ***(A) FGE-FAM*** *polyester DA-CANs with different bismaleimides and* ***(B) TFBZ*** *polyester DA-CANs with different bismaleimides. Obtained from uniaxial tensile testing using a 10 mm.min^{-1} extension rate.*

From the resulting stress-strain curves, the stress at break (σ_b), Young's modulus (E_y) (linear regression in the 0-2% strain interval), elongation at break (ε_b) and modulus of toughness (U_T), (the total area under the stress-strain curve) can be calculated for each polyester DA-CAN (***Table 5.8***).

Table 5.8 *Mechanical properties of polyester DA-CANs.*

DA-CAN	f_g (mol.kg^{-1})	σ_b[a] (MPa)	E_y[a] (MPa)	U_T[a] (MPa)	ε_b[a] (%)
1,12-DD-FGE-FAM	2.33	9.20 ± 0.6	2.50 ± 0.1	1108 ± 206	300 ± 37
1,12-DD-TFBZ	2.25	14.72 ± 0.8	265.0 ± 10	1617 ± 281	147 ± 20
C_{36}-FGE-FAM	1.67	3.28 ± 0.3	0.48 ± 0.02	428 ± 60	279 ± 39
C36-TFBZ	1.63	13.20 ± 1.0	16.80 ± 0.9	1863 ± 305	337 ± 43
HPBD1000-FGE-FAM	0.88	2.32 ± 0.3	0.76 ± 0.05	350 ± 51	272 ± 30
HPBD1000-TFBZ	0.88	4.63 ± 0.5	2.72 ± 0.08	1000 ± 198	407 ± 61
HPBD2000-FGE-FAM	0.70	1.58 ± 0.3	0.57 ± 0.03	216 ± 34	233 ± 27
HPBD2000-TFBZ	0.70	3.04 ± 0.4	0.46 ± 0.04	597 ±102	353 ± 55
HPBD3000-FGE-FAM	0.45	1.14 ± 0.2	0.12 ± 0.01	313 ± 56	509 ± 85
HPBD3000-TFBZ	0.45	2.10 ± 0.3	0.45 ± 0.03	563 ± 95	468 ± 73

[a] *determined by uniaxial tensometry using an extension rate 10 mm.min^{-1}. Mean values ± standard deviation from measurements conducted independently on 5 specimens.*

The tensile data demonstrated that increasing network f_g caused an increase in stress at break, Young's modulus, and toughness as more DA reversible cross-links must be broken, increasing the stiffness and strength of the DA-networks. Generally, higher DA cross-link densities resulted in less flexible networks

with lower fracture strains, where fracture occurs because the molecules can't accommodate the mechanical strain. The stress-strain curve of **1,12-DD-TFBZ** displayed a yield point, characteristic of a semi-crystalline material, leading to a significantly higher Young's modulus, (E_Y of 265 MPa) than the amorphous polyester DA-CANs. Polyester DA-CANs incorporating **TFBZ** cross-linker exhibited higher Young's modulus, network strength, and flexibility than those containing **FGE-FAM**, exhibiting more pronounced strain-hardening, especially for the **C36 and 1,12-DD** bismaleimide backbones (***Figure 5.30***). This effect is likely due to the higher degree of stiffness and physical interactions, such as π–π stacking in the **TFBZ** cross-linker, leading to greater resistance to polymer chain alignment at higher strains. This increase in strain-hardening was not as pronounced for the **HPBD** polyester DA-CANs, where $f_g < 1$ and the high flexibility of the HPBD backbone instead governed mechanical performance.

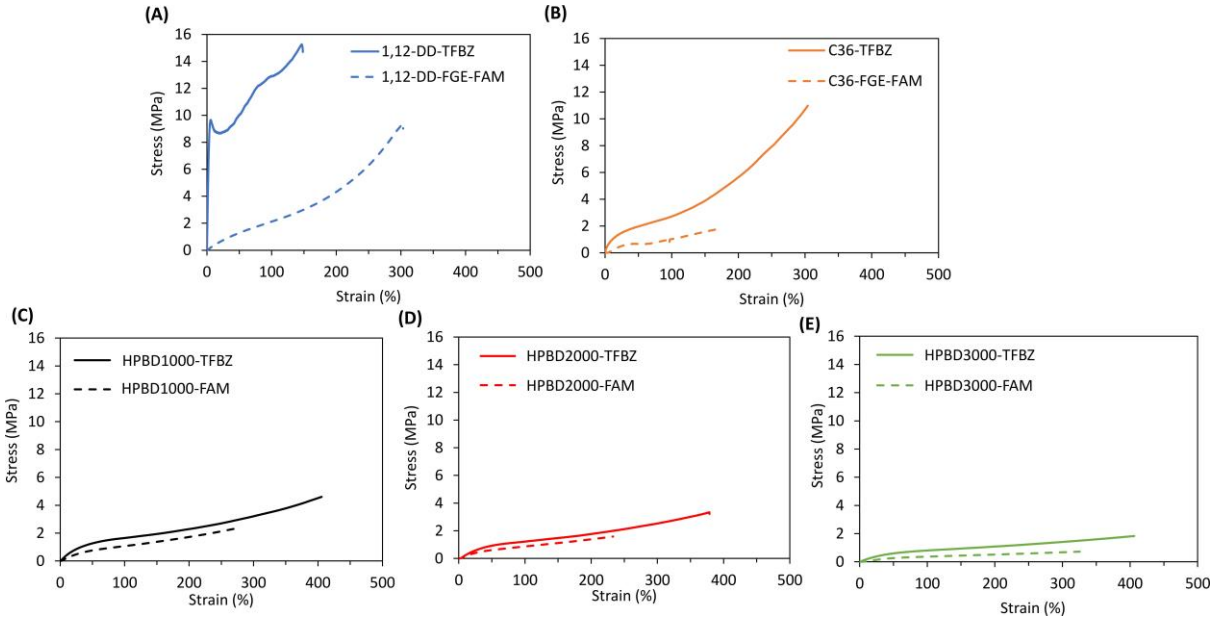

Figure 5.30 *Representative stress-strain curves of* ***(A) 1.12-DD-TFBZ*** *and* ***1,12-DD-FGE-FAM, (B) C36-TFBZ*** *and* ***C36-FGE-FAM, (C) HPBD1000-TFBZ*** *and* ***HPBD1000-FGE-FAM, (D) HPBD2000-TFBZ*** *and* ***HPBD2000-FGE-FAM*** *and* ***(E) HPBD3000-TFBZ*** *and* ***HPBD3000-FGE-FAM****. Obtained from uniaxial tensile testing using a 10 mm.min^{-1} extension rate.*

5.2.7 Synthesis and characterisation of FGE-P1075 polyester DA-CANs.

The biobased tetrafuran cross-linker **FGE-P1075** (1151.66 g.mol^{-1}) (***Figure 5.31 (A)***) was copolymerised with three different molar mass bismaleimides: **6-MCA-1,12-DD** (588.75 g.mol^{-1}), **6-MCA-C$_{36}$** (946

g.mol^{-1}) and **6-MCA-HPBD2000** (2695 g.mol^{-1}) (***Figure 5.31 (B)***), to produce **1,12-DD-FGE-P1075**, **C_{36}-FGE-P1075** and **HPBD2000-FGE-P1075** polyester DA-networks with f_g values of 1.72, 1.32 and 0.61 mol.kg^{-1}, respectively. **6-MCA-C_{36}** is also biobased, meaning that the **C_{36}-FGE-P1075** network is fully biobased. Copolymerisation was achieved *via* solvent casting in chloroform, followed by solvent removal, then compression moulding to give 1 mm thick elastomeric sheets, which were conditioned for 7 days at 25 °C prior to testing.

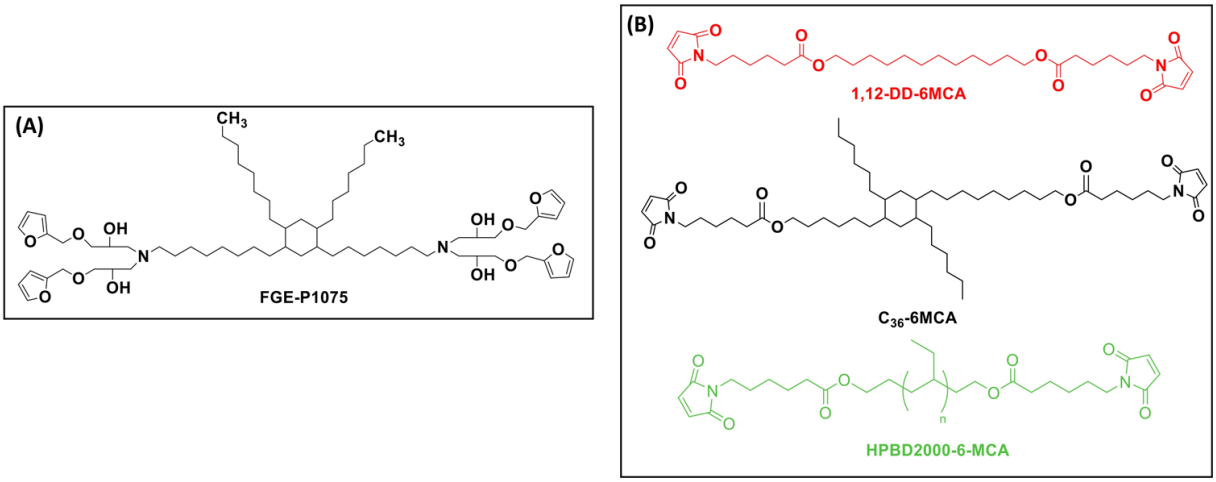

Figure 5.31 *Structures of* ***(A) FGE-P1075*** *cross-linker and* ***(B) 1,12-DD-6MCA, C_{36}-6MCA*** *and* ***HPBD2000-6MCA*** *bismaleimides.*

ATR-FTIR spectroscopy of the **FGE-P1075** polyester DA-CANs showed minimal transmittance at ν_{max} = 696 cm^{-1} after conditioning at 25 °C for 7 days, confirming that most free maleimide groups had successfully copolymerised to form DA-cycloadducts (***Figure 5.32***). The overlayed ATR-FTIR spectra also showed that the intensity of the FTIR bands at ν_{max} = 1695, 1150 and 732 cm^{-1} increased with increasing network f_g, confirming an increase in the concentration of maleimide and furan functional groups, as seen with the previous polyester DA-CANs. Additionally, the intensity of FTIR bands at ν_{max} = 3445 and 1733 cm^{-1} increased with network f_g, indicating an increase in concentration of β-hydroxy groups formed *via* the ring-opening addition of FGE and ester carbonyl stretching from the lower molar mass bismaleimides. Finally, the transmittance of the FTIR band at ν_{max} = 1775 cm^{-1} increased with increasing network f_g, suggesting an increase in DA-cycloadduct concentration.

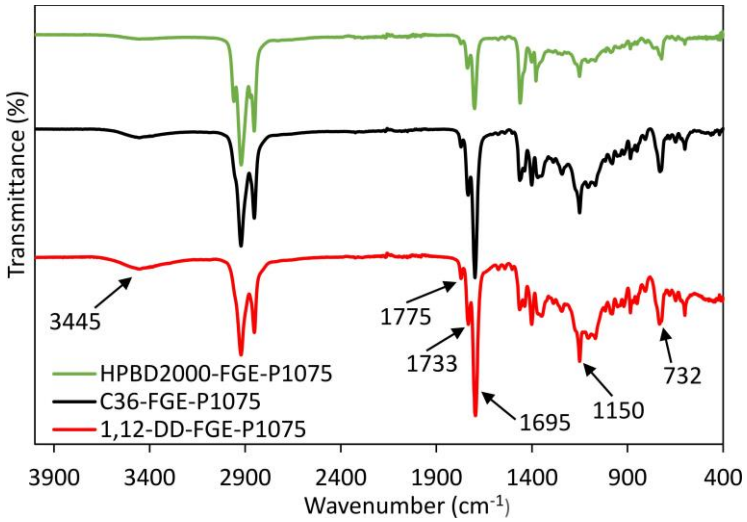

Figure 5.32 *ATR-FTIR spectra of* ***HPBD2000-FGE-P1075***, ***C36-FGE-P1075***, *and* ***1,12-DD-FGE-P1075*** *polyester DA-CANs. Network f_g increases from top to bottom.*

24 hour-Soxhlet extractions were performed on the **FGE-P1075** polyester DA-CANs in THF. All DA-networks exhibited high gel fractions (≥ 90%), demonstrating that most material was successfully incorporated into the networks through DA cross-linking with only small amount of sol fraction (non-incorporated material) (***Table 5.9***).

Table 5.9 *Gel fractions of* ***FGE-P1075*** *DA-CANs.*

DA-CAN	Gel fraction [a](%)
1,12-DD-FGE-P1075	98
C_{36}-FGE-P1075	93
HPBD2000-FGE-P1075	95

[a] *determined via Soxhlet extractions in THF after 24 hours.*

The **FGE-P1075** DA-networks were also analysed by DSC after conditioning for 7 days at 25 °C to determine their thermal properties (***Figure 5.33*** and ***Table 5.10***). The thermal data showed that there was a clear increase in T_g with increasing network f_g, due to an increase in the DA cross-link density which restricts network mobility. The DSC thermograms of all **FGE-P1075** DA-CANs revealed characteristic double *endo* and *exo* endothermic peaks between 110 and 160 °C, representing the rDA reaction. DA-CANs with higher f_g and DA cross-link densities exhibited more pronounced endothermic rDA peaks, with higher ΔH_{rDA} values due to a higher concentration of DA-cycloadducts that can be disrupted during temperature elevation, resulting in greater heat absorption.[19] Similar to the previous

polyester DA-CANs, the increased constraint from networks with higher cross-link densities promoted the formation of an increased proportion of sterically hindered *endo* DA-cycloadducts.[15] The T_{rDA} was not affected by network f_g.

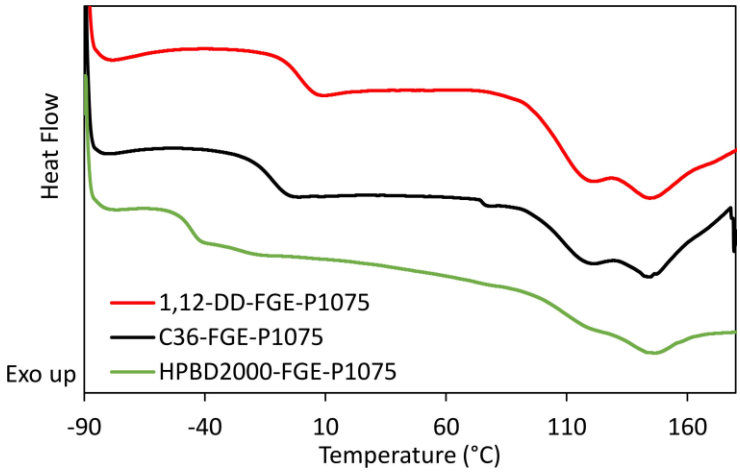

Figure 5.33 *DSC thermograms (1st heating cycles) of polyester* ***FGE-P1075*** *polyester DA-CANs measured after 7 days at 25 °C, 10 °C.min-1 heating rate.*

Table 5.10 *DSC thermal data of polyester* ***FGE-P1075*** *DA-CANs.*

DA-CAN	f_g (kg.mol^{-1})	T_g [a] (°C)	T_{rDA} [a] (°C)	ΔH_{rDA} [a] (J.g^{-1})
1,12-DD-FGE-P1075	1.72	-1.3	119 & 146	43.0
C_{36}-FGE-P1075	1.32	-13	119 & 144	32.0
HPBD2000-FGE-P1075	0.61	-48	120 & 144	15.0

[a] determined from DSC analysis using 1st heating cycle, heating rate of 10 °C.min-1.

DMA was performed on the **FGE-P1075** polyester DA-CANs to study their viscoelastic behaviour as a function of temperature (***Figure 5.34*** and **Table 5.11**). The *E'* and tan δ against temperature plots revealed that T_g increased with increasing f_g and DA cross-link density due to reduced mobility in the amorphous networks, in agreement with DSC analysis. All DA-CANs displayed extensive rubbery plateaus above T_g until the onset of viscous flow (T_f) above 100 °C due to DA-equilibrium shifting to lower molecular weight furan and maleimide precursors. Increasing network f_g and DA cross-link density caused an increased in $E'_{rubbery}$, due to an increase in stiffness and mechanical reinforcement. The T_f values of the polyester DA-CANs increased with increasing crosslink density, suggesting an increase in thermal stability, due to the higher concentrations of DA-cycloadducts. The tan δ curve of **HPBD2000-FGE-P1075** displayed an additional softening transition above the T_g at 20 °C, which is likely

to originate from physical interactions due to microphase separation of the non-polar HPBD matrix from the polar **FGE-P1075** cross-linker.

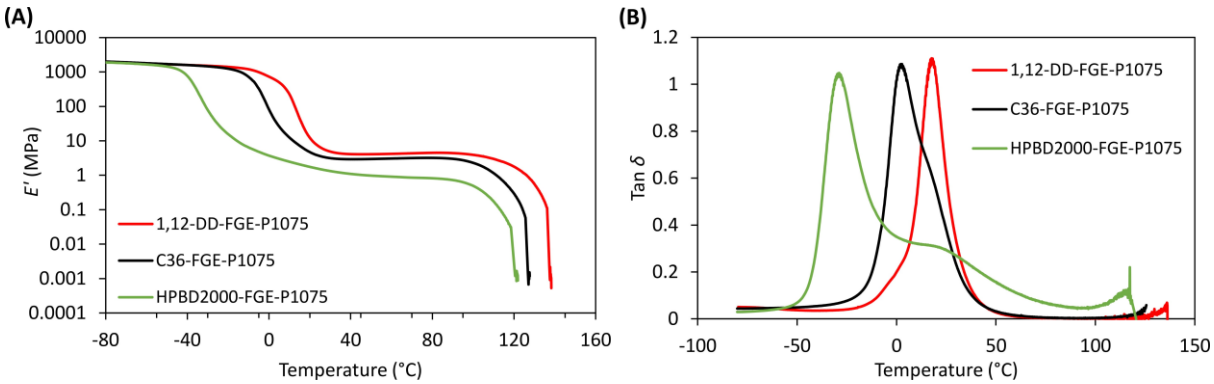

Figure 5.34 *Variation of* ***(A)*** *E' with temperature and* ***(B)*** *Tan δ with temperature for* ***FGE-P1075*** *DA-CANs with different bismaleimides.*

Table 5.11 *DMA thermal data of* ***FGE-P1075*** *DA-CANs using a heating rate of 3 °C.min^{-1}.*

DA-CAN	f_g (kg.mol^{-1})	E' ($T < T_g$) [a] (MPa)	T_g [b] (°C)	E' ($T > T_g$) [c] (MPa)	T_f [d] (°C)
1,12-DD-FGE-P1075	1.72	1766	17.6	12.3	136
C_{36}-FGE-P1075	1.32	1792	2.2	4.7	126
HPBD2000-FGE-P1075	0.61	1658	-29.0	1.8	118

[a] Storage modulus measured at -60 °C. [b] Measured as peak in tan δ. [c] Storage modulus measured at 20 °C. [d] Measured as onset of viscous flow.

Uniaxial tensile testing was performed on the **FGE-P1075** polyester DA-CANs to determine their mechanical properties at room temperature (***Figure 5.35***). The stress at break (σ_b), Young's modulus (E_y) (linear regression in the 0-2% strain interval), elongation at break (ε_b) and modulus of toughness (U_T), (the total area under the stress-strain curve) were calculated from the resulting stress-strain curves (***Table 5.12***). The mechanical data of the DA-CANs revealed that Young's modulus, tensile strength, and toughness increased with network f_g as more force is required to break the higher concentration of DA cross-links, causing a more pronounced strain-hardening effect. Network flexibility generally decreased with increasing f_g and crosslink density, due to an increase in T_g and reduction in the rubber chain mobility.

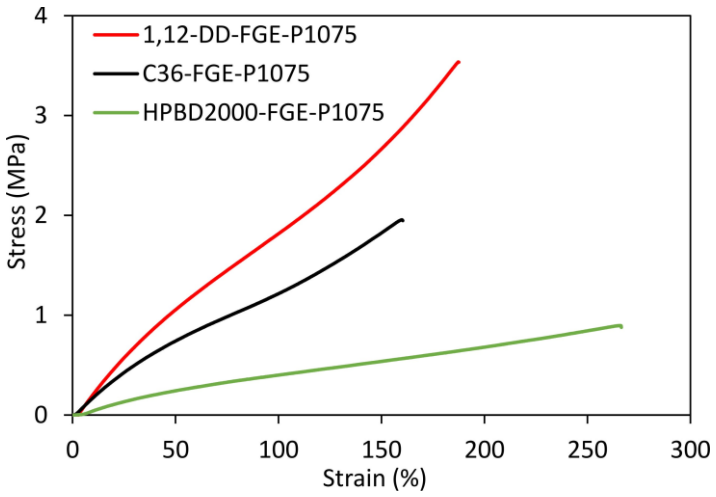

Figure 5.35 *Representative stress-strain curves of* ***FGE-P1075*** *polyester DA-CANs with different bismaleimides. Obtained from uniaxial tensile testing using a 10 mm.min^{-1} extension rate.*

Table 5.12 *Mechanical data of* ***FGE-P1075*** *DA-CANs.*

DA-CAN	f_g (kg.mol^{-1})	σ_b[a] (MPa)	E_γ[a] (MPa)	U_T[a] (MPa)	ε_b[a] (%)
1,12-DD-FGE-P1075	1.72	3.50 ± 0.3	0.7 ± 0.06	326 ± 34	186 ± 23
C_{36}-FGE-P1075	1.32	1.94 ± 0.1	0.7 ± 0.04	164 ± 25	159 ± 18
HPBD2000-FGE-P1075	0.61	0.89 ± 0.05	0.1 ± 0.01	129 ± 21	264 ± 32

[a] determined from uniaxial tensile testing using strain-controlled experiments at a 10 mmmin^{-1} extension rate. Mean values ± standard deviation from measurements conducted independently on 5 specimens.

To ensure that the incorporation of DA-cycloadducts into polyester-CANs enables thermal reprocessing (unlike conventional, thermoset elastomers), **1,12-DD-FGE-P1075** was subjected to reprocessing *via* compression moulding, using mild conditions (120 °C, 3 MPa, 10 minutes), before remeasurement of mechanical properties (R1) (***Figure 5.36***). This process was repeated a further two times (R2 and R3). The representative stress-strain curves after recycling demonstrated similar mechanical properties, with only a small loss in tensile strength or elongation, showing promising recycling potential.

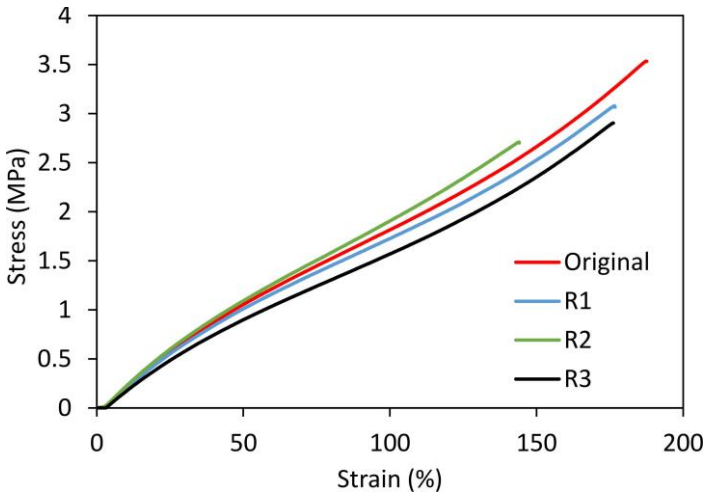

Figure 5.36 *Representative stress-strain curves of original* ***1,12-DD-FGE-P1075*** *sample and the same material after 3 reprocessing cycles (R1, R2 and R3). Determined from uniaxial tensile testing, using a 10 mm.min^{-1} extension rate.*

5.3 Conclusions

A novel series of polyester DA-CANs has been synthesised *via* the copolymerisation of hydrocarbon bismaleimides with multifunctional furan cross-linkers. Five bismaleimides with different molar masses were synthesised from the Fischer esterification of polyols with 6-MCA. Amorphous **FGE-P1075** and **FGE-FAM** were synthesised *via* the ring-opening addition of FGE with FAM and P1075, respectively whilst highly crystalline **TFBZ** cross-linker was synthesised *via* reaction between 1,3,5-benzenetricarbonyl chloride and furfuryl alcohol.

From these materials, two structure-property relationships were established: the first determining the effect of network f_g and DA-concentration, through the use of different molar mass bismaleimides, and the second evaluating the effect of furan cross-linker backbone (**FGE-FAM** versus **TBFZ**) on the thermomechanical properties of polyester DA-CANs. All DA-networks exhibited high gel-fractions (≥88%) *via* Soxhlet extraction, showing that most material was successfully incorporated into networks. Thermal analysis revealed that T_g increased with network f_g, and this effect became more prominent at higher DA concentrations, causing a decrease in network flexibility, evidenced from tensile testing. DSC revealed that the ΔH_{rDA} increased whilst DMA showed that the $E'_{rubbery}$ increased

with increasing cross-link density, resulting in an increase in network strength and toughness *via* tensile testing. DA-cycloadduct dissociation occurred in DA-CANs between 100-155 °C, *via* a double melting endotherm by DSC and a sharp drop in *E'* in DMA. The T_f of the DA-CANs generally increased with f_g, especially in the **FGE-P1075** series, showing that a higher concentration of DA-cycloadducts provides additional thermal stability. At similar f_g values, DA-CANs containing **TFBZ** displayed higher T_g, $E'_{rubbery}$ and T_f/T_{rDA} values *via* thermal analysis, whilst exhibiting higher network strength and toughness than those containing **FGE-FAM**, providing enhanced mechanical and thermal reinforcement to the resulting DA-CANs.

The work outlined in this chapter demonstrates how the thermomechanical properties of polyester DA-networks can be altered *via* monomer molecular weight and structure, enabling optimisation of properties to fit specific demands imposed by desired applications. Biobased furan and maleimide precursors (**FGE-FAM**, **FGE-P1075** and **6-MCA-C_{36}**) were also incorporated into polyester DA-CANs to yield partially or fully biobased, recyclable DA-networks, providing a significant sustainability advantage.

5.4 Experimental

5.4.1 Materials

Pripol™ 2033 and Priamine™ 1075 were supplied by Cargill. Nippon Soda supplied GI-1000, GI-2000, and GI-3000. 1,12-dodecanediol, chloroform, dichloromethane, deuterated chloroform ($CDCl_3$, 99.8 atom % D), 6-maleimidocaproic acid (6-MCA), p-Toluenesulfonic acid (PTSA), toluene, epichlorohydrin (ECH), furfuryl alcohol (FA), furfuryl amine (FA), tetrabutylammonium bromide (TBAB), 1,3,5-benzenetricarbonyl and triethylamine were all purchased from Sigma-Aldrich. All materials were used as supplied.

5.4.2 General procedure for synthesis of 6-MCA capped bismaleimides

The general procedure was as follows using the synthesis of 1,12-dodecyl bismaleimidocaproate (**6-MCA-1,12-DD**) as an example: 1,12-dodecanediol (1,12-DD, 20 g, 98.8 mmol) was added into a 250 mL round bottom flask, followed by 2.1 molar equivalents of 6-maleimidocaproic acid (6-MCA, 43.82 g, 207.5 mmol) then 0.1 molar equivalents of p-Toluenesulfonic acid (PTSA, 1.88 g, 9.9 mmol). A magnetic stirrer was added followed by 150 ml of toluene. The round bottom flask was securely clamped into a 250 mL heating block and the solution was left to stir at room temperature until all of the components had dissolved. A 30 mL Dean-Stark trap was then secured on top of the round bottom flask and filled with 20 mL of toluene, followed by a waterless reflux condenser. The reaction mixture was heated to reflux (110 °C) for at least 6 hours or until the expected theoretical amount of water was collected in the Dean-Stark trap. The trap was drained, and 50 mL of toluene solvent was distilled off of the reaction to remove trace moisture and drive the esterification equilibrium to completion. The reaction was allowed to cool to room temperature, additional toluene (20 mL) was added, and the solution was washed with saturated $NaHCO_3$ aq. (100 mL) then distilled water (100 mL). The organic layer was isolated and dried over anhydrous $MgSO_4$, and the solvent removed in vacuo to yield a light orange solid (14.4 g, 72 %). The material can be further purified by eluting a toluene solution of the resin through a short plug of silica or alumina. For **HPBD**-based bismaleimides the purification step differed. After the reactions were allowed to cool down, 50 mL of toluene was removed in vacuo using a rotatory evaporator. The product solutions were then precipitated in cold methanol (800 mL). Methanol and trace toluene were removed in vacuo to yield viscous orange oils (13.6 g, 68%).

1,12-dodecyl bismaleimidocaproate (6-MCA-1,12-DD): ^{1}H NMR (400 MHz, $CDCl_3$, 298 K): δ = 6.67 (s, 4H, NOC-*H*C=C*H*-CON), 4.04 (t, $^{3}J^{H\text{-}H}$ = 6.8 Hz, 4H, COO-CH_2CH$_2$), 3.51 (t, $^{3}J^{H\text{-}H}$ = 7.3 Hz, 4H, N-CH_2CH$_2$), 2.28 (t, $^{3}J^{H\text{-}H}$ = 7.5 Hz, 4H, N-CH$_2$CH$_2$CH$_2$CH$_2$CH_2-COO), 1.62 (m, 12H, N-CH$_2$CH_2, N-CH$_2$CH$_2$CH$_2$CH_2 and COO-CH$_2$CH_2) and 1.30 (m, 20H, N-CH$_2$CH$_2$CH_2 and all other remaining CH$_2$ protons) ppm. **^{13}C NMR** (125 MHz, $CDCl_3$, 298 K) δ = 173.81 (C=C-*C*(=O)-N), 171.05 (O-*C*(=O)-CH$_2$), 134.29 (*C*=*C*-C(=O)-N), 64.74 (O-

C(=O)-*C*H$_2$ and O-C(=O)-*C*H$_2$(CH$_2$)$_4$-N), 37.88 (N-*C*H$_2$(CH$_2$)$_4$COO), 34.34 (N-CH$_2$*C*H$_2$(CH$_2$)$_3$COO), 29.73-24.68 ppm all other remaining protons. **ATR-FTIR** ν_{max} = 2919 and 2850 (C-H stretching), 1734 (ester C=O stretching), 1695 (imide C=O stretching), 1170 and 1131 (C-O stretching), and 696 (maleimide C=C deformation mode) cm^{-1}. EI-MS (*m/z*) = 611.2 [M $^{+}$ Na $^{+}$].

Bismaleimidocaproyl C$_{36}$ dimerate (6-MCA-C$_{36}$): ^{1}H NMR (400 MHz, CDCl$_3$, 298 K): δ = 6.68 (s, 4H, NOC-*H*C=C*H*-CON), 4.04 (t, $^{3}J^{H-H}$ = 6.8 Hz, 4H, COO-C*H*$_2$CH$_2$), 3.50 (t, $^{3}J^{H-H}$ = 7.2 Hz, 4H, N-C*H*$_2$CH$_2$), 2.28 (t, $^{3}J^{H-H}$ = 7.5 Hz, 4H, N-CH$_2$CH$_2$CH$_2$CH$_2$C*H*$_2$-COO), 1.60 (m, 12H, N-CH$_2$C*H*$_2$, N-CH$_2$CH$_2$CH$_2$C*H*$_2$ and COO-CH$_2$C*H*$_2$), 1.25 and 0.87 (all remaining protons) ppm and 1.30 (m, 20H, N-CH$_2$CH$_2$C*H*$_2$ and all other remaining CH$_2$ protons) ppm. **^{13}C NMR** (125 MHz, CDCl$_3$, 298 K) δ = 173.80 (C=C-*C*(=O)-N), 171.04 (O-*C*(=O)-CH$_2$), 134.28 (*C*=*C*-C(=O)-N), 64.75 (O-C(=O)-*C*H$_2$ and O-C(=O)-*C*H$_2$(CH$_2$)$_4$-N), 37.88 (N-*C*H$_2$(CH$_2$)$_4$COO), 34.34 (N-CH$_2$*C*H$_2$(CH$_2$)$_3$COO), 29.73-22.92 (all other remaining protons) ppm. **ATR-FTIR** ν_{max} = 2921 and 2855 (C-H stretching), 1731 (ester C=O stretching), 1704 (imide C=O stretching), 1167 and 1134 (C-O stretching), and 696 (maleimide C=C deformation mode) cm^{-1}.

HPBD-bismaleimides (6-MCA HPBD) (same for 6-MCAHPBD1500, 6MCA-HPBD2000 and 6-MCA-HPBD3000): ^{1}H NMR (400 MHz, CDCl$_3$, 298 K): δ = 6.68 (s, 4H, NOC-*H*C=C*H*-CON), 4.06 (dt, $^{3}J^{H-H}$ = 13.4, 6.9 Hz, 4H, COO-C*H*$_2$CH$_2$), 3.51 (t, $^{3}J^{H-H}$ = 7.3 Hz, 4H, N-C*H*$_2$CH$_2$), 2.28 (t, $^{3}J^{H-H}$ = 7.5 Hz, 4H, N-CH$_2$CH$_2$CH$_2$CH$_2$C*H*$_2$-COO), 1.60 (m, 12H, N-CH$_2$C*H*$_2$, N-CH$_2$CH$_2$CH$_2$C*H*$_2$ and COO-CH$_2$C*H*$_2$) and 1.24-0.82 (all remaining protons) ppm. **^{13}C NMR** (125 MHz, CDCl$_3$, 298 K) δ = 173.78 (C=C-*C*(=O)-N), 171.03 (O-*C*(=O)-CH$_2$), 134.29 (*C*=*C*-C(=O)-N), 64.77 (O-C(=O)-*C*H$_2$ and O-C(=O)-*C*H$_2$(CH$_2$)$_4$-N), 37.90 (N-*C*H$_2$(CH$_2$)$_4$COO), 34.38 (N-CH$_2$*C*H$_2$(CH$_2$)$_3$COO), 39.38, 38.66, 36.37, 33.64, 30.94-10.46 (all other remaining protons) ppm. **ATR-FTIR** ν_{max} = 3030-2790 (C-H stretching), 1734 (ester C=O stretching), 1711 (imide C=O stretching), 1379 (C-O stretching), and 696 (maleimide C=C deformation mode) cm^{-1}.

5.4.3 Synthesis of FGE

Furfuryl alcohol (FA, 9.82 g, 0.100 mol) and tetrabutylammonium bromide (TBAB, 0.450 g, 14.0 mmol) were added to a three-necked flask equipped with a reflux condenser, a thermometer, and a

mechanical stirrer. Epichlorohydrin (ECH 10.2 g, 0.110 mol) was dropped into the flask under inert gas protection and the reaction mixture was stirred vigorously at room temperature for 4 h. Then, the mixture was cooled to 10 °C with an ice bath and 50 wt% NaOH aqueous solution (20 mL) was slowly added into the flask. After the reaction mixture was stirred for 2 h at ambient temperature, 30 mL deionized water was added. The product was extracted with 10 mL ethyl acetate and the organic phase was separated in a separator. The extraction was conducted three times. The organic extracted product was collected and washed three times with deionized water. The organic phase was separated out, dried with anhydrous Na_2SO_4, and filtrated to give a transparent solution. Then, the solvent in solution was removed under reduced pressure to get an orange-yellow liquid product (FGE, yield 78%).

^{1}H-NMR (400 MHz, $CDCl_3$, 298 K) δ = 7.44–7.39 (t, $^3J^{H-H}$= 7.1 Hz, 1H, -O-C**H**=CH-), 6.38–6.31 (m, 2H, =C**H**-C**H**=), 4.53 (m, 2H, C-C**H$_2$**-O), 3.80–3.40 (ddd, $^3J^{H-H}$= 17.3, 11.5, 4.5 Hz, 2H, -O-C**H$_2$**-CH), 3.16 (m, 1H, C**H**-CH_2 oxirane ring), 2.80–2.61 (dd, $^3J^{H-H}$= 4.9, 4.2, 2H, CH-C**H**$_2$ oxirane ring). **^{13}C-NMR** (125 MHz, $CDCl_3$, 298 K) δ = 151.52 (C-O-**C**-CH_2 furan), 148.08 (C=**C**-O furan), 109.75 (OC=**C**-C=CO-CH_2 furan), 110.45 (OC=C-**C**=CO-CH_2 furan), 70.71 (CH_2 next to oxirane ring), 65.18 (C-O-C-**C**H_2-O), 50.87 (O-CH_2-**C**H-(O)-CH_2, oxirane ring) and 44.44 (O-CH_2-CH-(O)-**C**H_2, oxirane ring) ppm. **ATR-FTIR** ν_{max} = 3146, 3125(=C-H, υ), 3062 (-C-H on the oxirane ring, υ), 1504 (-C=C-, υ), 1257, 850 (C-O-C on the oxirane ring, υ), 1217, 1084 (CH_2-O-CH_2, υ), 1150 (C-O-C on the furan ring, υ), 1018 (C-O-C on the furan ring, δ), 918 (C-O-C on the oxirane ring, δ), and 751 (single-substituted furan ring, δ), cm^{-1}. **EI-MS** (*m*/*z*): 154 $[M]^+$, 97 [M- 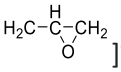]$^+$, 81 [M- 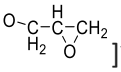]$^+$.

5.4.4 Synthesis of FGE-FAM

Furfuryl amine (FAM, 5g, 51.48 mmol) was added to a 30 mL glass vial. A stoichiometric amount of furfuryl glycidyl ether (FGE, 15.87 g, 0.103 mol) was added to the vial followed by a magnetic stirrer. The mixture was heated at 80 °C for 24 hours in bulk to allow for the epoxy ring opening reaction to

occur. The reaction was allowed to cool down to room temperature to give an orange-brown oil as the product (**FGE-FAM**, 20.87 g, 100% yield). No further purification was necessary.

^{1}H NMR (400 MHz, $CDCl_3$, 298 K) δ = 7.40 (s, 2H, O-CH_2C-(=CH)-O-C**H**=CH furan), 7.35 (s, 1H, N-CH_2C-(=CH)-O-C**H**=CH furan), 6.33 (m, 5H total, 2H, O-CH_2C-(=CH)-O-CH=C**H**, 2H, O-CH_2C-(=C**H**)-O-CH=CH and 1H, N-CH_2-(=CH)-O-CH=C**H** furan), 6.17 (m, 1H, N-CH_2-(=C**H**)-O-CH=CH furan), 4.48 (s, 4H, O-C**H**$_2$C(=CH)O), 3.83 (m, 2H, C**H**-OH), 3.73 (d, $^{3}J^{H\text{-}H}$ = 7.4 Hz, 2H, N-C**H**$_2$C(=CH)O), 3.50-3.40 (m, 4H, O-C**H**$_2$CH-OH), 3.11-3.03 (d, $^{3}J^{H\text{-}H}$ = 33.0 Hz, 2H, O**H**-CH), and 2.60 (m, 4H, N-C**H**$_2$CH-OH) ppm. **^{13}C-NMR** (125 MHz, $CDCl_3$, 298 K) δ = 152.20 (O-CH_2**C**-(=CH)-O-CH=CH furan), 151.80 (N-CH_2**C**-(=CH)-O-CH=CH furan), 143.06 (O-CH_2C-(=CH)-O-**C**H=CH furan), 142.33 (N-CH_2C-(=CH)-O-**C**H=CH furan), 110.49 and 110.35 (O-CH_2C-(=CH)-O-CH=**C**H furan), 109.69 (N-CH_2C-(=CH)-O-CH=**C**H furan), 109.04 (O-CH_2C-(=**C**H)-O-CH=CH furan), 72.40 (O-**C**H_2CHOH), 68.45 and 68.07 (O-CH_2**C**HOH), 65.43 and 65.39 ((O-**C**H_2C-(=CH)-O-CH=CH), 57.62 and 57.17 and 51.51 (N**C**H_2CHOH) and 51.46 (N-**C**H_2C-(=CH)-O-CH=CH) ppm. **EI-MS** (*m*/*z*): 405.186 $[M]^+$, 428.18 $[M^+ Na^+]$.

5.4.5 Synthesis of FGE-P1075

Priamine^{TM} 1075 (P1075, 5g, 9.14 mmol) was added to a 30 mL glass vial. A stoichiometric amount of furfuryl glycidyl ether (FGE, 5.63 g, 36.54 mol) was added to the vial followed by a magnetic stirrer. The mixture was heated at 80 °C for 24 hours in bulk to allow for the epoxy ring opening reaction to occur. The reaction was allowed to cool down to room temperature to give a viscous orange liquid as the product (**FGE-P1075**, 10.63 g, 100% yield). No further purification was necessary.

^{1}H NMR (400 MHz, $CDCl_3$, 298 K) δ = 7.40 (s, 4H, O-CH_2C-(=CH)-O-C**H**=CH furan), 6.33 (dd, $^{3}J^{H\text{-}H}$ = 5.1, 3.5 Hz, 8H, O-CH_2C-(=C**H**)-O-CH=C**H** furan), 4.49 (s, 8H, O-C**H$_2$**C-(=CH)-O-CH=CH furan), 3.82 (m, 4H, OCH_2C**H**OH), 3.44 (m, 8H, OC**H$_2$**CHOH), 3.06 (s, 4H, OCH_2CHO**H**), 2.50 (m, 16H, NC**H$_2$**CHOH, NC**H**$_2$CH_2(CH) and NCH_2C**H$_2$**(CH)), 1.70-0.75 (P1075 backbone protons) ppm. **^{13}C-NMR** (125 MHz, $CDCl_3$, 298 K) δ = 151.81 (O-CH_2**C**-(=CH)-O-CH=CH furan), 143.03 (O-CH_2C-(=CH)-O-**C**H=CH furan), 110.48 (O-

CH_2C-(=CH)-O-CH=**C**H furan), 109.66 (O-CH_2C-(=**C**H)-O-CH=CH furan), 72.58 (O-**C**H_2CHOH),68.40 and 68.00 (O-CH_2**C**HOH), 65.44 and 65.40 (O-**C**H_2C-(=CH)-O-CH=CH), 58.14 and 57.73 (N**C**H_2CHOH), 55.88 (N**C**H_2CH_2(CH)), 52.10 (CH_2**C**H bottom cyclohexane), 50.09 (CH_2**C**H top cyclohexane), 32.15 (**C**$H_2(CH)_2$ cyclohexane), 29.92 (CH**C**H_2CH_2), 27.59 and 27.24 (NCH$_2$**C**H_2(CH)), 22.91 (CH_3**C**H_2) and 14.36 (**C**H_3CH_2) ppm. **EI-MS** (*M*/*z*): 1151.84 $[M]^+$, 997.675 $[C_{60}H_{104}N_2O_9]^+$ and 843.581 $[C_{52}H_{94}N_2O_6]^+$.

5.4.6 Synthesis of TFBZ

In a 3-necked flask equipped with a mechanical stirrer and nitrogen inlet 1,3,5-benzenetricarbonyl chloride (20.0 g, 75.3 mmol) was weighed in CH_2Cl_2 (200 mL). The mixture was cooled using an ice-water mixture to approximately 0 °C. Triethylamine (NEt_3, 26.7 g, 263 mmol) was added and the mixture stirred for 15 minutes at the same temperature. Furfuryl alcohol (FA, 22.2 g, 226 mmol) was added dropwise using an addition funnel. The rate of addition was carefully controlled so that the reaction temperature did not rise above 20 °C. After the addition was complete, the reaction mixture was stirred further for two hours. TLC monitoring gave an indication about completion of the reaction. CH_2Cl_2 was evaporated under reduced pressure and 500 mL of ethyl acetate added to the mixture. The NEt_3 salt was filtered and washed with ethyl acetate. The filtrate was washed three times with water (100 mL) to remove any amine salt and dried over anhydrous $MgSO_4$. Solvent evaporation gave the product as a light brown coloured solid (**TFBZ**, 33.76 g, 85% yield).

^{1}H NMR (400 MHz, $CDCl_3$, 298 K) δ = 8.85 (s, 3H, benzene C**H**), 7.44 (s, 3H, O-CH_2C-(=CH)-O-C**H**=CH furan), 6.51 (t, $^3J^{H\text{-}H}$ = 3.6 Hz, 3H, O-CH_2C-(=C**H**)-O-CH=CH furan), 6.39 (m, 3H, O-CH_2C-(=CH)-O-CH=C**H** furan), 5.34 (s, 6H, O-C**H$_2$**C-(=CH)-O-CH=CH) ppm. **^{13}C-NMR** (125 MHz, $CDCl_3$, 298 K) δ = 164.84 (**C**(=O)O), 149.17 (O-CH_2**C**-(=CH)-O-CH=CH furan), 143.75 (O-CH_2C-(=CH)-O-**C**H=CH furan), 135.15 (benzene **C**H(=C)), 131.26 (benzene CH(=**C**)), 111.57 and 110.89 (O-CH_2C-(=**C**H)-O-CH=**C**H furan) and 59.29 (O-**C**H_2C-(=CH)-O-CH=CH) ppm. **ATR-FTIR** ν_{max} = 1727 (ester C=O, υ), 1609 (aromatic C=C, υ), 1232 (ester C-O, υ), 1150 (C-O-C on the furan ring, υ), 1018 (C-O-C on the furan ring, δ), and 736 (single-substituted furan ring) cm^{-1}.

5.4.7 Synthesis of polyester DA-CANs

All polyester DA-CANs were synthesised *via* solvent casting in chloroform. Equimolar amounts of bismaleimide and multifunctional furan cross-linker were added to a 50 mL glass vial, ensuring a 1 : 1 stoichiometric ratio of furan : maleimide functional groups. 20 mL of chloroform was added, followed by a magnetic stirrer. The mixture was stirred at room temperature until a homogenous solution formed. The solution was then cast into a PTFE-lined petri dish and left in the fume hood until most of the solvent evaporated. Residual solvent was removed in the vacuum oven at 40 °C overnight. 5 g of the bulk DA-network was then chopped up and compression moulded at 100-130 °C for 10 minutes using 3 MPa of pressure, producing approximately a 1 mm thick elastomeric sheet. This sheet was conditioned at 25 °C for 7 days before characterisation and testing to allow DA-network formation to equilibrate.

1,12-DD-FGE-FAM: **ATIR-FTIR** ν_{max} = 3445 (β-OH, υ), 2918 and 2850 (C-H, υ), 1755 (C=O DA, υ), 1725 (ester C=O, υ), 1689 (imide C=O, υ), 1150 (C-O-C on the furan ring, υ),and 730-720 (single-substituted furan ring, δ), cm^{-1}. **DSC**: T_g (12.4 °C), T_{rDA} (110 & 143 °C), and ΔH_{rDA} (52.0 $J.g^{-1}$).

1,12-DD-TFBZ: **ATIR-FTIR** ν_{max} = 2918 and 2850 (C-H, υ), 1755 (C=O DA, υ), 1726 (ester C=O, υ), 1692 (imide C=O, υ), 1232 (ester C-O, υ), 1150 (C-O-C on the furan ring, υ) and 738 (single-substituted furan ring, δ) cm^{-1}. **DSC:** T_m (57.6 °C), ΔH_m (5.9 $J.g^{-1}$), T_{rDA} (122 & 148 °C), and ΔH_{rDA} (47.0 $J.g^{-1}$).

C_{36} -FGE-FAM: ATIR-FTIR ν_{max} = 3445 (β-OH, υ), 2918 and 2850 (C-H, υ), 1755 (C=O DA, υ), 1730 (ester C=O, υ), 1692 (imide C=O, υ), 1150 (C-O-C on the furan ring, υ) and 730-720 (single-substituted furan ring, δ) cm^{-1}. **DSC**: T_g (3.5 °C), T_{rDA} (110 & 137 °C), and ΔH_{rDA} (41.0 $J.g^{-1}$).

C_{36} -TFBZ: **ATIR-FTIR** ν_{max} = 2920 and 2850 (C-H, υ), 1755 (C=O DA, υ), 1730 (ester C=O, υ), 1697 (imide C=O, υ), 1230 (ester C-O, υ), 1150 (C-O-C on the furan ring, υ) and 739 (single-substituted furan ring, δ) cm^{-1}. **DSC**: T_g (27.0 °C), T_{rDA} (124 & 152 °C), and ΔH_{rDA} (35.0 $J.g^{-1}$).

HPBD-1000-FGE-FAM: ATIR-FTIR ν_{max} = 3445 (β-OH, υ), 2955, 2912, 2868 and 2850 (C-H, υ), 1755 (C=O DA, υ), 1730 (ester C=O, υ), 1701 (imide C=O, υ), 1150 (C-O-C on the furan ring, υ) and 730-720 (single-substituted furan ring, δ) cm^{-1}. **DSC**: T_g (-31.0 °C), T_{rDA} (112 & 137 °C), and ΔH_{rDA} (33.0 $J.g^{-1}$).

HPBD-1000-TFBZ: ATIR-FTIR ν_{max} = 2957, 2915, 2871 and 2850 (C-H, υ), 1755 (C=O DA, υ), 1738 (ester C=O, υ), 1695 (imide C=O, υ), 1231 (ester C-O, υ), 1150 (C-O-C on the furan ring, υ) and 737 (single-substituted furan ring, δ) cm^{-1}. **DSC**: T_g (-31.0 °C), T_{rDA} (123 & 153 °C), and ΔH_{rDA} (32.0 $J.g^{-1}$).

HPBD-2000-FGE-FAM: ATIR-FTIR ν_{max} = 3445 (β-OH, υ), 2955, 2912, 2868 and 2850 (C-H, υ), 1755 (C=O DA, υ), 1742 (ester C=O, υ), 1695 (imide C=O, υ), 1150 (C-O-C on the furan ring, υ) and 730-720 (single-substituted furan ring, δ) cm^{-1}. **DSC**: T_g (-31.0 °C), T_{rDA} (116 & 136 °C), and ΔH_{rDA} (18.0 $J.g^{-1}$).

HPBD-2000-TFBZ: ATIR-FTIR ν_{max} = 2961, 2913, 2869 and 2848 (C-H, υ), 1755 (C=O DA, υ), 1739 (ester C=O, υ), 1698 (imide C=O, υ), 1231 (ester C-O, υ), 1150 (C-O-C on the furan ring, υ) and 738 (single-substituted furan ring, δ) cm^{-1}. **DSC**: T_g (-31.0 °C), T_{rDA} (124 & 149 °C), and ΔH_{rDA} (16.0 $J.g^{-1}$).

HPBD-3000-FGE-FAM: ATIR-FTIR ν_{max} = 2955, 2912, 2868 and 2850 (C-H, υ), 1755 (C=O DA, υ), 1732 (ester C=O, υ), 1697 (imide C=O, υ), 1150 (C-O-C on the furan ring, υ) and 730-720 (single-substituted furan ring, δ) cm^{-1}. **DSC**: T_g (-33.0 °C), T_{rDA} (132 °C), and ΔH_{rDA} (16.0 $J.g^{-1}$).

HPBD-3000-TFBZ: ATIR-FTIR ν_{max} = 2962, 2914, 2871 and 2850 (C-H, υ), 1755 (C=O DA, υ), 1732 (ester C=O, υ), 1700 (imide C=O, υ), 1231 (ester C-O, υ), 1150 (C-O-C on the furan ring, υ) and 738 (single-substituted furan ring, δ) cm^{-1}. **DSC**: T_g (-33.0 °C), T_{rDA} (123 & 150 °C), and ΔH_{rDA} (12.0 $J.g^{-1}$).

1,12-DD-FGE-P1075: ATIR-FTIR ν_{max} = 3445 (β-OH, υ), 2918 and 2849 (C-H, υ), 1755 (C=O DA, υ), 1729 (ester C=O, υ), 1693 (imide C=O, υ), 1150 (C-O-C on the furan ring, υ) and 730-720 (single-substituted furan ring, δ) cm^{-1}. DSC: T_g (-1.3 °C), T_{rDA} (119 & 146 °C), and ΔH_{rDA} (43.0 $J.g^{-1}$).

C_{36}-FGE-P1075: ATIR-FTIR ν_{max} = 3445 (β-OH, υ), 2918 and 2850 (C-H, υ), 1755 (C=O DA, υ), 1730 (ester C=O, υ), 1696 (imide C=O, υ), 1150 (C-O-C on the furan ring, υ) and 730-720 (single-substituted furan ring, δ) cm^{-1}. DSC: T_g (-13 °C), T_{rDA} (119 & 144 °C), and ΔH_{rDA} (32.0 $J.g^{-1}$).

HPBD2000 FGE-P1075: ATIR-FTIR ν_{max} = 2963, 2916, 2877 and 2850 (C-H, υ), 1755 (C=O DA, υ), 1741 (ester C=O, υ), 1697 (imide C=O, υ), 1150 (C-O-C on the furan ring, υ) and 730-720 (single-substituted furan ring, δ) cm^{-1}. **DSC**: T_g (-48 °C), T_{rDA} (120 & 144 °C), and ΔH_{rDA} (15.0 $J.g^{-1}$).

5.4.8 Instrumental methods.

Proton (^{1}H) nuclear magnetic resonance (^{1}H NMR) spectra were recorded using a Bruker AV or AVIIIHD 400 MHz spectrometer at room temperature with ~ 10 mg of sample fully dissolved in deuterated chloroform ($CDCl_3$). Chemical shifts were recorded in parts per million (ppm) relative to the reference peak of chloroform solvent at δ = 7.26 ppm. Spectra were analysed on MestReNova v6.0.2. **Carbon (^{13}C) nuclear magnetic resonance (^{13}C NMR)** spectra were recorded at 125 MHz using ~ 40 mg of sample. Chemical shifts were recorded in parts per million (ppm) relative to a reference peak of chloroform solvent at δ = 77.16 ppm. **Electrospray ionisation- time of flight (ESI-ToF)** spectra were recorded using a Waters G2 Synapt Q-TOF mass spectrometer, equipped with a solid-state laser delivering laser pulses at 355 nm with a positive ion ToF detection performed using an accelerating voltage of 10 kV. Samples were spotted onto analytical plates through application of 1 µL of a solution containing 2,5-dihydroxybenzoic acid (DHB) (10 mg/mL in THF) as a matrix and analyte (10 mg/mL in THF) followed by solvent evaporation. The samples were measured in reflection ion mode. **Attenuated Total Reflectance Fourier Transform Infrared (ATR-FTIR)** spectra were collected on a PerkinElmer FT-Infra-red spectrometer equipped with a UATR Two accessory. Eight scans were taken in the range of 4000 – 400 cm^{-1}. Analysis was performed on PerkinElmer Spectrum software. **Differential scanning calorimetry (DSC)** was performed using a TA instruments Discovery DSC 25. Less than 3 mg of sample was accurately weighed on a microbalance and loaded into a T_{zero} aluminium pan. Heating and cooling ramps (from -90 °C to 200 °C) were conducted under a N_2 flow (40 mL min^{-1}) at a standard rate of 10 °C

min^{-1}. T_g was taken as the midpoint of inflexion. T_m and T_{rDA} were measured as the temperature at the minimum heat flow of the appropriate endotherms. Analysis was performed on TRIOS v5.1.1 software. **Dynamic Mechanical Analysis (DMA)** was performed using a TA Instruments Q800 DMA using tensile clamps. Sample dimensions were typically 10 mm length by 5 mm width by 1 mm thickness. Samples were evaluated between -80 °C and 200 °C at a heating rate of 3 °C min^{-1}. A deformation frequency of 1 Hz and a strain of 0.05% were used. **Monotonic uniaxial extension experiments** were carried out on a Zwick line tensometer according to ISO 527 (10 $mm.min^{-1}$ extension rate). Dumbbell specimens were cut out of approximately 1 mm thick compression moulded sheets using a Zwick Roell® knee manual cutting press ZCP 020 with cutting device for ISO 527-2 type 5B die attachment. (Length= 35 mm, gauge length = 12 mm, width = 2 mm). Before testing, thickness of each specimen was measured using a digital calliper and recorded on the software.5 specimens were tested for each material. Results were analysed on TestXpert II software.

5.4.9 Soxhlet experiments

An accurately measured mass of DA-CAN compression moulded sheet (0.5 g) was folded into a pre-weighed piece of filter paper and labelled carefully with pencil. A repeat sample was made up in the same way. A piece of blank filter paper containing no sample was included as a control. Samples were inserted into a 250 mL Soxhlet extractor on top of a 500 mL round-bottom flask containing THF solvent (300 mL) with a reflux condenser attached above. THF was heated to reflux for 24 hours. Sample mass was recorded before and after extraction. The sample mass difference was used to calculate the gel fraction of the material, which provides insight into how successfully it has cross-linked. The gel fraction is defined as the weight ratio of dried network polymer (W_2) after extraction to that of the polymer before (W_1).

5.4.10 Compression moulding

5 g of each DA-PU CAN (bulk material) was chopped into small pieces and spread evenly into a metal compression mould lined with a thin sheet of PTFE. Another PTFE sheet was placed on top followed

by the metal mould lid which was then placed between two preheated metal plates at 100-130 °C. The metal mould was then placed between the two preheated metal plates and 3 MPa of pressure was applied for ten minutes to melt and spread the material into an even film. The mould was then removed from the heat and once cooled to room temperature, the material was removed, giving a 1 mm thick elastomeric sheet.

5.5 References

[1] C. J. Kloxin, T. F. Scott, B. J. Adzima and C. N. Bowman, *Macromolecules*, 2010, **43**, 2643-2653.

[2] A. Cornille, R. Auvergne, O. Figovsky, B. Boutevin and S. Caillol, *Eur. Polym. J.*, 2017, **87**, 535-552.

[3] S. Kamarulzaman, Z. M. Png, E. Q. Lim, I. Z. S. Lim, Z. Li and S. S. Goh, *Chem.*, 2023, **9**, 2771-2816.

[4] M. Thys, J. Brancart, G. Van Assche, R. Vendamme and N. Van den Brande, *Macromolecules*, 2021, **54**, 9750-9760.

[5] P. Tanasi, M. Hernández Santana, J. Carretero-González, R. Verdejo and M. A. López-Manchado, *Polymer*, 2019, **175**, 15-24.

[6] C. Zeng, H. Seino, J. Ren, K. Hatanaka and N. Yoshie, *Macromolecules*, 2013, **46**, 1794-1802.

[7] L. M. Sridhar, M. O. Oster, D. E. Herr, J. B. D. Gregg, J. A. Wilson, and A. T. Slark, *Green Chem.*, 2020, **22**, 8669-8679.

[8] J. Ding, W. Peng, T. Luo and H. Yu, *RSC Adv.*, 2017, **7**, 6981-6987.

[9] M. Chatterjee, T. Ishizaka, and H. Kawanami, *Green Chem.*, 2016, **18**, 487-496.

[10] N. Faggio, A. Marotta, V. Ambrogi, P. Cerruti and G. Gentile, *J. Mater. Sci.*, 2023, **58**, 7195-7208.

[11] R. Cucciniello, D. Cespi, M. Riccardi, E. Neri, F. Passarini and F. M. Pulselli, *Green Chem.*, 2023, **25**, 5922-5935.

[12] T. Woldbæk, P. Klaboe and C. J. Nielsen*, J. Mol. Struct.*, 1975, **27**, 283-301.

[13] J. Wang, J. Li, J. Zhang, S. Liu, L. Wan, Z. Liu and F. Huang, *Polymers*, 2023, **15**, 3470.

[14] S. Terryn, J. Brancart, E. Roels, R. Verhelle, A. Safaei, A. Cuvellier, B. Vanderborght and G. Van Assche, *Macromolecules*, 2022, **55**, 5497-5513.

[15] Q. Zhou, Z. Sang, K. K. Rajagopalan, Y. Sliozberg, F. Gardea and S. A. Sukhishvili, *Macromolecules*, 2021, **54**, 10510-10519.

[16] R. C. Boutelle and B. H. Northrop, *J. Org. Chem.*, 2011, **76**, 7994-8002.

[17] C.-J. Huang and E. Y. Li, *RSC Adv.*, 2019, **9**, 7246-7250.

[18] I. M. Barszczewska-Rybarek, A. Korytkowska-Wałach, M. Kurcok, G. Chladek and J. Kasperski, *Acta Bioeng. Biomech.*, 2017, **19**, 47-53.

[19] A. Safaei, J. Brancart, Z. Wang, S. Yazdani, B. Vanderborght, G. Van Assche and S. Terryn, *Polymers*, 2023, **15**, 3527.

6. Conclusions and future work

6.1 Conclusions

This thesis focussed on developing novel structure-property relationships of thermally reversible DA polymers with healing and reprocessing abilities for elastomeric applications. Despite the chemistry of the furan-maleimide DA-reaction being well documented in the literature, fundamental understanding of material behaviour and structure-property relationships is still lacking.

Initially, TPUs comprising similar concentrations of DA-cycloadducts (f_g) but different SS backbones (PCL, PCL.LA, PBD or HPBD) were synthesised *via* copolymerisation of the PU prepolymers comprising maleimide and furan end-groups. Cycloadduct formation was measured as requiring 7 days at 25 °C or 2 days at 60 °C to reach an equilibrium *via* FTIR spectroscopy and DSC analysis. Thermal analysis confirmed the rDA reaction *via* a double melting endotherm and a substantial drop in *E'* between 117 and 145 °C. The thermomechanical properties of DA-TPUs varied with SS backbone, with DA-PCL and DA-PBD exhibiting enhanced mechanical and thermal properties due to synergistic reinforcement of the thermally reversible DA-bonds through physical interactions resulting from crystallinity and phase separation, respectively. All DA-TPUs were thermally reprocessable under mild conditions and DA-PBD/ DA-PCL displayed excellent self-healing ability.

The synthesis of DA-TPUs comprising different molecular weight PCL SS was then investigated to determine the effect of equivalent concentration of furan and maleimide functional groups (f_g) and thus DA-cycloadduct concentration on material properties. DA-TPUs incorporating higher molecular weight PCL displayed enhanced mechanical properties due to higher PCL crystallinity with reduced thermal stability and elasticity due to lower DA-cycloadduct concentrations. Mixed DA-(PBU-*co*-PEU) copolymers were then synthesised and compared to DA-TPU's containing 100 wt.% PBU or PEU backbone. The effect of PBU : PEU composition on material properties was evaluated, with DA-(50PBU-*co*-50PEU) displaying a pronounced synergistic effect and the best elastomeric properties.

A series of 12 PU-DA networks (CANs) was then synthesised *via* the copolymerisation of three trifuran (TF) cross-linkers containing different H-bonding capable groups: TF ester, TF urethane, and TF urea

with the four telechelic bismaleimide prepolymers based on PCL, PCL.LA, PBD or HPBD SSs from earlier. Increased cross-linker H-bonding led to a systematic increase in network strength, stiffness, and delegation temperature (T_{gel}), crucial for processing, across all polymer backbones, suggesting synergistic reinforcement of DA-covalent cross-links. However, increased cross-linker H-bonding also caused a significant decrease in network flexibility and a resulting reduction in tensile toughness. PCL and PCL.LA PU-DA networks displayed enhanced elongation and toughness over PBD and HPBD networks, due to the greater ability of PCL to strain-crystallise. PCL-DA networks also displayed the highest network strength due to reinforcement from semi-crystalline PCL segments. Like thermosets, at room temperature the PU-DA CANs displayed robust mechanical properties and solvent resistance *via* Soxhlet extraction however the DA-CANs could also be thermally reprocessed above 100 °C, maintaining excellent mechanical properties.

Focus then shifted towards adjusting design parameters in polyester-DA networks. The effect of network f_g and DA-cross-link density on thermomechanical properties was explored *via* copolymerising different molar mass bismaleimides (synthesised *via* the esterification of polyols with 6-MCA) with three multifunctional furan cross-linkers: amorphous FGE-FAM and FGE-P1075, made *via* the ring-opening addition of FGE with FAM and P1075 dimer diamine, respectively, and crystalline 1,3,5-trifuryl benzoate (TFBZ), synthesised from the reaction of 1,3,5-benzenetricarbonyl chloride with furfuryl alcohol. Thermal analysis revealed that increasing DA cross-link density increased T_g, T_f and ΔH_{rDA} whilst tensile testing showed that network strength and Young's modulus increased but network flexibility decreased, due to an increase in the concentration of rigid DA-cycloadducts. At similar f_g values, DA-networks incorporating TFBZ cross-linker displayed higher T_g and T_{rDA} values *via* DSC analysis and higher $E'_{rubbery}$ and T_f values from DMA than those containing FGE-FAM, demonstrating higher stiffness and thermal stability. TFBZ polyester DA-CANs also exhibited higher Young's modulus, stress and elongation at break and tensile toughness due to enhanced strain-hardening effects.

In this project, novel design parameters have been systematically investigated in DA-polymers to determine their individual effect on the resulting thermomechanical and morphological properties. The work outlined in this thesis has demonstrated the large variety of material properties that can be achieved through careful adjustment of DA design parameters to optimise properties to meet specific requirements for diverse applications and reprocessing techniques. Moreover, self-healing and reprocessing capabilities of DA-polymers have been demonstrated, in addition to synthesis of biobased furan/maleimide monomers, presenting a sustainability advantage over current thermoset elastomers.

6.2 Future work

In the future it would be beneficial to conduct creep experiments on the DA-elastomers, since the occurrence of creep in CANs at ambient temperature is a well-known problem, due to constant bond exchange and stress-relaxation.[1] It would be particularly interesting to test the creep-resistance of the more phase separated DA-polymers, since hydrogen-bonding in microphase-separated structures of CANs has been reported to significantly reduce creep.[2,3] SAXS and WAXS experiments on the polyester DA-CANs from Chapter 5 would have been interesting to determine if the influence of maleimide/furan structure and network DA-cross-link density on morphology. Moreover, in *situ* heating SAXS/WAXS experiments of phase-separated/crystalline materials could be useful to explore how heat affects the morphology of these lamellar structures. Further thermal reprocessing tests on DA-CANs would confirm whether all networks can be recycled whilst maintaining good mechanical properties whilst further self-healing studies could be conducted to determine whether the difference DA-design parameters such as the degree of cross-linker H-bonding in Chapter 4 affect self-healing efficiency/ conditions. Studies on whether the morphology is affected by repeated processing cycles would be important and could be achieved *via* collecting DMA, DSC, SAXS and WAXS data between reprocessing of materials. Post-processing thermal treatment (annealing) studies on the PU-based materials could also improve mechanical properties at elevated temperatures and enhance low

temperature performance by reducing the T_g of the SS due to better alignment of HS domains.[4] The investigation of DA-cycloadducts to comptabilise other immiscible SSs outside of PBD and PCL could also be useful.

6.3 References

[1] F. Van Lijsebetten, T. Debsharma, J. M. Winne and F. E. Du Prez, *Angew. Chem., Int. Ed.*, 2022, **61**.

[2] Y. Liu, Z. Tang, D. Wang, S. Wu and B. Guo, *J. Mater. Chem. A*, 2019, **7**, 26867–26876.

[3] L. Wang, Y. Liu, Y. Qiao, Y. Wang, Z. Cui, S. Zhu, F. Dong, S. Fang and A. Du, *Polym. Chem.*, 2022, **13**, 4144–4153.

[4] M. Amirkhosravi, L. Yue, T. Ju and I. Manas-Zloczower, *Polymer*, 2021, **214**, 123254.